Nonlinear response of earth dams and foundations in earthquakes.

Chang, Chi-Tso

NONLINEAR RESPONSE OF EARTH DAMS AND FOUNDATIONS IN EARTHQUAKES

by

Chi-Tso Chang, B.Sc.; M.Eng.; P.E.

Thesis submitted to the University of Wales in Candidature for the degree of Doctor of Philosophy, University College of Swansea.

JANUARY, 1979

C/Ph/53/79

ACKNOWLEDGEMENTS

The author wishes to express his deepest gratitude to his supervisors, Professor O.C. Zienkiewicz and Dr. E. Hinton for their invaluable help and continued guidance and encouragement throughout this study.

Thanks are also due to Dr. D.W. Kelly, Dr. Peter Bettess, Dr. G.N. Pande, Dr. D.J. Naylor, Mr. K. Johnson, Dr. N. Bicanic, Mr. G.D. Tong, Dr. K.K. Raju, Mr. K.H. Leung, Mr. S. Baraka, Mr. W.Abdullah and Mr. A. Salem for many useful discussions and to the staff of the Computer Centre for providing computer facilities.

The author is very grateful to the Science Research Council of the United Kingdom for affording him the Research Grant GR/2602.8 and to Sinotech Engineering Consultants Inc., Taiwan, ROC, especially to Mr. Rogers Y. Cheng for enabling him to study in the United Kingdom.

Appreciation is also expressed to the members of the Reprographic Staff - Mrs. J. Pugh, Mrs. A. McGairl and to Mr. D. Gabriel for their assistance in the preparation of this thesis and also to Mrs M.P. Jones and Mrs. M.A. Williams for their skill and patience in typing this manuscript.

Finally, the author wishes to express his sincere appreciation to his wife, Fuying, for her continuous encouragement throughout the course of this study. The author also expresses his appreciation to his children, Weian, Weiling and Yu, for overcoming considerable hardship caused by their father's absence from home.

SUMMARY

This thesis is devoted to the study of nonlinear response of earth dams in earthquakes and the problems of soil liquefaction. The finite element method is employed for the spatial discretization of the continuum and the dynamic equations of motion are solved using step by step time integration schemes. Both the implicit and the explicit time stepping schemes are studied and the efficiency of two schemes are compared.

The essential cause of the growth of pore pressure during cyclic loading is identified as an "autogenous" shrinkage or densification of the solid phase of the soil and this is related to a strain path parameter. Introduction of this shrinkage coupled with nonlinear constitutive laws of the soil skeleton allows a full nonlinear dynamic analysis to be conducted up to the point of structural failure.

The detail of the basic formulation of the dynamics of a nonlinear two phase material based on the finite element method is developed and illustrated by application to a variety of problems.

Finally, the fully nonlinear responses of earth dams in earthquakes are extensively investigated. The results which are presented graphically are readily applicable to the evaluation of the safety of the dam in earthquakes.

CONTENTS

CHAPTER 1

INTRODUCTION AND THESIS LAYOUT

1.1 Introduction:

When an earth dam is constructed in a seismic high risk zone, the safety of the dam in terms of its performance during a major earthquake must be ensured in order to avoid the catastropic events which are certain to follow any failure in the dam. To evaluate safety, four steps are required:

(1) An appropriate mathematical model must be established for the dam.

(2) The expected ground motion must be defined.

(3) An analysis must be made to determine the model's dynamic response to the expected ground motion.

(4) The analytical results must be interpreted in terms of the prototype behaviour.

The present study attempts to cover these points.

1.2 Physical Reality:

The different physical elements of an earth dam during an earthquake consist of: the soil mass and the foundation; the reservoir; and the applied earthquake. The soil mass and the foundation form a three-dimensional continuum which is usually composed of anisotropic, nonhomogenous inelastic materials. In addition to a set of initial stresses due to self weight and the construction process, the dam is also subjected to a hydrostatic force from the reservoir, an inertia force and a hydrodynamic force induced by the earthquake.

1.3 Design Considerations:

An earth dam which is located in a region of high seismic risk must be designed to withstand without disastrous failure the most severe earthquake that may take place. If the dam is able to resist the earthquake then a major catastrophe involving loss of life and property can be avoided. Therefore, the main objective of every dam engineer is to design and construct a dam which is not only economically viable but which is also safe under any probable loading condition. The enormous size of the dam structure makes the factors of both economy and safety particularly important. While an excessively conservative design of a dam increases the cost of the project, the failure of a dam implies disastrous results and fatalities to the communities downstream.

In order to assess the best design for a dam, it is essential for an engineer to carry out a thorough investigation to understand the true structural behaviour of the dam and to estimate the magnitude of any potential deformation. The magnitude of any deformation must remain within allowable limits so that the system is able to remain in constant operation.

Failure of an earth dam under seismic loading may be due to overtopping, piping, liquefaction, shear failure or a combination of these factors. During an earthquake, mass landslide may occur upstream of the dam, which in turn can create huge wavefronts and, where these are inadequate spillways, the results could lead to overtopping. Piping will result if the dam cracks or if there is a build up of excess pore pressure. Liquefaction will take place if the excess pore pressure reaches the total mean stress of

the soil resulting in a zero effective stress and thus causing the soil to lose its strength completely. Finally, shear failure may occur when the stress induced by the earthquake exceeds the maximum strength of the soil. Apart from overtopping these failure modes are completely dependent on the response of the dam during an earthquake. Since the constitutive laws of the materials used in earth dams rarely follow linear patterns, in this context, the practical importance of the present study (that is the nonlinear behaviour of earth dams and foundations in earthquakes) is self evident.

1.4 Literature Review:

Before the advent of the electronic computer, the analysis of an earth dam under earthquake loading was carried out by the pseudo static method, in which the dynamic load per unit volume of the dam induced by an earthquake was taken as the product of w, the unit weight of the dam, and α is a seismic coefficient which depends on the earthquake's intensity at the damsite (the higher the earthquake intensity the larger the values of α adopted). Usually α_h, the horizontal seismic coefficient, ranges from 0.1 to 0.3 and α_v, the vertical seismic coefficient, ranges from 0.06 to 0.15. With such static forces defined, the slip circle method can be applied to find the "factor of safety" against sliding or overturning or local slope instability. It can be seen that the pseudo static method is capable of predicting the factor of safety, but it can not predict either the potential stress or deformation of the dam, both of which are of practical importance. Furthermore, in recent major earthquakes, some dams which were designed according to the accepted pseudo static method have been damaged.

A comprehensive study of the effects of earthquakes on dams

has been presented by Newmark[1]. The first mathematical treatment of the dynamic response of earth dams during earthquakes was made by reducing the problem to a one-dimensional form. The dam was assumed to be a prismatic wedge of infinite length, under uniform load along its length. Thus the problem was basically one of plane strain. Furthermore, the displacements within the cross sections were assumed to involve only horizontal shear. Thus, the system was further reduced to a vertical shear beam with linearly varying width. The dynamic behaviour of such a system was first discussed by Mononobe, et al[2]. Further studies of the earthquake behaviour of the wedge shaped shear beam were published by Hatanaka[3]. Ambraseys[4] extended the analysis to include the effects of end constraint, assuming that shear distortions could develop along vertical as well as horizontal sections.

All of these analyses only took into account shearing distortions in the earth dam material, a very limited approximation of the true behaviour. The first attempt to include the complete two-dimensional nature of the cross-sectional deformations in a dynamic analysis was made by Ishizaki, et al[5]. They treated the dynamic plane strain problem using finite differences to solve the Navier equations of equilibrium at discrete intervals of time. Comparison of these results with results from the shear wedge type analysis demonstrated that (1) the assumption of pure shear deformation is reasonable near the vertical axis of the cross-section, but no longer correct near the upstream and downstream faces; and (2) horizontal displacements near the faces of the dam may be significantly different from the centre line displacements given by the shear wedge theory. Since the design criteria for earth dams

are based largely on slope stability which is controlled by conditions near the faces of the dam, it is clear that the shear wedge analysis does not give an adequate measure of the dam behaviour.

The finite difference method, however, does not appear to be the most advantageous method for studying the two-dimensional dynamic response problem. The arbitrary geometry and nonhomogeneity of a typical earth dam cross-section must inevitably lead to difficulties in the finite difference formulation. Conversely, the finite element method automatically takes into consideration any arbitrary geometry or material property variations, thus, it is ideally suited to earth dam analysis. The first attempt to apply the finite element method to the earthquake stress analysis of an earth dam was made by Clough, et al[6] in 1966. They considered a simple triangular section with homogenous elastic properties, subjected to the El Centro earthquake of 18th May, 1940. Meanwhile, Chopra[7] pointed out the inadequacy of the shear wedge approach for obtaining the response of earth dams to earthquakes by comparing results with those produced by the finite element method. From these results it was concluded that the finite element method offered considerable advantages over the shear wedge method. The study of the elastic response of earth dams subjected to travelling seismic waves was carried out by Dibaj, et al[8]. They concluded that the spatial variation of the earthquake excitation was negligible only when the ratio of base width to wave velocity, (i.e. the time required for the travelling wave to move across the base of the dam) was less than 0.1 to 0.2 seconds. For other situations the spatial variation present in earthquake ground motions, if neglected, was very likely to lead to a serious underestimation of the safety factors.

The dynamic response of a dam resting on an elastic foundation was given by Chopra, et al[9,10]. They illustrated that the elasticity of the foundation might have an important influence on the natural frequencies as well as the mode shapes, and large amounts of energy might be dissipated by wave propagation into the infinite foundation. Soil can be considered as a two-phase material composed of a porous granular solid skeleton saturated with water. Ghaboussi, et al[11] studied a dynamic model in which the soil was treated as a two phase material. The solid skeleton and the fluid which were treated as independent elastic materials had separate material properties. The linearly elastic constitutive properties were not capable of representing such important features of the soil behaviour as dilatancy under the shear deformation, which has a significant influence on the pore pressure. However this study could be considered as an initial step towards the determination of pore pressures and theintergranular stresses in soil structures under seismic loading. The study of several significant parameters that could affect the performance of a dam-foundation system were carried out by Idriss, et al[12]. These parameters were the fundamental periods of the dam and of the foundation layer, the lateral extent of the foundation, and the material properties of the dam and of the foundation layer. They concluded that the interaction effects could not be uniquely related to either the ratio of the period of the dam to the period of the foundation layer, or to the relation between the material properties of the dam and the foundation layer but the interaction effects were found to be uniquely related to the ratio D/B, where D is the depth of the foundation layer and B is the width of the dam section as shown in Figure 1.1. For values of D/B less than unity, strong interaction

effects were obtained and the dam foundation system must be analysed as a coupled system. For values of D/B greater than unity, the interaction appeared negigible and the dam and its foundation layer can be decoupled. It should be noted, however, that for very small values of D/B the interaction effects would decrease because as D approaches zero (or, as the foundation layer becomes much stiffer than the dam) there would be no interaction.

The Bureau of Reclamation[13], United States Department of the Interior, proposed certain procedures for the dynamic analysis of embankment dams. The procedures allow viscous damping to be introduced in the construction of the stiffness matrix and use the equivalent linear method to describe soil moduli and damping. The main output of the finite element programs based on such procedures is the irregular stress-time history and the maximum shear stress within each element. It is then assumed that the irregular shear stress-time history can be represented by an equivalent number of uniform cycles. This refers to the stress magnitude which would cause the same effect on the soil and is used in laboratory tests to relate experimental work to the computed stress. The procedure for converting the irregular shear stress time histories to an equivalent number of uniform cycles was given by Seed[14]. This leads to the determination of a "strain potential" for each element in the structure, which consequently forms a basis for evaluating the embankment dam stability.

These and other studies [15-20] related to actual case histories of recording the behaviour of earth dams during earthquakes, and particularly of the major slide in the Lower San Fernando Dam[21]

during the earthquake of 9th February, 1971 indicate that the nonlinear response of a structure foundation system subjected to an earthquake may be completed by various approximate processes involving a sequence of linear analyses in which the secant moduli of the materials were amended as computation proceeded. However though such methods were able to give reasonable predictions of the possible areas of liquefaction or overstress, they were incapable of giving any indication of the extent or the permanence of any damage or deformation after the passage of an earthquake. Therefore a more precise evaluation by a finite element nonlinear solution appears to be necessary for important structures. This subject is further emphasized by Clough and Zienkiewicz[22] and forms the main topic of the present thesis.

1.5 Scope and Layout of the thesis:

The main object of the present study is to investigate the nonlinear behaviour of earth dams during earthquakes. This is particularly important in seismic design since the energy absorption which results from the plastic deformation and creep of the material affects the motion of the structure considerably. The study concentrates on the following areas:

(1) the development of an efficient time stepping algorithm.

(2) consideration of suitable elasto-plastic models or elasto-viscoplastic models.

(3) liquefaction phenomena.

A mathematical model for the analysis of the structural response to earthquakes which allows the investigation of the above aspects, is described in Chapter 2. In this chapter, the structural approximation made, and the material model adopted are

presented and the selection of design earthquakes is discussed. Chapter 3 deals with finite element spatial discretization. The equation solving techniques are presented in Chapter 4. Chapter 5 is devoted entirely to the theory of liequefaction, i.e., the behaviour of saturated sand under cyclic loading in undrained conditions. Chapter 6 presents the densification of dry sand or saturated sand under fully drained conditions during cyclic loading. The partially drained analysis of saturated sand undergoing cyclic loading is presented in Chapter 7. The results of the nonlinear response study of earth dams in earthquakes are presented in Chapter 8. Finally, the conclusions and recommendations based on the present study are made in Chapter 9. A brief summary of the thesis is presented in Figure 1.2.

REFERENCES

1. NEWARK, N.M.,
'Effects of Earthquakes on Dams and Embankments,
Geotechnique, London, England, Vol. 15, No. 2, 39-160 (1965)

2. MONONOBE, N., TAKATA, A. and MATUMURA, M.,
'Seismic Stability of an Earth Dam,
Transactions, 2nd Congress on Large Dams, Washington D.C. Vol.IV (1936)

3. HATANAKA, M., Fundamental Considerations on the Earthquake
'Resistant Properties of the Earth Dam',
Bulletin No. 11, Disaster Prevention Research Inst., Kyoto University,
Kyoto, Japan (1955)

4. AMBRASEYS, N.N.,
'The Seismic Stability of Earth Dams,
Proceedings, 2nd World Conf. on Earthquake Engineering, Tokyo,
Japan, Vol. 2 (1960)

5. ISHIZAKI, H. and HATAKEYAMA, N.,
'Considerations on the Vibrational Behaviours of Earth Dams',
Bulletin No. 52, Disaster Prevention Research Inst., Kyoto
University, Kyoto, Japan (1962)

6. CLOUGH, R.W. and CHOPRA, A.K.
'Earthquake Stress Analysis in Earth Dams',
Journal of the Engineering Mech. Division, ASCE, Vol. 92, 197-212 (1966)

7. CHOPRA, A.K.
'Earthquake Response of Earth Dams',
Journal of the Soil Mechanics and Foundations Division, ASCE,
Vol. 93, No. SM2, 65-81 (1967)

8. DIBAJ, M. and PENZIEN, J.
'Response of Earth Dams to Travelling Seismic Waves'
Journal of the Soil Mechanics and Foundations Division, ASCE
Vol.95, No. SM2, 541-560 (1969)

9. CHOPRA, A.K., DIBAJ, M., CLOUGH, R.W., PENZIEN, J. and SEED, H.B.
'Earthquake Analysis of Earth Dams'
4th World Conference on Earthquake Engineering, Santiago, Chile (1969)

10. CHOPRA, A.K. and PERUMALSWAMI
'Dam Foundation Interaction During Earthquake'
Proceeding, 4th World Conference on Earthquake Engineering,
Santiago, Chile (1969)

11. GHABOUSSI, J. and WILSON, E.L.,
'Seismic Analysis of Earth Dam-Reservoir Systems'
Journal of the Soil Mechanics and Foundations Division, ASCE
Vol.99, No. SM10, 849-862 (1973)

12. IDRISS, I.M., MATHUR, J.M. and SEED, H.B.,
'Earth Dam-Foundation Interaction During Earthquakes'
International Journal of Earthquake Engineering and Structural Dynamics, Vol. 2, 313-323 (1974)

13. ARTHUR, H.G., et al
'Dynamic Analysis of Embankment Dams'
United States Department of the Interior, Bureau of Reclamation Engineering and Research Center, Denver, Colorado (1976)

14. SEED, H.B. and IDRISS, I.M.
'Influence of Soil Conditions on Ground Motions During Earthquake'
Journal of the Soil Mechanics and Foundations Division, ASCE, Vol. 95, 99-137 (1969)

15. AKAY, H.U. and GULKAN, P.
'Earthquake Analysis of Keban Dam'
Proceedings of the Fifth European Conference on Earthquake Engineering, Paper No. 36, Istanbul (1975)

16. AKAY, A.U. and GULKEN, P.
'Evaluation of the Reservoir Effect on The Dynamics of Dams'
Proceedings of the International Symposium on Earthquake Structural Engineering, St. Louis, Missouri, U.S.A. (1976)

17. DEFFENSE, G.V.
'Nonlinear Seismic Analysis of Earth Dams by the Finite Element Method'
M.Sc. Thesis, University of Wales, Swansea (1976)

18. KRAMER, R.W., MacDONALD, R.B., TIEDEMANN, D.A. and VIKSNE, A.
'Dynamic Analysis of Tsengwen Dam'
Bureau of Reclamation, Denver, Colorado (1975)

19. NAYLOR, D.J., STAGG, K.G. and ZIENKIEWICZ, O.C.,
'Criteria and Assumptions for Numerical Analysis of Dams'
Proceedings of an International Symposium Held at Swansea, U.K.(1975)

20. VULPE, A., BARBAT, H., BREABAN, V. and IONESEU, C.,
'Seismic Analysis of a Rockfill Dam'
Proceedings of the Fifth European Conference on Earthquake Engineering, Paper No. 48, Istanbul (1975)

21. SEED, H.B., LEE, K.L., IDRISS, I.M. and MAKDISI, F.,
'Slides in the San Fernando Dams During the Earthquake of February 9th, 1971'
Journal of the Geotechnical Division, ASCE, 651-688 (1975)

22. CLOUGH, R.W. and ZIENKIEWICZ, O.C.,
'Finite Element Methods in Analysis and Design of Dams' (A survey of Present Developments, Practical Assumptions and Outstanding Problems)
Proceedings of an International Symposium Held at Swansea, U.K. (1975)

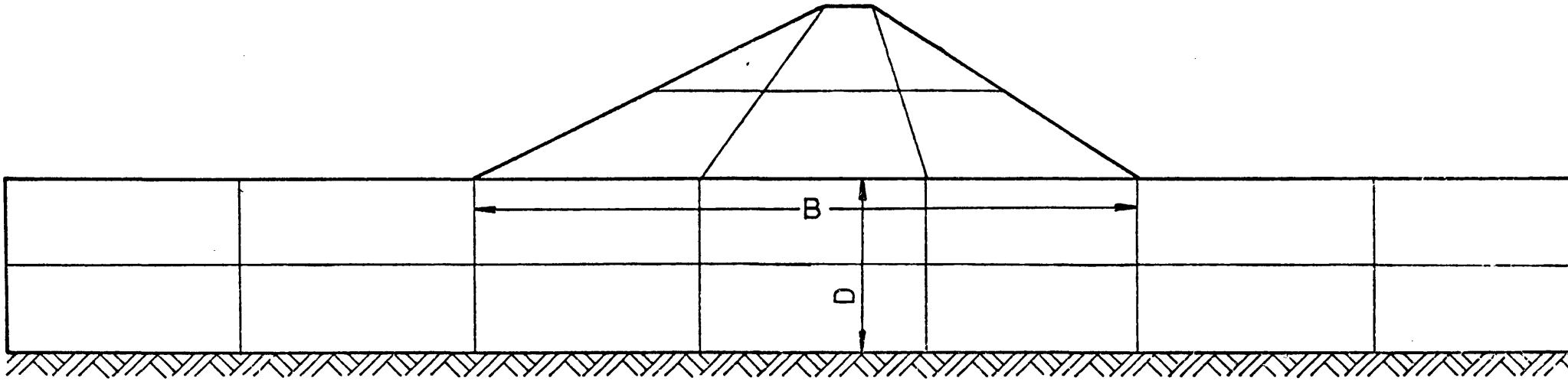

Fig. 1.1: DAM-FOUNDATION SYSTEM

1. Introduction and thesis layout

*Introduction
*Physical reality
*Design considerations
*Literature review
*Scope and layout of the thesis

2. The mathematical model

*Introduction
*Structural idealization
*Structural approximation of fluid
*Material model
 Stresses, strains, and constitutive law
 Plasticity
 Viscoplasticity
 No tension model
*The extent of foundation length included in structural model
*Modelling of boundary
*Selection of design earthquake

3. Finite element spatial discretization

*Introduction
*Dynamic formulation
*Mass matrix
*Damping matrix
*Evaluation of isoparametric elements

4. Solution technique

*Introduction
*Implicit time stepping scheme
*Explicit time stepping scheme
*Comparison of the implicit time stepping scheme and the explicit time stepping scheme

5. Liquefaction

*Introduction
*Physical reality of liquefaction
*Undrained soil behaviour under cyclic loading
*Factors affecting liquefaction
*Evaluation of "autogenous" volumetric strain " ε_v^o"
*Examples

6. Densification of sand

*Introduction
*Factors governing the densification of dry sand
*Densification of sand
 Densification in terms of volumetric strain
 Densification in terms of void ratio
*Comparison of the theoretical evaluation with experimental results
*Discussions

Fig. 1.2: A brief summary of the thesis

7. Partially drained analysis of transient problems in porous media

*Introduction
*Basic formulation of seepage equation
*Examples

8. Nonlinear response of earth dams in earthquakes

*Introduction
*Procedures to carry out the dynamic analysis of embankment dams
*Effects of vertical component of earthquake on dam response
*Undrained analysis of earth dam on earthquake
*Undrained vs partially drained analysis of earthquake on dam response
*Evaluation of dam safety

9. Conclusions and recommendations

*Conclusions
*Recommendations

APPENDIX A LIST OF SYMBOLS

APPENDIX B AN INTRODUCTION TO DYNAMIC RELAXATION

APPENDIX C NONLINEAR RESPONSE OF QUALL WALL IN EARTHQUAKE

APPENDIX D COMPUTER IMPLEMENTATION

Fig. 1.2(cont'd)

CHAPTER 2

THE MATHEMATICAL MODEL

2.1 Introduction:

A proper mathematical model must be developed to represent the physical reality of a dam. The model must incorporate the following features:

(1) an adequate structural idealization.
(2) a suitable model for the reservoir water.
(3) a material constitutive law.
(4) suitable boundary conditions.
(5) the selection of the design earthquake.

These items will be discussed in the subsequent sections.

2.2 Structural Idealization:

In the present study, a two-dimensional analysis is carried out in which the plane strain conditions are assumed. The plane strain conditions are justified if the thickness of the dam is large enough in comparison with the vertical and horizontal dimensions of the dam and if the dam is constructed on a fairly uniform foundation. It has been shown [1,2] in static loading conditions that the 2D and 3D solutions give essentially the same results if the above conditions prevail.

In any continuum the actual number of degrees of freedom is infinite and unless a closed form solution is available, an exact solution is impossible. For any numerical approach, an approximate solution is attempted by assuming that the behaviour of the continuum can be represented by a finite number of unknowns.

Therefore, the dam is divided into a series of elements which are connected at a finite number of points known as nodal points. A typical example of an earth dam is shown in Figure 2.1.

2.3 Structural approximation of Fluid:

The water in the reservoir can be treated as a continuum with its own material properties. If a fluid element is employed, the water can be simply considered as an elastic material with zero shear resistance. Thus the standard procedure for evaluating the internal resisting force can be adopted with an appropriate elasticity matrix $\underset{\sim}{D}$. While for an elastic solid any isotropic or anisotropic behaviour can be used, the $\underset{\sim}{D}$ matrix for a fluid is essentially isotropic. The complete set of six three-dimensional stress strain relationship can be presented in terms of the bulk modulus K and the shear modulus G as[3]

$$\begin{pmatrix} \sigma_x \\ \sigma_y \\ \sigma_z \\ \tau_{xy} \\ \tau_{yz} \\ \tau_{zx} \end{pmatrix} = \begin{pmatrix} K+\frac{4}{3}G & K-\frac{2}{3}G & K-\frac{2}{3}G & 0 & 0 & 0 \\ K-\frac{2}{3}G & K+\frac{4}{3}G & K-\frac{2}{3}G & 0 & 0 & 0 \\ K-\frac{2}{3}G & K-\frac{2}{3}G & K+\frac{4}{3}G & 0 & 0 & 0 \\ 0 & 0 & 0 & G & 0 & 0 \\ 0 & 0 & 0 & 0 & G & 0 \\ 0 & 0 & 0 & 0 & 0 & G \end{pmatrix} \begin{pmatrix} \varepsilon_x \\ \varepsilon_y \\ \varepsilon_z \\ \gamma_{xy} \\ \gamma_{yz} \\ \gamma_{zx} \end{pmatrix} \qquad (2.1)$$

For a normal fluid it is now simply necessary to insert an appropriate bulk modulus K and set G = 0 in equation (2.1). Obviously, with G = 0, equation (2.1) will result in zero shear stress. Therefore, in the finite element context, the hydrostatic force as well as the hydrodynamic force induced by an earthquake can be evaluated directly using the fluid element. The displacement time histories at the

crest of the dam shown in Figure 2.1 obtained by (i) including the fluid and (ii) excluding the fluid in the reservoir are presented in Figure 2.2. It should be noted that at the present stage of study, the responses are assumed to correspond with the fully drained condition. This was done simply to focus attention on various computational comparisons. The results show that the effect of external hydrodynamic force is negligible.

2.4 Material Model:

To describe the material model, it is necessary to start from the stress strain relationship defining the constitutive law for soil. Here the concept of yield functions which define the combinations of stress at which the material yields according to the theory of plasticity or viscoplasticity is given. Soil is different from rock or concrete in the sense that although soil can not resist tensile stress, it is able to heal itself after tensile stress has disappeared. Therefore, a simple no-tension cut off model is employed in the present study.

2.4.1 Stresses, Strains and Constitutive Law:

It is well known that a load applied to a saturated soil is carried partly by the pore water and partly by the soil skeleton. If tension is considered as positive then the total stresses can be represented in the following vector form[4,5]

$$\underset{\sim}{\sigma} = \{ \sigma_x, \sigma_y, \sigma_z, \tau_{xy}, \tau_{yz}, \tau_{zx} \}^T \tag{2.2}$$

This total stress can be divided into two parts, i.e. the effective

stresses, $\underset{\sim}{\sigma}'$ and the pore pressure p. Thus

$$\underset{\sim}{\sigma} = \underset{\sim}{\sigma}' + \underset{\sim}{m}\, p \tag{2.3}$$

in which $\underset{\sim}{\sigma}' = \{ \sigma_x' , \sigma_y' , \sigma_z' , \tau_{xy}' \quad \tau_{yz}' , \tau_{zx}' \}^T$

and $\underset{\sim}{m} = \{1, 1, 1, 0, 0, 0 \}^T$

The displacement of the solid skeleton is defined as

$$\underset{\sim}{u} = \{ u, v, w \}^T \tag{2.4}$$

The strain is defined in Langrangian terms to allow for large deformations which may occur during collapse. Thus

$$\underset{\sim}{\varepsilon} = \{\varepsilon_x, \varepsilon_y, \varepsilon_z, \gamma_{xy}, \gamma_{yz}, \gamma_{zx}\}^T \tag{2.5}$$

and assume

$$\underset{\sim}{\varepsilon} = \underset{\sim}{\varepsilon}^I + \underset{\sim}{\varepsilon}^{II} \tag{2.6}$$

in which $\underset{\sim}{\varepsilon}^I$ is the usual linear, infinitesimal strain vector defined as

$$\underset{\sim}{\varepsilon}^I = \begin{Bmatrix} \varepsilon_x \\ \varepsilon_y \\ \varepsilon_z \\ \gamma_{xy} \\ \gamma_{yz} \\ \gamma_{zx} \end{Bmatrix} = \begin{bmatrix} \frac{\partial}{\partial x} & 0 & 0 \\ 0 & \frac{\partial}{\partial y} & 0 \\ 0 & 0 & \frac{\partial}{\partial z} \\ \frac{\partial}{\partial y} & \frac{\partial}{\partial x} & 0 \\ 0 & \frac{\partial}{\partial z} & \frac{\partial}{\partial y} \\ \frac{\partial}{\partial z} & 0 & \frac{\partial}{\partial y} \end{bmatrix} \begin{Bmatrix} u \\ v \\ w \end{Bmatrix} = \underset{\sim}{L}\ \underset{\sim}{u} \tag{2.7}$$

and $\underset{\sim}{\varepsilon}^{II}$ is the nonlinear contribution which can be presented as

$$\underset{\sim}{\varepsilon}^{II} = \frac{1}{2} \begin{bmatrix} \underset{\sim}{\theta}_x^T & 0 & 0 \\ 0 & \underset{\sim}{\theta}_y^T & 0 \\ 0 & 0 & \underset{\sim}{\theta}_z^T \\ \underset{\sim}{\theta}_y^T & \underset{\sim}{\theta}_x^T & 0 \\ 0 & \underset{\sim}{\theta}_z^T & \underset{\sim}{\theta}_y^T \\ \underset{\sim}{\theta}_z^T & 0 & \underset{\sim}{\theta}_x^T \end{bmatrix} \begin{bmatrix} \underset{\sim}{\theta}_x \\ \underset{\sim}{\theta}_y \\ \underset{\sim}{\theta}_z \end{bmatrix} \qquad (2.8)$$

$$\underset{\sim}{\theta}_x = \{ \frac{\partial u}{\partial x}, \frac{\partial u}{\partial x}, \frac{\partial w}{\partial x} \}^T, \quad \underset{\sim}{\theta}_y = \{ \frac{\partial u}{\partial y}, \frac{\partial v}{\partial y}, \frac{\partial w}{\partial y} \}^T$$

$$\underset{\sim}{\theta}_z = \{ \frac{\partial u}{\partial z}, \frac{\partial v}{\partial z}, \frac{\partial w}{\partial z} \}^T$$

It is assumed that the stresses are given as the Piola-Kirchhoff stresses and the strains are as given by equation (2.6) and these can also be expressed in incremental form and assumed to be separable into the following terms:

$$d\underset{\sim}{\varepsilon} = d\underset{\sim}{\varepsilon}^{\sigma'} + d\underset{\sim}{\varepsilon}^{c} + \underset{\sim}{m} \frac{d\varepsilon_v^o}{3} \qquad (2.9)$$

where $d\underset{\sim}{\varepsilon}^{\sigma'}$ is the effective stress dependent strain increment, $d\underset{\sim}{\varepsilon}^{c}$ is the strain increment due to creep and is equivalent to the viscoplastic strain, $d\underset{\sim}{\varepsilon}_{vp}$, which will be discussed later on, while $d\varepsilon_v^o$ is defined here as the autogenous volumetric strain increment to reflect the compaction of the grain configuration due to cyclic loading and will be described in detail in Chapter 5. Thus the constitutive law can be written directly in terms

of effective stresses as

$$d\underset{\sim}{\sigma}' = \{ D_T \} \left(d\underset{\sim}{\varepsilon} - d\underset{\sim}{\varepsilon}^c - \underset{\sim}{m} \frac{d\varepsilon_v^o}{3} \right) \tag{2.10}$$

where $\{ D_T \}$ stands for the tangent constitutive matrix.

If pore pressure changes are assumed to cause no strain in the soil skeleton, (i.e. the grain compressibility is zero) then for the undrained conditions any overall volumetric strain is entirely absorbed by the fluid compressibility. Thus

$$dp = \alpha \, d\varepsilon_v \tag{2.11}$$

where $d\varepsilon_v = \underset{\sim}{m}^T d\varepsilon = d\varepsilon_x + d\varepsilon_y + d\varepsilon_z$ and $\alpha = \frac{K_f}{\eta}$, K_f being the fluid bulk modulus, η being the porosity of the soil.

Relations (2.3) to (2.11) give a complete description of the undrained soil behaviour provided that appropriate constitutive tangent matrix, creep relations and increments of autogenous volumetric strain can be determined . Thus the complete effective stress can be written as

$$^{t+\Delta t}\underset{\sim}{\sigma}' = {}^t\underset{\sim}{\sigma}' + \{D_T\} \left(d\underset{\sim}{\varepsilon} - d\underset{\sim}{\varepsilon}^c - \underset{\sim}{m} \frac{d\varepsilon_v^o}{3} \right) \tag{2.12}$$

in which superscripts t, t + Δt represent times t and t + Δt. Similarly the total pore water pressure at t + Δt is given as

$$^{t+\Delta t}p = {}^t p + \alpha d\varepsilon_v \tag{2.13}$$

At some initial time t = 0, ${}^o\sigma' = \sigma'_o$, ${}^oP = P_o$ are taken and while σ'_o and P_o are the initial effective stress and initial pore water pressure determined prior to the earthquake.

It is of interest to note that for drained conditions the pore water pressure remains unchanged, i.e.

$$t + \Delta t_p = {}^{o}p \tag{2.14}$$

Upon substitution of equations (2.12), (2.13) and (2.14) into equation (2.3), the following expression is obtained

$$t+\Delta t\underset{\sim}{\sigma} = \{D_T\}\,{}^{t+\Delta t}\underset{\sim}{\varepsilon} - \{D_T\}\left({}^{t+\Delta t}d\underset{\sim}{\varepsilon}^{c} + \underset{\sim}{m}\frac{d\underset{\sim}{\varepsilon}^{o}_{v}}{3}\right) + {}^{t}\underset{\sim}{\sigma}' + \underset{\sim}{m}\,{}^{t}p \tag{2.15}$$

in which $\{\bar{D}_T\} = \{D_T\} + \{D_u\}$ for the undrained conditions

$\{\bar{D}_T\} = \{D_T\}$ for the drained conditions

While D_u represents the stiffness matrix of the pore water and can be expressed as

$$\{D_u\} = \underset{\sim}{m}\,\alpha\,\underset{\sim}{m}^{T} = \alpha\begin{bmatrix} I_3 & 0_3 \\ 0_3 & 0_3 \end{bmatrix}$$

in which I_3 is a 3 x 3 matrix, all elements of which are unity, and 0_3 are 3 x 3 null matrices.

It is of interest to investigate what happens when no change of total stress occurs and $d\underset{\sim}{\varepsilon}^{c} = 0$ but $d\underset{\sim}{\varepsilon}^{o}_{v} \neq 0$. We now have from equation (2.3)

$$d\underset{\sim}{\sigma}' = -\underset{\sim}{m}\,dp \tag{2.16}$$

Equation (2.10) can be rewritten as

$$d\underset{\sim}{\varepsilon} - m\frac{d\varepsilon^{o}_{v}}{3} = \{C_T\}\,d\underset{\sim}{\sigma}' \tag{2.17}$$

in which $\{C_T\} = \{D_T\}^{-1}$. Multipying the above equation by $\underset{\sim}{m}^{T}$ and

inserting into equation (2.16) leads to

$$d\varepsilon_v - d\varepsilon_v^o = - \underset{\sim}{m}^T \{C_T\} \underset{\sim}{m} \, d\, p \tag{2.18}$$

We note that

$$\underset{\sim}{m}^T \{C_T\} \underset{\sim}{m} = \frac{1}{K_T} \tag{2.19}$$

in which K_T is the bulk tangential modulus relating the change of volumetric strain $d\varepsilon_v$ to the change of mean effective stress, $d\sigma_m' = \frac{1}{3}(d\sigma_x' + d\sigma_y' + d\sigma_z')$ and can be represented as

$$K^T = \frac{d\sigma_m'}{d\varepsilon_v} = \frac{E_T}{3(1-2\nu)} \tag{2.20}$$

where E_T and ν are tangent modulus and Poisson's ratio of the material respectively.

Inserting equation (2.11) into (2.18) yields

$$\frac{n}{K_f} d\, p - d\varepsilon_v^o = - \frac{1}{K_T} d\, p \tag{2.21}$$

Rearranging, finally yields

$$d\, p = \beta d\varepsilon_v^o \tag{2.22}$$

where

$$\beta = \frac{1}{n/K_f + 1/K_T} \tag{2.23}$$

Normally, the compressibility of pore water is much higher than that of soil skeleton, i.e. $K_f \gg K_T$, and porosity is small, then

equation (2.23) can be simply expressed as

$$\beta = K_T \tag{2.24}$$

in which K_T is also known as the "rebound modulus" of soil.

2.4.2 Plasticity:

When an increment of stress is applied to a material, two types of strain may occur; one is elastic or reversible strain and the other is plastic or irreversible strain. The basic nature of plastic strain was first suggested by Saint Venant (Hill, 1950)[6], who proposed that the principal axes of the increments of plastic strain should coincide with the principal axes of stress and not of stress increment. This behaviour contrasts sharply with the behaviour of elastic materials, in which the principal axes of the increments of strain coincide with the principal axes of stress increment and not of stress. Thus, the basic nature of plastic strain is quite different from that of elastic strain.

Based on experimental evidence[7], the soil behaves approximately as an elastic material at low stress levels and approximately as a plastic material at high stress levels. Therefore an accurate model for the stress strain behaviour of the soil should take into account the plastic nature of the strain at high stress levels.

In the elastoplastic analysis, the total strain increments $\underset{\sim}{\varepsilon}^{\sigma'}$ due to incremental stress can be postulated as the sum of an elastic component $\underset{\sim}{\varepsilon}_E$ and a plastic component $\underset{\sim}{\varepsilon}_p$, thus

$$\underset{\sim}{\varepsilon}^{\sigma'} = \underset{\sim}{\varepsilon}_E + \underset{\sim}{\varepsilon}_p \tag{2.25}$$

These strains can be obtained separately, the elastic strain is obtained using an elastic constitutive law while the plastic strain is calculated using a plastic constitutive law. The plastic strain is only mobilized when the stress exceeds some state at which yield starts, which is defined by a yield function F as follows

$$F(\sigma', \kappa) = 0 \tag{2.26}$$

in which κ is a hardening or softening parameter. This yield condition can be visualized as a surface in n-dimensional stress space with the position of the surface dependent on the instantaneous value of the parameter κ.

To define a complete strain rate law in an explicit form, it is necessary to introduce the concept of a plastic potential Q (e.g. Hill 1950).[6]

$$Q = Q(\sigma') \tag{2.27}$$

the derivatives of which define the directions of the straining. If $d\underset{\sim}{\varepsilon}_p$ denotes the increment of plastic strain then

$$d\underset{\sim}{\varepsilon}_p = \lambda \frac{\partial Q}{\partial \sigma'} \tag{2.28}$$

in which λ is a proportionality constant, as yet undetermined. The rule is known as the normality principle because equation (2.28) can be intepreted as requiring the normality of the plastic strain increment vector to the plastic potential surface in the space of n stress dimensions.

The particular case when Q = F is known as associative plasticity; when this relation is not satisfied the plasticity

is nonassociated. In equation (2.25), the elastic strain increments are related to stress increments by a symmetric elasticity matrix of constant $\underset{\sim}{D}$ as usual. Now equation (2.25) can be rewritten, in view of equation (2.28) as

$$d\underset{\sim}{\varepsilon}^{\sigma'} = \{D\}^{-1} d\sigma' + \lambda \frac{\partial Q}{\partial \underset{\sim}{\sigma}'} \tag{2.29}$$

When plastic yield occurs the stresses are on the yield surface as given by equation (2.26) which after differentiation gives

$$dF = \frac{\partial F}{\partial \sigma_1'} d\sigma_1' + \frac{\partial F}{\partial \sigma_2'} d\sigma_2' + \ldots + \frac{\partial F}{\partial \kappa} d\kappa = 0$$

or

$$\left(\frac{\partial F}{\partial \sigma'}\right)^T d\sigma' - A\lambda = 0 \tag{2.30}$$

in which

$$A = -\frac{1}{\lambda} \frac{\partial F}{\partial \kappa} d\kappa.$$

Equations (2.29) and (2.30) can be written in a simple matrix as

$$\begin{bmatrix} d\underset{\sim}{\varepsilon}^{\sigma'} \\ 0 \end{bmatrix} = \begin{bmatrix} \{D\}^{-1} & \frac{\partial Q}{\partial \underset{\sim}{\sigma}'} \\ \left(\frac{\partial F}{\partial \sigma'}\right)^T & -A \end{bmatrix} \begin{bmatrix} d\underset{\sim}{\sigma}' \\ \lambda \end{bmatrix} \tag{2.31}$$

The indeterminate constant λ can be eliminated. This results in an explicit expression which determines the stress changes in terms of imposed strain changes with

$$d\underset{\sim}{\sigma}' = \{D_{EP}\}\, d\underset{\sim}{\varepsilon} \tag{2.32}$$

where

$$\{D_{EP}\} = \{D\} - \{D\} \left\{\frac{\partial Q}{\partial \underset{\sim}{\sigma}'}\right\} \left\{\frac{\partial F}{\partial \underset{\sim}{\sigma}'}\right\}^T \{D\} \left(A + \left\{\frac{\partial F}{\partial \underset{\sim}{\sigma}'}\right\}^T \{D\} \left\{\frac{\partial Q}{\partial \underset{\sim}{\sigma}'}\right\}\right)^{-1}$$

Thus the elastoplastic matrix $\{D_{EP}\}$ takes the place of the elasticity matrix $\{D_T\}$ in incremental analysis.

Various yield functions and plastic potentials can be incorporated in the formulation depending on the nature of the materials used. The most commonly used expressions for soils are those of Mohr-Coulomb or a simplified form given by Drucker and Prager[8]. In such expressions the failure condition of soil is equated with yield. Details are described by Nayak and Zienkiewicz[9,10].

For Mohr-Coulomb,

$$F = \sigma'_m \sin\phi + \left(\cos\alpha - \frac{\sin\alpha \sin\phi}{\sqrt{3}}\right)\bar{\sigma}' - C\cos\phi \tag{2.33}$$

For Drucker-Prager

$$F = \frac{3 \sin\phi}{(3+\sin^2\phi)^{\frac{1}{2}}}\sigma'_m \quad \bar{\sigma}' - \frac{3 C \cos\phi}{(3+\sin^2\phi)^{\frac{1}{2}}} \tag{2.34}$$

where C, ϕ are respectively the cohesion and angle of internal friction of the material and,

$$\sigma'_m = \frac{J_1}{3} = \frac{1}{3}\left(\sigma'_x + \sigma'_y + \sigma'_z\right)$$

$$\bar{\sigma}' = J_2^{\frac{1}{2}} = \tfrac{1}{2}\left(s'^2_x + s'^2_y + s'^2_z\right) + \tau'^2_{xy} + \tau'^2_{yz} + \tau'^2_{zx}\Big)^{\frac{1}{2}}$$

$$\alpha = \frac{1}{3}\sin^{-1}\left(-\frac{3\sqrt{3}}{2}\frac{J_3}{\bar{\sigma}^3}\right) \text{ with } -\frac{\pi}{6} < \alpha < \frac{\pi}{6}$$

in which

$$J_3 = s'_x s'_y s'_z + 2\tau'_{xy}\tau'_{yz}\tau'_{zx} - s'_x\tau'^2_{yz} - s'_y\tau'^2_{zx} - s'_z\tau'^2_{xy}$$

and

$$s'_x = \sigma'_x - \sigma'_m, \quad s'_y = \sigma'_y - \sigma'_m, \quad s'_z = \sigma'_z - \sigma'_m$$

It is well known that Tresca and Von Mises yield surfaces can be readily obtained by simply setting $\phi = 0$ in equations (2.33) and (2.34) respectively. Various yield surfaces are as shown in Figure 2.3.

Critical state yield surfaces: Roscoe, Schofield and Wroth[11] proposed a model which successfully distinguished between yielding and ultimate collapse by introducing the concept of a "critical state line" in conjunction with a strain dependent yield surface. They suggested that an element of soil undergoing shear deformation could pass through a yield point without collapse and continue to deform until eventually a critical state was reached at which point the soil could continue to deform without further change of voids ratio or stress. When projected onto the axes of the first two stress invariants, the critical state line was represented by the equation

$$\sqrt{3}\,\bar{\sigma}' = -M_{cs}\,\sigma'_m \qquad (2.35)$$

In a later paper Roscoe and Burland showed that an elliptical shape for the strain dependent yield surface, which became known as the Modified Cam clay model, fitted experimental data satisfactorily. The original theory was developed for triaxial stress conditions but was also extended to cover the case of plane strain. The material parameters for the plane strain case can be determined from triaxial tests.

An elliptical yield surface of this type is shown in Figure 2.4 and it can be seen that it is a function of the first two stress

invariants. It has a constant shape that is a circle of revolution around the σ_m' axis. The ellipse passes through the origin and is centred on the point $\sigma_m' = -P_o$, $\sqrt{3}\bar{\sigma}' = 0$, P_o being equal to half the preconsolidation pressure. In terms of the parameters σ_m', $\bar{\sigma}'$, P_o and M_{cs}, the equation representing the elliptical yield surface can be written as

$$\frac{(\sigma_m' + P_o)^2}{P_o^2} + \frac{3\bar{\sigma}'^2}{(M_{cs}P_o)^2} = 1 \qquad (2.36)$$

which can be rearranged to give

$$F = 3\bar{\sigma}'^2 + M_{cs}^2(\sigma_m'^2 + 2\sigma_m' P_o) = 0 \qquad (2.37)$$

This yield surface has been implemented in the computer program. In order to show the effect of various yield surfaces on dynamic response, an earth dam and foundation subjected to the N-S component of El Centro May 1940 earthquake has been studied and the results are presented in Figure 2.5. The results shown in Figure 2.5 can be improved if the critical state line coincide with the Mohr Coulomb surface. This has the effect of making the gradient of the critical state line a function of the third stress invariant. The detail can be seen in Ref.[12,13].

2.4.3 Viscoplasticity:

The stress strain relationship of soil can be time dependent and the proper rate effects need to be considered. For this reason, the viscoplastic model is also employed in the present study but for which the appropriate physical constants are assumed values as experimental evidence is lacking.

In the analysis of elasto/viscoplastic material behaviour, the total incremental strain can be postulated as the sum of an elastic strain and viscoplastic strain, i.e.[12-17] ,

$$\underset{\sim}{\varepsilon} = \underset{\sim}{\varepsilon}_E + \underset{\sim}{\varepsilon}_{vp} \tag{2.38}$$

where the instantaneous response is elastic and the viscoplastic component is considered to be a delayed effect and includes both the viscous and plastic effects lumped together. The delayed viscoplastic strain can be treated in the same manner as prescribed initial strain. The viscoplastic flow rule imples that viscoplastic strain rates occur only when the state of stress exceeds a certain threshold static yield surface.

In associative form, the flow rule is given by

$$\dot{\underset{\sim}{\varepsilon}}_{vp} = \gamma < \phi\,(F) > \frac{\partial F}{\partial \underset{\sim}{\sigma}}, \tag{2.39}$$

where γ is a material fluidity parameter, F is a scaler yield function as given in the previous section and the notation $< >$ imples that

$$< \phi\,(F) > = \begin{cases} \phi\,(F) & \text{when } \phi\,(F) > 0 \\ 0 & \text{when } \phi\,(F) \leq 0 \end{cases} \tag{2.40}$$

It may be noted that the viscoplastic strain rate exists only when $\phi\,(F)$ exceeds zero and depends on the amount by which the static yield surface is exceeded. The choice of function $\phi(F)$ must be in accordance with the rate dependent properties of the materials considered. Perzyna[18] has discussed the use of various functions for $\phi(F)$ and

proposed amongst others the following types

(1) linear law $\quad \phi(F) = F/F_o$

(2) power law $\quad \phi(F) = (F/F_o)^n$

(3) exponential law $\quad \phi(F) = \exp(F/F_o) - 1$

where F_o denotes any reference value of F to render the function $\phi(F)$ nondimensional and to so enable the same constant γ to be used for any function $\phi(F)$.

While $F > 0$ constitutes an inadmissible state in the theory of invicid plasticity, the plastic state being identified by $F = 0$, it is admissible in viscoplasticity and causes viscoplastic deformations to take place.

For nonassociative flow rule $\frac{\partial Q}{\partial {}^t\sigma'}$ replaces $\frac{\partial F}{\partial {}^t\sigma'}$ in equation (2.39) where Q is a separate plastic potential as described in the previous section.

Various yield functions and plastic potentials given in the previous section can equally be applied to the elasto/viscoplastic model.

Using the viscoplastic strain rate given by equation (2.39) the total viscoplastic strain at time $t + \Delta t$ can be obtained as

$$ {}^{t+\Delta t}\underset{\sim}{\varepsilon}_{vp} = {}^t\underset{\sim}{\varepsilon}_{vp} + \int_t^{t+\Delta t} {}^{\tau}\dot{\underset{\sim}{\varepsilon}}_{vp}\, d\tau \qquad (2.41) $$

If an assumption of constant viscoplastic strain rate during each time step is made, then the second term of the right hand side in equation (2.41) can be written explicitly as $\dot{\underset{\sim}{\varepsilon}}_{vp}\Delta t$.

It is worthwhile noting that the static computations with the elasto/viscoplastic model and an explicit scheme described above are conditionally stable, i.e., they are unstable if a time step exceeding a critical value is used. Numerical stability in the quasi-static viscoplastic computation has been derived by Cormeau[19,20]. For an associative Mohr-Coulomb yield criterion, the critical time step length is given by the expression

$$\Delta t_{m-c} \leq \frac{4(1+\nu)\ (1-2\nu)\ C\ \cos\phi}{\gamma\ E\ (1-2\nu\ +\ \sin^2\phi\ )} \tag{2.42}$$

The elastoplastic solution can be obtained from the elasto/viscoplastic algorithm as a limiting case in which $\gamma \to \infty$ or at $t \to \infty$. However the time step length requirement of equation (2.42) will become critical as γ increases. If the critical time step length is selected a priori from the stability requirement of dynamic computation, with this critical time step length, Δt_D, the largest value of γ which can be used is given as

$$(\gamma \Delta t_D)_{crit} = \beta_1 \frac{4(1+\nu)(1-2\nu)\ C\ \cos\phi}{E\ (1-2\nu + \sin^2\phi)} \tag{2.43}$$

The reduction factor β_1 is a loading type dependent factor and is usually less than unity. For a uniform dynamic load as shown in Figure 2.6, a value of $\beta_1 = 1$ was found to give a reasonably good approximation of the elastoplastic response using the elasto/viscoplastic model.

The elastic solution can easily be obtained from the elasto/viscoplastic solution by simply putting $\gamma = 0$. The response obtained with various values of γ are presented in Figure 2.6.

In order to illustrate the behaviour of the elastoplastic model and the elasto/viscoplastic model, an earth dam with the dimensions and material properties shown in Figure 2.7 is subjected to the base accelerations of the first 10 seconds of the N-S component of 1940 El Centro earthquake. The results of this study are presented in terms of the time history of displacements as well as stresses. Figures 2.8 and 2.9 show respectively the displacement time history of the dam crest and the shear stress time history at the Gauss point marked by x. Figure 2.10 shows the displacement contours with the principal stress distributions every second through the passage of the earthquake. It can be seen from both Figures 2.8 and 2.9 that the elastic solution leads to cyclic response and the highest shear stress while the plastic solution yields permanent deformation and the lowest shear stress, and the elasto/viscoplastic solution with $\gamma\Delta t = 0.5(\gamma\Delta t_D)_{crit}$ lies in between elastic and plastic responses.

2.4.4 No Tension Model:

In general, the soil does not take any tensile stress. This condition can be met if a proper cut off yield surface has been carried out. A detailed description of the no tension model for the Mohr-Coulomb yield surface which is most commonly used in soil mechanics is given below.

The Mohr-Coulomb yield surface as given in equation (2.33) is recalled as follows

$$F = \sigma'_m \sin\phi + \frac{\bar{\sigma}'}{\sqrt{3}} (\sqrt{3}\cos\alpha - \sin\alpha\sin\phi) - \bar{c}\cos\phi \qquad (2.44)$$

It can be shown that the no tension yield surface is available by setting $\phi = \frac{\pi}{2}$ in equation (2.44). Therefore, the no tension cut off yield surface can be represented as

$$F_{NT} = \sigma'_m + \frac{\bar{\sigma}'}{\sqrt{3}} (\sqrt{3} \text{ Cos } \alpha - \text{ Sin } \alpha) \tag{2.45}$$

This yield surface can be represented in $\sigma'_m - \frac{\bar{\sigma}'}{\sqrt{3}}$ plane as shown in Figure 2.11 in which the co-ordinates of corner $B(\sigma'_m, \frac{\bar{\sigma}'}{\sqrt{3}})$ can be obtained by using equations (2.44) and (2.45) and are given as follows

$$B\ (\sigma'_m, \frac{\bar{\sigma}'}{\sqrt{3}}) = B\ (-\ C\ \text{Cos}\phi\ \frac{1 - \frac{1}{\sqrt{3}} \tan\phi}{1 - \text{Sin } \alpha},\ \frac{C\ \text{Cos}\phi}{\sqrt{3}\ \text{Cos}\ \alpha\ (1 - \text{Sin}\ \phi)}) \tag{2.46}$$

2.5 The Treatment of Singularity of Yield Surfaces:

It is observed that the Mohr-Coulomb type yield surface or no tension cut off model is inherent singularity at the corners. In order to preclude any singularity at the corners, the yield surfaces must have a smooth transition around the corners. This can be simply achieved by taking the mean values of yield functions at the left hand side and the right hand side, i.e.

$$F_{cor} = \frac{1}{2} (F_l + F_r) \tag{2.47}$$

or by choosing a smooth function such as shown in Figure 2.10, at corner B,

$$F_{cor} = \left[(\sigma'_m - \frac{\bar{\sigma}'}{\sqrt{3}} \text{Sin}\alpha + \sigma' \text{Cos}\alpha - \sigma'_{1\ cor})^2 + (\sigma'_m - \frac{\bar{\sigma}'}{\sqrt{3}} \text{Sin}\alpha - \sigma' \text{Cos}\alpha - \sigma'_{2\ cor})^2 \right]^{\frac{1}{2}} \tag{2.48}$$

and at corner A ($\sigma'_{1\ cor} = \sigma'_{2\ cor} = 0$)

$$F_{cor} = \left(2\{ (\sigma'_m + \bar{\sigma}'\cos\alpha)^2 + \frac{\bar{\sigma}'^2}{3} \sin^2\alpha \} \right)^{\frac{1}{2}} \qquad (2.49)$$

A similar procedure can be applied to the plastic potential functions.

2.6 The Extent of Foundation Length included in Structural Model:

For the seismic response analysis of earth dams, the proper choice of the foundation dimensions is crucial. The error introduced by the fictitious boundary is that the seismic excitation induced waves in the foundation are reflected back towards the structure rather than being allowed to propagate outwards indefinitely. If a large enough foundation block is adopted, the waves reflected from the boundary will not significantly influence the response of the structure. However, if the foundation block is extended to an unnecessary length, the computing time as well as the cost of analysis will increase drastically. A study of the effect of different extents of foundation length on the response of the structure has been carried out and the results are shown in Figure 2.12. It can be seen that extending the foundation block in both upstream and downstream directions by a length identical to the base length of the dam effectively nullified the influence of reflected waves.

It has been shown[21] that if the foundation is much stiffer than the dam, there will be no interference of response between the dam and the foundation. Thus in the proper model in this case, it can simply be assumed that the dam is fixed along its base.

2.7 Modelling of Boundary:

If the structure-foundation-fluid interaction is to be taken into consideration, then the proper modelling of boundaries is of practical importance. For an earthquake type of loading and for a sufficiently long extent of boundaries, it is common practice to treat the boundaries along both ends of the foundation as only permitting free movement in a horizontal direction.

2.8 Selection of Design Earthquake:

To investigate the behaviour of dams in earthquakes, it is necessary first to establish the ground motion characteristics of the design earthquakes and the maximum probably earthquake at the proposed damsite[22-26]. This can be achieved by studying the available earthquake history of the region. As a result of the seismological study, the design earthquake and the maximum possible earthquake in terms of their magnitude and distance from the damsite can be defined. Of course, the magnitude of the design earthquake and its distance from the damsite do not directly indicate the ground motion which a dam should resist. In order to fulfill the design requirements, it is necessary to relate these basic seismological parameters to the intensity and other characteristics of the accelerations expected at the damsite. One of the simplest ways of defining the expected ground motions is to make use of the accelerogram of a past earthquake which had a comparable magnitude and was recorded at an appropriate distance. However, it is not sufficient to represent the response of the dam by the use of a single record only. This can be compensated for by modifying and distorting an

actual earthquake record so that it represents an event of different magnitudes and distances. For instance, the intensity of motion may be adjusted by means of a single amplitude scaling factor, the frequency content may be modified by a change of time scale, and the duration of the earthquake may be changed by truncating or duplicating portions of the record. However, because all significant earthquake motions are generated by processes that are essentially random, the characteristics of the ground motions associated with a particular magnitude and distance can vary widely from one event to the next. Therefore, it is becoming common practice to derive artificial earthquake records which represent the desired design earthquake[24,26]. The present study is based on the recorded El Centro May 1940 earthquake. Three components of this accelerogram, i.e., N-S, E-W and vertical components, are shown in Figure 2.13.

REFERENCES

1. EISENSTEIN, Z., KRISHNEYYE and MORGENSTERN, N.R.,
'An Analysis of Cracking in Earth Dams'
Symposium on Application of Finite Element Methods in Geotechnical Engineering, Vickslung, Mississippi (1972)

2. SIMMONS, J.B.
'Three Dimensional Analysis of Mica Dam'
M.Sc. Thesis, University of Alberta, Edmonton, Canada (1974)

3. FUNG, Y.C.
'Foundation of Solid Mechanics'
Prentice Hall Ins., (1965)

4. ZIENKIEWICZ, O.C.
'The Finite Element Method'
McGraw-Hill, London (1977)

5. LAMBE, T.W. and WHITMAN, R.V.
'Soil Mechanics'
John Wiley and Sons Inc., (1969)

6. HILL, R.
'The Mathematical Theory of Plasticity'
Oxford, Clarendon Press (1950)

7. SCHOFIELD, A.N. and WORTH, C.P.
'Critical State Soil Mechanics'
McGraw-Hill, London (1968)

8. DRUCKER, D.C. and PRAGER, W.
'Soil Mechanics and Plastic Analysis on Limit Design'
Q. Appl. Mathematics, 10, 157-165 (1952)

9. NAYAK, G.C. and ZIENKIEWICZ, O.C.
'Elastoplastic Stress Analysis'
A Generalization for Various Constitutive Relations Including Strain Softening
Int. Journal Num. Meth. Engng., 5, 113-135 (1972)

10. NAYAK, G.C. and ZIENKIEWICZ, O.C.
'Convenient Form of Stress Invariants for Plasticity'
Proceedings Am. Soc. Civ. Engrs., 98, ST4, 949-954 (1972)

11. ROSCOE, K.H., SCHOFIELD, A.N. and WROTH, C.P.
'On the Yielding of Soils'
Geotechnique, 8, 22-53 (1958)

12. HUMPHESON, C.
'Finite Element Analysis of Elasto-viscoplastic Soils'
Ph.D. Thesis, University of Wales, Swansea (1976)

13. ZIENKIEWICZ, O.C., NORRIS, V.A., WINNICKI, L.A., NAYLOR, D.J. and LEWIS, R.W.
'A unified approach to the Soil Mechanics Problems of Offshore Foundations'
Numerical Methods in Offshore Engineering, Ed. by ZIENKIEWICZ, O.C., LEWIS, R.W. and STAGG, K.G.
John Wiley & Sons (1978)

14. NAYLOR, D.J.
'Nonlinear Finite Element Models for Soils'
Ph.D. Thesis, University of Wales, Swansea (1975)

15. ZIENKIEWICZ, O.C.
'Visco-plasticity, Creep and Visco-plastic flow'
Lecture Presented at Int. Conf. on Computation Method
in Nonlinear Mechanics
University of Texas, Austin, Texas (1974)

16. ZIENKIEWICZ, O.C. and CORMEAU, I.C.
'Visco-plasticity Solution by the Finite Element Process,
Arch. Mech., 24, 873-888 (1972)

17. ZIENKIEWICZ, O.C. and CORMEAU, I.C.
'Viscoplasticity-plasticity and Creep in Elastic Solids.
A unified Numerical Solution Approach,
Int. Jnl. Num. Meth. Engng. 8, 821-845 (1974)

18. PERZYNA
'Fundamental Problems in Viscoplasticity'
Adv. Appl. Mech. 9, 243-377 (1966)

19. CORMEAU, I.C.
'Numerical Stability in Quasi-Static Elasto-Viscoplasticity'
Int. Jnl. Num. Meth. Engng. 9, 109-127 (1975)

20. CORMEAU, I.C.
'Viscoplasticity and Plasticity in the Finite Element Method'
Ph.D. Thesis, University of Wales, Swansea (1976)

21. IDRISS, I.M., MATHUR, J.M. and SEED, H.B.
'Earth Dam-Foundation Interaction During Earthquakes'
Int. Jnl. of Earthquake Engineering and Structural Dynamics,
Vol. 2, 313-323 (1974)

22. WIEGEL, R.L.
'Earthquake Engineering'
Prentice-Hall (1970)

23. BOGGS, H.L., et al
'Method of Estimating Design Earthquake Rock Motions'
United States Department of the Interior, Bureau of Reclamation,
Engineering and Research Center, Denver, Colorado (1972)

24. HOUSNER, G.W. and JENNINGS, P.C.
'Generation of Artificial Earthquakes'
Jnl. Eng. Mech. Division, ASCE, Vol. 90, EM1, 113-150 (1964)

25. HOUSNER, G.W.
'Spectrum Intensities of Strong Motion Earthquakes'
Proceedings of Symposium on Earthquakes and Blast Effects on
Structures, Los Angeles, California (1952)

26. JENNKINGS, P.C., HOUSNER, G.W. and TSAI, N.C.
'Simulated Earthquake Motions'
Report of Earthquake Engineering Research Lab., California
Institute of Technology (1968)

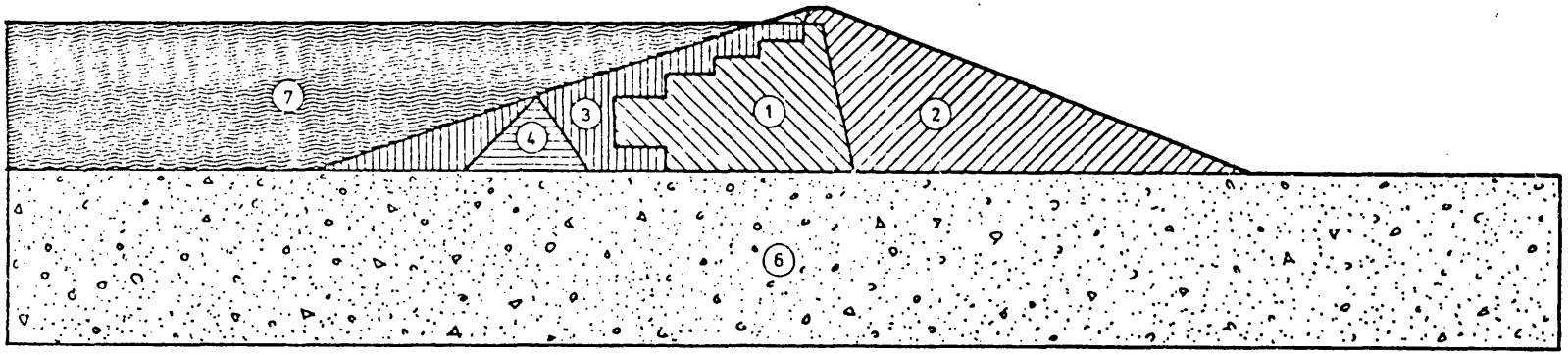

(1)

Material zone	E MN/m²	ν	φ degree	C KN/m²	Unit weight Kg/m³
1	100	0.45	33	10	2260
2	100	0.40	33	10	2260
3	230	0.45	38	80	2400
4	100	0.45	33	10	2160
5	230	0.45	38	80	2400
6	10,000	0.20			2650
7	2250*	0.50	-	-	1000

*Bulk mod.

(3)

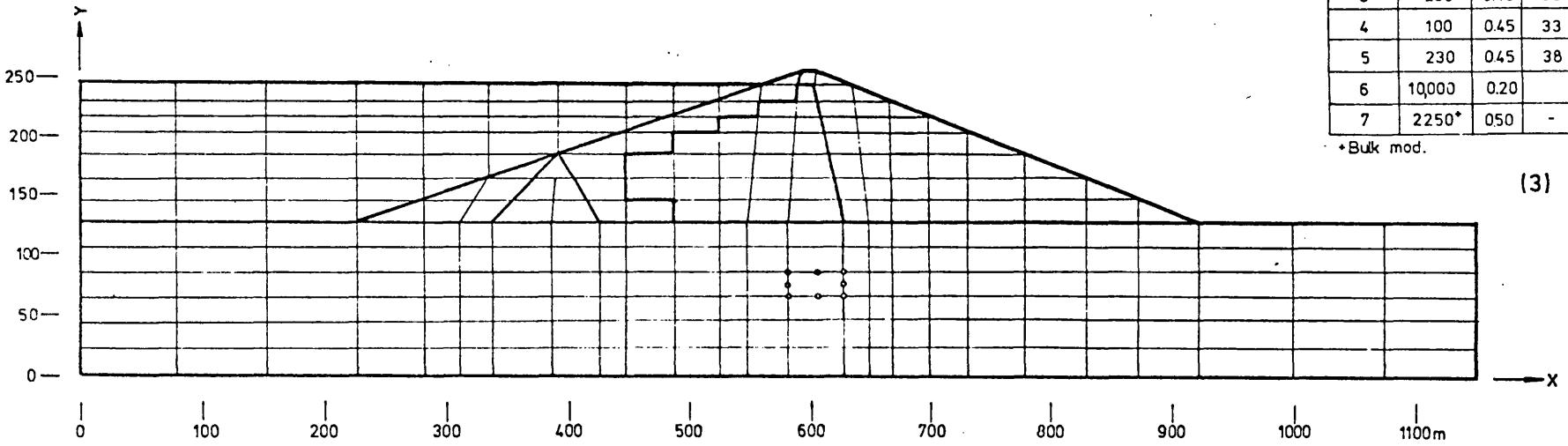

(2)

Fig. 2.1 A typical earth dam and its foundation.

(1) Material Zones (2) Finite Element Mesh (3) Material Properties

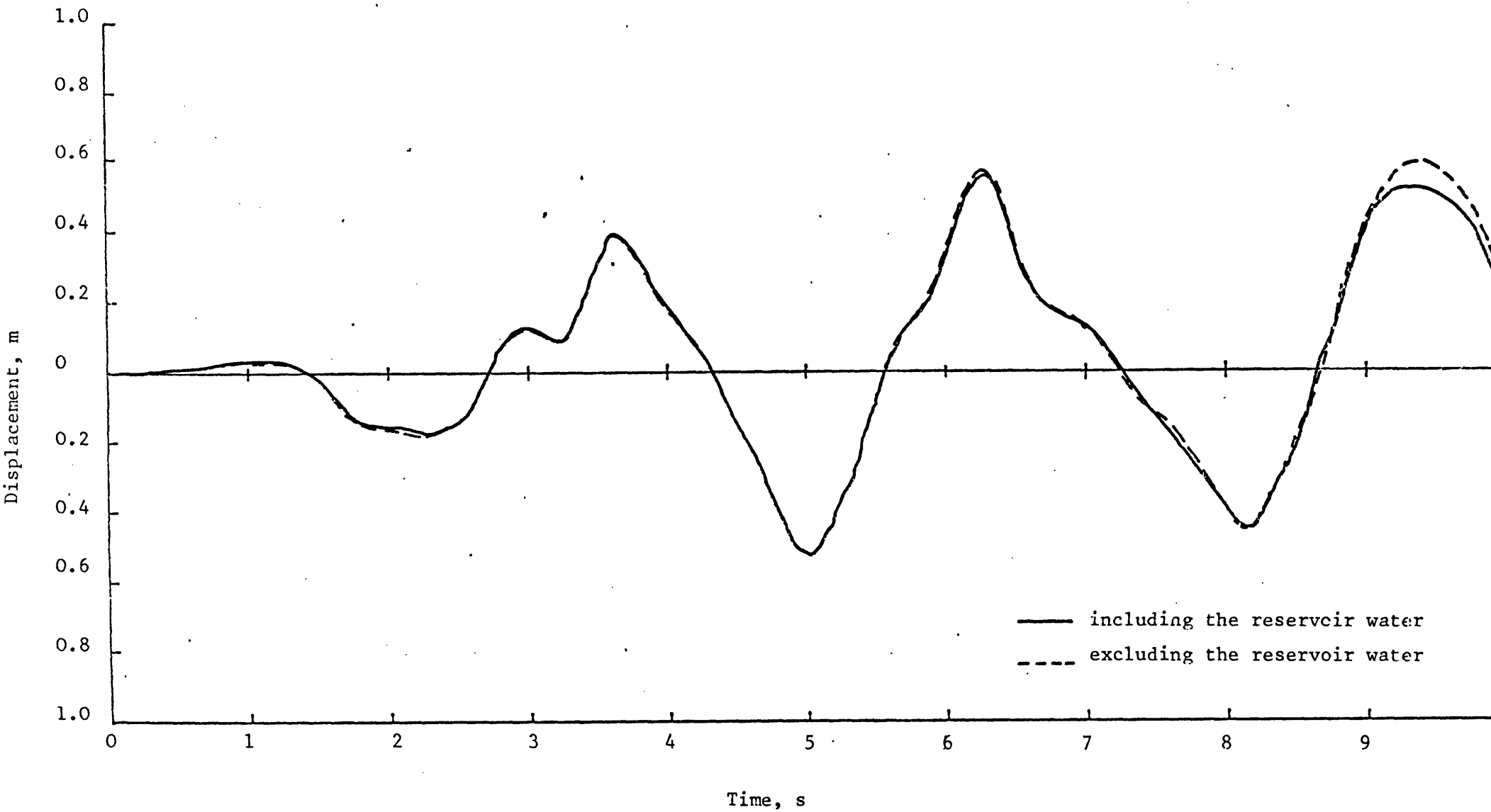

Fig. 2.2 Horizontal displacement time history at dam crest with including and excluding of the reservoir water (drained conditions).

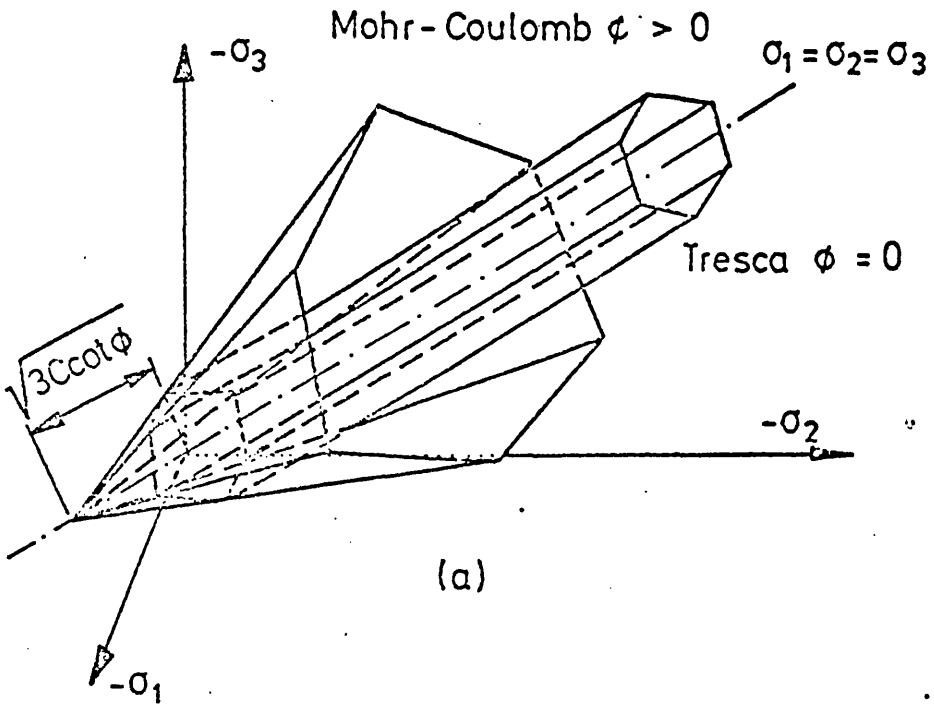

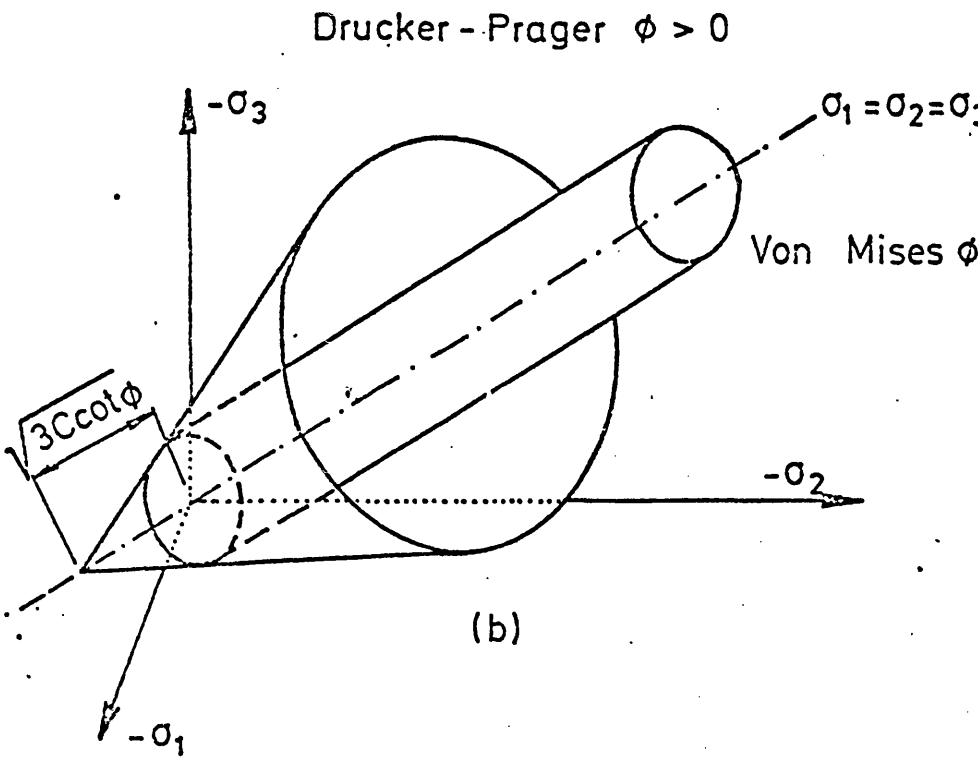

FIGURE 2.3 YIELD SURFACES

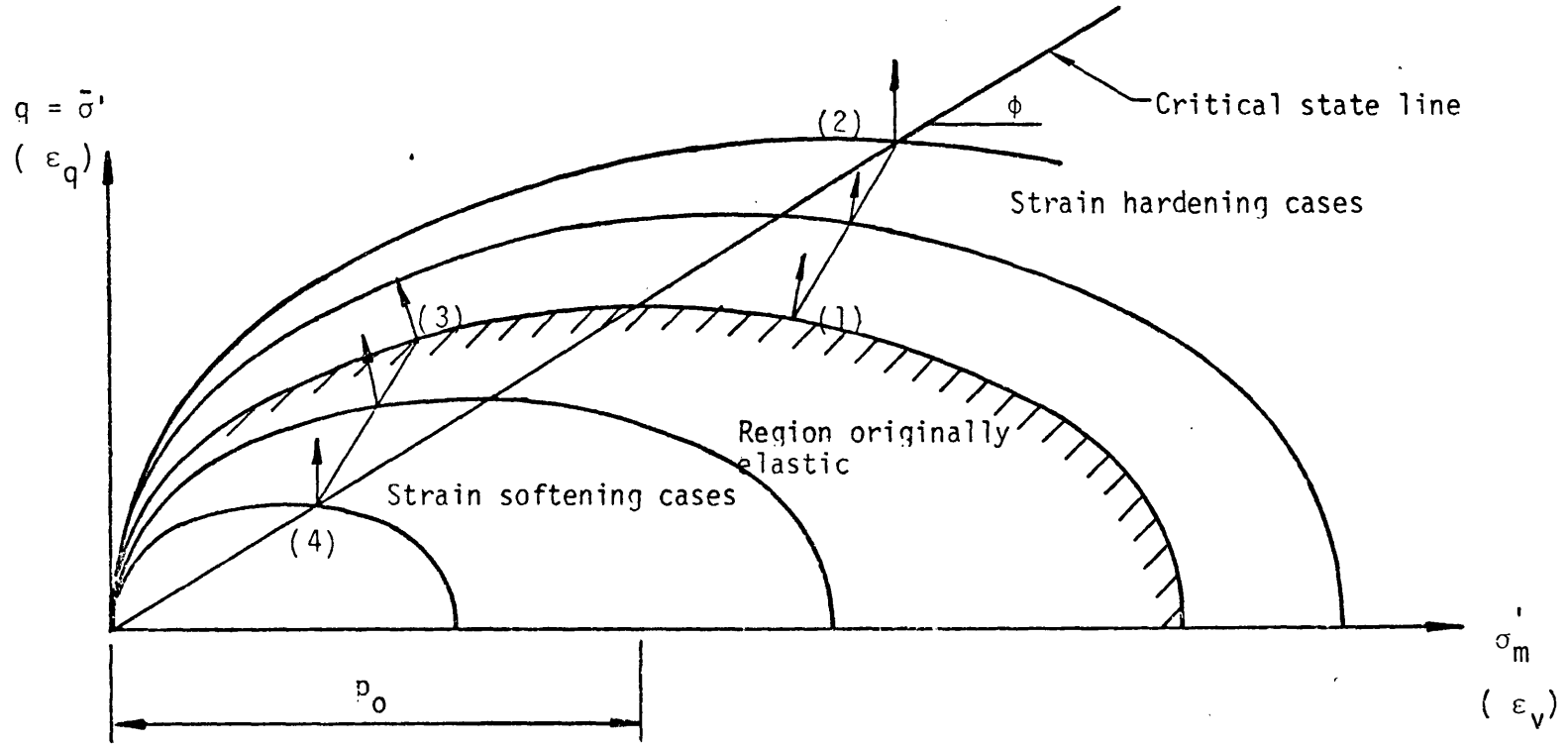

FIGURE 2.4 (1) GRAPHICAL REPRESENTATION OF YIELD SURFACES IN SPACE OF THE TWO STRESS INVARIANTS σ'_m , $\bar{\sigma}'$

(2) STRAIN HARDENING BEHAVIOUR

(3) STRAIN SOFTENING BEHAVIOUR

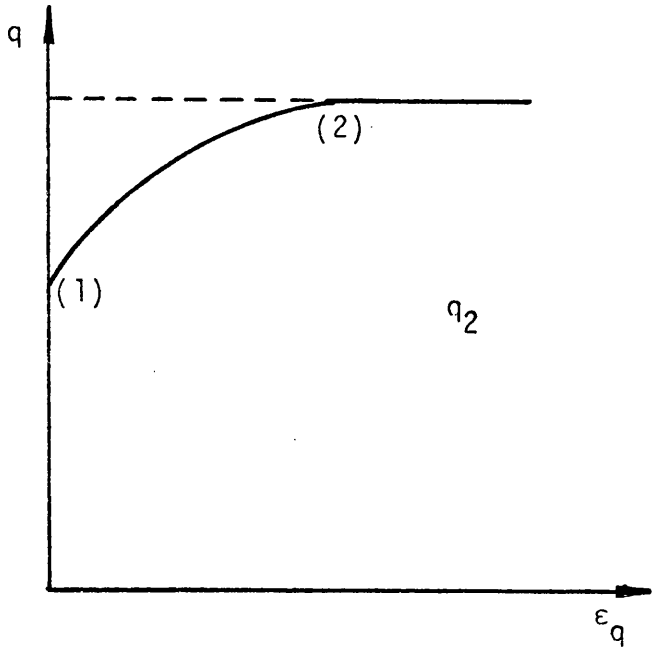

(2)

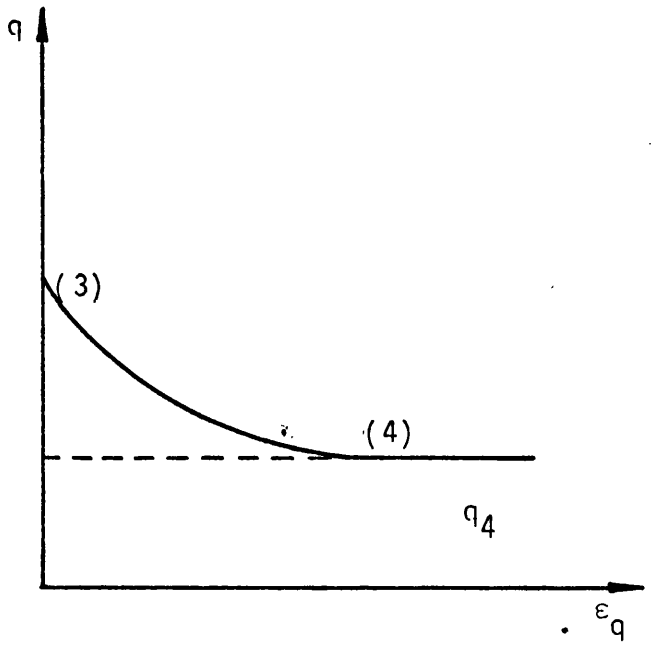

(3)

FIGURE 2.4(cont'd)

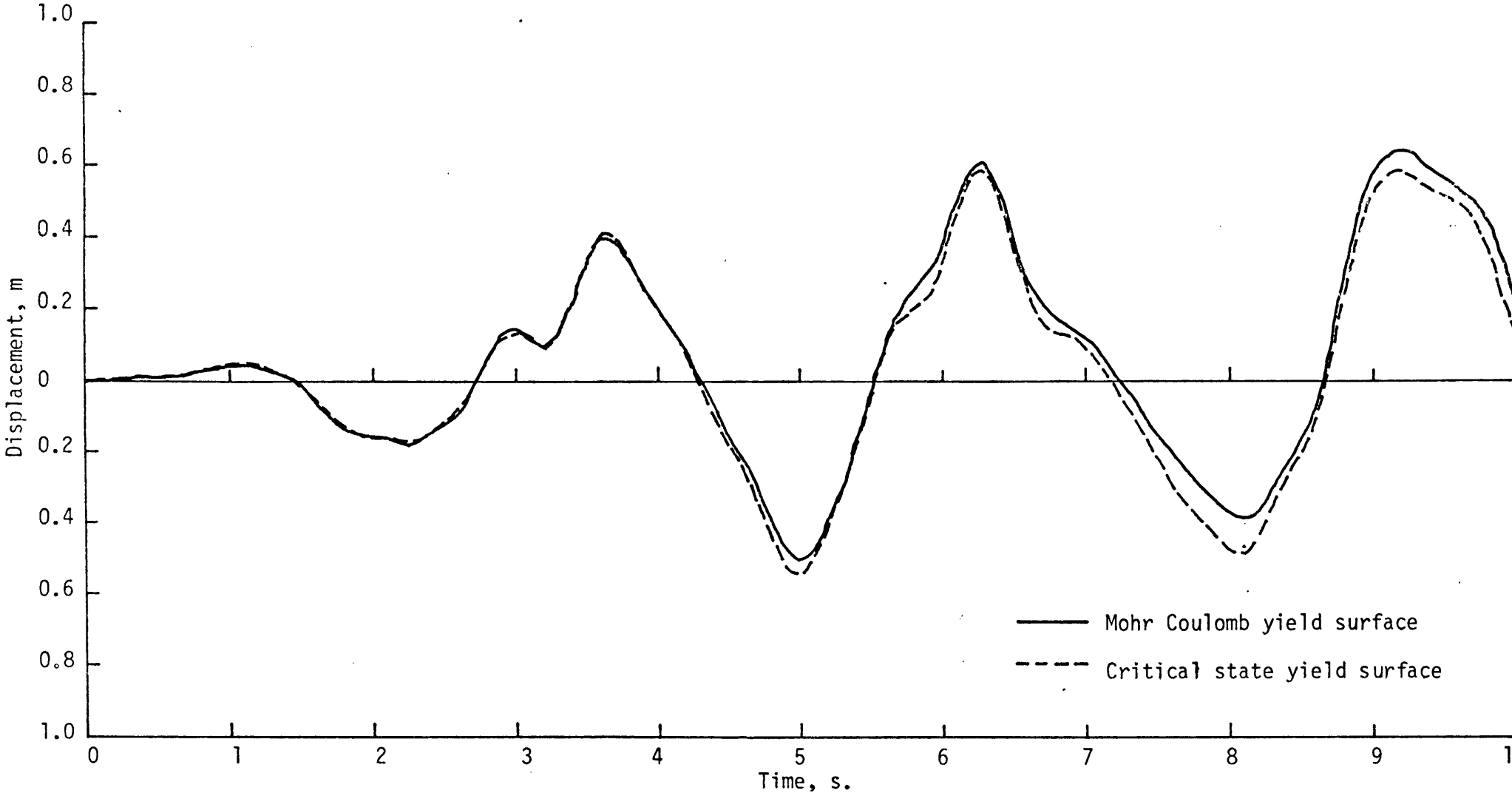

FIGURE 2.5 HORIZONTAL DISPLACEMENT TIME HISTORY AT DAM CREST WITH MOHR COULOMB YIELD SURFACE AND CRITICAL STATE YIELD SURFACE (DRAINED CONDITIONS)

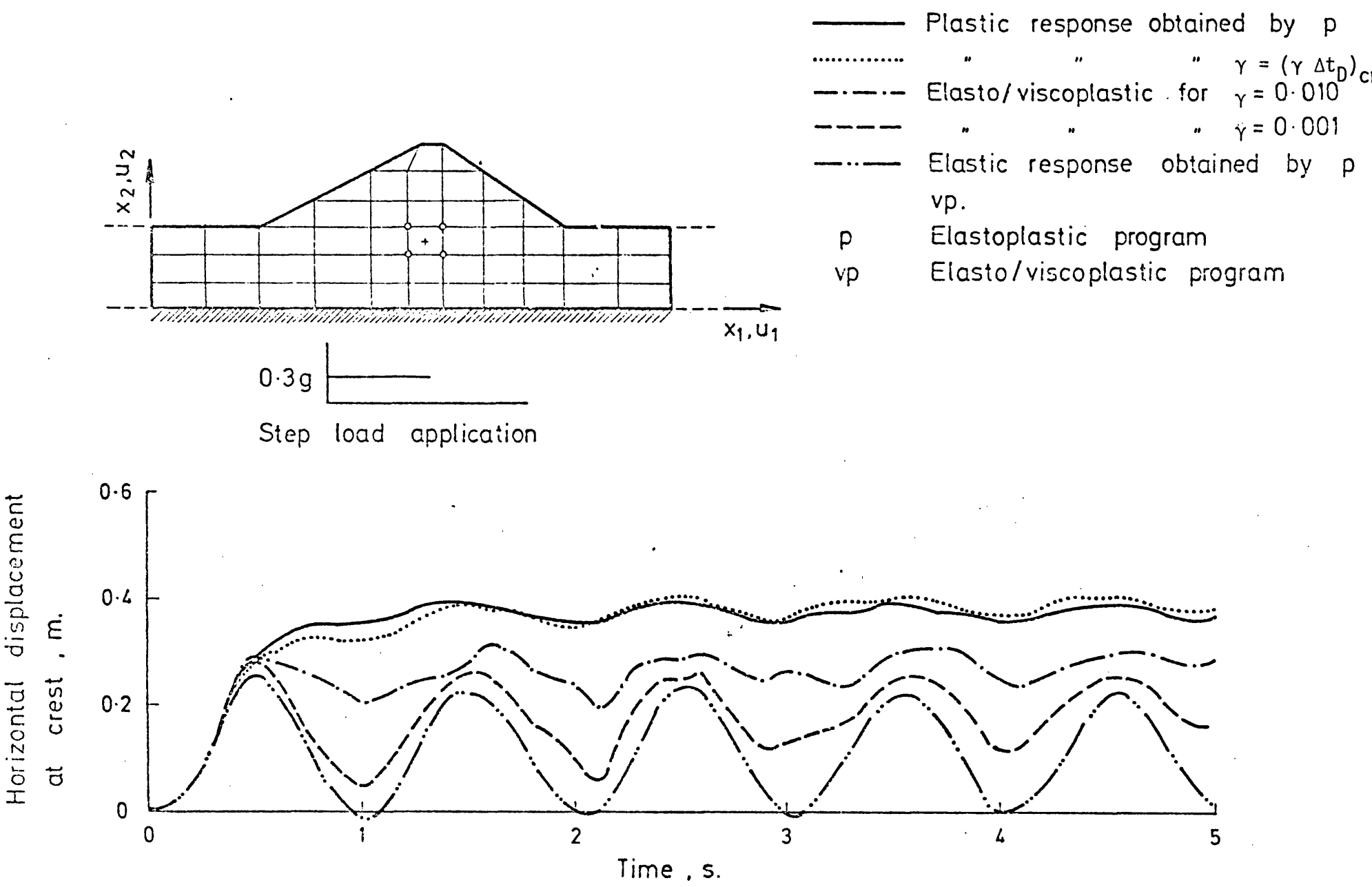

FIGURE 2.6 RESPONSES WITH VARIOUS VALUES OF FLUIDITY PARAMETER, γ (COMPUTER TIME ON A CDC 7600 IS 56s EACH)

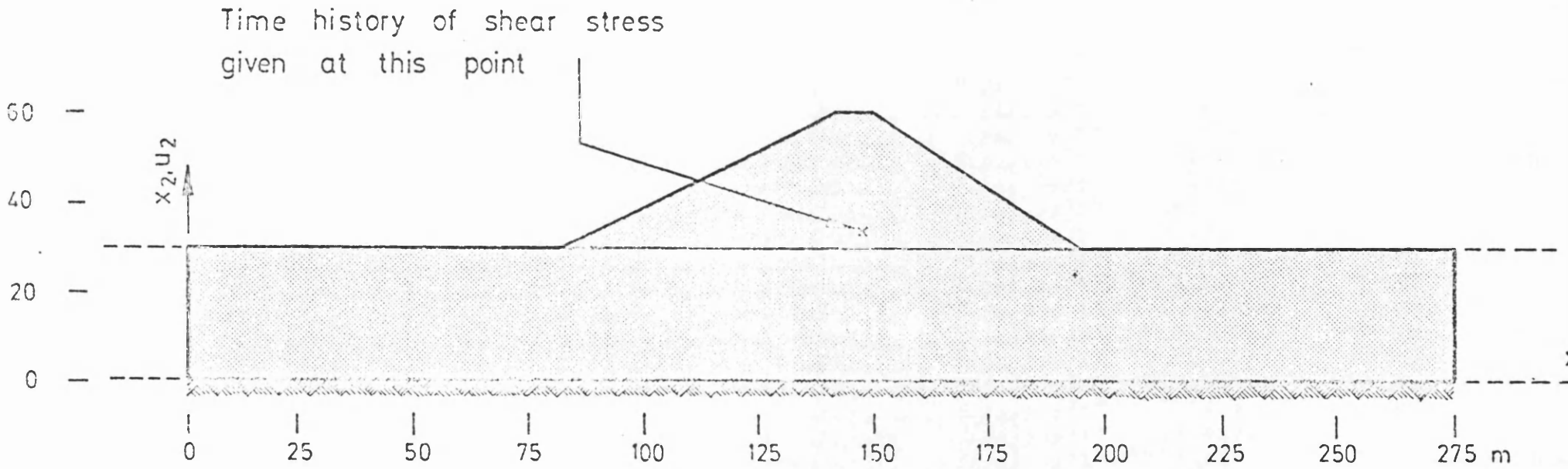

Material properties : Young's mod E = 130,000 kN/m^2 Mass density = 1740 kg/m^3
Poisson ratio = 0·333 Cohesion = 35 kN/m^2
Hardening parameter = 1,300 kN/m^2 Friction angle = 30°

FIGURE 2.7 EARTHDAM

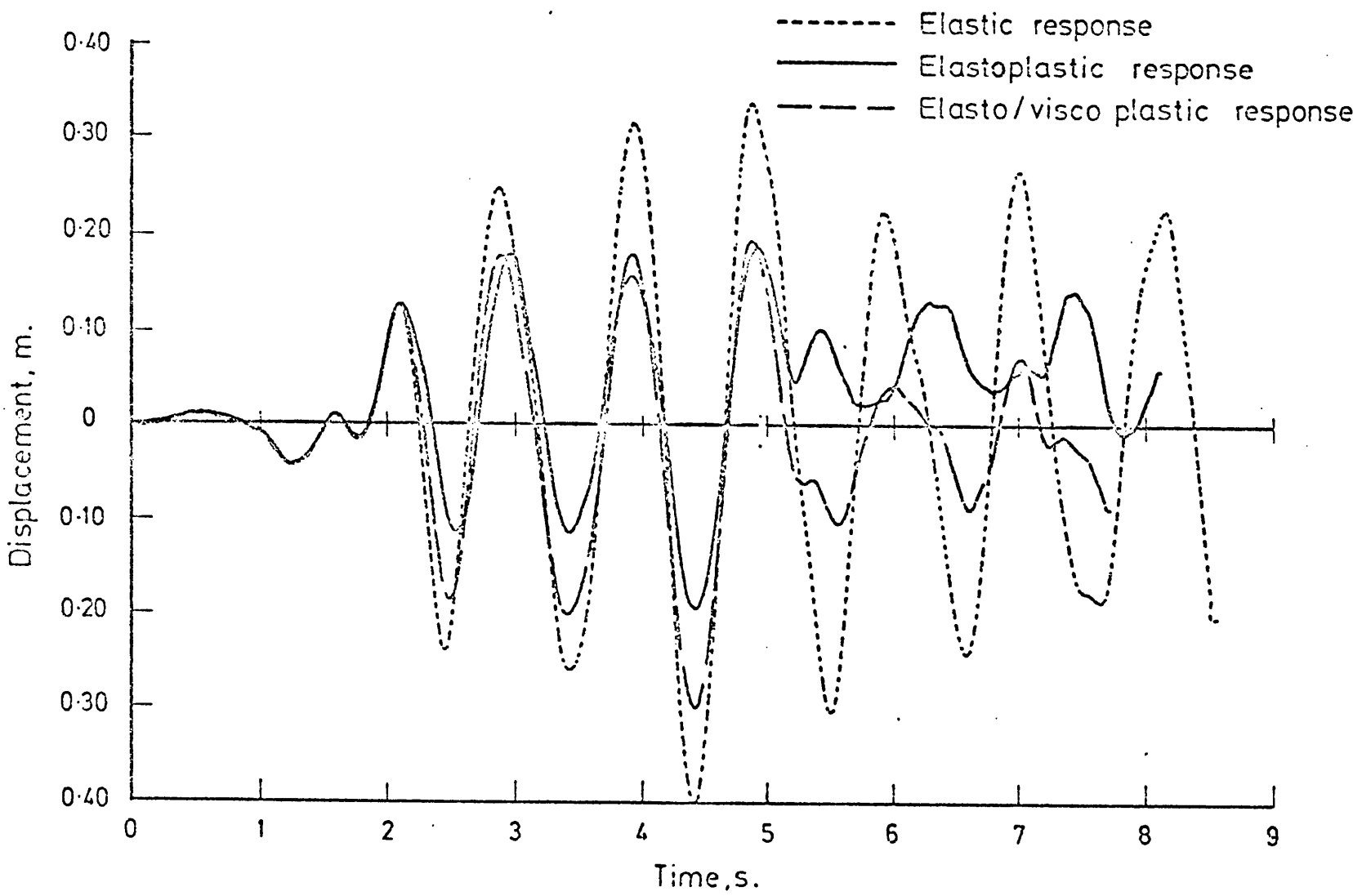

FIGURE 2.8 HORIZONTAL DISPLACEMENT, ${}^{t}U_1$, TIME-HISTORY AT DAM CREST (COMPUTER TIME ON A CDC 7600 IS 160s EACH)

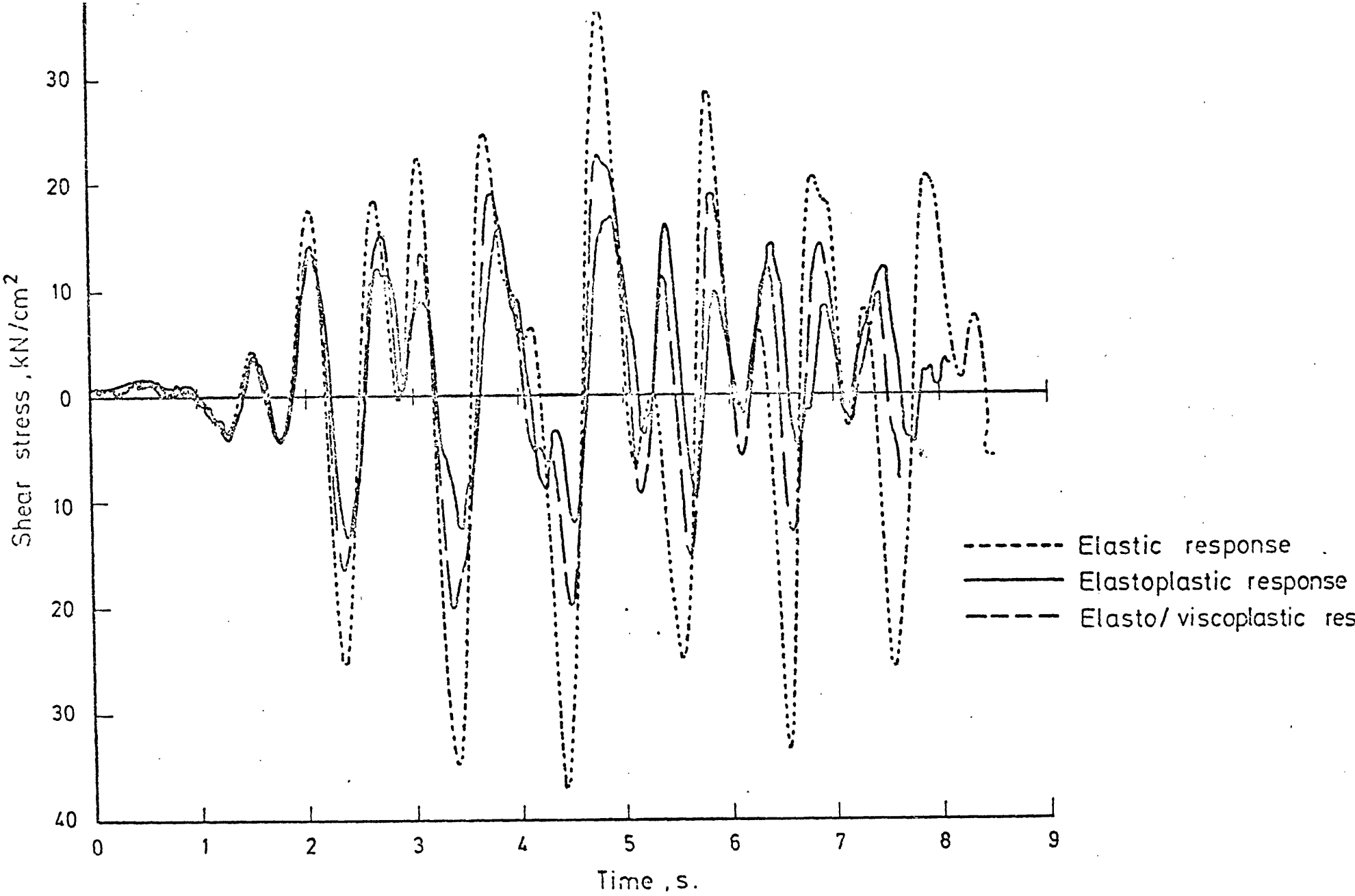

FIGURE 2.9 SHEAR STRESS TIME HISTORY AT THE POINT GIVEN IN FIGURE 11.4

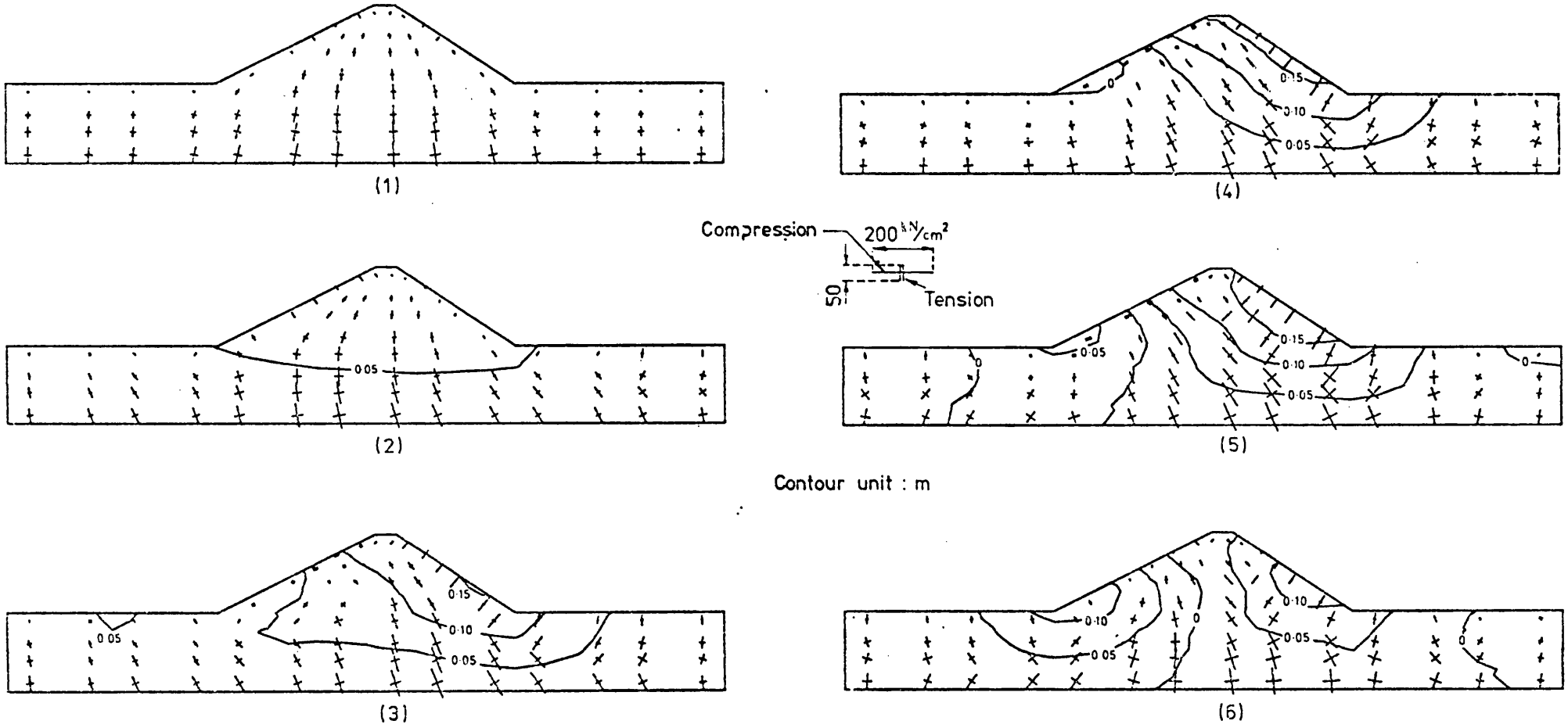

FIGURE 2.10 PRINCIPAL STRESS DISTRIBUTION AND X-COMPONENT DISPLACEMENT CONTOUR AT TIME: (1) 1s, (2) 2s, (3) 3s, (4) 4s, (5) 5s, (6) 6s.

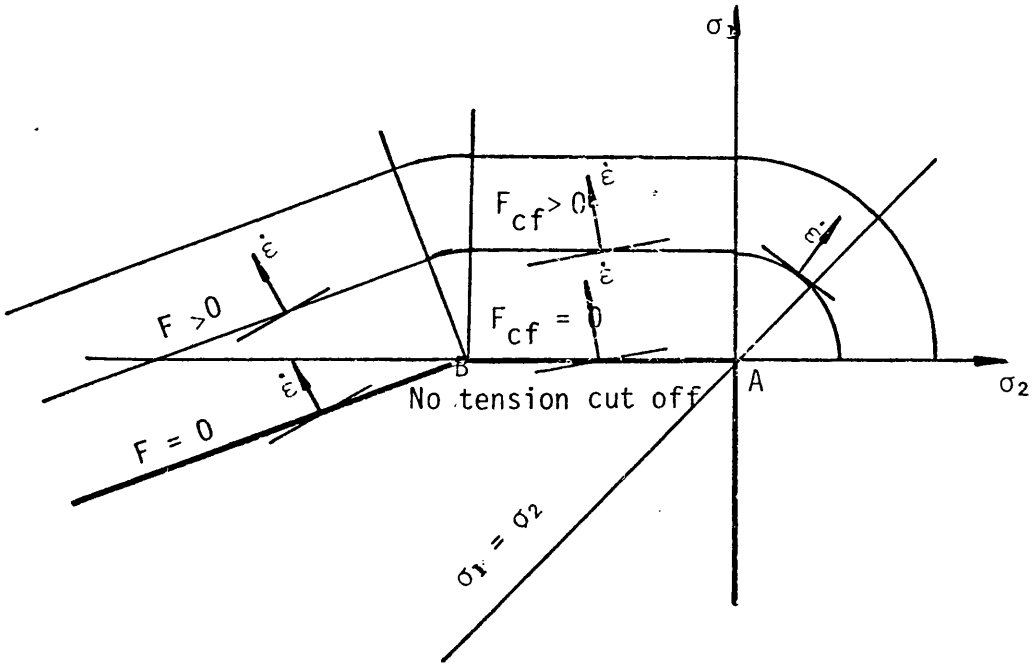

(1) On principal stress plane

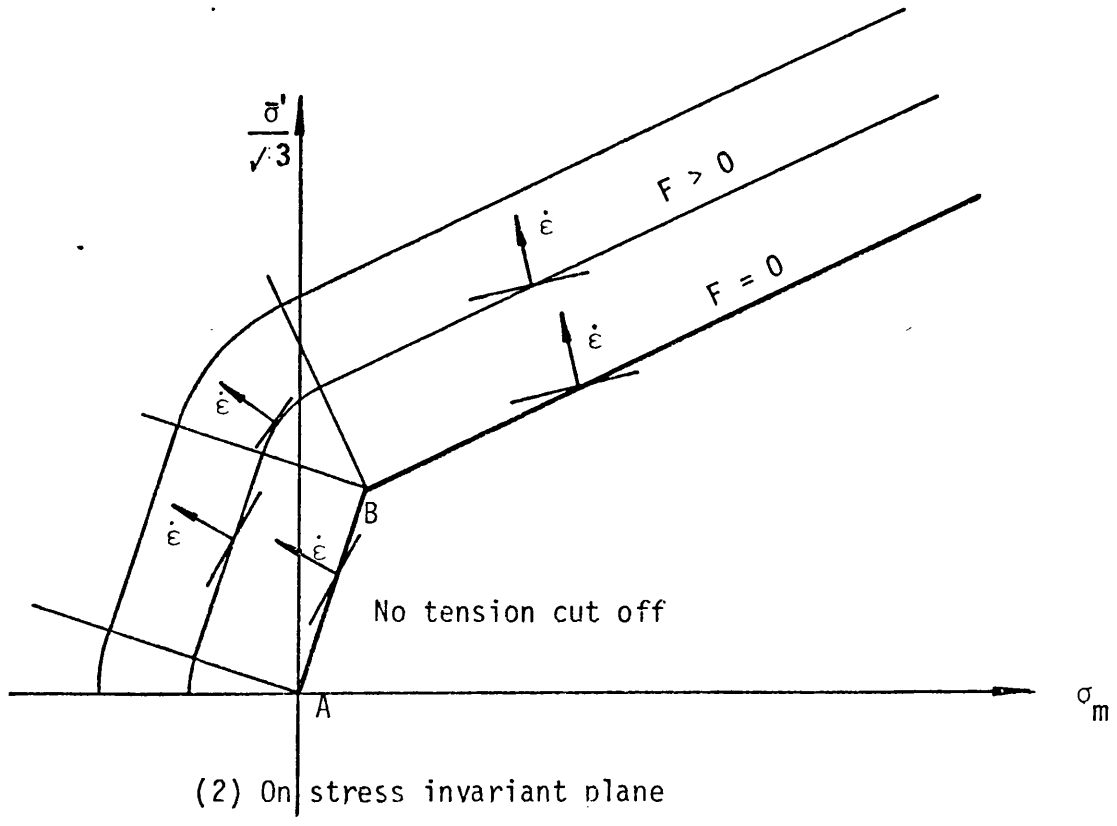

(2) On stress invariant plane

FIGURE 2.11 NO TENSION CUT OFF MODEL

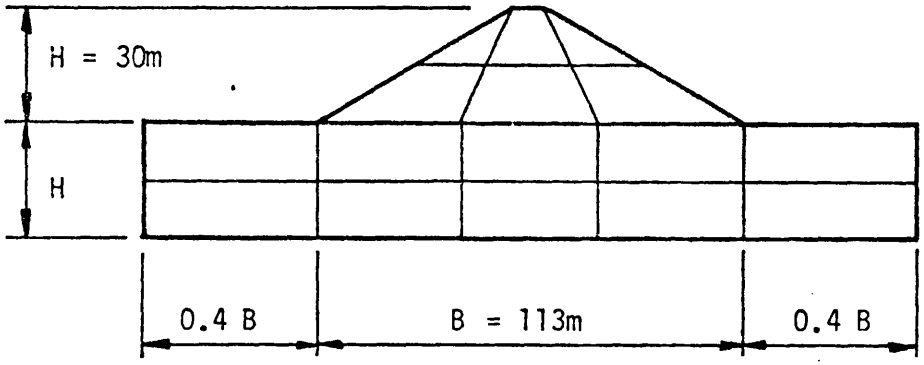

(1)

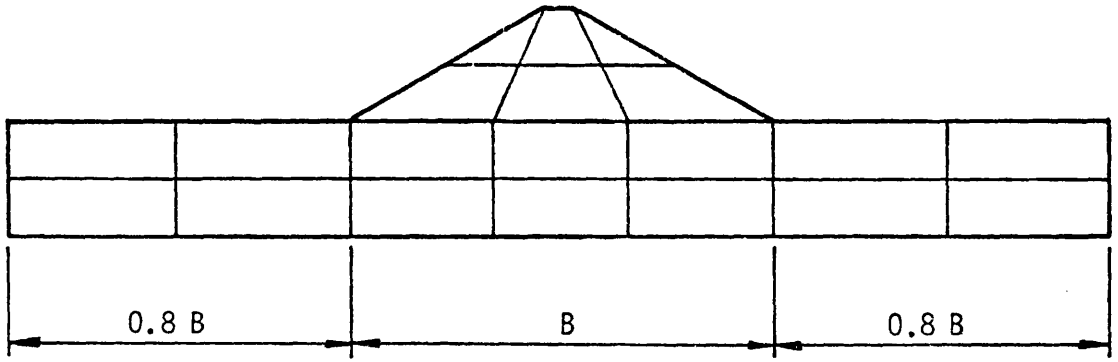

(2)

FIGURE 2.12 (to be cont'd)

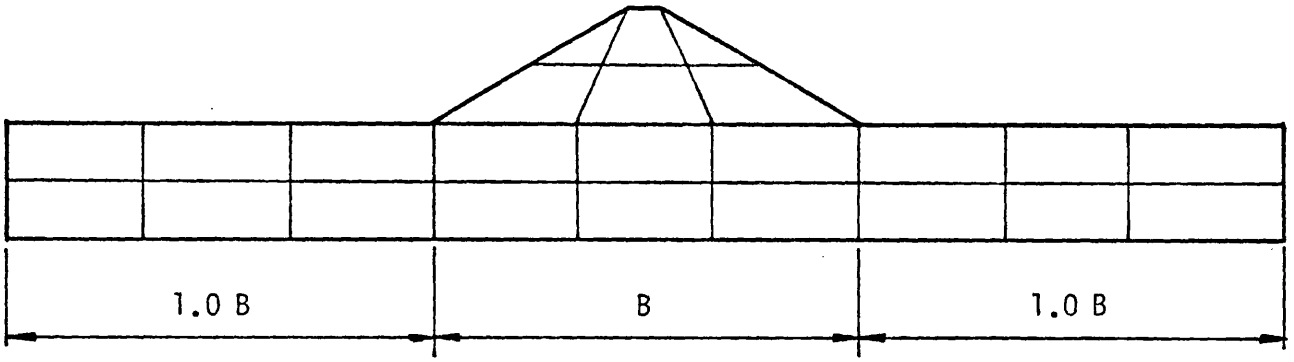

(3)

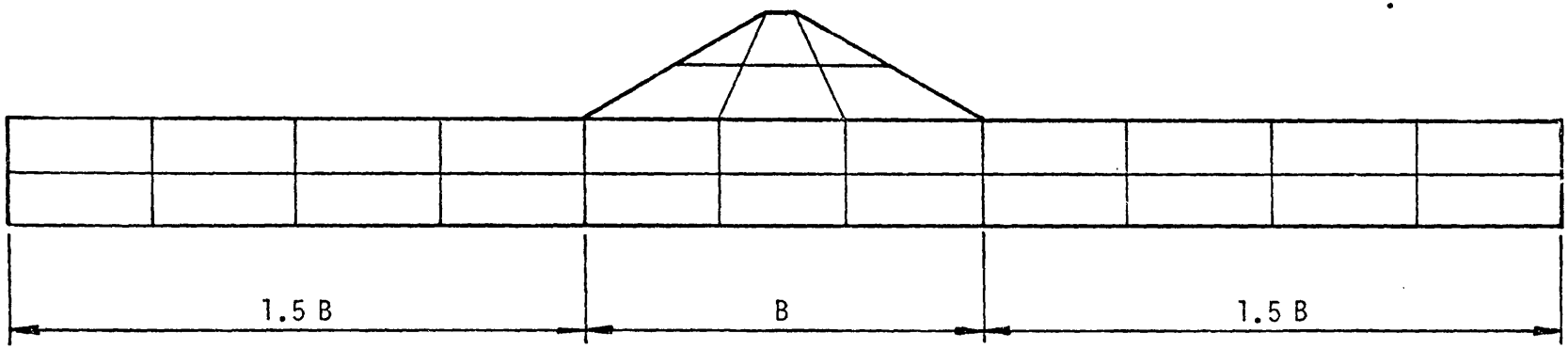

(4)

FIGURE 2.12 (to be cont'd)

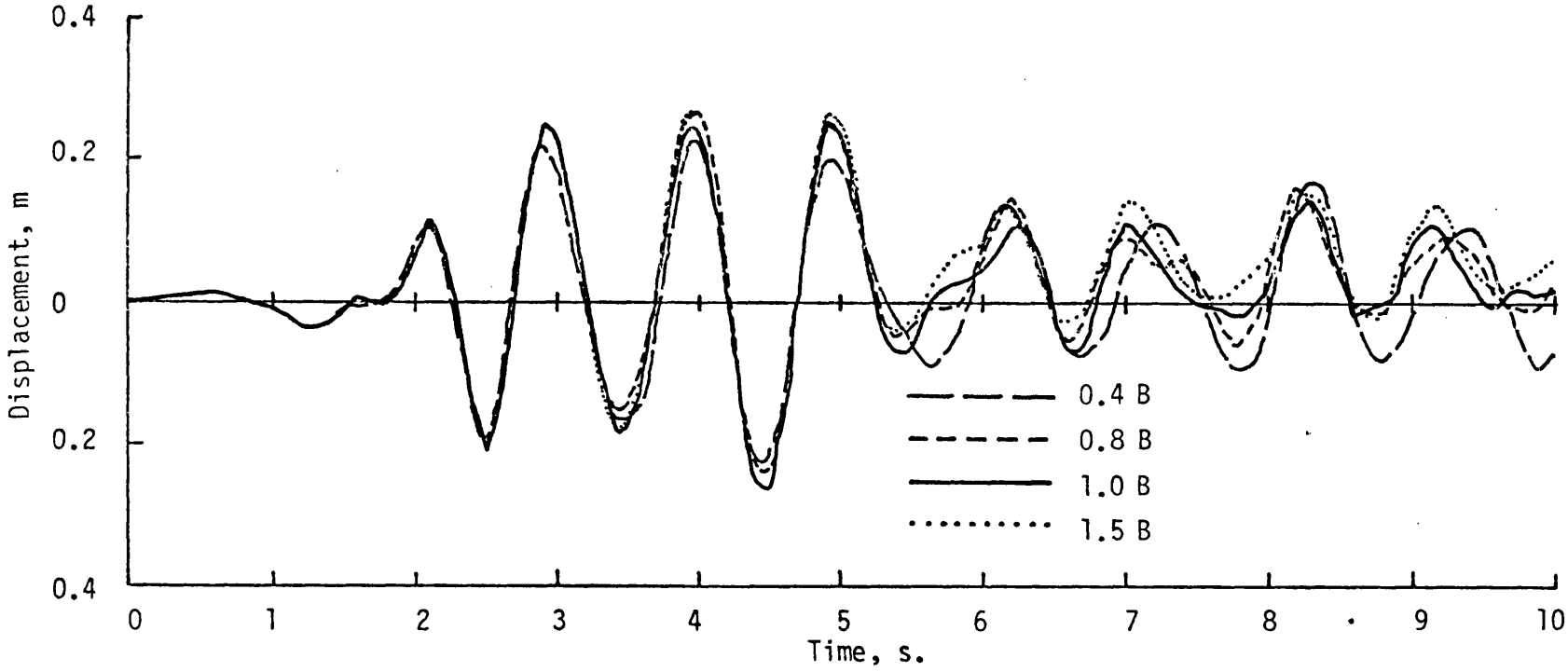

(5)

FIGURE 2.12 EFFECT OF DIFFERENT EXTENTS OF FOUNDATION LENGTH
(1) 0.4 B, (2) 0.8 B, (3) 1.0 B, (4) 1.5 B
(5) HORIZONTAL DISPLACEMENT TIME HISTORY AT DAM CREST

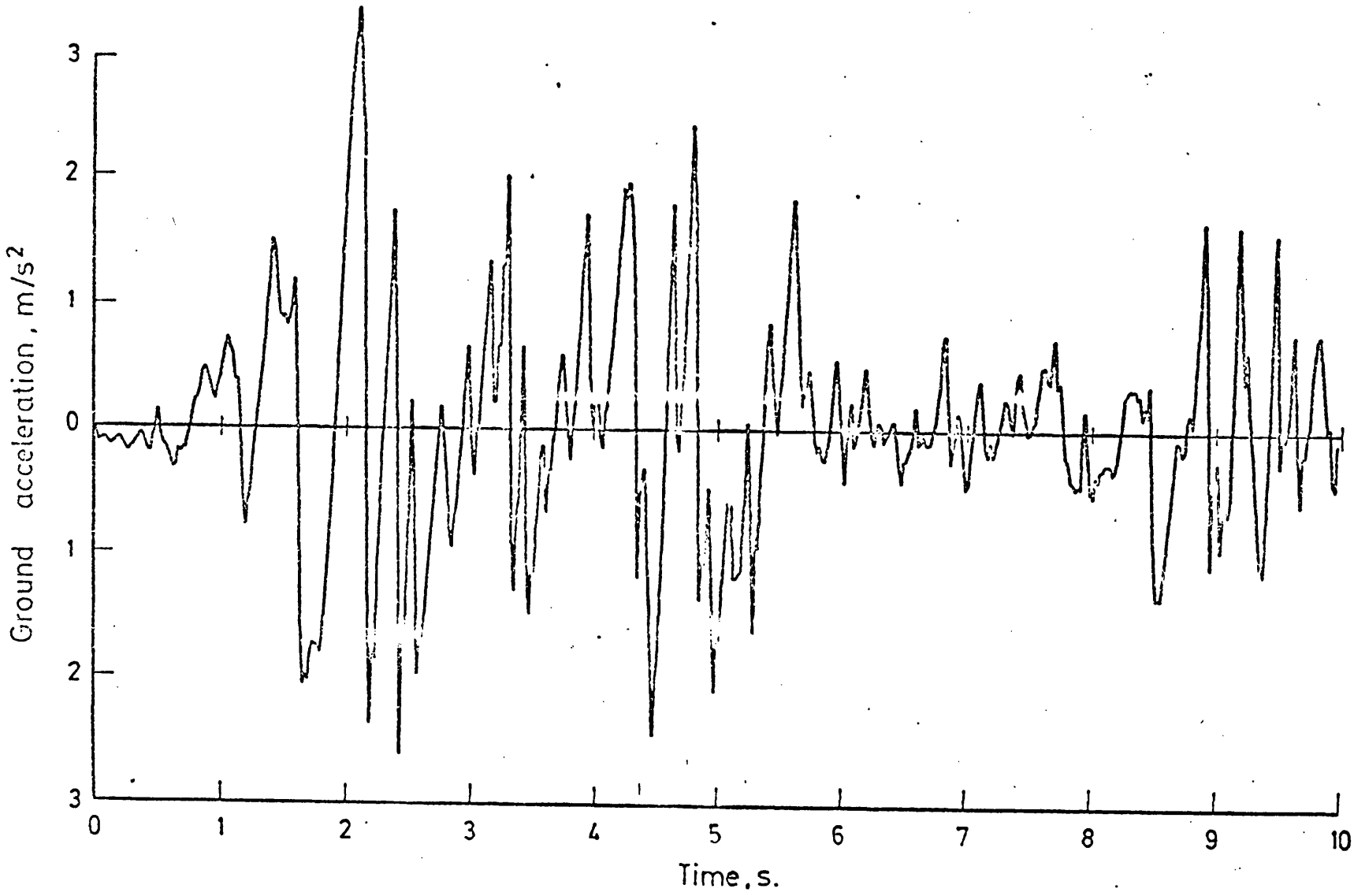

FIGURE 2.13(a) ACCELEROGRAM FROM EL CENTRO EARTHQUAKE, (MAY 1940), N-S COMPONENT

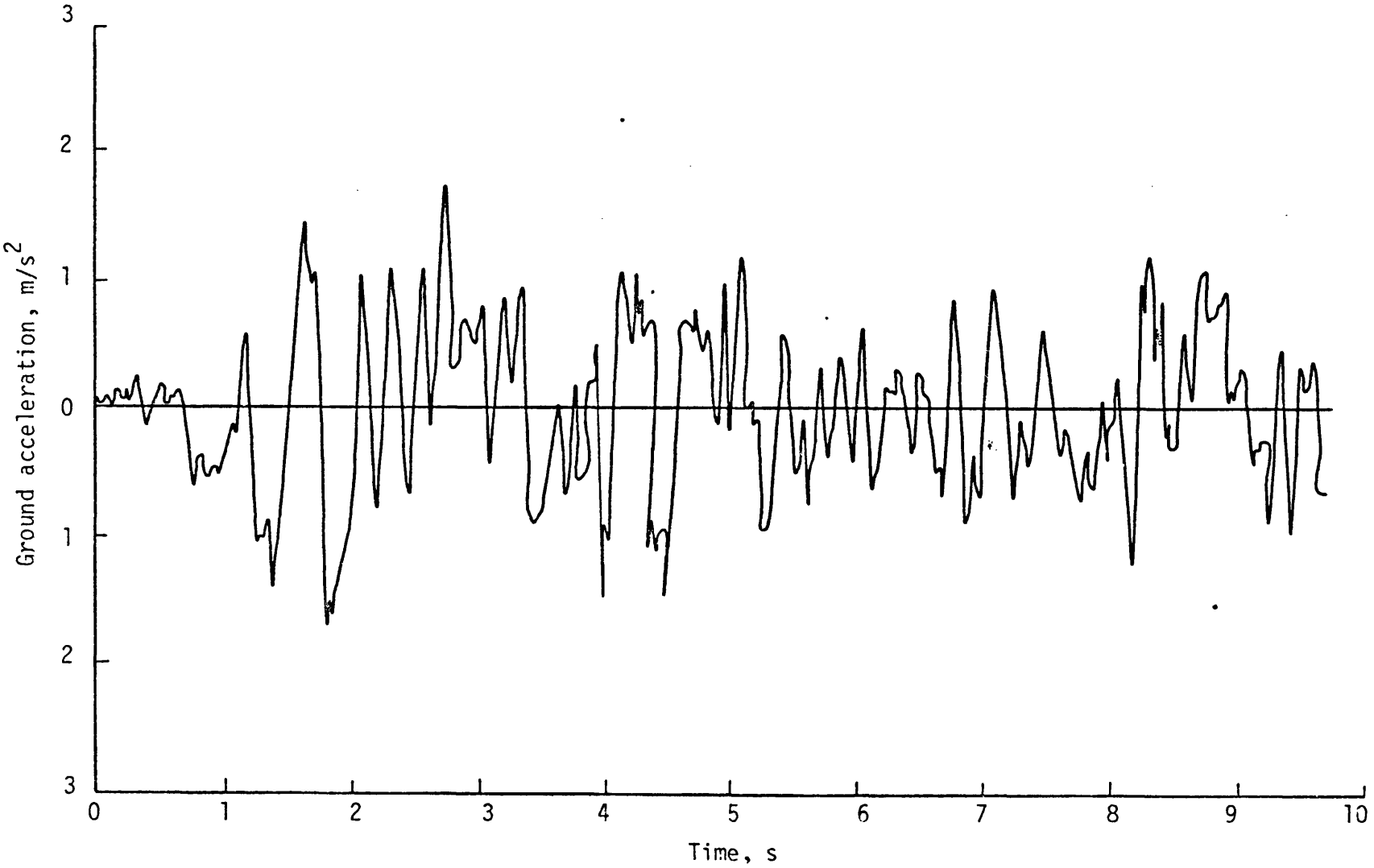

FIGURE 2.13(b) ACCELEROGRAM FROM EL CENTRO EARTHQUAKE (MAY 1940), E-W COMPONENT

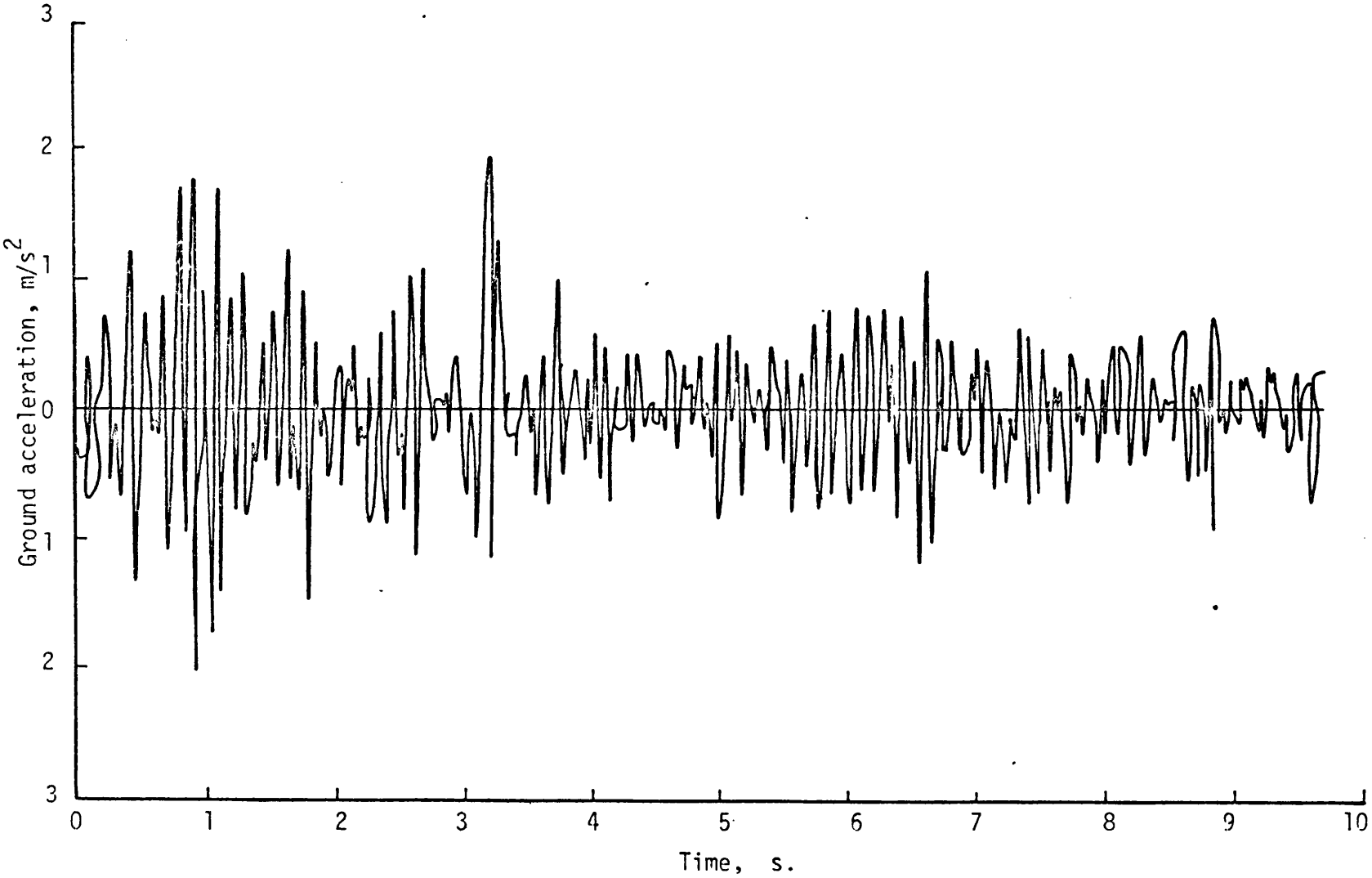

FIGURE 2.13(c) ACCELEROGRAM FROM EL CENTRO EARTHQUAKE (MAY 1940), VERTICAL COMPONENT

CHAPTER 3

FINITE ELEMENT SPATIAL DISCRETIZATION

3.1 INTRODUCTION

Nonlinear structural analysis is today, carried out almost exclusively by the finite element method. In nonlinear dynamic analysis, the finite element method can be applied both in space and in time. However, it appears more practical to use the finite element method in space and the finite difference method in time although, as shown by Zienkiewicz[1] both processes are identical in the time domain. This approach is adopted in the present study. In this chapter the finite element spatial discretization is presented. The temporal discretization will be discussed in the next chapter.

3.2 DYNAMIC FORMULATION

In the present formulation, the displacement based finite element procedure is adopted and the principle of virtual displacements is used to express the equilibrium of the body in the configuration at time t. Assuming that the direction and magnitude of the body loading and inertia loading is independent of the configuration (i.e., the path independent loading only is considered), the principle of virtual displacements requires that[1-3]

$$\int_{\Omega} \rho\, {}^{t}\ddot{\underset{\sim}{u}}\, \delta\underset{\sim}{u}\, d\Omega + \int_{\Omega} \mu\, {}^{t}\dot{\underset{\sim}{u}}\, \delta\underset{\sim}{u}\, d\Omega + \int_{\Omega} {}^{t}\underset{\sim}{\sigma}\, \delta\, {}^{t}\underset{\sim}{\varepsilon}\, d\Omega$$

$$= \int_{\Omega} \underset{\sim}{f}\, \delta\underset{\sim}{u}\, d\Omega + \int_{\Omega} \rho\, {}^{t}\ddot{\underset{\sim}{u}}\, \delta u\, d\Omega \qquad (3.1)$$

in which dots represent differentiation with respect to time; $\delta\underset{\sim}{u}$ is a virtual variation in the current displacement components ${}^{t}\underset{\sim}{u}$; $\underset{\sim}{f}$ is the

initial body forces; $\ddot{\underset{\sim}{u}}$ represents a given base accelerogram, in general, it is obtained from earthquake records and discretized at equally spaced time intervals; ρ, μ are mass density and viscosity of the material respectively. Finally, the stress vector ${}^{t}\underset{\sim}{\sigma}$ and the strain vector ${}^{t}\underset{\sim}{\varepsilon}$ at time t are respectively as presented in Chapter 2.

The equilibrium equation (3.1) is now integrated by using the isoparametric finite element spatial discretization. It is unnecessary to recall here the full description of the finite element process and only a brief summary of the salient points is included using the standard notation used by Zienkiewicz[1].

Consider the 8 noded parabolic isoparametric element shown in Figure 3.1. If the coordinates of the nodes are denoted as (x_i, y_i) and the corresponding displacements as (u_i, v_i) (where i various from 1 to 8), then any point (x, y) within the element and the corresponding displacement (u, v) can be represented as

$$\begin{aligned} x &= \sum_{i=1}^{8} N_i\, x_i \quad ; \quad y = \sum_{i=1}^{8} N_i\, y_i \\ u &= \sum_{i=1}^{8} N_i\, u_i \quad ; \quad v = \sum_{i=1}^{8} N_i\, v_i \end{aligned} \tag{3.2}$$

where N_i's are the shape functions which are location dependent. Table 3.1 lists the shape functions in terms of curvilinear coordinates ξ, η for 4 noded linear and the 8 noded parabolic isoparametric elements.

If the standard finite element discretization implied by equation (3.2), is inserted into (3.1) then the following expression is obtained

$$\underset{\sim}{M}\,\ddot{\underset{\sim}{a}} + \underset{\sim}{C}\,\dot{\underset{\sim}{a}} + \underset{\sim}{P}(a) = \underset{\sim}{F}(t) \tag{3.3}$$

in which $\underset{\sim}{M} = \int_{\Omega} \underset{\sim}{N}^T \rho \, \underset{\sim}{N} \, d\Omega$

$\underset{\sim}{C} = \int_{\Omega} \underset{\sim}{N}^T \mu \, \underset{\sim}{N} \, d\Omega$

$\underset{\sim}{F}(t) = \int_{\Omega} \underset{\sim}{N}^T \underset{\sim}{f} \, d\Omega + \underset{\sim}{M} \, t\ddot{\underset{\sim}{u}}$

and $\underset{\sim}{P}(a) = \int_{\Omega} B^T \sigma \, d\Omega$

It is understood in the above that σ represents the total stress as described in the previous chapter. Under drained conditions (with P = 0) and for linear problems $\int_{\Omega} B^T \sigma \, d\Omega$ can be replaced by $\underset{\sim}{K} \, \underset{\sim}{a}$ while $\underset{\sim}{K} = \int_{\Omega} \underset{\sim}{B}^T \underset{\sim}{D} \, \underset{\sim}{B} \, d\Omega$ and $\underset{\sim}{D}$ is the elasticity matrix.

3.3 MASS MATRIX

The mass matrix $\underset{\sim}{M}$ given in equation (3.3) uses the shape functions as employed in the calculation of the load vectors and in the evaluation of the internal resisting forces. Thus a consistent load vector and a consistent mass matrix have been evaluated. When, as in this thesis, the explicit time stepping scheme is used, the "diagonalized" or "lumped" mass matrix is more convenient. A lumped mass matrix of such kind can be obtained by the use of suitable shape functions N_i which have values of unity in a certain part of the element surrounding the node i and zero elsewhere. Without overlapping of such functions all terms containing products are zero and only diagonal terms remain, i.e.,

$$\int_{\Omega} \underset{\sim}{N}_i^T \rho \, \underset{\sim}{N}_j \, d\Omega = 0 \quad (i \neq j) \qquad (3.4).$$

In the present study, the special mass lumping scheme given by Hinton, et. al.[4] is used. This lumping scheme takes the consistent mass matrix and lumps in proportion to the diagonal terms of the consistent mass matrix.

In this scheme the consistent mass matrix of each element is firstly evaluated by the following expression

$$M_{ij} = \int_{\Omega} \underset{\sim}{N}_i^T \rho \underset{\sim}{N}_j \, d\Omega \tag{3.5}$$

Then the element diagonal term M_i^e is computed as

$$M_i^e = M_{ii}^e \frac{M}{\Sigma M_{ii}^e} \tag{3.6}$$

where $M = \int_{\Omega} \rho \, d\Omega$ (3.7)

Having evaluated all element diagonal terms, each diagonal term can be obtained by simply summing the values of all elements contributing to that particular term, i.e.,

$$M_i = \sum_{e=1}^{m} M_i^e \tag{3.8}$$

where the subscript e stands for a particular element and m denotes the number of elements contributing to i^{th} diagonal term.

Use of piecewise "lumping" functions suggested here results in a loss of accuracy and it is possible to devise alternative procedures of lumping for certain elements by special integration rule which are more accurate. These have been proposed by Fried and others[5] and are fully discussed in reference (1).

3.4 DAMPING MATRIX

In practice, it is not generally possible to define and determine the viscosity μ from which the damping matrix C is determined. Thus it has become a common practice to adopt Rayleigh damping which can be written as

$$\underset{\sim}{C} = \alpha \underset{\sim}{M} + \beta \underset{\sim}{K} \tag{3.9}$$

in which α and β are determined experimentally. Furthermore, it can be shown that the damping matrix adopted is $\zeta_r C_r$ where C_r is the damping matrix associated with critical damping of the r^{th} mode. The damping ratio ζ_r associated with the r^{th} mode of the system can be expressed in terms of α and β by the relation

$$\zeta_r = \frac{\alpha}{2\omega_r} + \frac{\beta \omega_r}{2} \tag{3.10}$$

where ω_r is the circular frequency in the r^{th} mode. In a low frequency dominant system, which prevails in the most structural dynamics, usually the contribution of the second term in equation (3.10) is negligible. Therefore, the damping ratio ζ_r can be simplified as

$$\zeta_r = \frac{\alpha}{2\omega_r} \text{ or } \alpha = 2\zeta_r \omega_r \tag{3.11}$$

Finally, the damping matrix can be written as

$$\underset{\sim}{C} = 2\zeta \omega_r \underset{\sim}{M} \tag{3.12}$$

Since $\underset{\sim}{C}$ is proportional to $\underset{\sim}{M}$, therefore it is also a diagonal matrix.

3.5 EVALUATION OF ISOPARAMETRIC ELEMENTS

In the static analysis, practical experience suggests that, for a given number of total degrees of freedom in a structure, greater accuracy is achieved by use of fewer complex elements in place of a larger number of simple elements. This fact is substantiated by theoretical error analysis provided the solution is sufficiently smooth. It would be of interest to study whether the same conclusion can be made in the dynamic context. Thus the earth dam, as shown in Figure 3.2, was studied. The earth dam is separately modelled by an 8 noded finite element mesh and a 4 noded finite element mesh as shown in Figures 3.3 and 3.4. Both models are subjected to the same base accelerations of

the N-S component of El Centro May 1940 earthquake. Figure 3.5 shows the time history of displacements at the dam crest. Figures 3.6 and 3.7 are respectively shown the deformed meshes for the 4 noded finite element mesh and the 8 noded finite element mesh at two second intervals from the start of motion. Table 3.2 presents the comparison of the two meshes. It can be seen from Figure 3.5 that, for the 4 noded isoparametric finite element mesh, the displacement time history at the dam crest leads to the uneven pattern of displacements while the 8 noded isoparametric finite element mesh gives a more realistic pattern of displacement. The reason for the uneven displacements obtained with the 4 noded isoparametric finite element mesh, is that the hourglassing mode participates in the dynamic response. The hourglassing mode can be eliminated by the use of the full integration rule (i.e., for the 4 noded element use 2x2 Gauss-Legendre integration rule). The deformed meshes obtained using the 4 noded element with full integration rule are presented in Figure 3.8. It can be seen from this figure that the hourglassing mode is no longer present. However, the use of full integration rule increases the computing cost. Therefore, the main advantage of using the 4 noded isoparametric finite element mesh, that is the fact that it is cheaper in computation cost compared with the 8 noded isoparametric finite element mesh, may be lost. Further, the use of 4 noded element requires more data preparation cost. Therefore, generally, in dynamic as well as static analysis, the 8 noded isoparametric element is preferred to the 4 noded element. A more detailed study of the performance of various isoparametric elements based on eigenvalue and mode shape analysis has been carried out by Bicanic[6].

REFERENCES

1. ZIENKIEWICZ, O.C.
'The Finite Element Method'
McGraw-Hill, London, (1977).

2. CLOUGH, R.W. and PENZIEN, J.
'Dynamics of Structures'
McGraw-Hill, New York, (1975).

3. NEWMARK, N.M. and ROSENBLUETH, E.
'Fundamentals of Earthquake Engineering'
Prentice-Hall, Englewood Cliffs, N.J., (1971).

4. HINTON, E., ROCK,T.A. and ZIENKIEWICZ, O.C.
'A note on mass lumping and related processes in the finite element method'
Int. Jnl. Earthquake Eng. and Struct. Dyn., 4, 245-249, (1976).

5. FRIED,I. and MELKUS,D.S.
'Finite element mass matrix lumping by numerical integration with the convergence rate loss'
Int. J. Solids Struct., 11, 461-5, (1975).

6. BICANIC,N.
'Nonlinear seismic response of concrete structures'
Ph.D. Thesis, Univ. of Wales, Swansea, (1978).

ELEMENT	NODES	SHAPE FUNCTION N_i
LINEAR (4 nodes)	CORNER $\xi_i = \pm 1, \quad \eta_i = \pm 1$	$\frac{1}{4}(1+\xi_o)(1+\eta_o)$
QUADRATIC (8 nodes)	CORNER $\xi_i = \pm 1, \eta_i = \pm 1$	$\frac{1}{4}(1+\xi_o)(1+\eta_o)(\xi_o+\eta_o-1)$
	MIDSIDE $\xi_i = 0, \quad \eta_i = \pm 1$	$\frac{1}{2}(1-\xi^2)(1+\eta_o)$
	MIDSIDE $\xi_i = \pm 1, \eta_i = 0$	$\frac{1}{2}(1+\xi_o)(1-\eta^2)$

Note: $\xi_o = \xi\xi_i, \quad \eta_o = \eta\eta_i$

TABLE 3.1 SHAPE FUNCTIONS FOR 2D ISOPARAMETRIC ELEMENTS

TABLE 3.2

TYPE	Nodes	Elements	Degrees of freedom	Gauss Points	Time step length (s)	Computation time (s)	Comments
4 node element	122	92	244	92	0.012	56	cheaper
8 node element	102	25	204	100	0.006	133	more accurate
Ratio	1.20	3.68	1.20	0.92	2	0.42	

Note: The computer time for 4 node element, 2x2 integration rule is 160 seconds (on a CDC 7600)

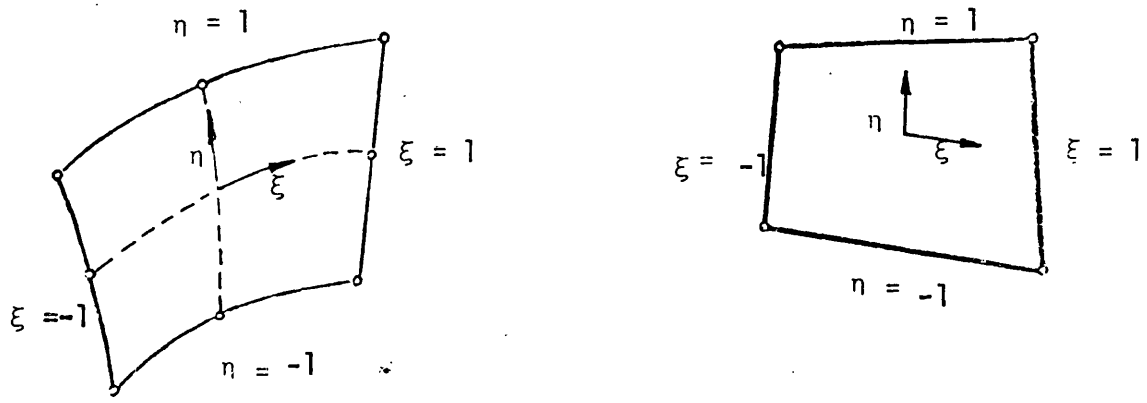

(1)

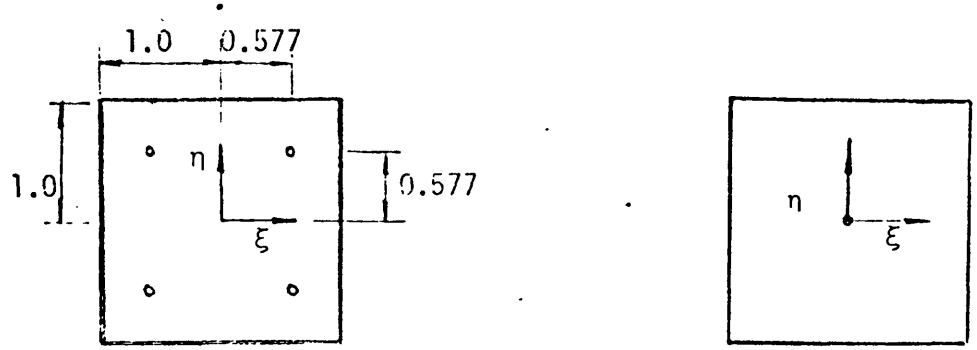

(2)

FIG: 3.1 (1) ISOPARAMETRIC ELEMENTS

(2) GAUSS INTEGRATION RULE

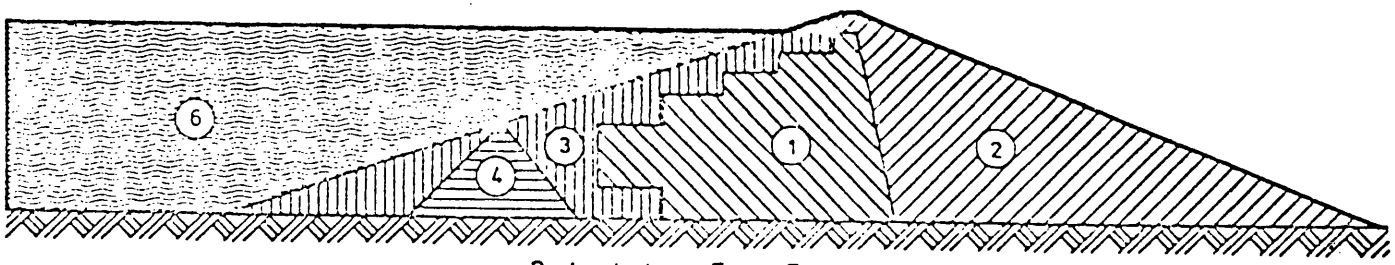

Material zone	E MN/m^2	ν	ϕ degree	C kN/m^2	Unit weight kg/m^3
1	100	0.45	33	10	2280
2	100	0.40	33	10	2280
3	230	0.45	38	80	2400
4	100	0.45	33	10	2160
5	230	0.45	38	80	2400
6	2250*	0.50	-	-	1000

* Bulk mod.

FIGURE 3.2 MATERIAL ZONES AND PROPERTIES

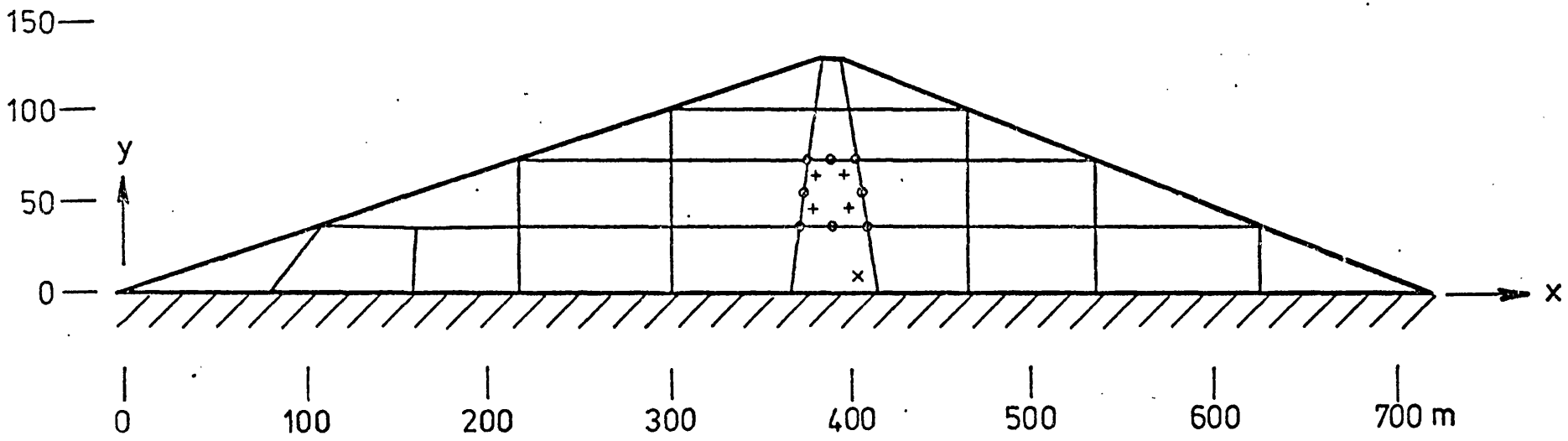

Fig. 3.3 Finite Element Mesh of 8 node elements

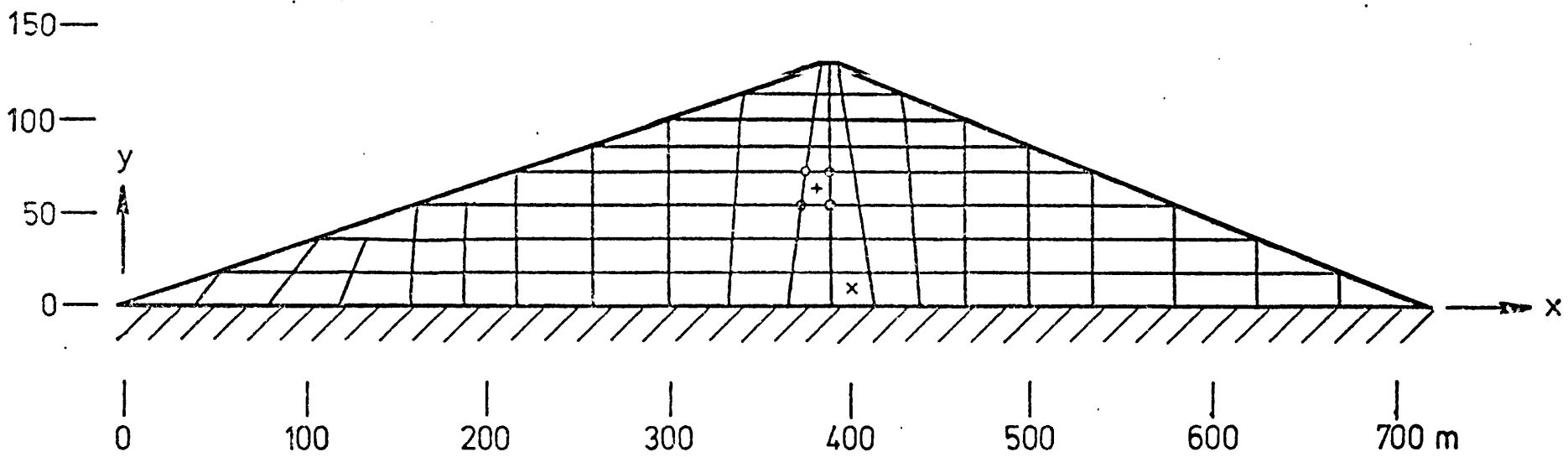

Fig.3.4 Finite Element Mesh of 4 node elements

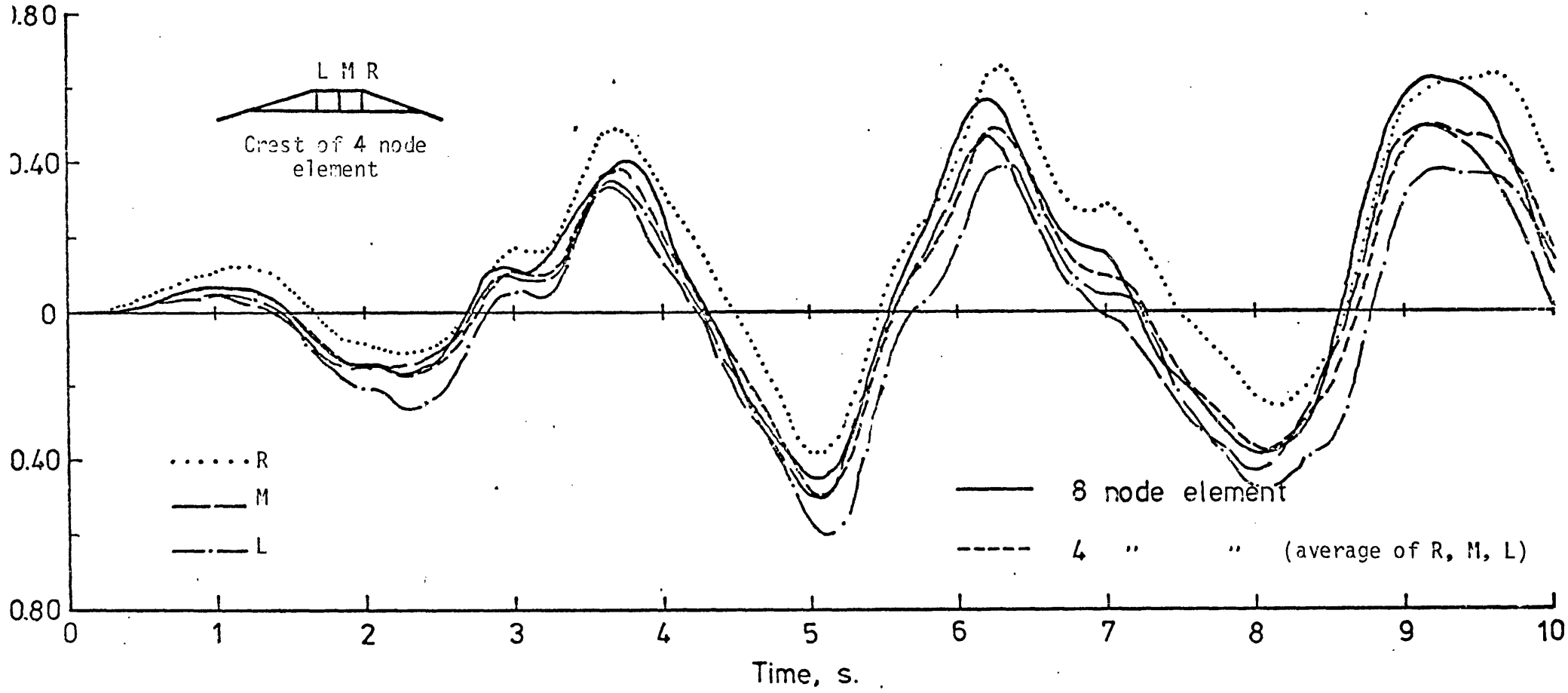

Fig.3.5 Horizontal Displacement Time History at Dam crest

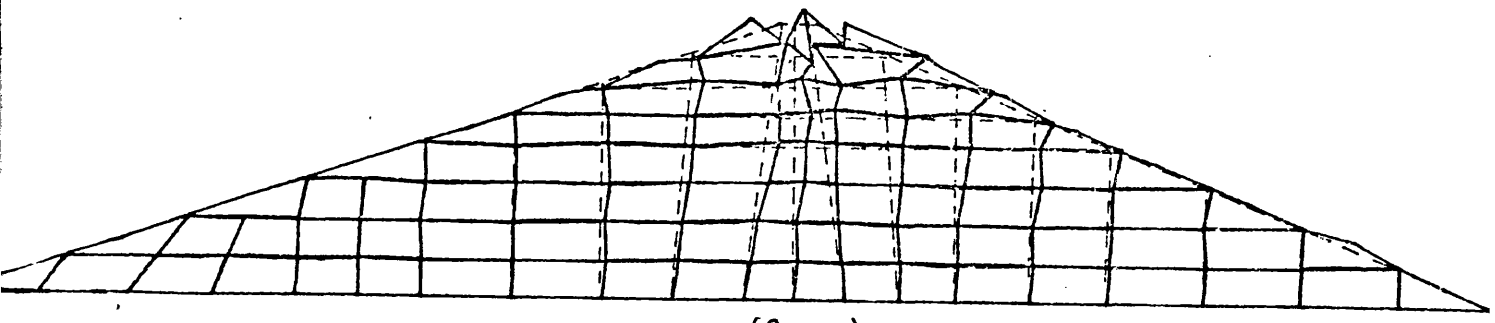

(2 sec)

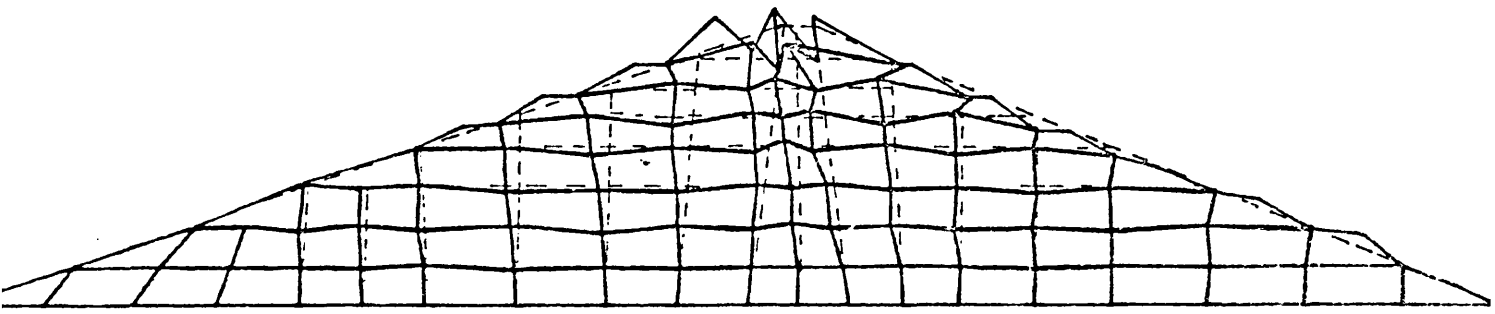

(4 sec)

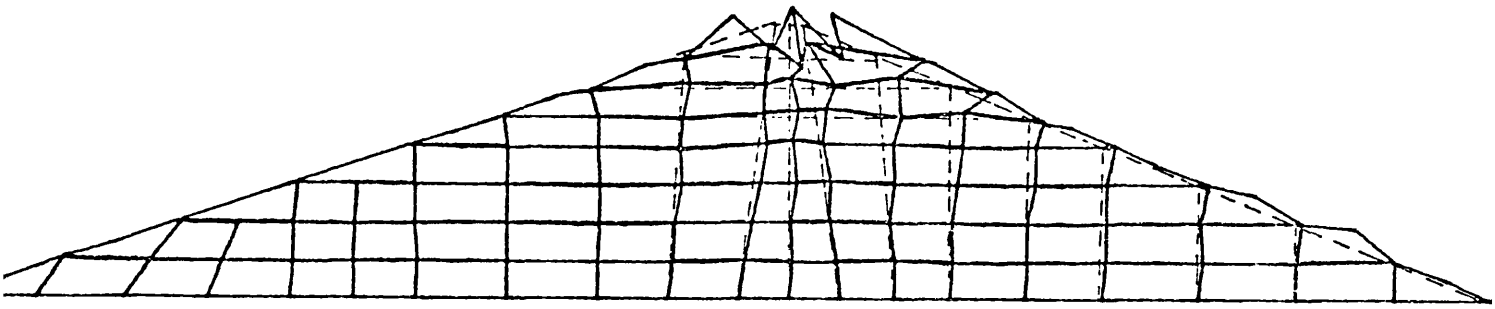

(6 sec)

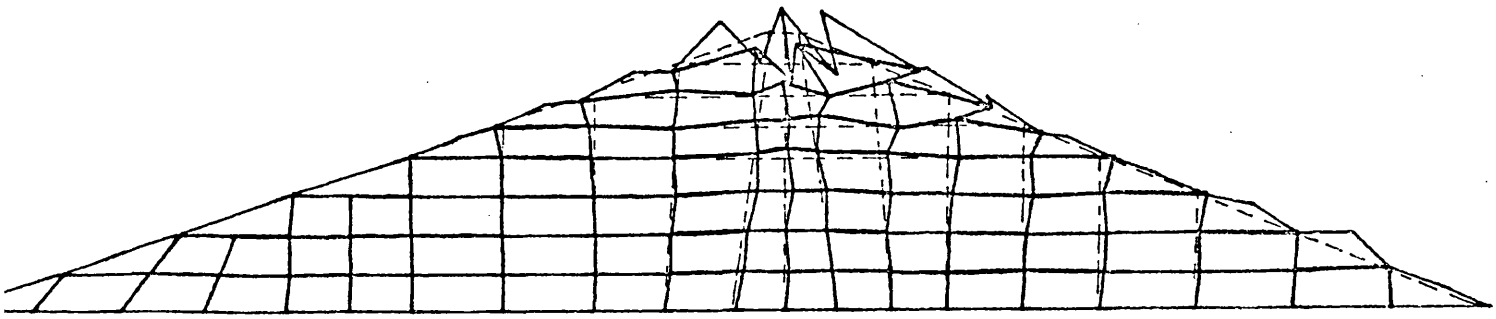

(8 sec)

g. 3.6 PREFORMED MESH OF 4-NODED FINITE ELEMENT MESH
USING 1 x 1 INTEGRATION RULE (DISPLACEMENT x 40)

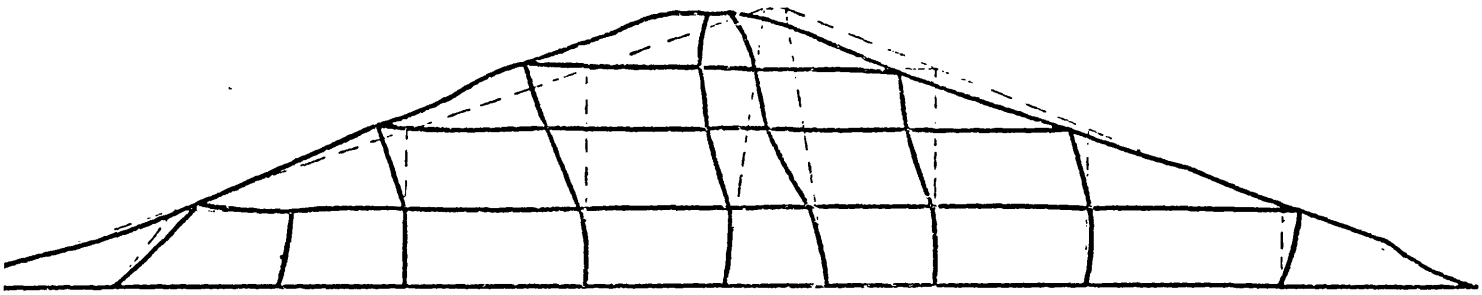

(2 sec)

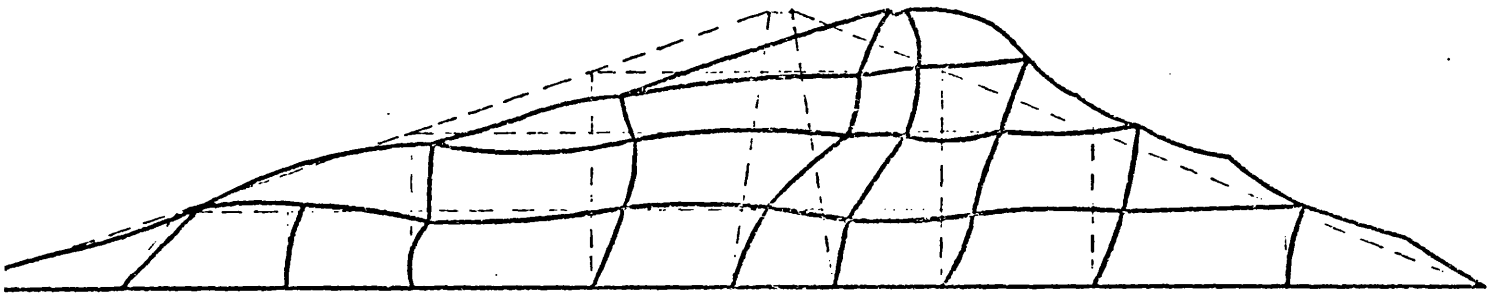

(4 sec)

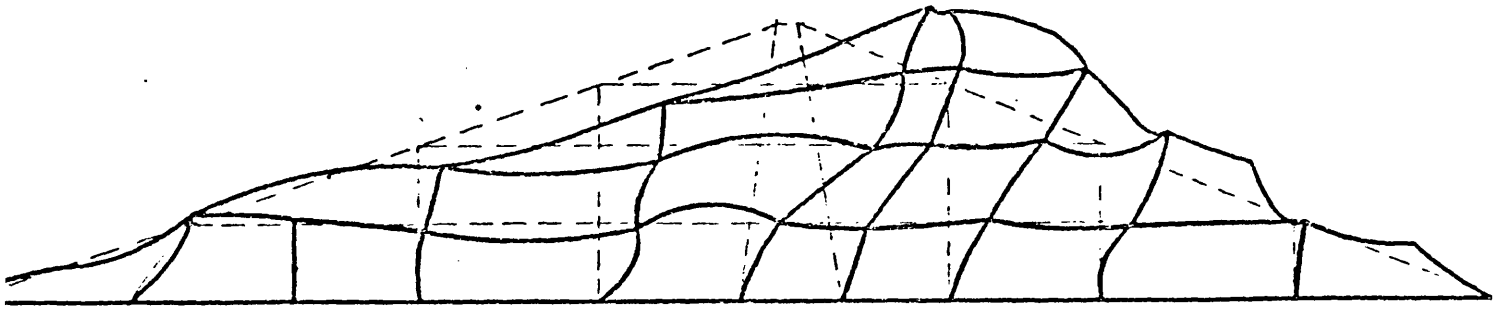

(6 sec)

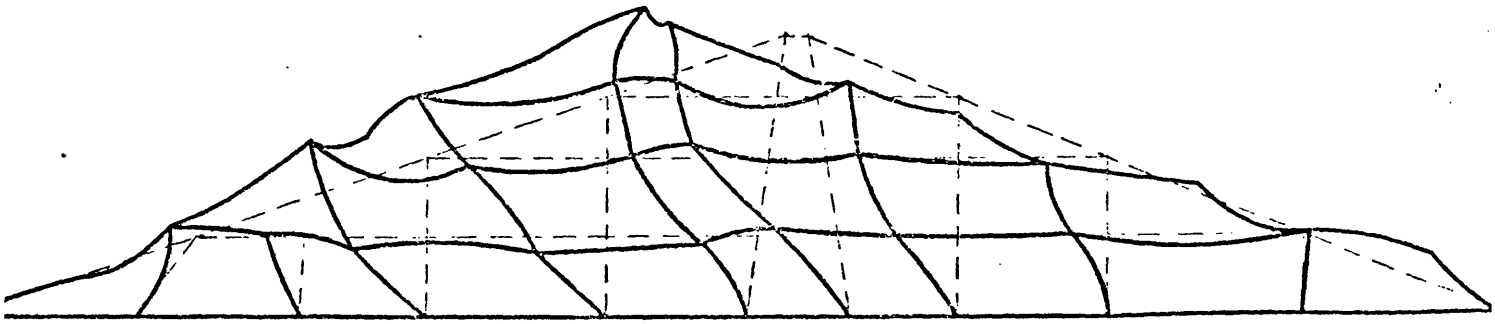

(8 sec)

Fig.3.7. DEFORMED MESH OF 8 NODED FINITE ELEMENT MESH
USING 2 x2 INTEGRATION RULE (DISPLACEMENT x 100)

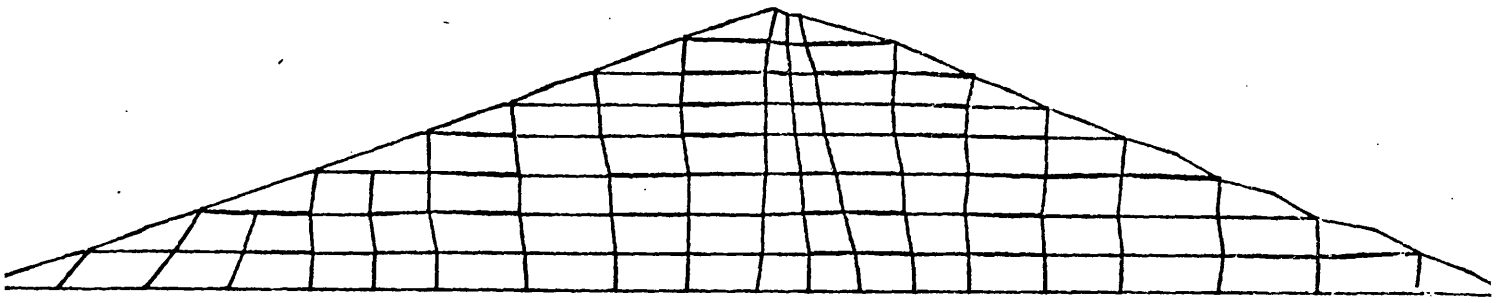

(2 sec)

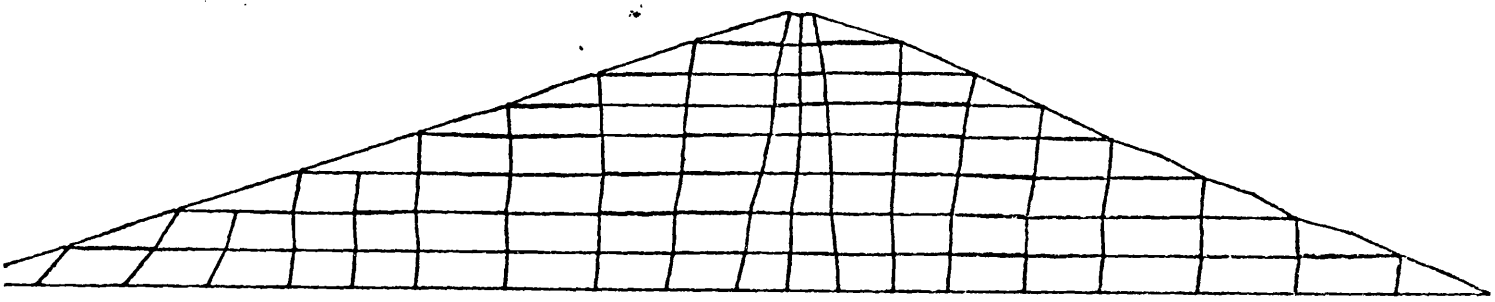

(4 sec)

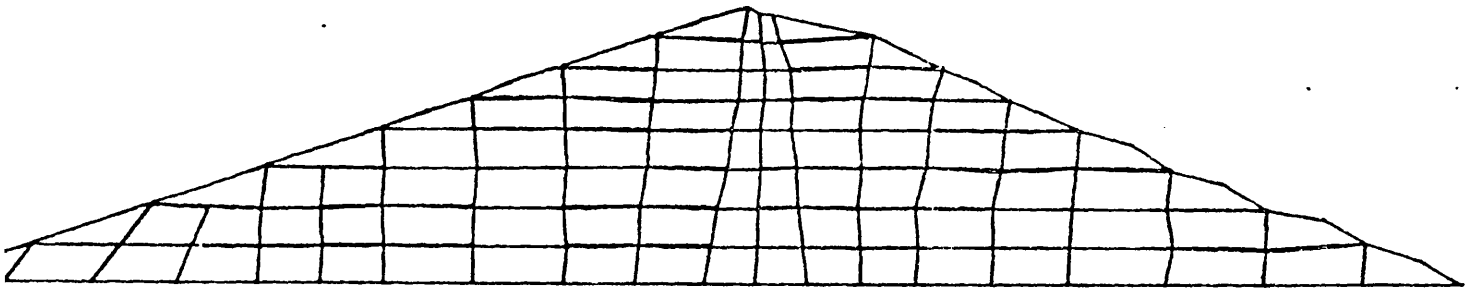

(6 sec)

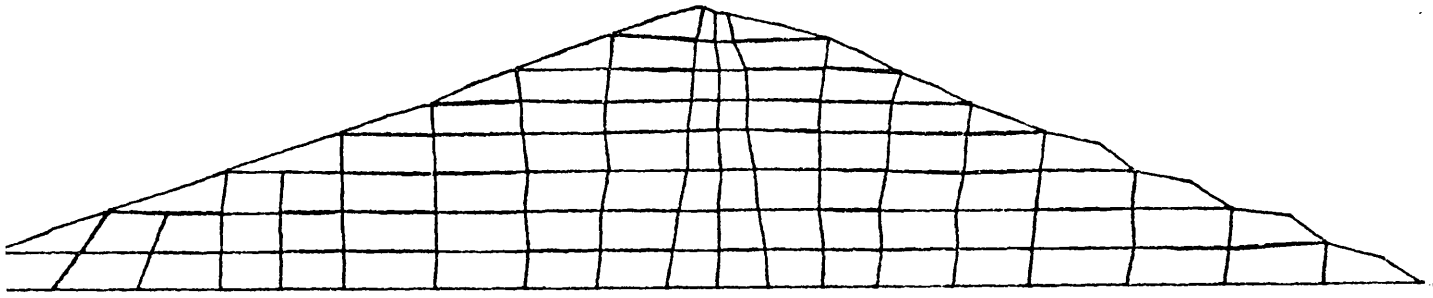

(8 sec)

Fig. 3.8 DEFORMED MESH OF 4 NODED FINITE ELEMENT MESH USING 2 x 2 INTEGRATION (DISPLACEMENT x 40)

CHAPTER 4

SOLUTION TECHNIQUE

4.1 INTRODUCTION

The use of finite element spatial discretization in nonlinear transient dynamic problems leads to a system of second order differential equations with respect to time as given in Chapter 3. It appears that the only generally applicable technique for nonlinear analysis of the coupled equations of motion is by the direct numerical step by step integration in time, where either implicit or explicit time stepping schemes may be utilized for the integration operators.

If the solution of time at $t + \Delta t$ is based on using the equilibrium conditions at time t, the integration procedure is called the explicit integration method. If the solution of time at $t + \Delta t$ is based on using the equilibrium conditions at time $t + \Delta t$ it is called the implicit integration method.

The implicit schemes result in the solution of coupled nonlinear algebraic equations at each time step and these schemes can be unconditionally stable[1,2]. On the other hand, the explicit schemes, if the mass and the damping matrices are diagonalized as described in Chapter 3, result in a system of uncoupled equations. Therefore, the computation can be carried out node by node involving only matrix multiplication with no need for matrix inversion. The programs based on the explicit method require a small amount of computer core and computing time per time step. However, the explicit schemes are conditionally stable and will be unstable if the time step length used is greater than the critical value.

For many elastoplastic problems, it has been shown[3,4] that the central difference explicit scheme is superior to any implicit scheme, especially, for a system of large bandwidth. The advantage of the implicit schemes in linear problems is the possible use of a relatively large time step, when these schemes are unconditionally stable. However, for materially nonlinear problems large time steps cannot be used, since the stress should follow the nonlinear material constitutive curve. In the case of a moderately or highly nonlinear material, the required material time step is often less than the dynamic stability limit, especially when the applied loads are changed rapidly as earthquake condition. In elasto/viscoplastic problems, pseudo time steps are allowed between each dynamic time step and stresses are permitted to be temporarily outside the yield surface. Therefore, the explicit scheme may not be superior to the implicit scheme. Consequently, it is of interest to compare the efficiency of both implicit and explicit schemes in the nonlinear dynamic analyses based on an elasto/viscoplastic constitutive model. In this chapter, the computation algorithms for both schemes are discussed and illustrated by an example.

4.2 IMPLICIT TIME STEPPING SCHEME

Equation (3.3) in the case of nonlinear systems can be written at time $t + \Delta t$ as[5,6,7]

$$\underset{\sim}{M}({}^{t}\ddot{\underset{\sim}{a}} + \Delta\ddot{\underset{\sim}{a}}) + \underset{\sim}{C}({}^{t}\dot{\underset{\sim}{a}} + \Delta\dot{\underset{\sim}{a}}) + \int_{\Omega} \underset{\sim}{B}^{T}({}^{t}\underset{\sim}{\sigma} + \Delta\underset{\sim}{\sigma})\, d\Omega = {}^{t+\Delta t}\underset{\sim}{R} \qquad (4.1)$$

in which $\Delta\ddot{\underset{\sim}{a}}$, $\Delta\dot{\underset{\sim}{a}}$, $\Delta\underset{\sim}{\sigma}$ are the changes in the acceleration, velocity and stress during the time increment Δt. Hence equation (4.1) can be written in incremental form as follows

$$\underset{\sim}{M}\,\Delta\ddot{\underset{\sim}{a}} + \underset{\sim}{C}\,\Delta\dot{\underset{\sim}{a}} + \int_{\Omega} \underset{\sim}{B}^{T}\,\Delta\underset{\sim}{\sigma}\,d\Omega = {}^{t+\Delta t}\underset{\sim}{R} - \underset{\sim}{M}\,{}^{t}\ddot{\underset{\sim}{a}} - \underset{\sim}{C}\,{}^{t}\dot{\underset{\sim}{a}} - \int_{\Omega} \underset{\sim}{B}^{T}\,{}^{t}\underset{\sim}{\sigma}\,d\Omega \qquad (4.2)$$

The incremental form of stress can be approximated as

$$\Delta\underset{\sim}{\sigma} = \underset{\sim}{D}\,(\underset{\sim}{B}\,\Delta\underset{\sim}{a} - \Delta\underset{\sim}{\varepsilon}_{VP}) \qquad (4.3)$$

in which $\Delta\underset{\sim}{\varepsilon}_{VP}$ is the viscoplastic strain increment as given in Chapter 2. If equation (4.3) is substituted into equation (4.2), the resulting incremental equations of motion can be written as

$$\underset{\sim}{M}\,\Delta\ddot{\underset{\sim}{a}} + \underset{\sim}{C}\,\Delta\dot{\underset{\sim}{a}} + \underset{\sim}{K}\,\Delta\underset{\sim}{a} = {}^{t+\Delta t}\underset{\sim}{R} - \underset{\sim}{M}\,{}^{t}\ddot{\underset{\sim}{a}} - \underset{\sim}{C}\,{}^{t}\dot{\underset{\sim}{a}} - {}^{t}\underset{\sim}{F}_{E} + \underset{\sim}{F}_{VP} \qquad (4.4)$$

in which $\underset{\sim}{K} = \int_{\Omega} \underset{\sim}{B}^{T}\,\underset{\sim}{D}\,\underset{\sim}{B}\,d\Omega$, ${}^{t}\underset{\sim}{F}_{E} = \int_{\Omega} \underset{\sim}{B}^{T}\,{}^{t}\underset{\sim}{\sigma}\,d\Omega$ and

$$\underset{\sim}{F}_{VP} = \int_{\Omega} \underset{\sim}{B}^{T}\,\underset{\sim}{D}\,\underset{\sim}{\varepsilon}_{VP}\,d\Omega$$

The numerical integration of equation (4.4) is carried out by Newmark's generalized acceleration method. This method uses two free parameters θ and β which indicate the effect of acceleration at the end of a time interval on the relation with velocity and displacement increments during the interval. It is worthwhile noting at this stage that in the following formulation, the unconditional stability persists if $\beta \geq \frac{1}{4}$ and the central difference time stepping scheme is regained if $\beta = 0$. An alternative derivation of recurrence formulae based on finite element approximation can be seen in the text by Zienkiewicz[2]. The expressions for incremental velocity and displacement are written as follows[8],

$$\Delta\dot{a} = \theta\,\Delta t\,{}^{t+\Delta t}\ddot{\underset{\sim}{a}} + (1-\theta)\,\Delta t\,{}^{t}\ddot{\underset{\sim}{a}} \qquad (4.5)$$

$$\Delta a = \beta\,\Delta t^{2}\,{}^{t+\Delta t}\ddot{\underset{\sim}{a}} + (0.5-\beta)\,\Delta t^{2}\,{}^{t}\ddot{\underset{\sim}{a}} + \Delta t\,{}^{t}\dot{\underset{\sim}{a}}$$

Making use of equation (4.5), $\Delta\ddot{\underset{\sim}{a}}$, and $\Delta\dot{\underset{\sim}{a}}$ can be represented in terms of $\Delta\underset{\sim}{a}$, ${}^{t}\dot{\underset{\sim}{a}}$, ${}^{t}\ddot{\underset{\sim}{a}}$ and substituting $\Delta\underset{\sim}{a}$, $\Delta\dot{\underset{\sim}{a}}$, $\Delta\ddot{\underset{\sim}{a}}$ into equation (4.4) and simplifying finally yields the equation in the following form,

$$\overset{*}{\underset{\sim}{K}}\ \Delta\underset{\sim}{a} = \overset{*}{\underset{\sim}{R}} \tag{4.6}$$

in which

$$\overset{*}{\underset{\sim}{K}} = \underset{\sim}{K} + \frac{\underset{\sim}{M}}{\beta\ \Delta t^2} + \frac{\theta\ \underset{\sim}{C}}{\beta\ \Delta t}$$

$$\overset{*}{\underset{\sim}{R}} = {}^{t+\Delta t}\underset{\sim}{R} - \underset{\sim}{M}\left[(1-\frac{1}{2\beta})\,{}^{t}\ddot{\underset{\sim}{a}} - \frac{{}^{t}\dot{\underset{\sim}{a}}}{\beta\Delta t}\right] + \underset{\sim}{C}\left[(\frac{\theta}{2\beta}-1)\,\Delta t\ {}^{t}\ddot{\underset{\sim}{a}} + (\frac{\theta}{\beta}-1)\,{}^{t}\dot{\underset{\sim}{a}}\right] - {}^{t}\underset{\sim}{F}_{E} + \underset{\sim}{F}_{VP}$$

Solving equation (4.6) for $\Delta\underset{\sim}{a}$ then the acceleration, velocity and displacement at time step $t + \Delta t$ can be obtained from the following equations

$$\begin{aligned}
{}^{t+\Delta t}\ddot{\underset{\sim}{a}} &= \frac{\Delta\underset{\sim}{a}}{\beta\ \Delta t^2} - \frac{{}^{t}\dot{\underset{\sim}{a}}}{\beta\ \Delta t} - \frac{{}^{t}\ddot{\underset{\sim}{a}}}{2\beta} + {}^{t}\ddot{\underset{\sim}{a}} \\
{}^{t+\Delta t}\dot{\underset{\sim}{a}} &= {}^{t}\dot{\underset{\sim}{a}} + \theta\Delta t\ {}^{t+\Delta t}\ddot{\underset{\sim}{a}} + (1-\theta)\ \Delta t\ {}^{t}\ddot{\underset{\sim}{a}} \qquad (4.7) \\
{}^{t+\Delta t}\underset{\sim}{a} &= {}^{t}\underset{\sim}{a} + \Delta t\ {}^{t}\dot{\underset{\sim}{a}} + \beta\Delta t^2\ {}^{t+\Delta t}\ddot{\underset{\sim}{a}} + (0.5-\beta)\ \Delta t^2\ {}^{t}\ddot{\underset{\sim}{a}}
\end{aligned}$$

A brief summary of the implicit time stepping scheme is given in Table 4.1.

4.3 EXPLICIT TIME STEPPING SCHEME

The ordinary differential equation (3.3) can also be solved using the central difference time stepping algorithm with[2,6,9]

$$\begin{aligned}
{}^{t}\ddot{a} &= \frac{1}{\Delta t^2}\{{}^{t-\Delta t}a - 2\,{}^{t}a + {}^{t+\Delta t}a\} \qquad (4.8) \\
{}^{t}\dot{a} &= \frac{1}{2\Delta t}\{-{}^{t-\Delta t}a + {}^{t+\Delta t}a\}
\end{aligned}$$

Substituting equation (4.8) into equation (3.3) leads to

$$\underset{\sim}{M}\,\frac{{}^{t+\Delta t}\underset{\sim}{a} - 2\,{}^{t}\underset{\sim}{a} + {}^{t-\Delta t}\underset{\sim}{a}}{\Delta t^2} + \underset{\sim}{C}\,\frac{{}^{t+\Delta t}\underset{\sim}{a} - {}^{t-\Delta t}\underset{\sim}{a}}{2\Delta t} + {}^{t}\underset{\sim}{F} = {}^{t}\underset{\sim}{R} \qquad (4.9)$$

in which $t+\Delta t$, t, $t-\Delta t$ denote three consecutive time intervals with time step length Δt, ${}^{t}\underset{\sim}{F} = \int_{\Omega} \underset{\sim}{B}^{T}\,{}^{t}\sigma\, d\Omega$ and ${}^{t}\underset{\sim}{R} = \int_{\Omega} \underset{\sim}{N}^{T}\,\underset{\sim}{f}\, d\Omega + \underset{\sim}{M}\,{}^{t}\ddot{\underset{\sim}{a}}$.

If values of ${}^{t}\underset{\sim}{a}$, ${}^{t-\Delta t}\underset{\sim}{a}$ are known, the value of ${}^{t+\Delta t}\underset{\sim}{a}$ can readily be obtained as

$${}^{t+\Delta t}\underset{\sim}{a} = \left[\underset{\sim}{M} + \underset{\sim}{C}\,\frac{\Delta t}{2}\right]^{-1} \left[(\Delta t)^2\,(-{}^{t}\underset{\sim}{F} + {}^{t}\underset{\sim}{R}) + 2\underset{\sim}{M}\,{}^{t}\underset{\sim}{a} - (\underset{\sim}{M} - \underset{\sim}{C}\,\frac{\Delta t}{2})\,{}^{t-\Delta t}\underset{\sim}{a}\right] \qquad (4.10)$$

Furthermore, upon introducing the diagonal lumped mass matrix and the damping matrix as presented in Chapter 3, equation (4.10) can be rewritten, for i^{th} term of the $\underset{\sim}{a}$ vector, as follows

$${}^{t+\Delta t}a_i = \frac{1}{M_i + C_i\,\frac{\Delta t}{2}} \left[(\Delta t)^2\,(-{}^{t}F_i + {}^{t}R_i) + 2M_i\,{}^{t}a_i - (M_i - C_i\,\frac{\Delta t}{2})\,{}^{t-\Delta t}a_i\right] \qquad (4.11)$$

The computation of ${}^{t+\Delta t}a_i$ is straightforward provided the forces ${}^{t}F_i$ and ${}^{t}R_i$ can be determined. In the finite element context, the total force at i is the summation of element contribution, i.e.,

$${}^{t}F_i = \sum_{e=1}^{m} {}^{t}F_i^{e} \;;\; {}^{t}R_i = \sum_{e=1}^{m} {}^{t}R_i^{e} \qquad (4.12)$$

where the superscript e stands for a particular element and m denotes the number of elements meeting at the i^{th} nodal point. It is therefore obvious that it is unnecessary to assemble the full vector of forces before the calculation starts and that the computation of ${}^{t+\Delta t}a_i$ can be

carried out node-by-node (or more exactly degree of frædom by degree of freedom) thereby avoiding large storage requirements.

It can be observed that with the central difference schemes, the calculation of ${}^{t+\Delta t}a$ involves ${}^{t}a$ and ${}^{t-\Delta t}a$. Therefore, to get the solution of time t=Δt, a special starting procedure must be used. Since ${}^{o}a$, ${}^{o}\dot{a}$ and ${}^{o}\ddot{a}$ are known, (note that with ${}^{o}a$ and ${}^{o}\dot{a}$ known, ${}^{o}\ddot{a}$ can be calculated using equation (3.3) at time t = 0) the relations in equation (4.8) can be used to obtain ${}^{-\Delta t}a$, i.e.,

$$ {}^{-\Delta t}a_i = {}^{o}a_i - \Delta t\, {}^{o}\dot{a}_i + \frac{\Delta t^2}{2}\, {}^{o}\ddot{a}_i \qquad (4.13) $$

A brief summary of the explicit time stepping scheme is given in Table 4.2.

It is noted that the stability of the explicit central difference time stepping schemes is conditional. If the highest frequency λ_{max} of the discretized system is available the critical time step is given as[10]

$$ \Delta t_{crit} \leq \frac{2}{\lambda_{max}} \qquad (4.14) $$

It appears that the estimate of the critical time step length, Δt_{crit}, necessitates the solution of the eigenvalue problem for the whole system. However, the bound on the highest eigenvalue can be simply obtained by the consideration of an individual element. This is established by an important theorem[11] that the highest system eigenvalue must always be less than the highest eigenvalue of the individual elements. This permits a very easy estimate of the critical time step length which will err on the safe side. Based on this theorem, the critical time step length in a plane strain elastic problem is given as[12,13]

$$\Delta t \leq \frac{\bar{\beta}L}{c} = \bar{\beta}L \left[\frac{\rho(1+\nu)\ (1-2\nu)}{E(1-\nu)}\right]^{\frac{1}{2}} \tag{4.15}$$

where c is the current wave speed, L is the smallest distance between any two adjacent nodes and $\bar{\beta}$ is a parameter less than unity and depends on the type of the element used. Generally, for linear elements, $\bar{\beta}$ ranges from 0.9 to 1.0, while for quadratic elements, $\bar{\beta}$ ranges from 0.2 to 0.6. In equation (4.15) E and ν are Young's modulus and Poisson's ratio of the material respectively. Although equation (4.15) is intended for elastic situations, experience indicates that it leads to conservative estimates for Δt in nonlinear problems.

When an elasto/viscoplastic material model is adopted then the critical time step associated with the evaluation of the viscoplastic strain rate may in certain circumstances govern the time step length used in time stepping schemes. The critical time step length for the quasi-viscoplastic analysis has already been discussed in Chapter 2[17,18].

4.4 COMPARISON OF THE IMPLICIT TIME STEPPING SCHEME AND THE EXPLICIT TIME STEPPING SCHEME

It has been noted previously that the implicit time stepping scheme is unconditionally stable, therefore, a relatively large time step length can be adopted compared with the explicit time stepping scheme. In practical applications, the size of time step for the implicit time stepping scheme is governed by the consideration of accuracy rather than by stability and it is usually taken as $\frac{1}{50}$ to $\frac{1}{100}$ of the longest period[15,16]. However, the advantage of large size of time step length for the implicit scheme might be eliminated due to the fact that this scheme involves the solution of a set of simultaneous equations. Consequently, it requires more computational effort per time step, also the computing time and computer core storage increase in direct proportion

to the bandwidth of the system. In an elasto/viscoplastic model the effect of material nonlinearity on dynamic time step length is not so crucial as it is in an elastoplastic model. In the elastoplastic analysis, the dynamic time step is, especially in highly nonlinear material, often limited by material plasticity. It will soon become unstable if the time step is too large. However the elasto/viscoplastic model has the advantage of allowing a separate pseudo time step within each dynamic time step so that the nonlinear internal resisting forces can be computed iteratively within each dynamic time step without increasing significantly the amount of computing time. And also, the viscoplastic model has the advantage of allowing stresses temporarily outside the yield surface, which is more reasonable. These permit us to choose freely the dynamic time step length as far as the numerical stability in the quasi-static viscoplastic computation is satisfied which for Mohr-Coulomb criterion with associative flow law can be recalled from Chapter 2 as follows

$$\Delta t_{M\text{-}C} \leq \frac{4(1+\nu)\ (1-2\nu)\ C\ \cos\phi}{\gamma E(1-2\nu + \mathrm{Sin}^2\phi)} \tag{4.16}$$

Furthermore, the use of efficient equation solvers such as FRONTAL solution techniques[14] could save a considerable amount of computer core storage and computation time. As a result, the implicit time stepping scheme could be a promising technique in the nonlinear dynamic study.

On the other hand, the explicit time stepping schemes as described previously involve no matrix factorization, therefore, compared with the implicit time stepping scheme less computer storage as well as computation effort per time step is needed and it is much easier to program, but this scheme is restricted to small time steps as given in equation (4.15).

It can be seen from equation (4.15) that the length of time step in the explicit time stepping scheme is directly related to the element type adopted and the coarseness of element mesh and is in direct proportion to the smallest distance between any adjacent nodes of the finite element mesh and in inverse proportion to the speed of wave propagation. Therefore, this scheme is rather inefficient in the quadratic element with very close nodes and irregular finite element mesh and where wave speeds are very high while the implicit time stepping scheme is not affected by these factors. On the other hand, because the explicit time stepping scheme requires no matrix factorization, it can be used to solve static problems with large bandwidths or frontwidths which are beyond the capability of static system solvers or which is anyway more easily solved by so called "dynamic relaxation techniques" (for details see Appendix B). It is quite obvious that a transient dynamic solution leads to static solution if critical damping is introduced and a steady state condition is reached, i.e., $\ddot{\underset{\sim}{a}} = \dot{\underset{\sim}{a}} = 0$.

It is worthwhile noting that the explicit time stepping scheme is incapable of dealing with high frequencies especially in the low frequency dominated systems while the implicit time stepping scheme, with suitable choice of time step length, is able to cut off frequencies which are not of interest.

In order to show the relative efficiency of the implicit time stepping scheme and the explicit time stepping scheme in elasto/visco-plastic transient dynamic studies, an earth dam subjected to base accelerations was analyzed. The earth dam with dimensions and material properties shown in Figure 4.1 is subjected to uniform base accelerations.

The displacement time histories of the dam crest obtained from both implicit and explicit schemes are presented in Figure 4.2. For comparison, the time step lengths and computation times used on a CDC 7600 computer are given in Table 4.3. It can be seen in Table 4.3 that the implicit scheme is more efficient than the explicit scheme. However, in the present study the explicit scheme is adopted because the complex material law in nonlinear analysis is much more easily incorporated in an explicit scheme.

REFERENCES

1. BATHE,K.J. and WILSON,E.L.
'Stability and accuracy analysis of direct integration methods'
Int. Jnl. Earthquake Eng. and Struct. Dyn., 1, 283-291, (1973).

2. ZIENKIEWICZ,O.C.
'The Finite Element Method'
McGraw-Hill, London, (1977).

3. WEEKS,G.
'Temporal operators for nonlinear structural dynamic problems'
Jnl. Eng. Mech. Div. ASCE, 98, 1087-1104, (1972).

4. BELYTSCHKO,T.
'Transient analysis'
Structural Mechanics Computer Programs, ed. by W. Pilkey et. al.,
(Univ. Press of Virginia) 255-276, (1974).

5. WARBURTON,G.B.
'Recent advances in structural dynamics'
Symp. on Dynamic Analysis of Structures, N.E.L., East Kilbride,
Scotland, (1975).

6. BATHE,K.J. and WILSON, E.L.
'Numerical Methods in Finite Element Analyses'
Prentice-Hall, (1976).

7. THAKKAR,S.K. and STAGG,K.G.
'Nonlinear dynamic analysis of stress wave propagation to
problems using parabolic isoparametric elements'
Report to S.R.C., (1977).

8. NEWMARK,N.M.
'A method of computation for structural dynamics'
Jnl. of Engg. Mech. Div., Proc. ASCE, 85, 67-94, (1959).

9. SHANTARAM,D.
'Dynamic transient analysis of structures including geometric
and/or material nonlinearity effects'
Ph.D. Thesis, Univ. of Wales, Swansea, (1976).

10. LEECH,J.W., HSU,P.T. and MACK,E.W.
'Stability of a finite difference method for solving matrix
equations'
AIAA, J. 3, 2172-2173, (1965).

11. IRONS,B.M.
'Applications of a theorem on eigenvalues to finite element
problems'
Univ. of Wales, Swansea, CR/132/70, (1970).

12. SHANTARAM,D., OWEN,D.R.J. and ZIENKIEWICZ,O.C.
'Dynamic transient behaviour of two and three-dimensional structures including plasticity, large deformation effects and fluid interaction'
Int. Jnl. Earthquake Eng. and STruct. Dyn., 4, 561-578, (1976).

13. BELYSCHKO,T., HOLMES,N. and MULLEN,R.
'Explicit integration-stability, solution properties, cost, finite element analysis of transient nonlinear structural behaviour'
Presented at the Winter Annual Meeting of the ASME, Houston, Texas, (1975).

14. HINTON,E. and OWEN,D.R.J.
'Finite Element Programming'
Academic Press, (1977).

15. CLOUGH,R.W. and PENZIEN,J.
'Dynamics of Structures'
McGraw-Hill Book Co., New York, (1975).

16. NEWMARK,N.M. and ROSENBLUETH,E.
'Fundamentals of Earthquake Engineering'
Prentice-Hall, Inc., Englewood Cliffs, N.J., (1971).

17. CORMEAU,I.C.
'Numerical stability in quasi-static elasto-visco/plasticity'
Int. Jnl. Num. Meth. Engng. 9, 109-127, (1975).

18. CORMEAU,I.C.
'Viscoplasticity and plasticity in the finite element method'
Ph.D. Thesis, Univ. of Wales, Swansea, (1976).

TABLE 4.1 SUMMARY OF THE IMPLICIT TIME STEPPING SCHEME

1. Basic Computation

   (1) Specify the parameters β, θ and time step t.

   (2) Compute the following constants

$$a_1 = \frac{1}{\beta\,\Delta t^2}, \quad a_2 = \frac{1}{\beta\,\Delta t}, \quad a_3 = \frac{1}{2\beta}, \quad a_4 = \frac{\theta}{\beta\,\Delta t}, \quad a_5 = \frac{\theta}{\beta}, \quad a_6 = \Delta t\,(\frac{\theta}{\beta} - 1)$$

   (3) Specify initial conditions: ${}^{o}\underset{\sim}{a}$, ${}^{o}\dot{\underset{\sim}{a}}$, ${}^{o}\ddot{\underset{\sim}{a}}$.

2. For each time step

   (4) Compute, if required, the effective stiffness matrix $\underset{\sim}{K}^{*}$ and form the effective force vector $\underset{\sim}{R}^{*}_{t}$ by equation (4.6).

   (5) Solve for $\Delta\underset{\sim}{a}_t$ by FRONTAL solution technique.

   (6) Update state of motion, at time $t+\Delta t$, by equation (4.7).

3. Computing $\underset{\sim}{F}_{VP}$ in equation (4.6) if required

   If at the beginning of a dynamic time step, state of stress falls outside the yield surface, compute $\dot{\underset{\sim}{\varepsilon}}_{VP}$, $d\underset{\sim}{\varepsilon}_{VP}$, and $d\underset{\sim}{F}_{VP}$ by using pseudo-time steps dt_{VP} as follows:

   (7) Compute $\dot{\underset{\sim}{\varepsilon}}_{VP}$ by equation (2.39).

   (8) Determine change in $\underset{\sim}{\varepsilon}_{VP}$ as $\Delta\underset{\sim}{\varepsilon}_{VP} = \dot{\underset{\sim}{\varepsilon}}_{VP}\, dt_{VP}$, while dt_{VP} is the pseudo-time step length which must satisfy the criteria given by Cormeau as $dt_{VP} = \frac{4(1+\nu)\,F_o}{3\,E}$ for Von Mises yield criterion.

   (9) Determine incremental force $d\underset{\sim}{F}_{VP} = \int_{\Omega} \underset{\sim}{B}^{T}\,\underset{\sim}{D}\,d\underset{\sim}{\varepsilon}_{VP}\,d\Omega$

   (10) Solve the equation $\underset{\sim}{K}^{*}\,d\underset{\sim}{a} = d\underset{\sim}{F}_{VP}$

   (11) Compute incremental changes in strain and stress.

TABLE 4.1 (cont'd)

(12) The values at $t_{VP} + \Delta t_{VP}$ (pseudo time) can be evaluated now

$$d\underset{\sim}{\varepsilon} = \underset{\sim}{B}^T d\underset{\sim}{a}$$

$$d\,{}^{t_{VP}+\Delta t_{VP}}\underset{\sim}{\sigma} = \underset{\sim}{D}(\underset{\sim}{B}\, d\underset{\sim}{a} - d\underset{\sim}{\varepsilon}_{VP})$$

$${}^{t_{VP}+\Delta t_{VP}}\underset{\sim}{\sigma} = {}^{t_{VP}}\underset{\sim}{\sigma} + d\,{}^{t_{VP}+\Delta t_{VP}}\underset{\sim}{\sigma}$$

$${}^{t_{VP}+\Delta t_{VP}}\underset{\sim}{\varepsilon} = {}^{t_{VP}}\underset{\sim}{\varepsilon} + d\underset{\sim}{\varepsilon}_{VP}$$

$${}^{t_{VP}+\Delta t_{VP}}F = {}^{t_{VP}}F + dF_{VP}$$

${}^{t_{VP}}\underset{\sim}{F} = 0$ at $t_{VP} = 0$ (at the beginning of pseudo-time step)

Note: displacements are not satisfied, i.e., ${}^{t+\Delta t}\underset{\sim}{a} = {}^{t}\underset{\sim}{a} + d\underset{\sim}{a}$ during pseudo time stepping, instead its effect is taken into account by adding pseudo load term $\underset{\sim}{F}_{VP}$ in the right hand side.

(13) Repeat steps 7 to 12 till steady state is reached, i.e., $\dot{\underset{\sim}{\varepsilon}}_{VP} \to 0$, the value of $\underset{\sim}{F}_{VP}$ at the end of steady state will be the value needed for equation (4.6).

4. $t \leftarrow t+\Delta t$ if $t \leq t_{max}$ go to step 2, otherwise stop.

TABLE 4.2 SUMMARY OF THE EXPLICIT TIME STEPPING SCHEME

1. Initialization

   (1) Specify initial conditions ${}^{0}\underset{\sim}{a}$, ${}^{0}\dot{\underset{\sim}{a}}$.

   (2) Select critical time step length.

2. Evaluation of displacement at node i, i.e., ${}^{t+\Delta t}\underset{\sim}{a}_i$.

   (3) Form $\int_{\Omega} \underset{\sim}{B}_i^T \, {}^{t}\underset{\sim}{\sigma}_i \, d\Omega$ and ${}^{t}\underset{\sim}{R}_i$.

   (4) Compute ${}^{t+\Delta t}\underset{\sim}{a}_i$ using equation (4.11).

3. Evaluation of ${}^{t+\Delta t}\underset{\sim}{\sigma}$ and ${}^{t+\Delta t}\dot{\underset{\sim}{\varepsilon}}_{VP}$ (required for next time step).

   (5) Compute the strains ${}^{t+\Delta t}\varepsilon = \underset{\sim}{B}_i^T \, {}^{t+\Delta t}\underset{\sim}{a}_i$

   (6) Compute the elastic strains ${}^{t+\Delta t}\underset{\sim}{\varepsilon}_E = {}^{t+\Delta t}\underset{\sim}{\varepsilon} - {}^{t+\Delta t}\underset{\sim}{\varepsilon}_{VP}$

   where ${}^{t+\Delta t}\underset{\sim}{\varepsilon}_{VP} = {}^{t}\underset{\sim}{\varepsilon}_{VP} + \dot{\underset{\sim}{\varepsilon}}_{VP} \Delta t$ and $\dot{\underset{\sim}{\varepsilon}}_{VP}$ is given by equation (2.39).

   (7) Calculate the stress ${}^{t+\Delta t}\sigma$ using equation (4.3).

4. $t \leftarrow t+\Delta t$ if $t \leq t_{max}$ go to 2, otherwise stop.

TABLE 4.3 COMPARISON OF IMPLICIT TIME INTEGRATION SCHEME AND EXPLICIT TIME INTEGRATION SCHEME

SCHEME	Time step length (s)	No. of time steps	Computing time (s)	Ratio of computing time
Implicit Scheme	T/100 = 0.01	1000	45	1.7
	T/50 = 0.02	500	26	1.0
	T/25 = 0.04	250	spurious response	
Explicit Scheme	0.0025	4000	104	4.0
	0.005	2000	unstable	

Notes: 1. Natural period T = 1.0 second.

2. Computer time is based on a CDC 7600.

3. Ratio of computing time is the computing time divided by that of T/50.

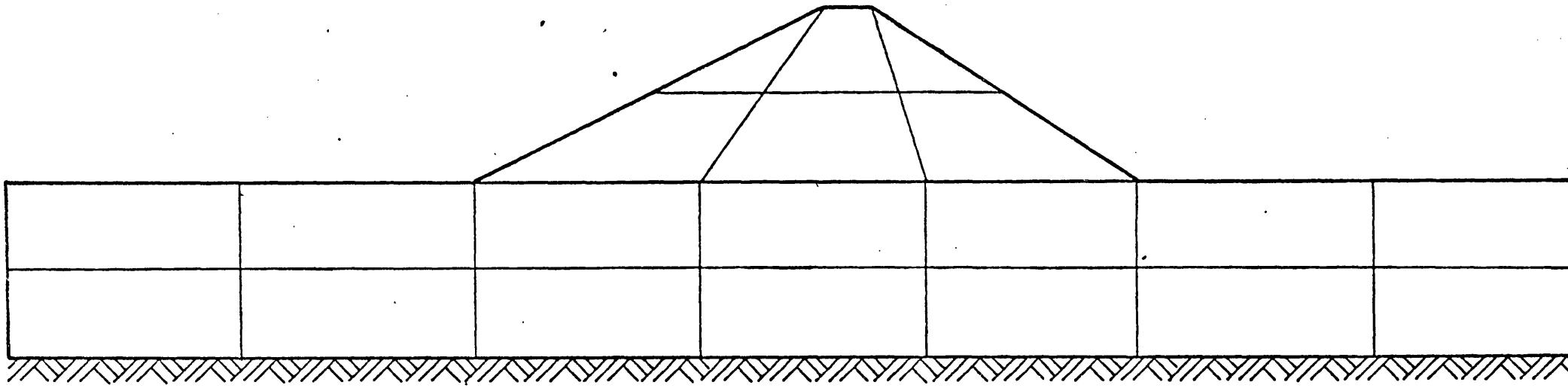

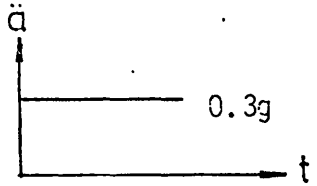

DIMENSIONS AND MATERIAL PROPERTIES ARE THE SAME AS FIG. 2.7

FIG. 4.1. EARTH DAM GEOMETRY AND BASE EXCITATION

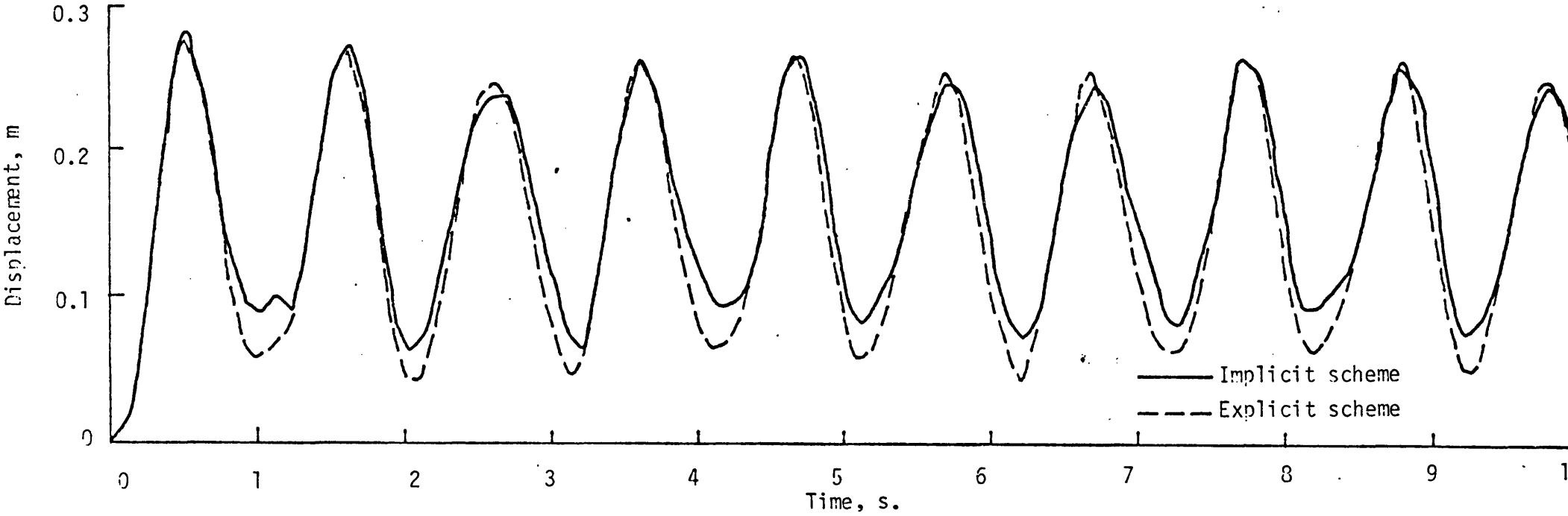

Fig. 4.2. HORIZONTAL DISPLACEMENT TIME HISTORY AT DAM CREST USING IMPLICIT TIME INTEGRATION SCHEME AND EXPLICIT TIME INTEGRATION SCHEME

CHAPTER 5

LIQUEFACTION

5.1 Introduction:

Loose saturated sand subjected to cyclic deviatoric stress will undergo volume change. This volume change in a drained condition produces densification whereas in an undrained condition it induces an excess pore pressure. When the excess pore pressure reaches the total mean stress then the sand loses its strength completely and behaves like a fluid. This is usually referred to as liquefaction. If the saturated sand can partially drain during shaking there will be simultaneous generation and dissipation of excess pore pressure. In this chapter, a completely undrained condition is presented. A fully drained condition, as well as dry sand, and a partially drained condition will be separately discussed in the next two chapters.

5.2 Physical Reality of Liquefaction:

Many failures of earth structures, slopes and foundations on saturated sands have been attributed in the relevant literature to the liquefaction of the sand. Liquefaction often occurs during or after earthquakes. The liquefaction of saturated sands physically manifests itself in the following ways[1].

(1) The soil loses its ability to support structures. Buildings sink into the soil. The most well known example was an apartment building which tilted some 80 degrees from the vertical during the Niigata earthquake of 1964[2,3].

(2) Slopes and embankments lose their strength and develop mud flows or soil flows. Two examples were the failure of both San Fernando dams during the earthquake in 1971[4].

(3) Sand boils, sand volcanos, sand cones, or sand fountains appear. These are ejections of sand and water from the surface. The water can squirt to heights of several feet. The sand, falling back to earth, forms a cone around the point of ejection. For this reason they are called boils or volcanos[5].

(4) Piles and caissons float out of the ground or lose lateral support. Extensive damage to the Alaskan highway and railroad bridges in the 1964 earthquake was caused by failure of the abutment piles in liquefied sands[6].

From numerous detailed studies of field cases under liequefaction and from other empirical evidence, it has been concluded that liquefaction occurs when the following conditions are present[7,8,9].

(1) The soil is a fine sand. The grain size, D_{50}, should be between 0.07^{mm} and 0.4^{mm}.

(2) The soil is uniform in grain size. Uniformity coefficients of 2 or less are common for liquefied soils.

(3) The soil is loose. It is generally accepted that soils denser than 70 percent relative density are not likely to liquefy.

(4) There is apparently a preferred zone for liquefaction. It has been indicated that the effective vertical stress should be less than $2.0^{kg/cm^2}$ to liquefy, which corresponds to a depth of less than 20 metres. Most instances of liquefaction have occurred at considerably shallower depths.

5.3 Undrained ~~Soil~~ Sand Behaviour under Cyclic Loading:

Typical undrained saturated sand tests show the following two phenomena[10,11,12]:

(1) An increase of pore pressure occurs with increasing number of cycles,

(2) The amplitude of strain increases until failure is reached at a large number of cycles.

Furthermore it appears that if failure is reached by cycling of if after cycling the sample is tested without drainage then its strength in terms of effective stress remains virtually unaltered, i.e. the strength decrease observed is simply related to the pore pressure increase. It is evident that the main effect of cycling is to cause the pore pressure to increase and this has to be correlated with cycling intensity.

Indeed if during cyclic loading, the pore pressure increases, the mean effective stress reduces to a value at which material failure is first observed. This point can be referred to as initial liquefaction. A further increase in the pore pressure reduces the mean effective stress to zero under which condition final liquefaction occurs and the soil flows like a fluid with zero shear resistance. Clearly the major phenomenon occuring during cycling is the compaction of the soil skeleton which transfers the total stress to the fluid.

5.4 Factors Affecting Liquefaction:

From the results of simple cyclic tests or triaxial tests, the factors affecting liquefaction, factors which are important for

choosing the proper parameters for numerical formulation, can be given as follows[13,14]:

(1) The shear stress or cyclic deviator stress required to cause liquefaction decreases with the number of cycles. Conversely, the number of cycles required to cause liquefaction decreases when shear stress or cyclic deviator stress increases.

(2) The shear stress or cyclic deviator stress and the number of cycles required to cause liquefaction decrease as the relative density decreases.

(3) For a given relative density and number of cycles, the required shear stress or deviator stress to cause liquefaction is directly proportional to the confining stress.

(4) Peacock and Seed[15] used a simple shear device to apply horizontal cyclic shear stresses rather than vertical cyclic loads. Their data showed only about half as much shear stress is required for liquefaction as would be predicted by the triaxial test results. This fact can be attributed to the rearrangement of soil particles which is mainly due to the deviatoric strain which is, in turn, directly related to the shear stress.

(5) Castro[16] found that loose sands tend to compress while being sheared and dense sands to dilate. There should be an intermediate density at which constant volume is maintained during shear. Casagrande proposed this as the critical void ratio and also indicated that it depends on the effective confining stress. The critical

void ratio is smaller for larger effective confining stresses. When a soil is saturated and undrained, dilatation is associated with a decrease in pore pressure. He also found that it was much more difficult to liquefy soils if their particles were angular than if they were rounded.

Therefore the main points affecting liquefaction can be again summarized as follows:

(1) The shear stress and shear strain,

(2) The confining stress,

(3) The relative density,

(4) The grain size and uniformity,

(5) The grain shape.

5.5 Evaluation of "autogenous" volumetric strain "ε_v^o"

As described in the previous sections, the cause of liquefaction in saturated sands is mainly due to the buildup of excess pore pressure during cyclic loading. Therefore, a full numerical analysis can be carried out if a means for evaluating the buildup of excess pore pressure is available. The description of the evaluation of excess pore pressure has been presented in Chapter 2, the mathematical model. The main points are recalled as follows:

The strain expressed in incremental form, as given by equation (2.9) can be represented as

$$d\underset{\sim}{\varepsilon} = d\underset{\sim}{\varepsilon}^{\sigma'} + d\underset{\sim}{\varepsilon}^{c} + \underset{\sim}{m}\frac{d\varepsilon_v^o}{3} \qquad (5.1)$$

The change of excess pore pressure with respect to the total

incremental volumetric strain, as given by equation (2.11), can be rewritten as

$$dp = \alpha \underset{\sim}{m}^T d\underset{\sim}{\varepsilon} \tag{5.2}$$

An alternative expression for pore pressure change (providing no change of total stress occurs and $d\varepsilon^c = 0$) is given by equation (2.22), i.e.,

$$dp = \beta d\varepsilon_v^o \tag{5.3}$$

From these expressions, it can be seen that the determination of the "autogenous" volumetric strain at any loading stage is clearly the crucial point of the present study. It is suggested that the autogenous volumetric strain ε_v^o is related to a quantity defining the total shear strain path and the relation of shear to mean stress. We shall thus write[17]

$$d\varepsilon_v^o = - f(\kappa)d\kappa \tag{5.4}$$

$$d\kappa = g(\theta)d\xi \tag{5.5}$$

in which the negative sign corresponds to the volume decrease and

$$d\xi = \sqrt{\tfrac{1}{2} d\underset{\sim}{e}^T d\underset{\sim}{e}} \tag{5.6}$$

and where

$$d\underset{\sim}{e} = d\underset{\sim}{\varepsilon} - \frac{\underset{\sim}{m}}{3} d\underset{\sim}{\varepsilon}_V \quad \text{and} \quad d\underset{\sim}{\varepsilon}_V = \underset{\sim}{m}^T d\underset{\sim}{\varepsilon} \tag{5.7}$$

represents the deviatoric strain increment, while θ is the ratio of the applied shear stress to the initial mean effective stress in the soil under simple shear tests. To generalize, the parameter θ will be defined as

$$\theta = \frac{\bar{\sigma}'}{\sigma'_{mo}} \tag{5.8}$$

where $\bar{\sigma}'$ is the second effective stress invariant and σ'_{mo} is the average effective mean stress at the start of cycling, i.e.,

$$\sigma'_{mo} = \underset{\sim}{m}^{To}\underset{\sim}{\sigma}'/3 \tag{5.9}$$

$$\bar{\sigma}' = (\tfrac{1}{2}\underset{\sim}{s} \cdot \underset{\sim}{s})^{\frac{1}{2}},\ \underset{\sim}{s} = \underset{\sim}{\sigma}' - \underset{\sim}{m}\,\sigma'_m/3 \text{ and } \sigma'_m = \underset{\sim}{m}^T\underset{\sim}{\sigma}' \tag{5.10}$$

and $f(\kappa)$ is a continuous monotonically decreasing function reflecting the fact that the densification increments decrease as the compaction occurs. Because $f(\kappa)$ is a monotonically decreasing function the simplest choice for $f(\kappa)$ is in the following form

$$f(\kappa) = \frac{A}{1 + B\kappa} \tag{5.11}$$

where A and B are constants for a given sand at a certain relative density. Based on experimental studies, $g(\theta)$ can be represented as

$$g(\theta) = \exp(r\theta) \tag{5.12}$$

in which r is a constant for the given sand.

One suitable expression which satisfies the conditions that A approaches zero as D_r approaches a certain critical density D_r^{cr}, and it must become negative when $D_r > D_c^{cr}$ to reflect the fact that shear at overcritical densities causes an increase in volume (called dilatancy) rather than densification, is

$$A = C\left(1 - \frac{D_r}{D_r^{cr}}\right)^n \tag{5.13}$$

in which C and n are constants for all densities of a given sand, and n must be an odd number. Substituting equations (5.13), (5.11) into

equation (5.4) and choosing n equal to unity, the following expression is obtained

$$d\varepsilon_v^o = -\frac{C(1-\frac{D_r}{D_{cr}})d\kappa}{1+B\kappa} = -\frac{Ad\kappa}{1+B\kappa} \tag{5.14}$$

(It is worthwhile mentioning that by properly choosing the sign of A, the expression (5.14) can represent densification as well as dilatancy). In the case of densification, the amount of volumetric strain is limited by the value of ε_v^o necessary to achieve the minimum void ratio, e_{min}. One such alternative form is given below. In place of equation (5.14), $d\varepsilon_v^o$ is given as

$$d\varepsilon_v^o = -\frac{C(\frac{e}{e_{min}}-1)^n d\kappa}{1+B\kappa} \tag{5.15}$$

where e is the current void ratio.

In the simple cyclic shear tests, the main volumetric strain is due to a rearrangement of grain configurations. Therefore, the change of excess pore pressure, by neglecting the contributions of elastic strain and creep, can be presented as

$$dp = d\varepsilon_v^o = \frac{\beta A d\kappa}{1+B\kappa} \tag{5.16}$$

or integrating yields

$$p = \frac{\beta A}{0.4343B}\log(1+B\kappa) \tag{5.17}$$

The way in which A, B and r are evaluated from the simple cyclic shear tests will now be explained. When the test is carried out, the values of the buildup of pore water pressure, p, and the development of cyclic shear strains γ are measured. In the special case of pure shear strain, $\gamma = 2e_{12}$ in which γ denotes the shear strain amplitude and $d\xi$ degenerates to [18,19]

$$d\xi = \left[\tfrac{1}{2}(d\underset{\sim}{e}^T d\underset{\sim}{e})\right]^{\frac{1}{2}} = (de_{xy}de_{xy} + de_{yx}de_{yx})^{\frac{1}{2}}\frac{1}{\sqrt{2}} = \left(\frac{\gamma}{2}\frac{\gamma}{2} + \frac{\gamma}{2}\frac{\gamma}{2}\right)^{\frac{1}{2}}\frac{1}{\sqrt{2}} = \frac{\gamma}{2} \qquad (5.18)$$

Therefore in the case of cyclic pure shear, the value of ξ at the end of every cycle, according to equation (5.18) is

$$\xi = 4\frac{\gamma}{2} = 2\gamma \qquad (5.19)$$

Hence the total straining path at the end of every cycle can be readily obtained by accumulating the values from equation (5.19). The pore pressure increases obtained from the tests are converted to an equivalent volumetric strain ε_v^o by the use of equation (5.16). This requires the introduction of a tangential bulk modulus of the dry sand and this value was taken here as

$$\beta = 100\ MN/m^2 \qquad (5.20)$$

The introduction of this parameter is not serious as it can be seen from equation (5.16) that βA can be considered as a single constant. Therefore with different values of β, simply change the value of A. After pore pressure is converted to an equivalent volumetric strain ε_v^o, the graph of ε_v^o against the length of the strain path ξ for each value of θ can be plotted. It is observed that $d\kappa$, evaluated using equation (5.5) is constant for a given volumetric strain, regardless of the value of θ. It has been found that the values of r remain nearly constant for all values of θ. Thus an average is adopted.

Having obtained r, the next step is to ascertain the values of A and B. The volumetric strain ε_v^o is plotted against κ, for all results obtained. Then the most suitable straight line is drawn through the points. Two points on this line are sampled then substituted into equation (5.17)

to give values of A and B. A better interpretation of the test results may be obtained by dividing the measurements into two parts: those obtained before initial liquefaction (i.e., where the excess pore pressure has reached a value of about 60 percent of the initial effective pressure) and those obtained after initial liquefaction. A straight line is then drawn through each set of results. Hence values of A and B are evaluated for both sets of results. The proposed empirical approach is based on data supplied for a sand tested by the Norwegian Geotechnical Institute (NGI)[20]. The tests were performed on a dense sand. The samples were consolidated to a vertical pressure, σ'_{vc}, of 20N/cm^2 under conditions of no lateral strain. Then a symmetrical two way cyclic horizontal shear stress amplitude, $\tau_{h,cy}$, was applied. (Note that $\theta = \frac{\tau_{h,cy}}{\sigma'_{vc}}$). The results are given as contours of pore pressure buildup and cyclic shear strain as shown in Figure (5.1) and Figure (5.2). The procedures outlined above were employed to estimate values of r, A and B. As illustrated in Figures (5.3 & 5.4). A value of 17.2 was obtained for r, while value of A = 0.012 and B = 55.5 were obtained from the data produced before initial liquefaction, and values of A = 0.0005 and B = 0.51 were obtained from the data produced after initial liquefaction.

The values of r, A and B may be used in equation (5.17) to give a simple, compact and accurate representation of the cyclic shear test results, and may be used in equation (5.14) for the numerical model in order to compute the autogenous volumetric strain.

5.6 Examples:

In order to illustrate the application of the method of analysis described in previous sections, a saturated sand layer

subjected to a sinusoidal acceleration as well as N-S component of El Centro Earthquake of May, 1940 scaled to 0.1g is given. This example is essentially one dimensional but it is solved here by the general procedure to obtain comparison with other published material[21,22,23

A 50 foot layer of sand with the water table at 5 feet below the ground surface is shown in Figure 5.5. This layer is subjected to a sinusoidal acceleration with a frequency of 2 cycles per second and with a maximum acceleration of 0.805 ft/sec^2 at the base of the stratum. The acceleration time history and displacement time history of the surface of the layer and the shear stress time history at point X are presented in Figures 5.6, 5.7 and 5.8 respectively. The rise of excess pore water pressure and normalized excess pore water pressure with depth at various times are presented in Figures 5.9 and 5.10 respectively. The build up of excess pore water pressure with respect to time at the critical layer is shown in Figure 5.11. It can be seen that for the method which does not take into account the autogenous volumetric strain, the motion in any layer quickly stabilized to a sinusoidal response at 2 cycles/sec. However the surface accelerations determined by the method which allow for the autogenous volumetric strain show a different response history. The responses are quite comparable with those of the method which take no account of autogenous volumetric strain up to 1 sec. This is attributable to the fact that in the early stages of the shaking the excess pore water pressures has not developed to the point where it has a significant effect on the dynamic response characteristics. After about 1 sec. the accelerations determined by the method which take into account of autogenous volumetric strain steadily decrease and reach zero after

final liquefaction.

It is worthwhile noting that the rate of build up of excess pore water pressure in the post-initial liquefaction range is faster than that of the pre-initial liquefaction range as shown in Figure 5.11. This trend is very similar to that occurring in simple cyclic shear tests as can be seen in Figure 5.4. The response of the same soil layer subjected to the N-S component of the El Centro earthquake scaled to a maximum acceleration of 0.1g has been studied and the results are presented in Figures 5.12 to 5.17. Figures 5.12, 5.13 and 5.14 show respectively the acceleration time history and displacement time history of the surface of the layer and the shear stress time history at point x. The rise of excess pore water pressure and the normalized excess pore water pressure with depth at various times are represented in Figures 5.15 and 5.16 respectively. The build up of excess pore water pressure with respect to time at the critical layer is shown in Figure 5.17. It can be seen that the proposed method predicts responses which are, qualitatively, similar to results obtained from site observation of Niigata earthquake in Japan in 1964[24].

It is of interest to mention that if the imposed frequency of the applied force is equal to or close to the natural frequency of a body, a beat will take place. In the present example, by chance, the natural frequency of the soil column is 2 cycles/sec which is exactly the same as the excitation force. Therefore, in free vibration, beating occurs as can be seen in Figures 5.18 to 5.20. However, in practical problems, this phenomenon rarely occurs. Beating can be eliminated by imposing a little damping to the system. The results with 5% of critical damping are also shown in the figures.

REFERENCES

1. CHRISTIAN, J.T.
'Liquefaction'
Course on Soil Dynamics for Earthquake Design, International Center for Computer Aided Design, Italy (1976)

2. SOILS AND FOUNDATIONS
Entire Issue Devoted to Soil Mechanics Aspects of the Niigata Earthquake, Vol. 6, No. 1 (1966)

3. SOILS AND FOUNDATIONS
Entire Issue Devoted to the Niigata Earthquake and Dynamic Properties of Soil, Vol. 6, No. 2 (1966)

4. SEED, H.B., LEE, K.L., IDRISS, I.M. and MAKDISI, F.
'Analysis of the Slides in the San Fernando Dams During the Earthquake of February 9th, 1971'
Earthquake Engineering Research Center, Report No. EERC 73-2, Univ. of California, Berkeley (1973)

5. SEED, H.B.
'Landslides During Earthquakes due to Soil Liquefaction'
Jnl. of the Soil Mechanics and Foundations Division, ASCE, Vol. 94, No. SM5, 1053-1122 (1968)

6. ROSS, G.A., SEED, H.B. and MIGLIACCIO, R.R.
'Bridge Foundation Behaviour in Alaska Earthquake'
Jnl. of the Soil Mechanics and Foundations Division, ASCE, Vol. 95, No. SM4, 1007-1036 (1969)

7. KISHIDA, H.
'Characteristics of Liquefied Sands During Mino-Owari Tohnankai and Fukui Earthquakes'
Soils and Foundations, Vol. 9, No. 1, 75-92 (1969)

8. KISHIKA, H.
'Characteristics of Liquefaction of Level Sandy Ground During the Tokachioki Earthquake'
Soils and Foundations, Vol. 10 No. 2, 103-111 (1970)

9. PALIT, R.M. and NATARAJAN,T.K.
'Susceptibility to Liquefaction of Submerged Sands'
Third Symposium on Earthquake Engineering, Roorkee, India, Vol. 1, 271-276 (1966)

10. LEE, K.L. and SEED, H.B.
'Cyclic Stress Conditions Causing Liquefaction of Sand'
Jnl. of the Soil Mechanics and Foundations Division, ASCE, Vol.93, No. SM5, 47-70 (1967)

11. LEE, K.L. and SEED, H.B.
'Dynamic Strength of Anisotropically Consolidated Sand'
Jnl. of the Soil Mechanics and Foundations Division, ASCE, Vol. 93, No. SM5, 169-190 (1967)

12. FINN, W.D.L., PICKERING, D.J. and BRANSBY, P.L.
'Sand Liquefaction in Triaxial and Simple Shear Tests'
Jnl. of the Soil Mechanics and Foundations Division,
ASCE, Vol. 97, No. SM4, 639-659 (1971)

13. SEED, H.B. and LEE, K.L.
'Liquefaction of Saturated Sands During Cyclic Loading'
Jnl. of the Soil Mechanics and Foundations Division, ASCE
Vol. 92, No. SM6, 105-134 (1966)

14. SEED, H.B.
'Evaluation of Soil Liquefaction Effects on Level Ground
During Earthquake'
Symposium on Soil Liquefaction, ASCE National Convention,
Philadelphia (1976)

15. PEACOCK, W.H. and SEED, H.B.
'Sand Liquefaction under Cyclic Loading Simple Shear
Conditions'
Jnl. of the Soil Mechanics and Foundations Division, ASCE,
Vol, 94, No. SM3, 689-708 (1968)

16. CASTRO, G.
'Liquefaction of Sands'
Harward Soil Mechanics Series No. 81, (1969)

17. ZIENKIEWICZ, O.C., CHANG, C.T. and HINTON, E.
'Nonlinear Seismic Response and Liquefaction'
Int. J. Num. Anal. Methods in Geomechanics, Vol. 2, 381-404 (1978)

18. BAZANT, Z.P. and KAIZEK
'Endochronic Constitutive Law for Liquefaction of Sand'
Jnl. of the Engineering Mechanics Division, ASCE, Vol. 102,
No. EM2, 225-238 (1976)

19. CUELLAR, V., BAZANT, Z.P., KAIZEK, R.J. and SILVER, M.L.
'Densification and Hysterisis of Sand under Cyclic Shear'
Jnl. of the Geotechnical Engineering Division, ASCE,
Vol. 103, No. GT5, 399-416 (1977)

20. ANDERSON, K.H.
'Private Communication'
An Interpretation of Data on Cyclic Load of Sand from Tests
given in Cyclic Loading in Simple Shear Test on Sand, Norwegian
Geotechnical Institute Report No. 51, 505-1 (1973)

21. FINN, W.D.L., BYRNE, P.M. and MARTIN, G.R.
'Seismic Response and Liquefaction of Sands'
Jnl. of the Geotechnical Engineering Division, ASCE
Vol. 102, No. GT8, 841-856 (1976)

22. GHABOUSSI, J. and WILSON, E.L.
'Liquefaction Analysis of Saturated Granular Soils'
5th World Conference on Earthquake Engineering, Rome, (1975)

23. GHABOUSSI, J. and DIKMEN, LASS-II
Computer Program for Analysis of Seismic Response and
Liquefaction of Horizontally Layered Saturated Sands,
Report No. UILU-ENG-77-2010, Department of Civil Engineering
University of Illinois at Urbana, Champaign, Urbana, Illinois (1977)

24. ISHIHARA, K., LYSMER, L., YASUDA, S. and HIRAS, H.
'Prediction of Liquefaction in Sand Deposits During Earthquakes,
Soils and Foundations, Vol. 16, No. 1 (1976)

25. ZIENKIEWICZ, O.C.
Lecture Note
Cyclic Loading, Progressive Deformation, Weaking and
Liquefaction, Course on Finite Elements in Geotechnical
Engineering Held at Swansea (1978)

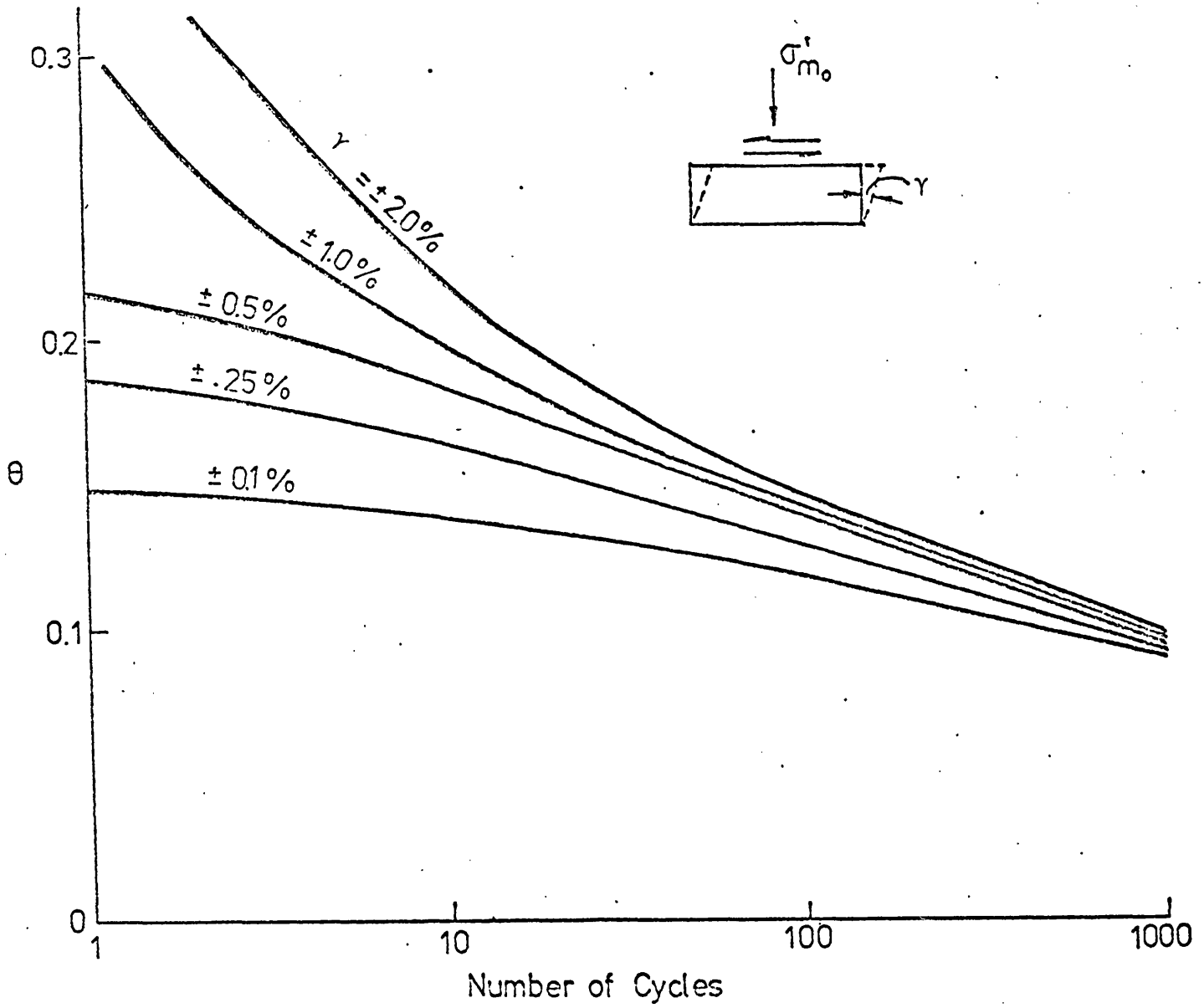

Fig. 5.1: Development of cyclic shear strains during undrained cyclic simple shear loading

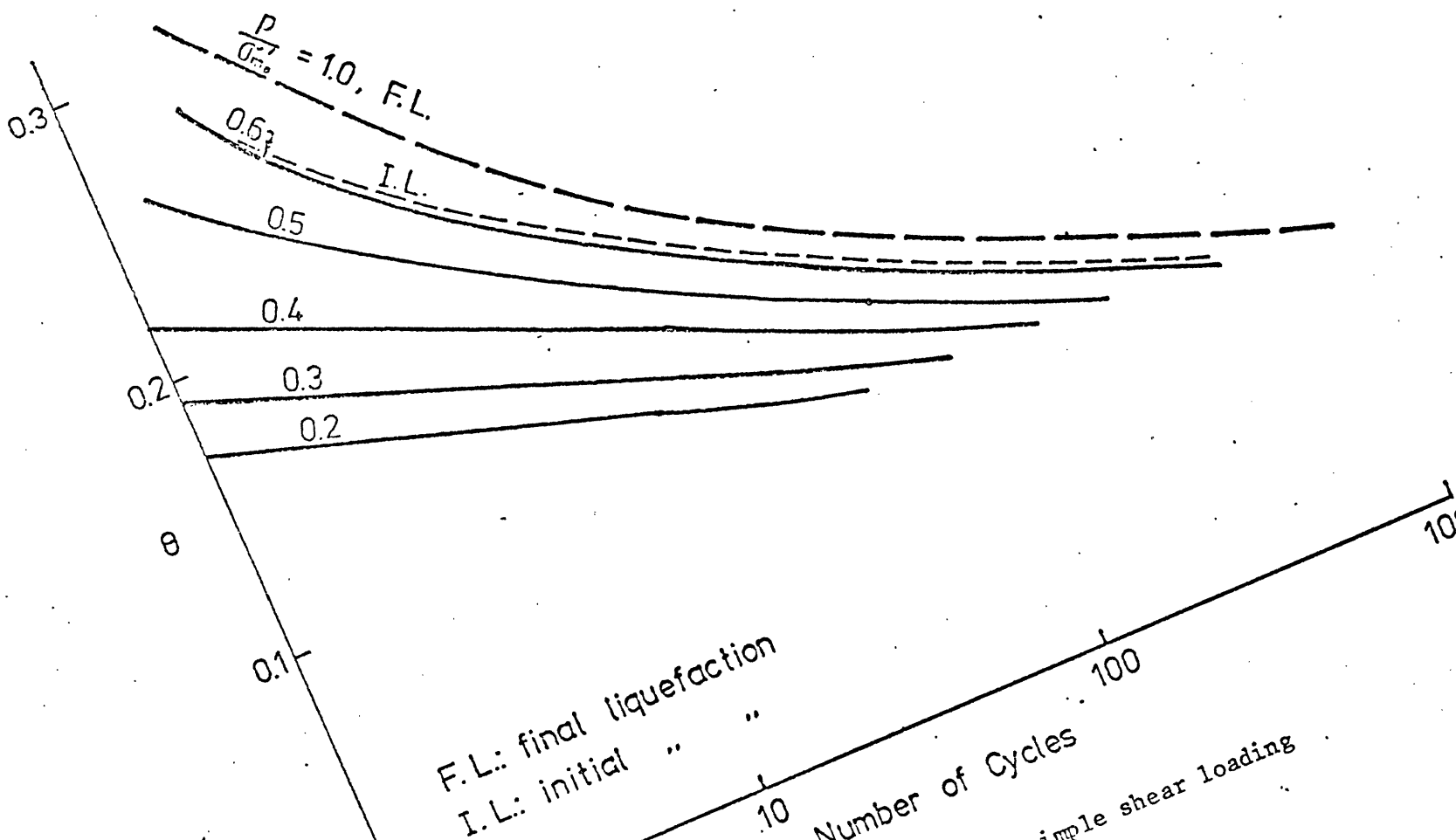
$\frac{p}{\sigma'_{vc}}$ = 1.0, F.L.
0.6
I.L.
0.5
0.4
0.3
0.2
0.3
0.2
0.1
θ
F.L.: final liquefaction
I.L.: initial " "
10
100
Number of Cycles
imple shear loading

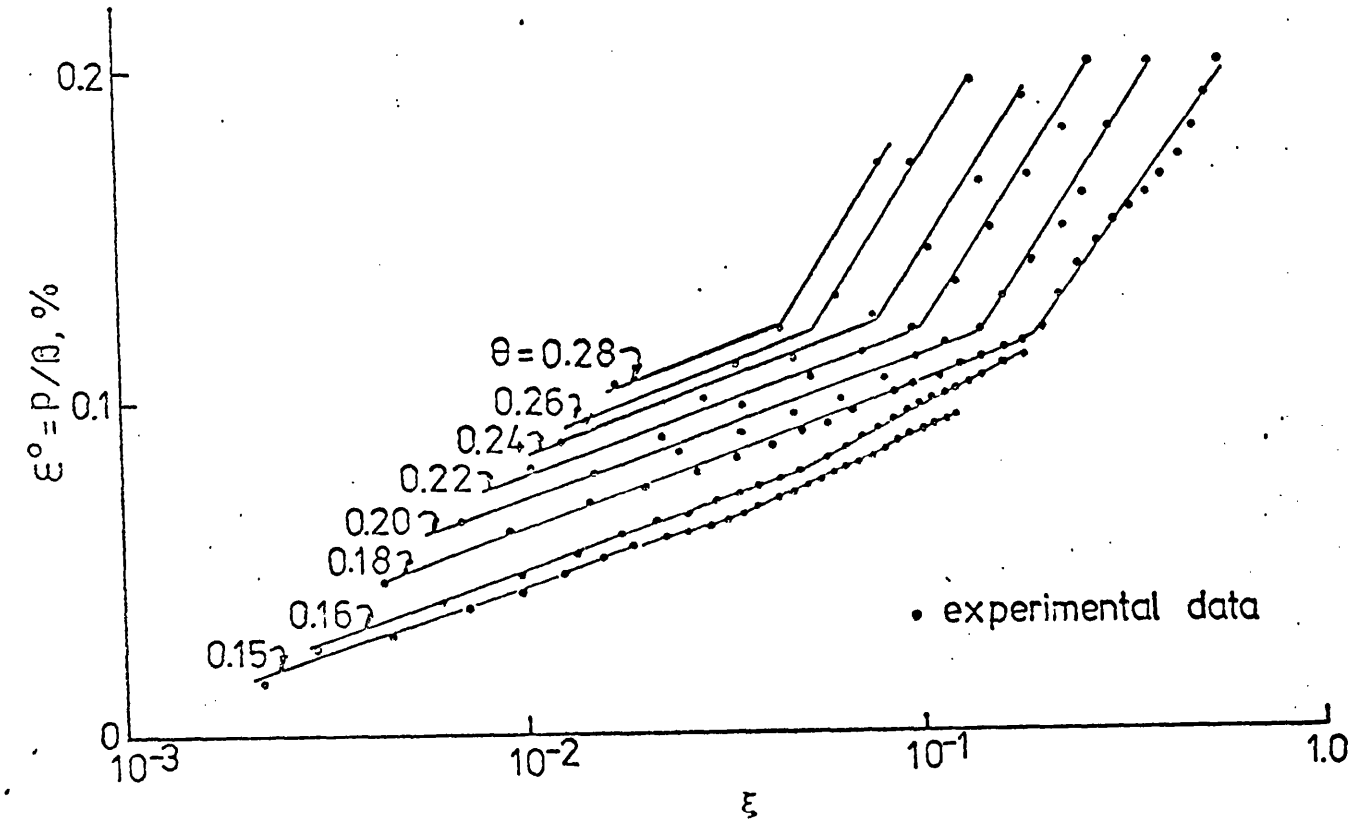

Fig.5.3:Autogenous volumetric strain versus the total strain path length ξ

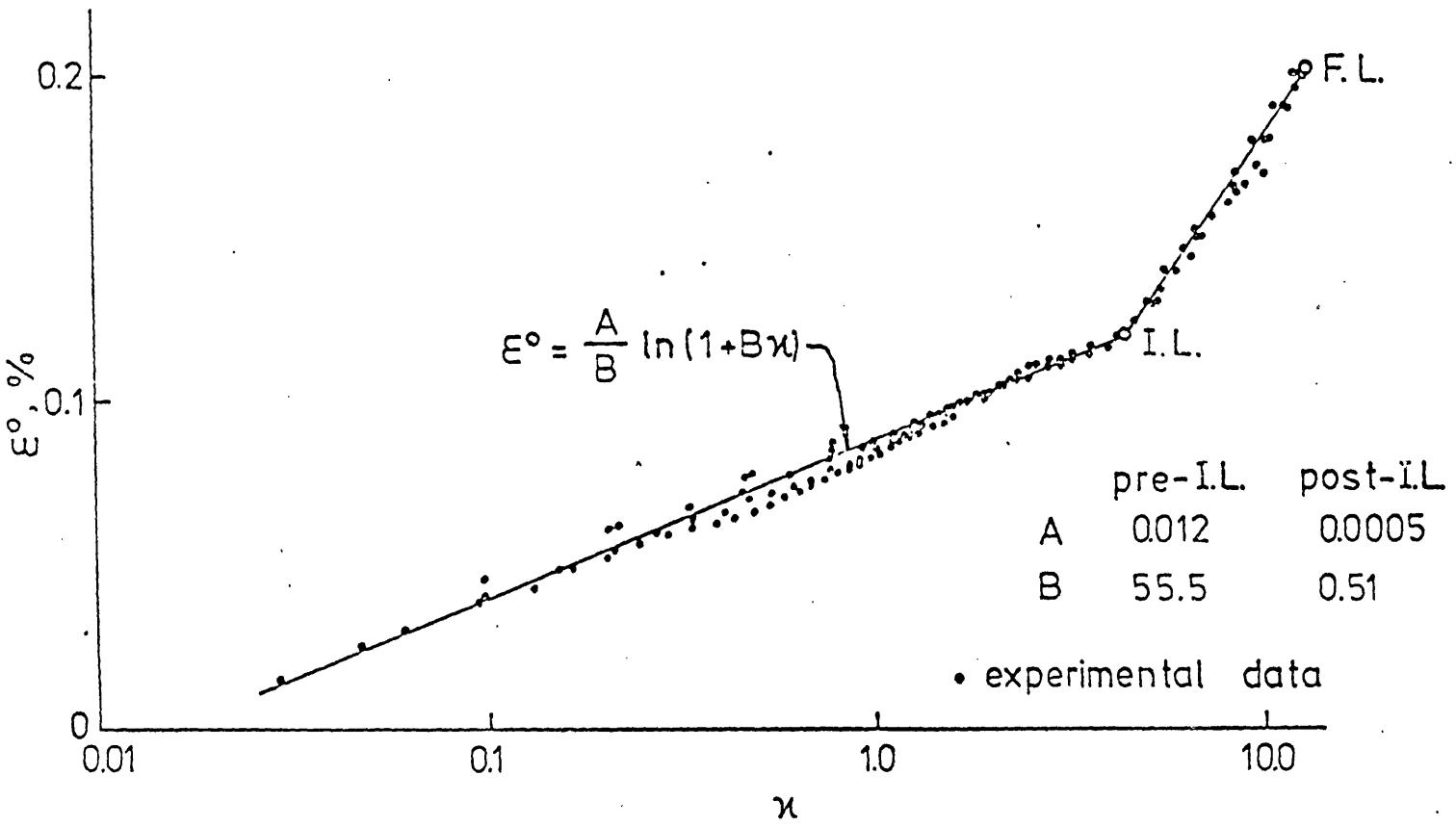

Fig. 5.4 Autogenous volumetric strain versus κ

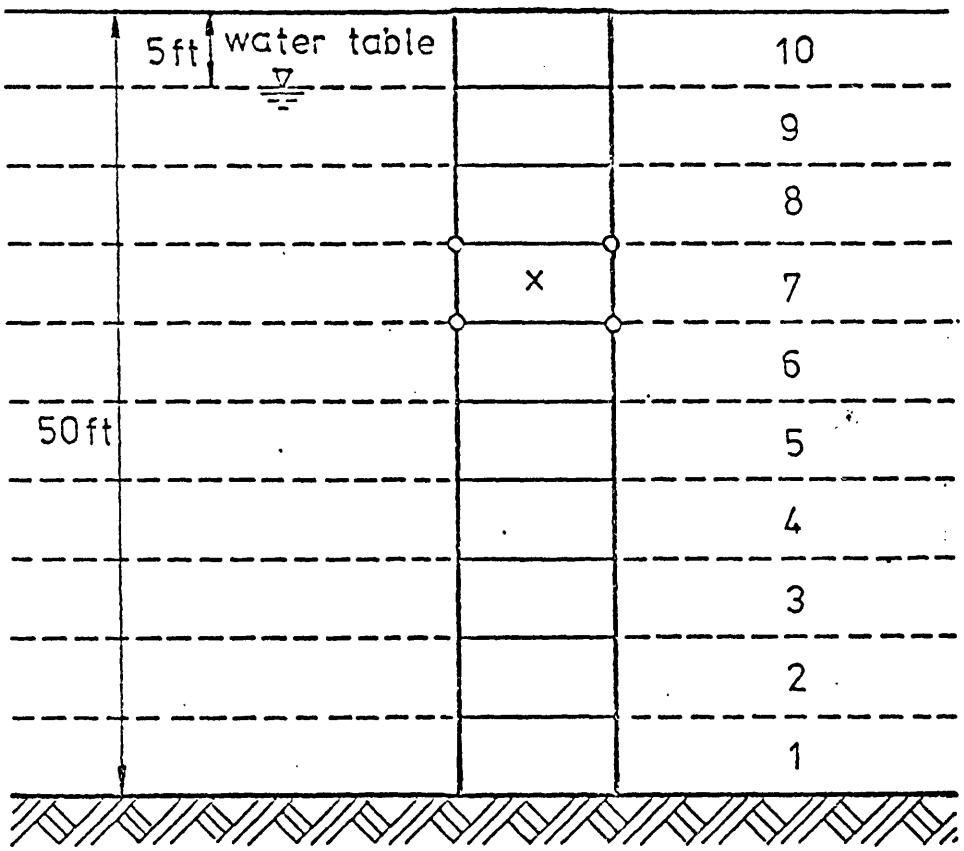

Material properties: Young's mod E = 2,000 kip/ft^2

Poisson ratio ν = 0.15

Friction angle ϕ = 40°

Cohesion C = 20 psf

Unit weight = 110 pcf

Fig. 5.5: Assumed soil stratum

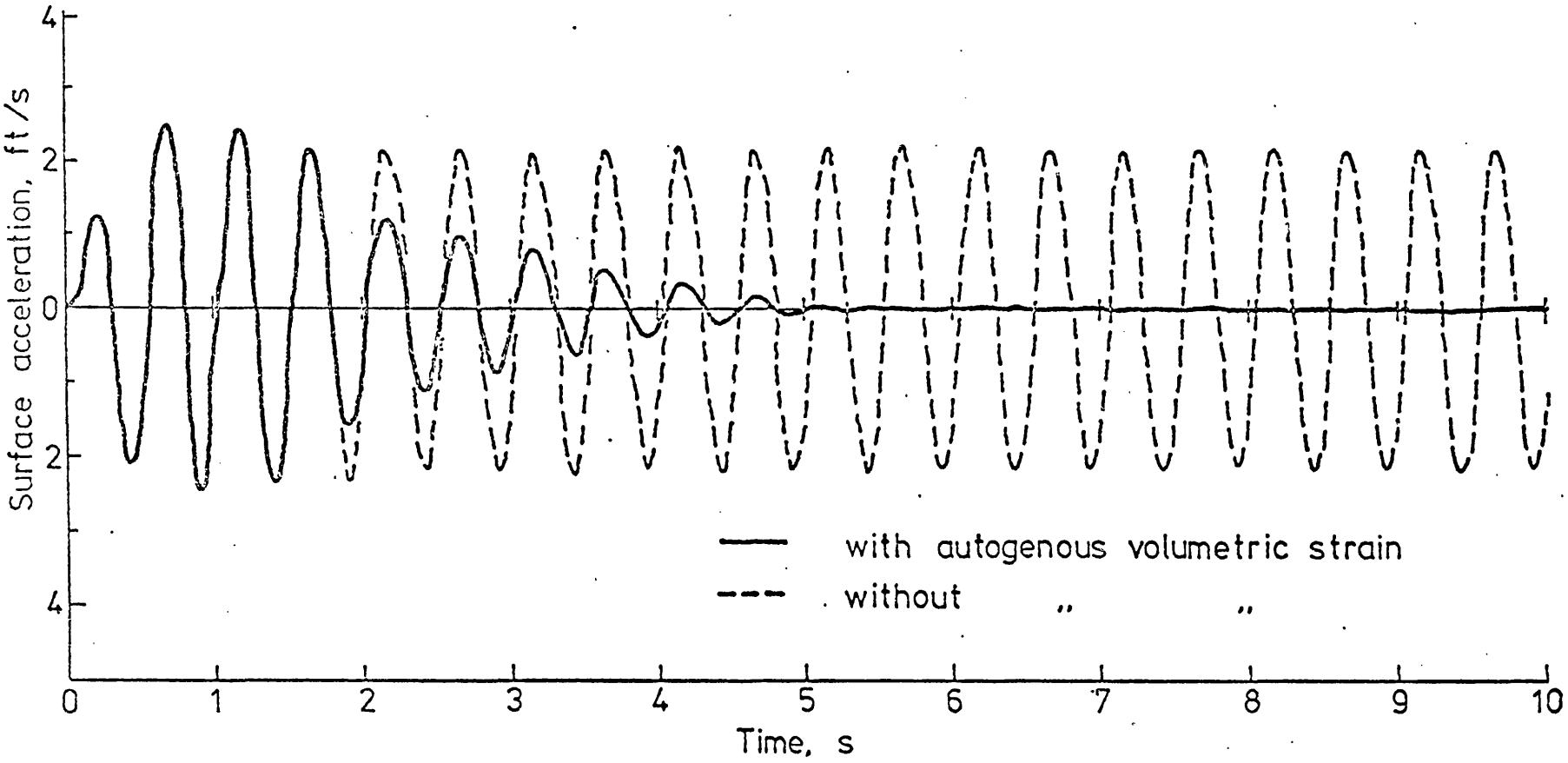

Fig.5.6: Surface horizontal acceleration time history of horizontal layered saturated soil subjected to sinusoidal acceleration at the base (1. Computations on a CDC 7600 is 44 s for each analysis; 2. Similar results have been shown by Finn et al[21])

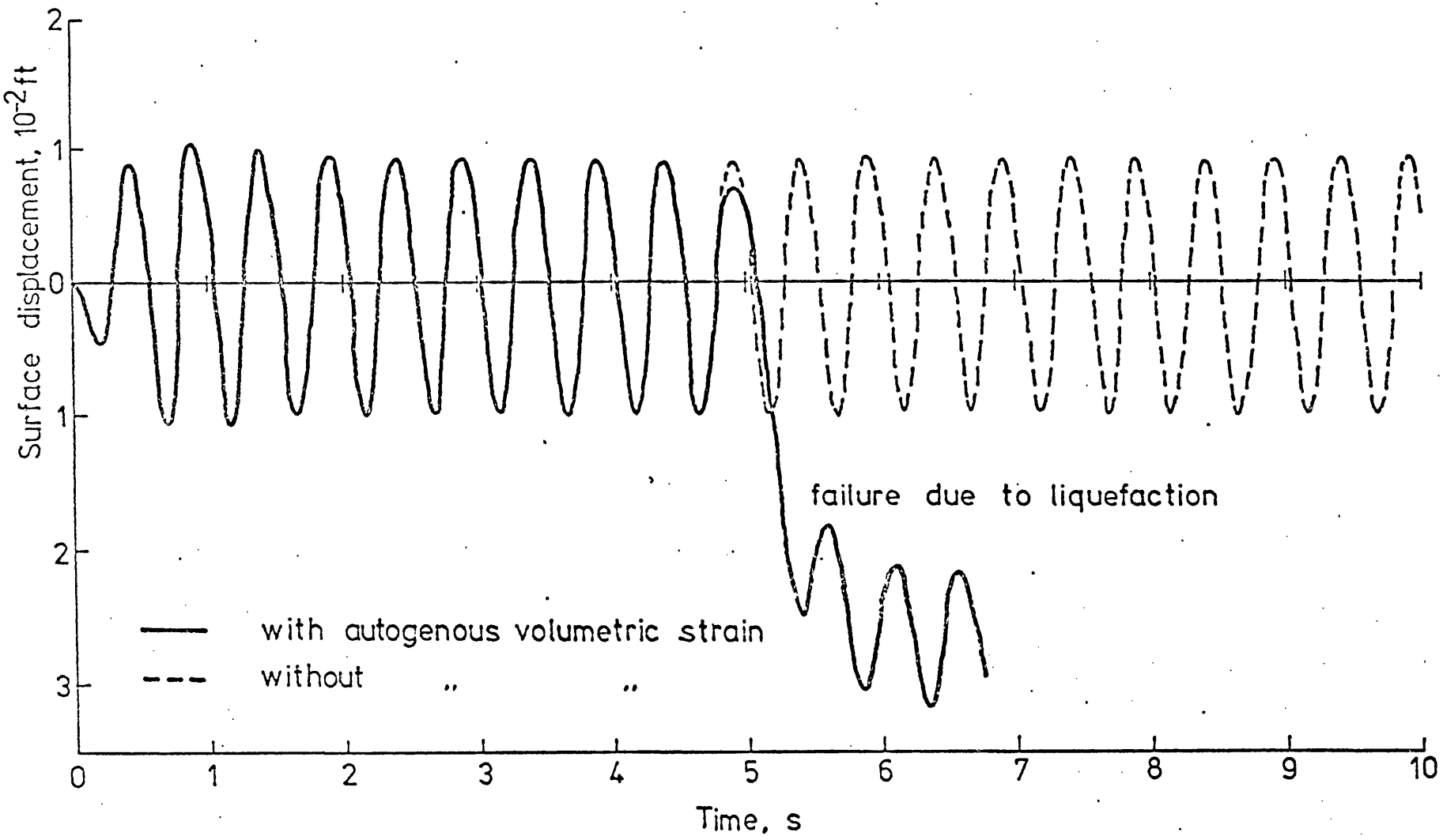

Fig.5.7: Surface horizontal displacement time history of horizontally layered saturated soil subjected to sinusoidal acceleration at the base.

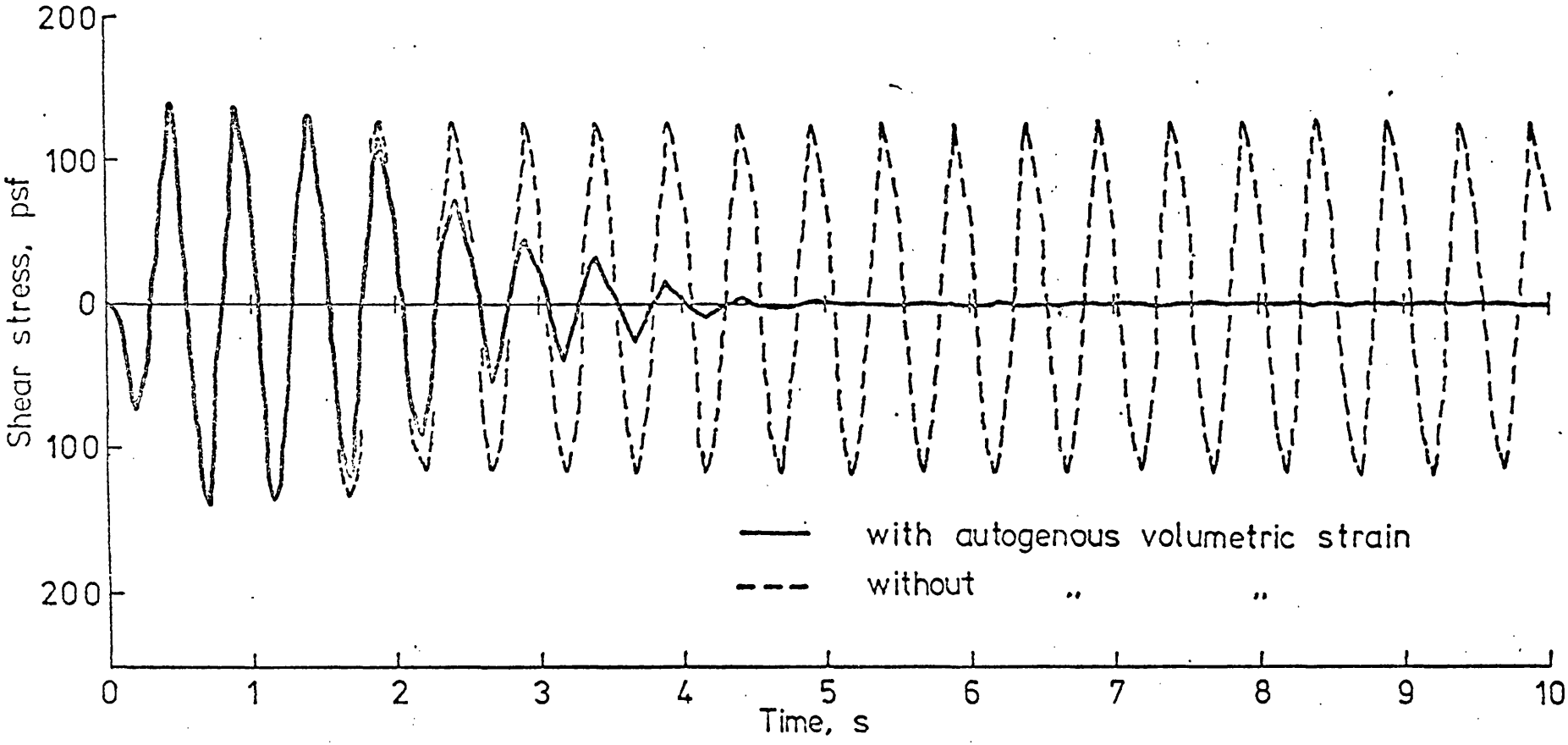

Fig.5.8:Shear stress time history in Layer 7 of horizontally layered saturated soil subjected to sinusoidal acceleration at the base (similar results have been shown by Finn et al(21)

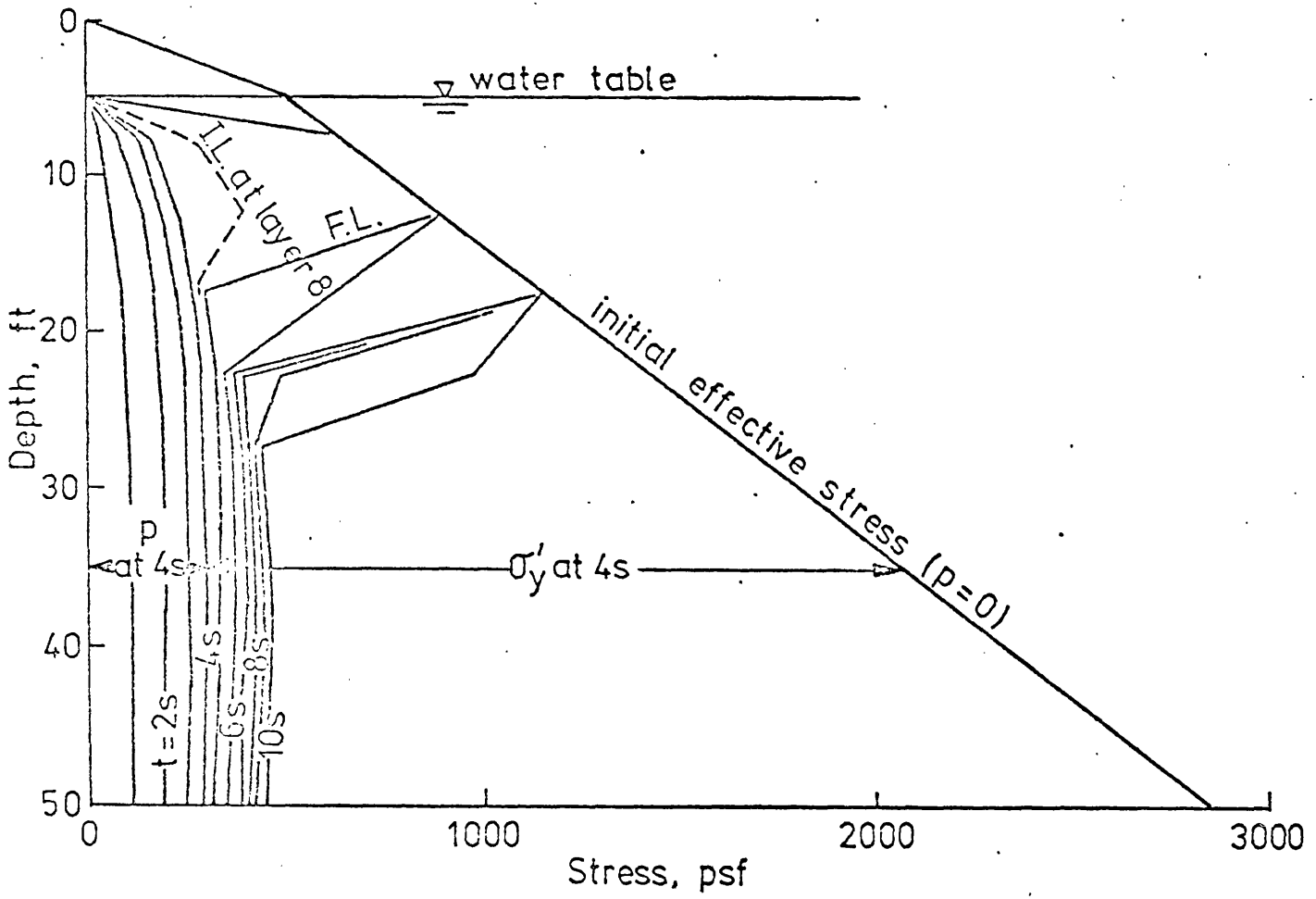

Fig. 5.9

Build up of excess pore water pressure at 1 s intervals from the start of motion

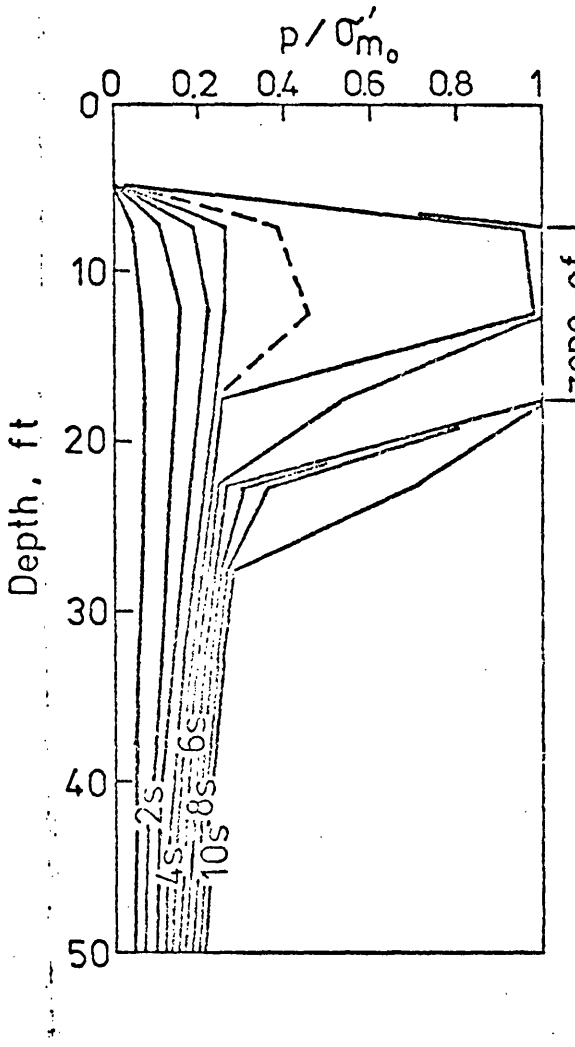

Fig.5.10

Normalized excess pore water wit
depth at 1 s intervals from the
of motion

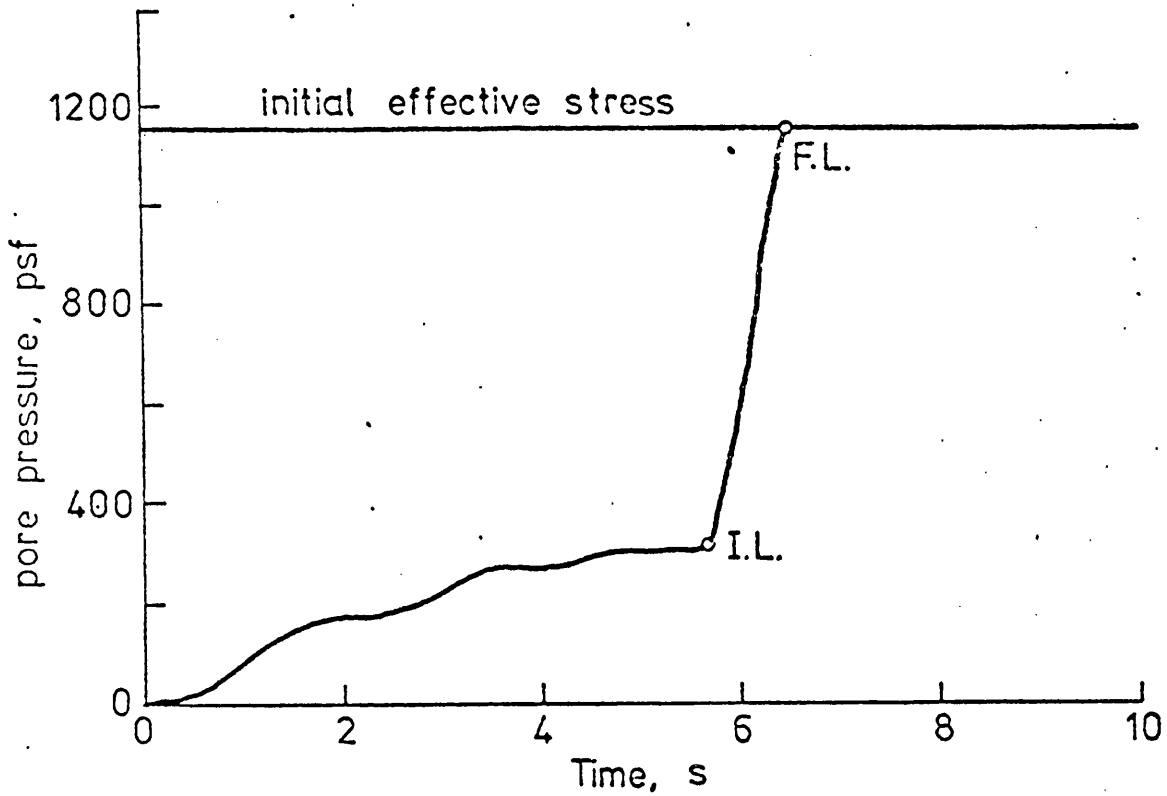

Fig.5.11: Build up of excess pore water pressure with respect to time in Layer 7 due to sinusoidal acceleration at the base.

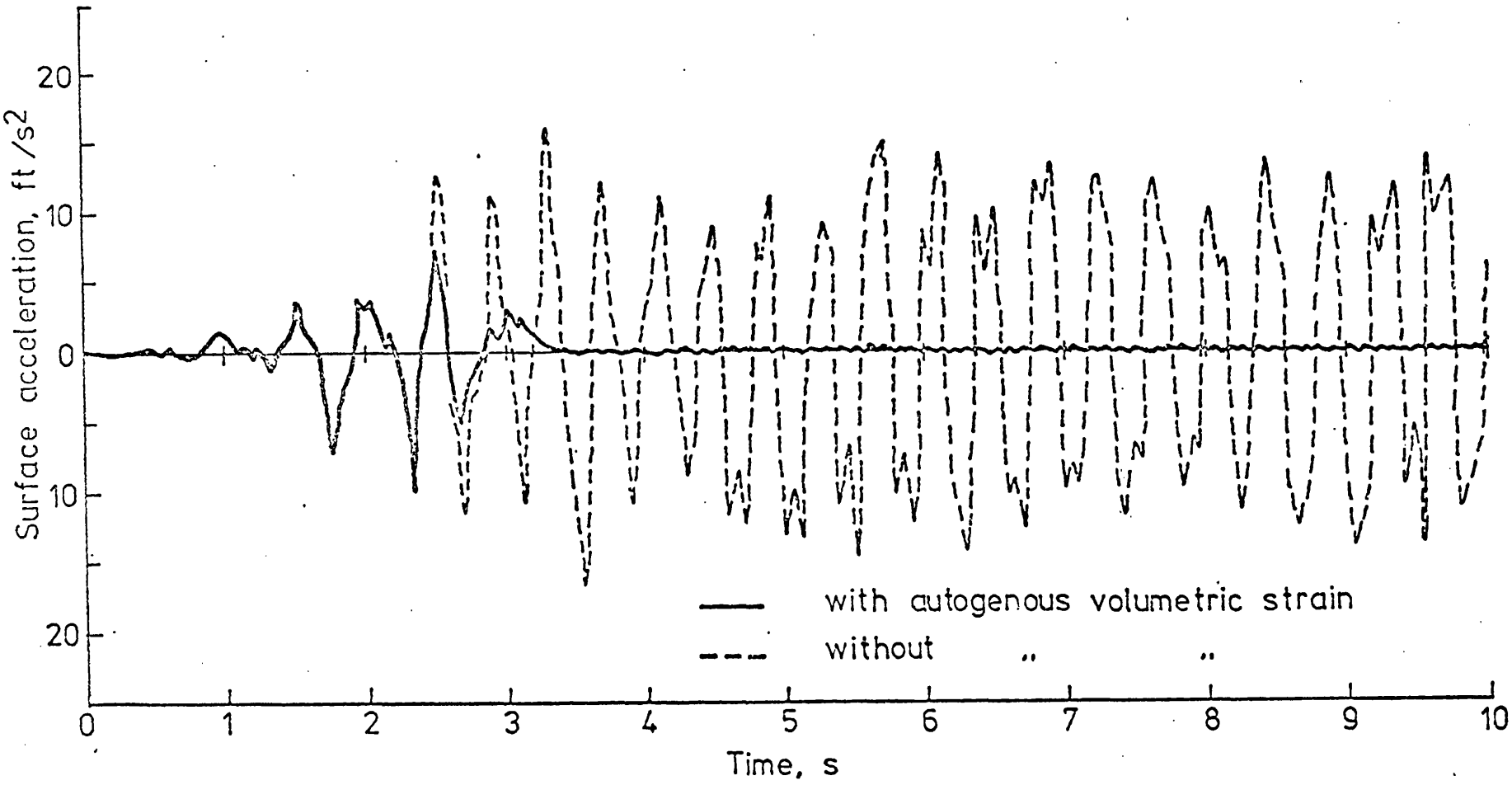

Fig.5.12: Surface horizontal acceleration time history of horizontally layered saturated soil subjected to El Centro earthquake of May 1940 scaled to 0.1g at the base (computer time on a CDC 7600 is 44 s for each analysis)

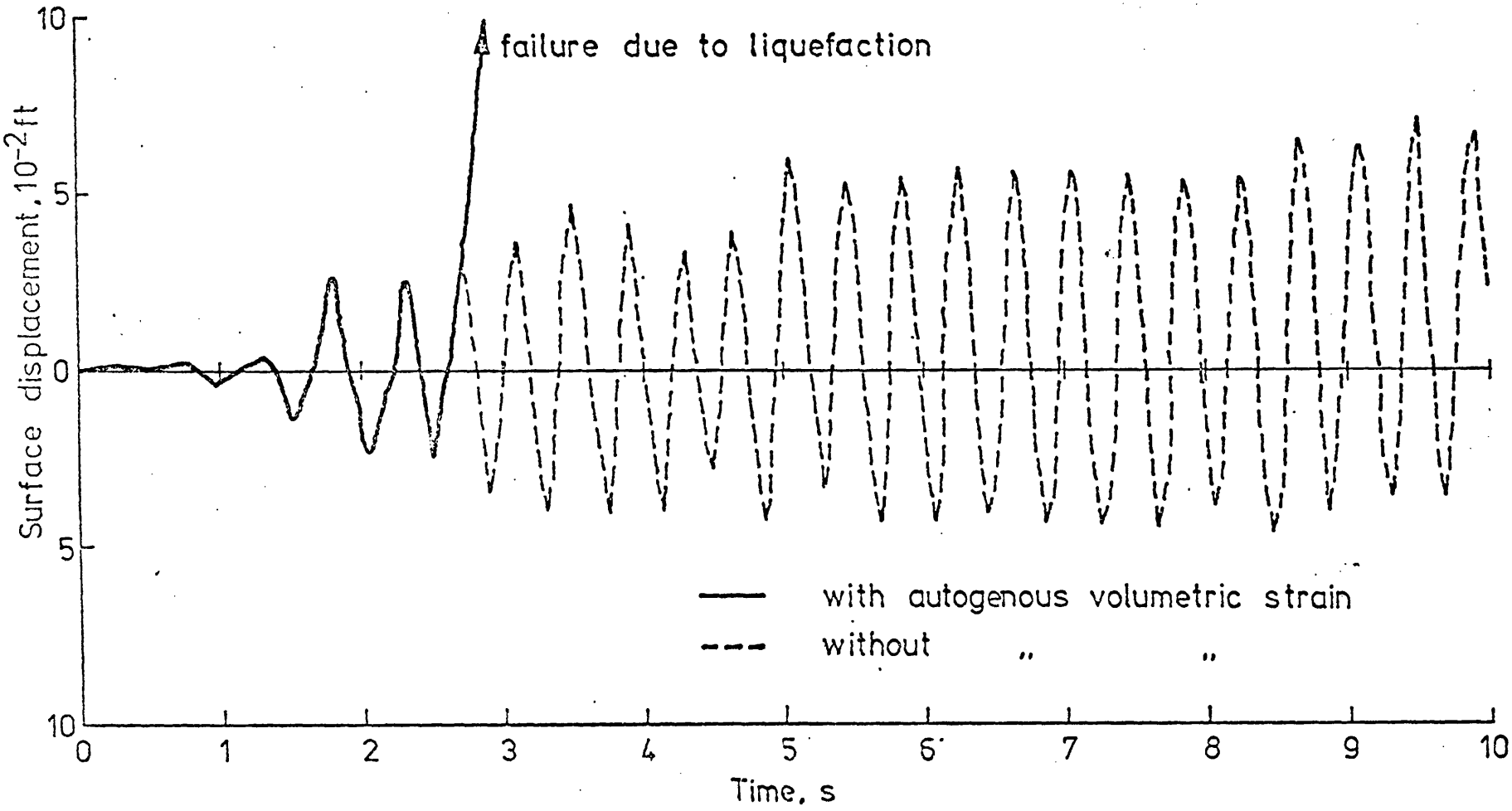

Fig.5.13: Surface horizontal displacement time history of horizontally layered saturated soil subjected to El Centro earthquake of May 1940 scaled to 0.1g at the base

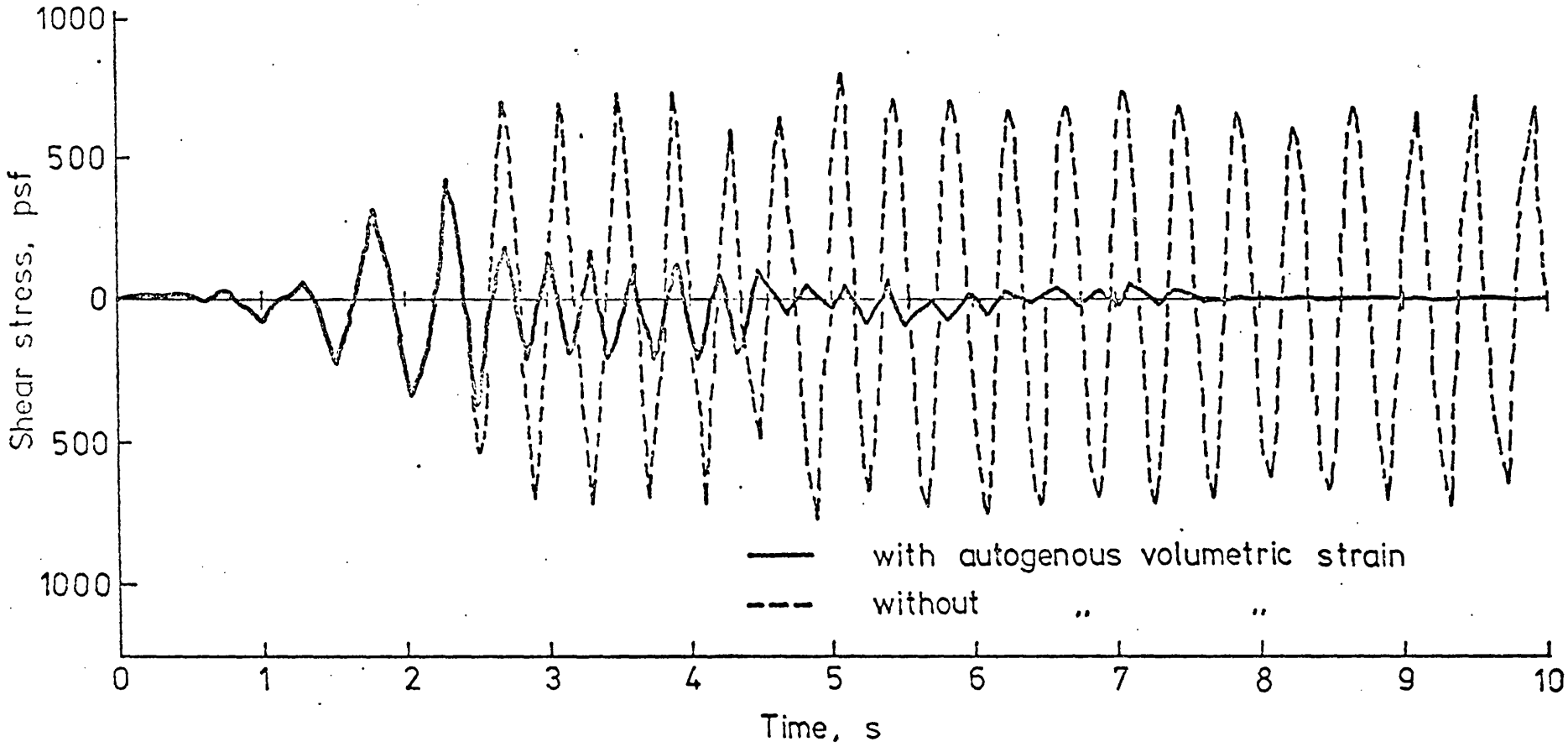

Figure 7 c.

Fig.5.14: Shear stress time history in Layer 7 of horizontally layered saturated soil subjected to El Centro earthquake of May 1940 scaled to 0.1g at the base

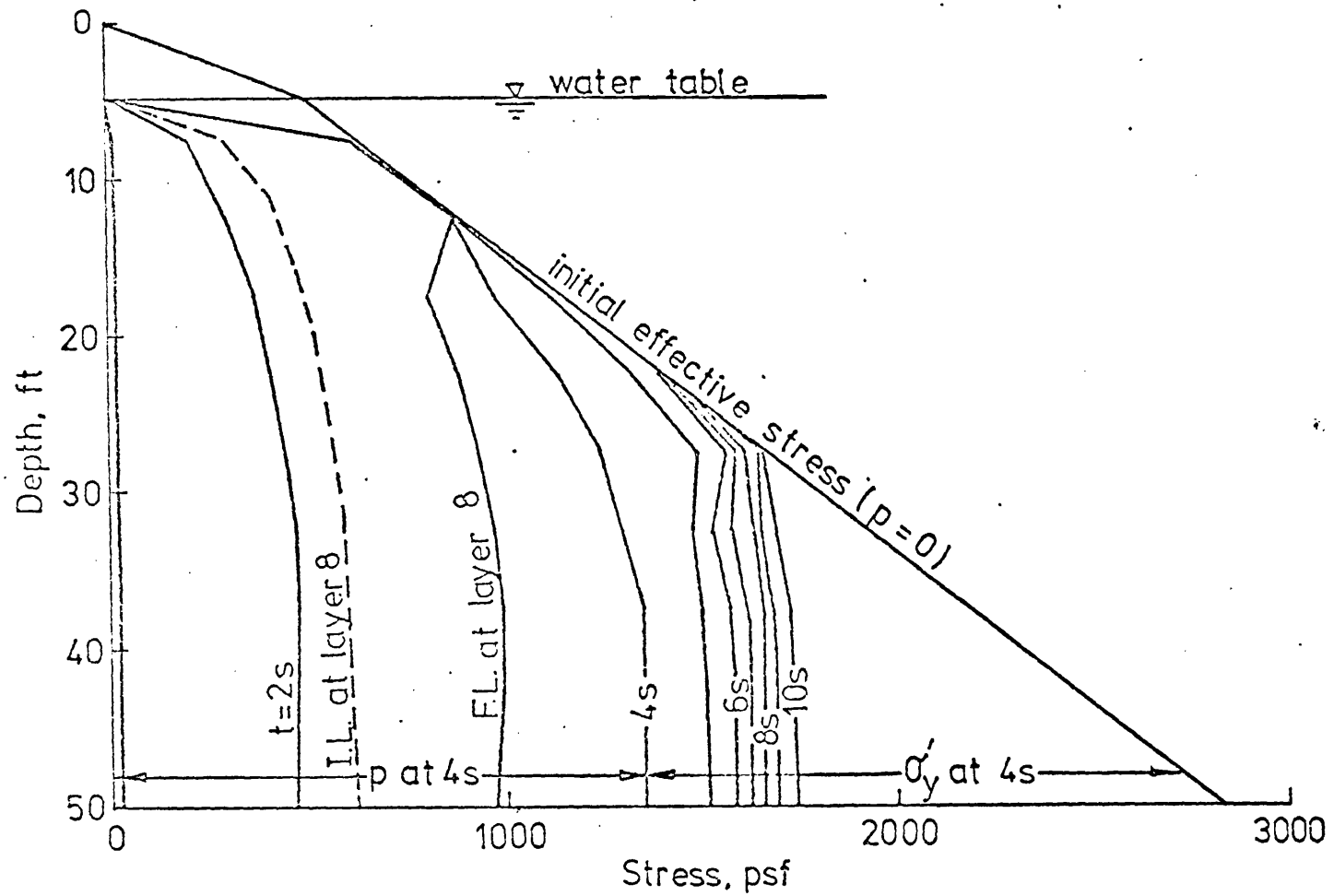

Fig.5.15

Build up of excess pore water pressure at 1 s intervals from the start of motion

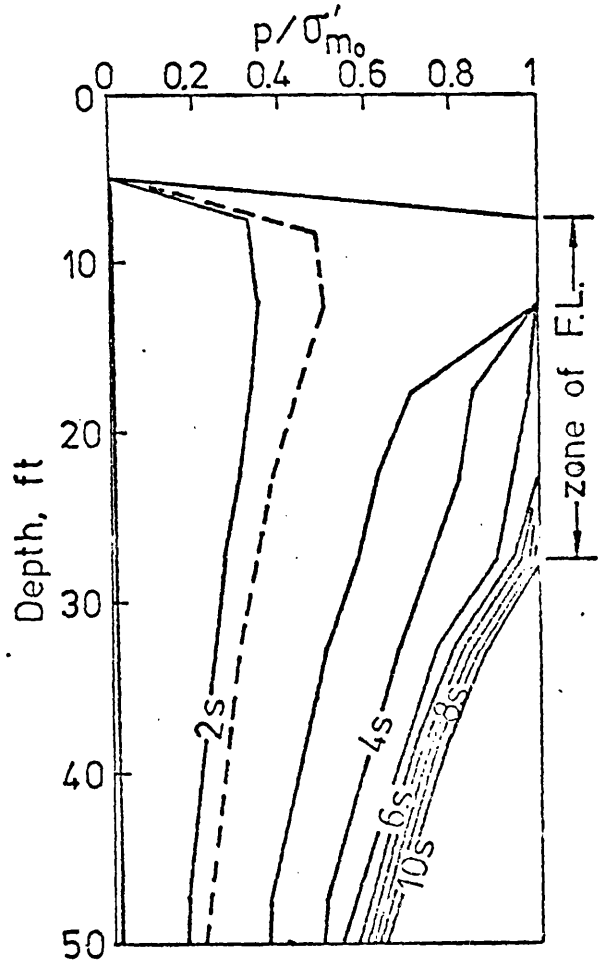

Fig. 5.16

Normalized excess pore water pressure with dep
at 1 s intervals from the start of motion (sim
results have been shown by K. Ishihara, J. Lys
S. Yasuda and H. Hinao[24])

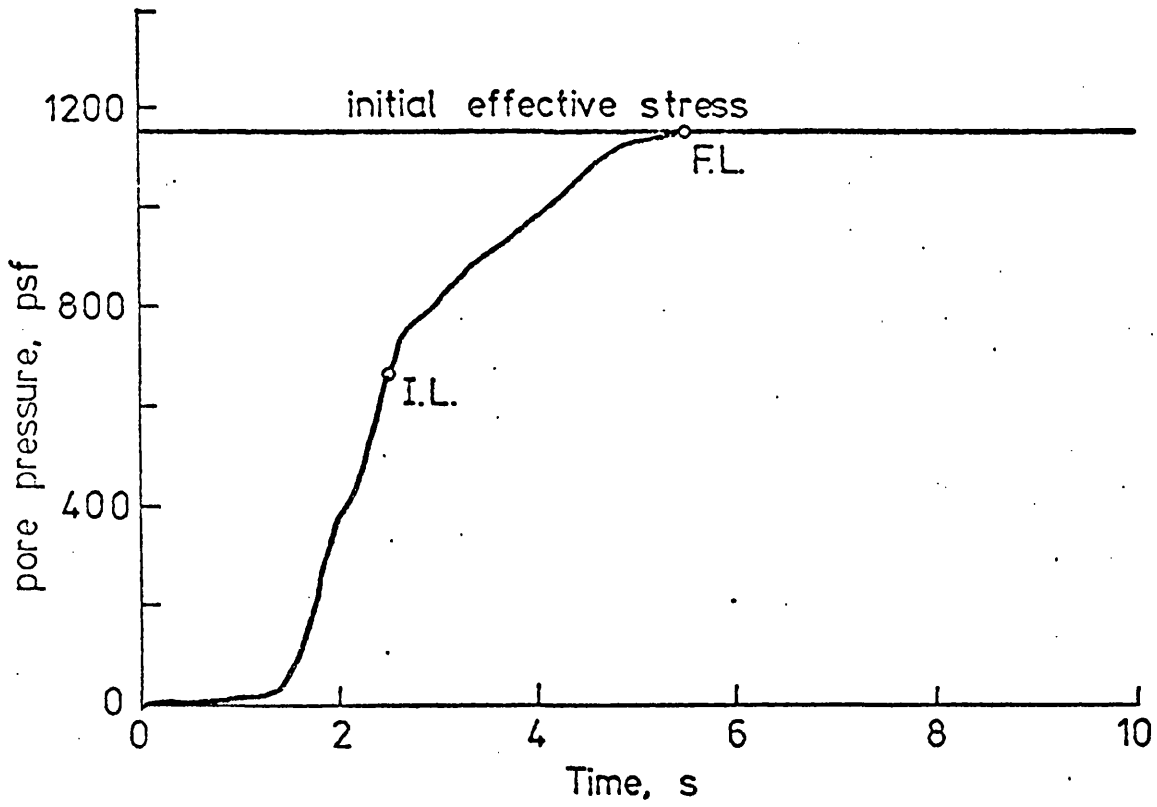

Fig. 5.17: Build up of excess pore water pressure with respect to time in Layer 7 due to El Centro earthquake of May 1940 scaled to 0.1g at the base.

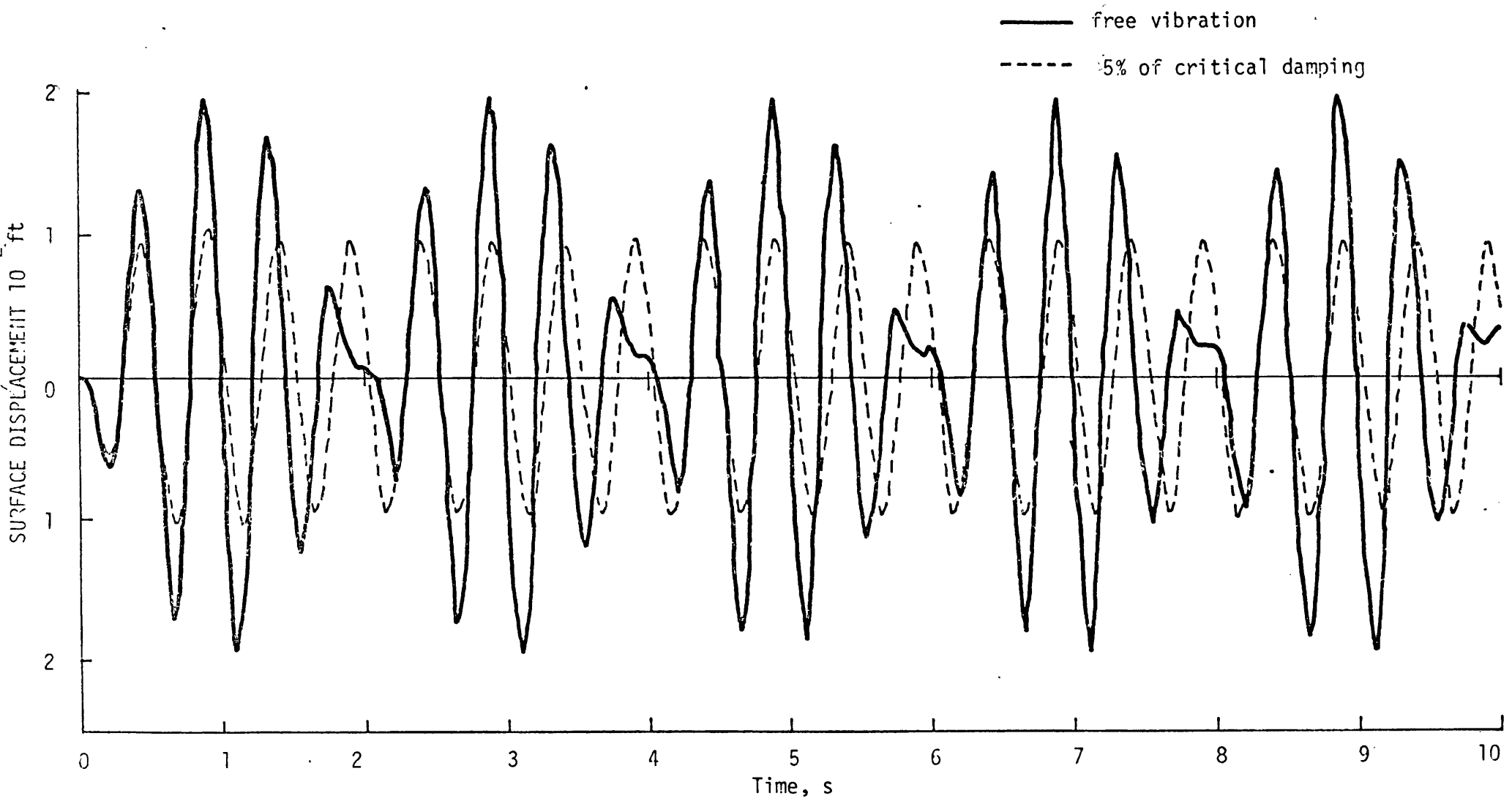

Fig.5.18 SURFACE DISPLACEMENT DUE TO SINUSOIDAL ACCELERATION AT BASE

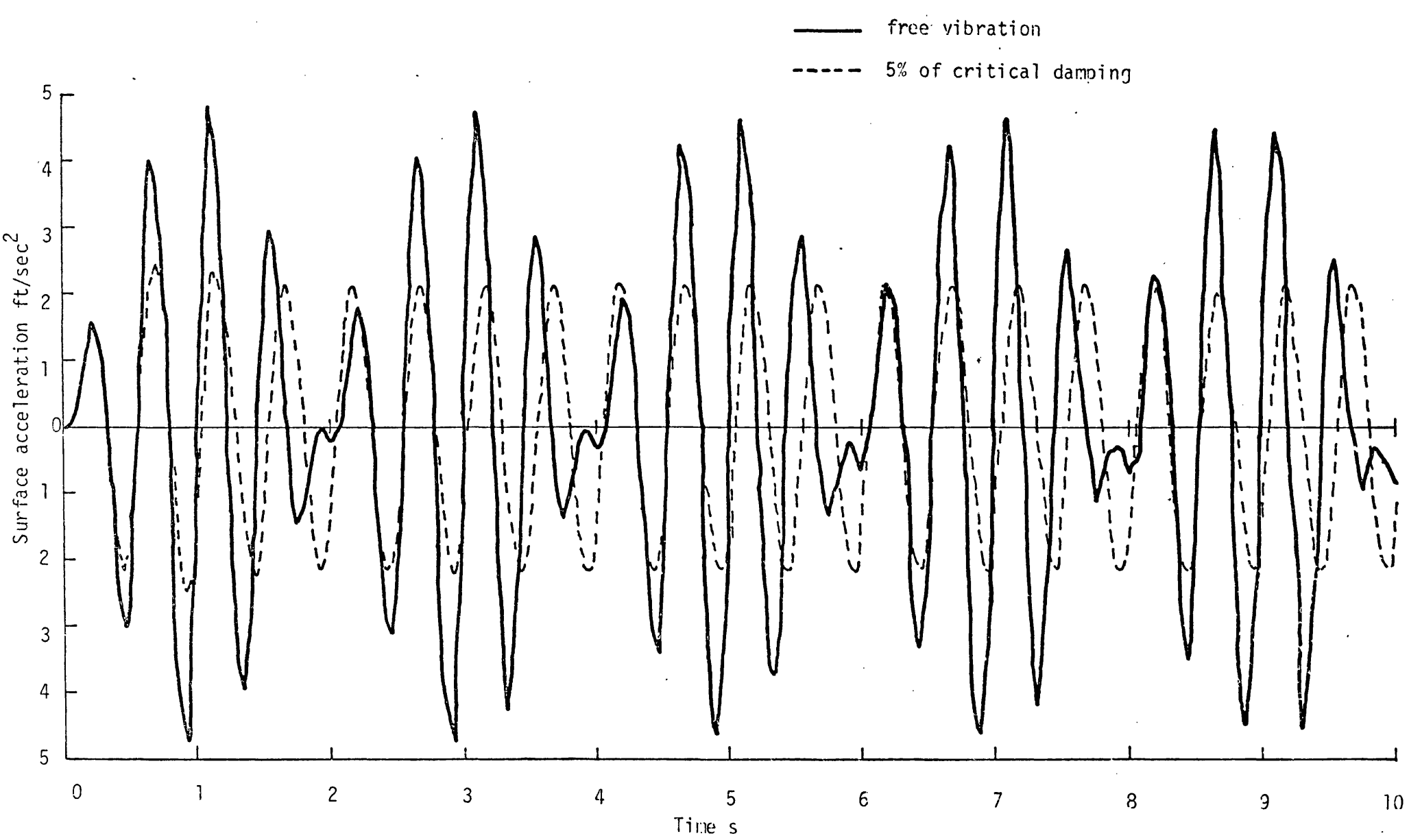

Fig.5 19: SURFACE ACCELERATION DUE TO SINUSOIDAL ACCELERATION AT BASE

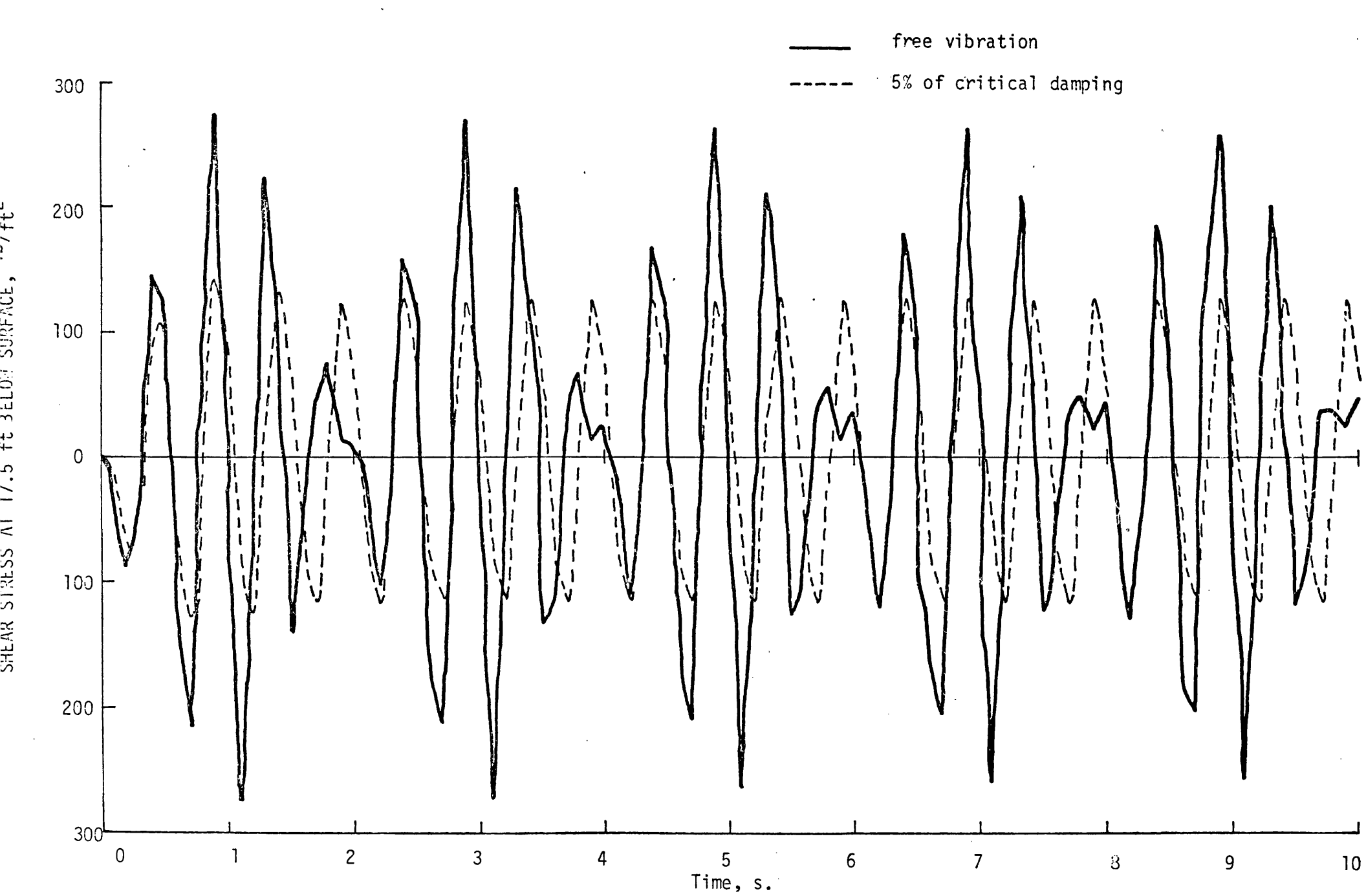

Fig. 5.20: SHEAR STRESS HISTORY AT LAYER 7 DUE TO SINUSOIDAL ACCELERATION AT BASE

CHAPTER 6

DENSIFICATION OF SAND

6.1 Introduction:

In the previous chapter, a saturated sand undergoing cyclic deviatoric stress with undrained conditions was presented. It was noted that the complete range of densification was not covered by the expression for the autogenous volumetric strain. However the expression did show the onset of densification, and also, the expression did agree with the physical phenomenon of the liquefaction of a saturated sand, i.e., liquefaction could occur within a small range of densification. In this chapter, the densification of dry sand or saturated sand under drained conditions is given. It will be seen that the same expression can be extended to cover the whole range of densification of dry sand.

6.2 Factors governing the Densification of Dry Sand:

As pointed out previously, shear strain is the primary factor causing the compaction of granular materials. Experimental evidence[1] shows that only a small amount of irreversible volumetric compression, or densification, occurs during the first few cycles of hydrostatic stressing of cubic sand samples in a soil test box. After this initial permanent densification of the sample, deformations during additional cycles of hydrostatic stressing were found to be nonlinear but completely elastic. Thus repeated cycles of volumetric strain acting alone have an essentially insignificant influence on densification. On the other hand, the experimental evidence [2,3] indicates that the amount of vertical strain, or densification, occuring in a given number of cycles increases with the shear strain

amplitude and the initial void ratio. This can be attributed to the fact that the densification or compaction of the loose sand under cyclic shearing is produced almost exclusively by interparticle slips that result in a rearrangement of grain configuration. The rearrangement of grain configuration is primarily dominated by shear strain as well as void ratio. Therefore, the progressive densification or an autogenous volumetric strain must be a function of shear strain and void ratio.

6.3 Densification of Sand:

It appears that the densification of sand can be represented either by volumetric strain or by void ratio. Therefore, two separate expressions are presented in this section.

6.3.1 Densification in Terms of Volumetric Strain:

Recall equation (5.14) as follows:

$$d\varepsilon_v^o = -\frac{A d\kappa}{1+B\kappa} \tag{6.1}$$

in which $d\kappa = g(\theta)d\xi$ as defined previously and A and B are constants to be evaluated from experimental studies. Although equation (6.1) was derived from the study of liquefaction, it is equally applicable to the densification of sand. This can be verified from the published test data by Silver and Seed[4].

Based on Silver and Seed's studies, the volumetric strains versus the number of cycles of shear strain for a sand with 60% of relative density under various vertical stresses have been presented and reproduced in Figure 6.1. From these test data the constants A and B and $g(\theta)$ in equation (6.1) can be evaluated. However due to lack of

information about the parameter θ, i.e., the ratio of applied shear stress to initial vertical stress, $g(\theta) = 1$ is assumed in the present study. A typical result to show the validity of equation (6.1) is presented in Figure (6.2), which corresponds to the curve for $\sigma'_v = 500$ lb/ft^2, and $\gamma = 0.041\%$ in Figure 6.1. Similar plots were obtained for $\gamma = 0.016\%$, 0.088% and 0.63% with $\sigma'_v = 500$ lb/ft^2 and also for $\sigma'_v = 2000$ lb/ft^2 and $\sigma'_v = 4000$ lb/ft^2 with various values of shear strains as shown in Figures 6.3, 6.4 and 6.5 respectively. It is certain that should the information about the parameter θ be available, a general expression to cover the whole range of test data presented by Silver and Seed could be derived.

6.3.2 Densification in Terms of Void Ratio:

It can be noted that equation (6.1) can be written in the following form, which was also presented in equation (5.15),

$$d\varepsilon_v^o = - \frac{A(\frac{e}{e_m} - 1)^n d\kappa}{1 + B\kappa} \qquad (6.2)$$

For a dry sand or saturated sand in drained conditions, this autogenous volumetric strain will produce a reduction in volume which can be represented by the void ratio change, i.e.,

$$d\varepsilon_v^o = \frac{de}{1 + e_o} \qquad (6.3)$$

in which e_o is the initial void ratio of the sand. Substituting equation (6.3) into equation (6.2) and integrating, finally the following expression is obtained

$$e = e_m + \left[(e_o - e_m)^{1-n} + C \ln (1 + B\kappa) \right]^{\frac{1}{1-n}} \qquad (6.4)$$

in which C is a constant depending on constants e_o, e_m, A, B and n. Therefore, the void ratio of sand at any time can be evaluated from its initial and minimum void ratios and κ provided that constants B,C and n have been obtained a priori from experimental studies.

It is of interest to note that equation (6.4) has the same form as the expression proposed by Nasser et al[5]. Their expression is quoted as follows:

$$e = e_m + \left[(e_o - e_m)^{1-n} + \bar{\nu} N \gamma_o^{1+\frac{1}{\beta}}\right]^{\frac{1}{1-n}} \tag{6.5}$$

in which ν, β and n are three constants to be determined from the experimental studies, γ_o is the amplitude of shear strain in repeated simple shear tests and N is the number of repeated loadings.

6.4 Comparison of Equation (6.4) with Experimental Results:

In a series of experiments reported by Youd[6], standard gradation Ottawa sands were densified in a Norwegian Geotechnical Institute type simple shear apparatus under repeated cycles of shear strains. In Figure 6.5 the solid curves represented Youd's results, where the initial void e_o is reported to be within the range 0.543 to 0.548, and the minimum void ratio to be about 0.412.

To evaluate the theoretical result, in equation (6.4), $e_o = 0.545$, $e_m = 0.412$ and $g(\theta) = 1$ have been adopted. Based on experimental data in Figure 6.5, the following expression has been derived from equation (6.4)

$$e = 0.412 + \left[7.52 + 4.52 \ln (1 + 2.23\kappa)\right]^{-1} \tag{6.6}$$

The dotted lines in Figure 6.5 are graphs of this equation for the indicated values of γ. Also shown in Figure 6.5 are results obtained by Nasser et al. It can be seen that over the range of 0.1% to 8% strain emplitudes, and for 1 to 100 cycles, the present theoretical results are reasonably consistent with the experiments, although a rather crude estimate of κ has been made. A more accurate theoretical estimate of e based on equation (6.4) should be obtainable if the information for evaluating $g(\theta)$ is available.

6.5 Discussions:

It has been observed that shear strain is the primary factor causing compaction of granular material. This shear strain can be generalized as the second deviatoric strain invariant. Therefore, the basic formulation presented here is a realistic mathematical model for the densification of sand subjected to cyclic deviatoric stress. The present formulation can be applied for arbitrary strain histories, for general states of stress and strain.

REFERENCES

1. KO, H.Y. and SCOTT, R.F.
'Deformation of Sand in Hydrostatic Compression'
Jnl. of the Soil Mechanics and Foundations Division,
ASCE, Vol. 93, No. SM3, 137-156 (1967)

2. YOUD, T.L.
'Densification and Shear of Sand During Vibration'
Jnl. of the Soil Mechanics and Foundations Division,
ASCE, Vol. 96, No. SM3, 863-880 (1970)

3. SILVER, M.L. and SEED, H.B.
'Deformation Characteristics of Sands under Cyclic Loading'
Jnl. of the Soil Mechanics and Foundations Division, ASCE,
Vol. 97, No. SM8, 1081-1098 (1971)

4. SILVER, M.L. and SEED, H.B.
'Volume Changes in Sands During Cyclic Loading'
Jnl. of the Soil Mechanics and Foundations Division,
ASCE, Vol. 97, No. SM9, 1171-1182 (1971)

5. NASSER, N.S. and SHOKOOH, A.
'A Unified Approach to Densification and Liquefaction
of Cohesionless Sand.
Earthquake Research and Engineering Lab. Technical Report
No. 77-10-3, Department of Civil Engineering, Northwestern
University, Evanston, Illinois (1977)

6. YOUD, T.L.
'Compaction of Sands by Repeated Shear Straining'
Jnl. of Soil Mechanics and Foundations Division, ASCE,
Vol. 98, No. SM7, 709-725 (1972)

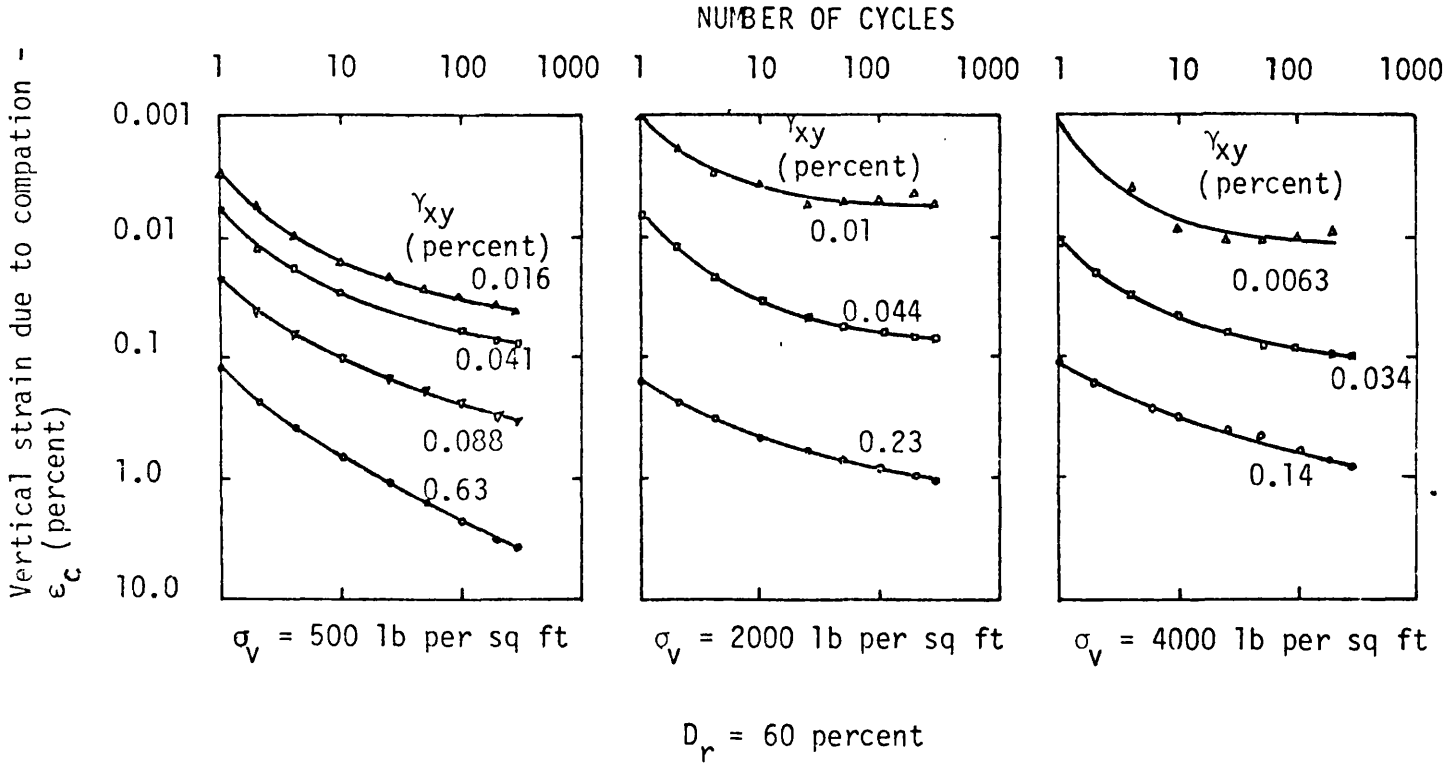

FIGURE 6.1 SETTLEMENT-SHEAR CYCLE RELATIONSHIP FOR MEDIUM DENSE SAND (D_r = 60%)

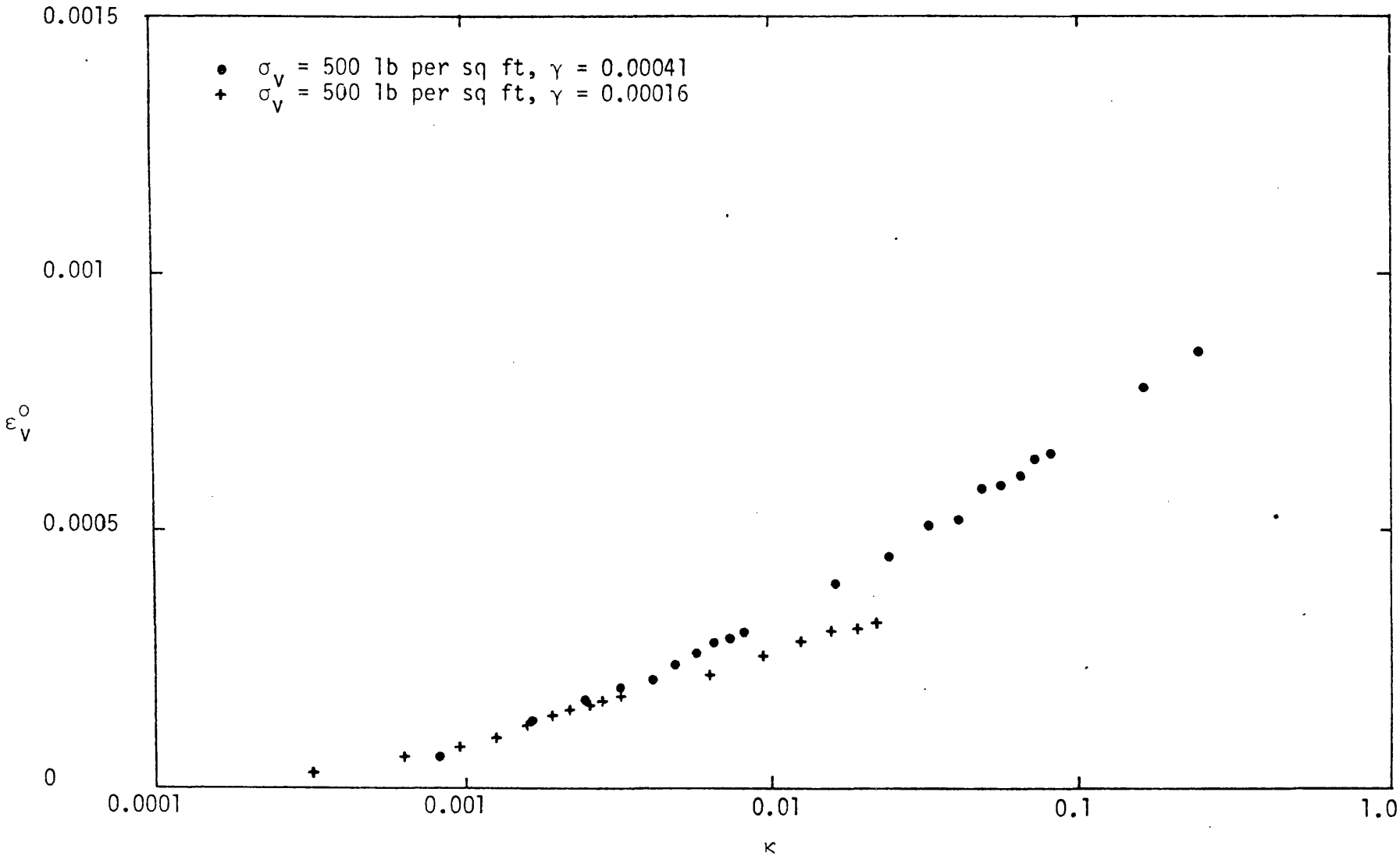

FIGURE 6.2 DENSIFICATION OF SAND VERSUS κ

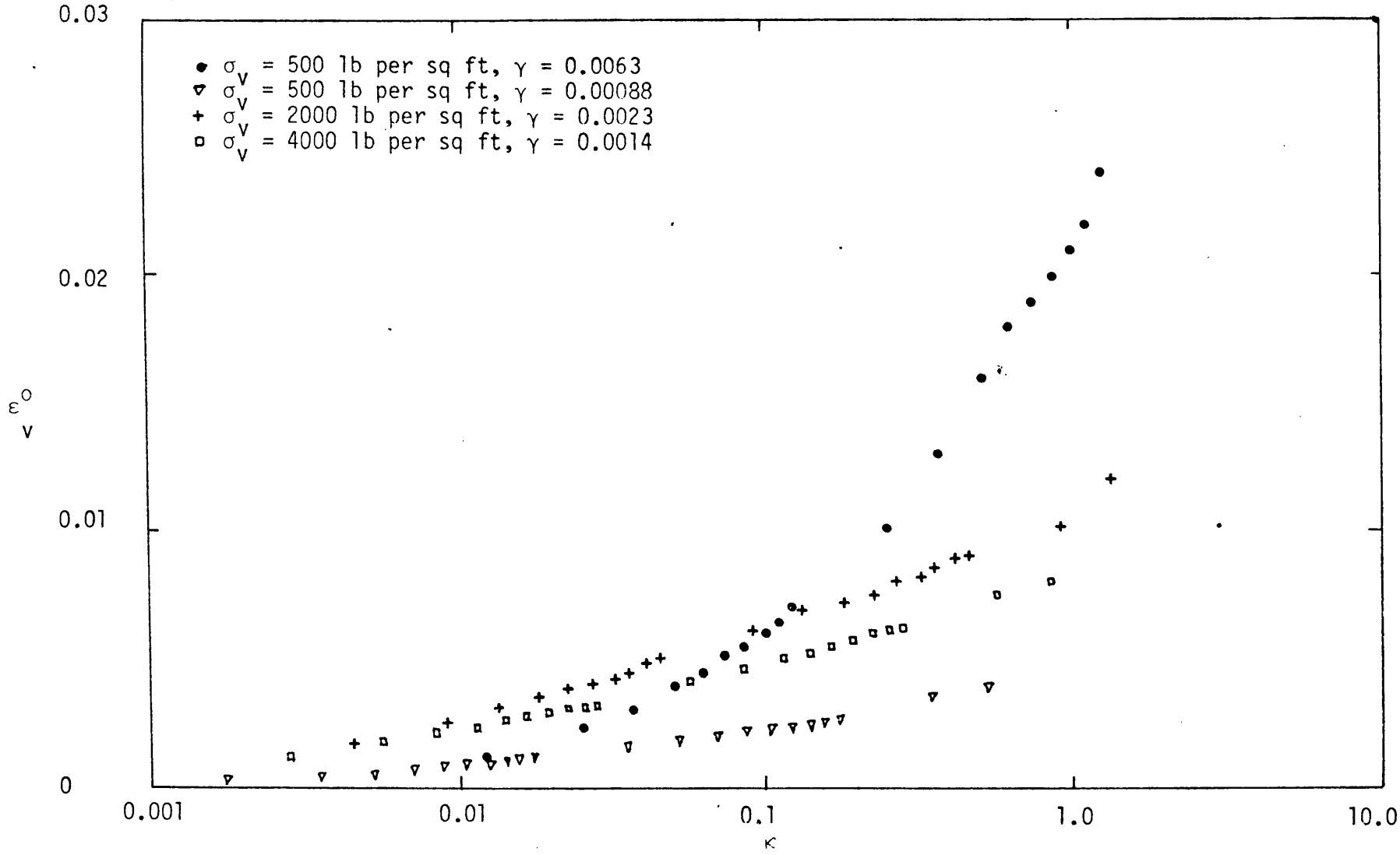

FIGURE 6.3 DENSIFICATION OF SAND VERSUS κ

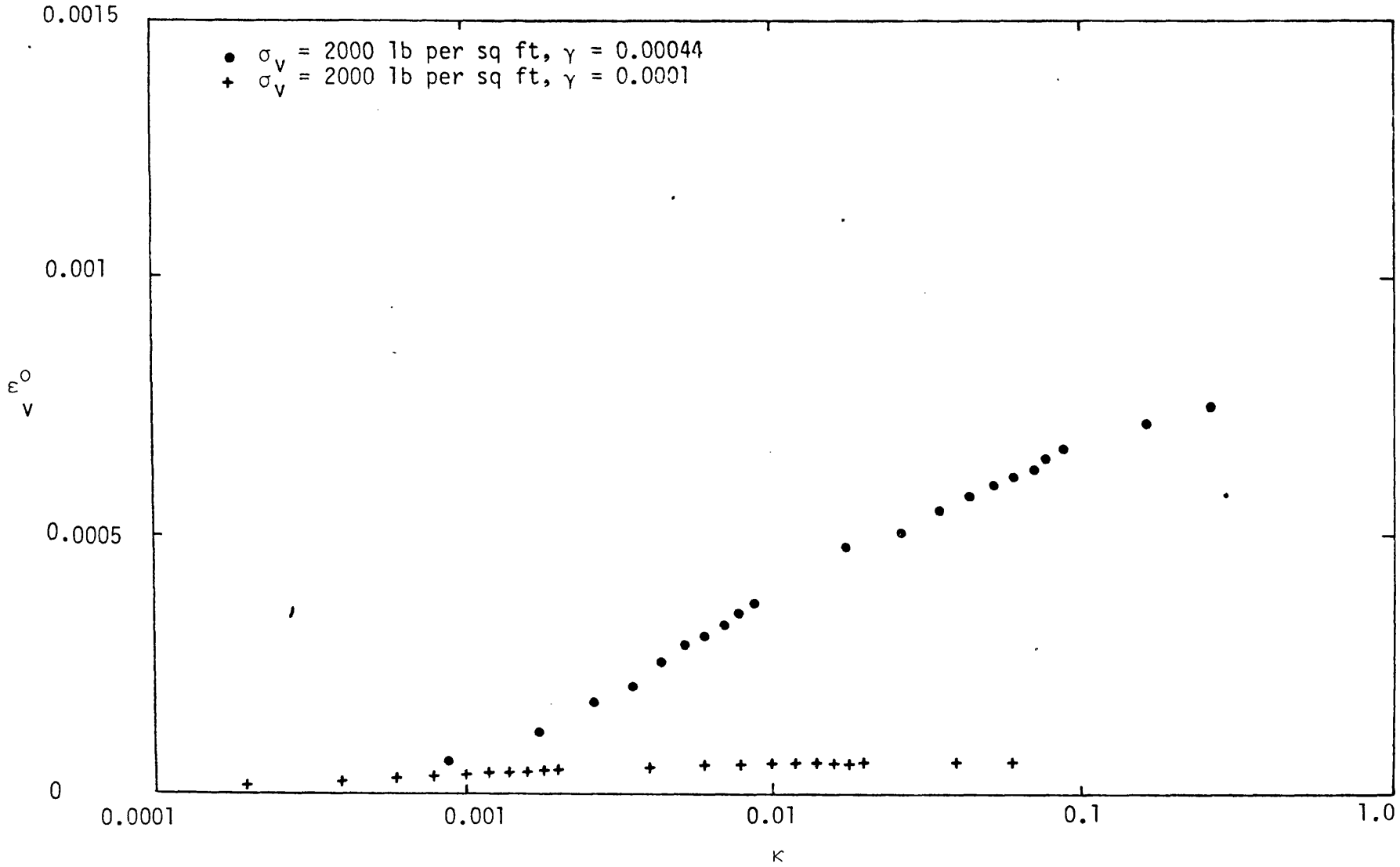

FIGURE 6.4 DENSIFICATION OF SAND VERSUS κ

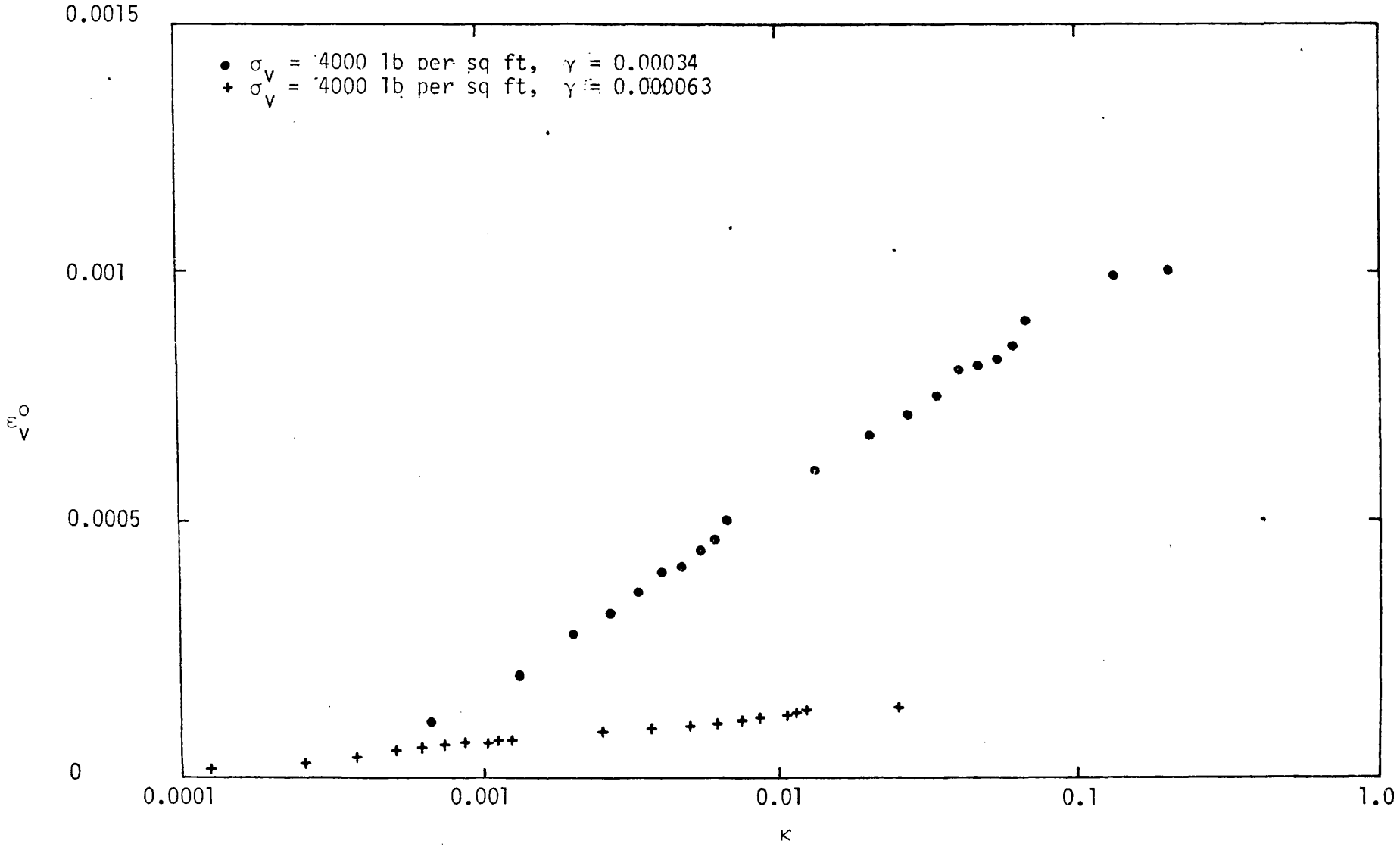

FIGURE 6.5 DENSIFICATION OF SAND VERSUS κ

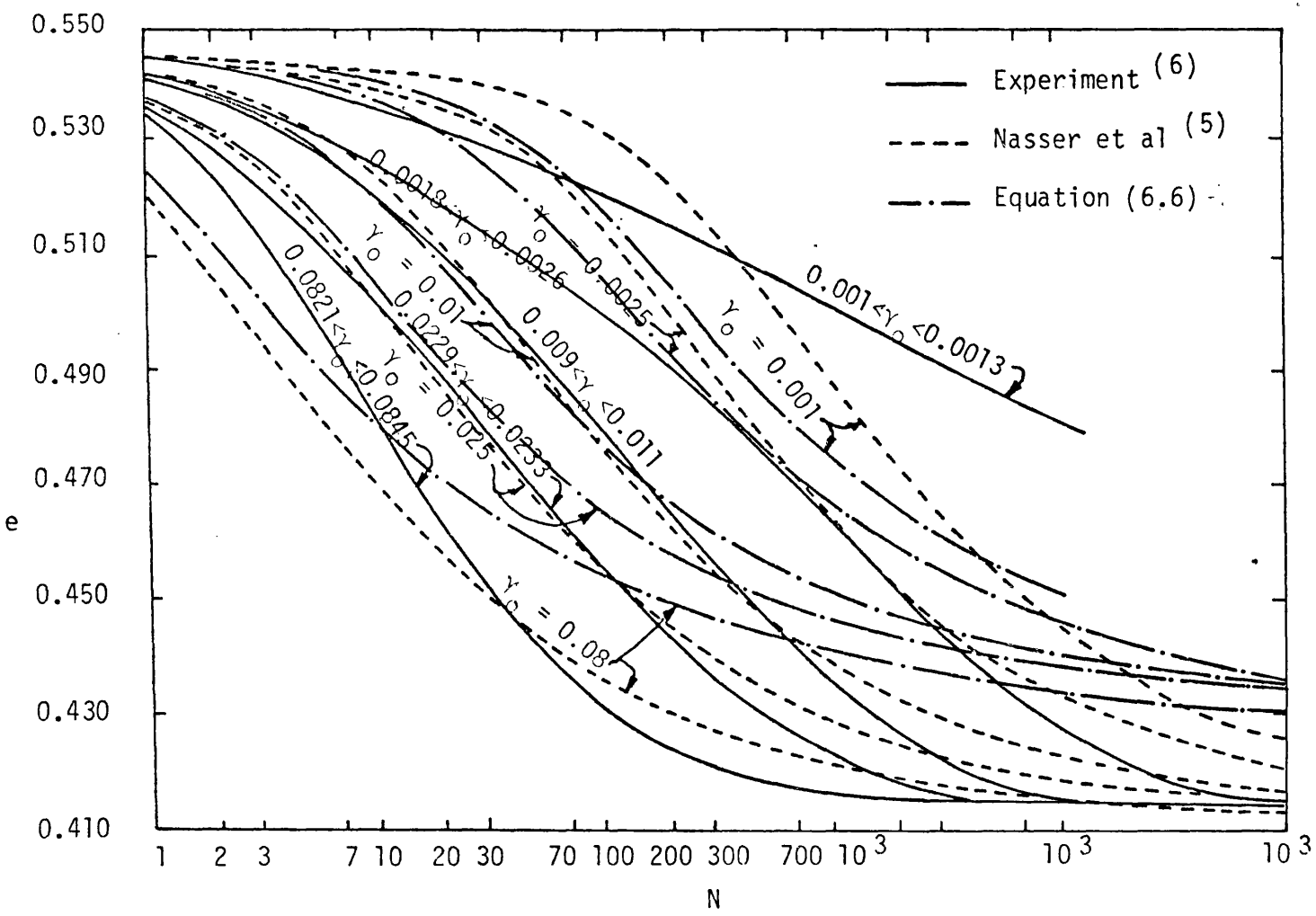

FIGURE 6.6 VOID RATIO e VS NUMBER OF CYCLES IN CYCLIC SHEARING OF DRY SAND (DATA FROM REF. 6) γ_o = MAXIMUM SHEAR STRAIN AMPLITUDE, N = NUMBER OF CYCLES

CHAPTER 7

PARTIALLY DRAINED ANALYSIS OF TRANSIENT PROBLEMS IN POROUS MEDIA

7.1 INTRODUCTION

In Chapter 5, it has been noted that a saturated granular material subjected to cyclic loading will show an increase in pore pressure if drainage is prevented. If permeability of the soil is relatively high or motion is slow, there will be simultaneous dissipation of excess pore pressure. If pore pressure generated in a soil mass is to some extent dissipated, then liquefaction may be averted, however in some cases, the dissipation of the pore pressure generated deep within a soil mass may lead to upward seepage and consequent liquefaction of the surface layers. This highlights the importance of taking the dissipation of excess pore pressure into consideration.

In this chapter a method of analysis of the equations governing pore pressure generation and dissipation, based on the finite element method is developed and illustrated by application to a variety of problems.

7.2 BASIC FORMULATION OF DYNAMICS OF TWO PHASE MATERIAL

The equations of motion for saturated elastic porous media were first given by Biot[1-4]. The independent variables of the problem in Biot's field equations are: the displacement of the solid and the displacement of the fluid with respect to the solid. These field equations have been used by Ghaboussi and Wilson[5-8] to systematically develop a variational formulation to solve the linear problem.

The application of finite element spatial discretization yields a set of ordinary differential matrix equations of motion. The independent displacements of the solids and the displacements of the fluid with respect to the solid are degrees of freedom at each node. As mentioned earlier, the Biot's formulation is based on a linear elastic theory. In practical problems, the constitutive laws of the soil rarely follow linear patterns. Therefore, it is imperative to study the dynamics of nonlinear porous media and to extend Biot's formulation to nonlinear cases.

Any porous media such as soil, rock, concrete or sintered metal saturated with fluid can be treated as two phase material, i.e., the solid skeleton and the fluid phase. Therefore, the basic formulation for both phases are separately presented as follows:

The solid skeleton: The basic formulation of the solid skeleton has already been discussed in Chapter 2. However, for completeness, it is briefly summarized in the following (tension is still taken as positive).

The total stress is divided into two parts, i.e., the effective stress, $\underset{\sim}{\sigma}'$ and the pore pressure p. Thus

$$\underset{\sim}{\sigma} = \underset{\sim}{\sigma}' + \underset{\sim}{m}\, p \tag{7.1}$$

The strain is defined as

$$\underset{\sim}{\varepsilon} = \underset{\sim}{L}\, \underset{\sim}{u} \tag{7.2}$$

in which

$$\underset{\sim}{L} = \begin{bmatrix} \frac{\partial}{\partial x} & 0 & 0 \\ 0 & \frac{\partial}{\partial y} & 0 \\ 0 & 0 & \frac{\partial}{\partial z} \\ \frac{\partial}{\partial y} & \frac{\partial}{\partial x} & 0 \\ 0 & \frac{\partial}{\partial z} & \frac{\partial}{\partial y} \\ \frac{\partial}{\partial z} & 0 & \frac{\partial}{\partial x} \end{bmatrix}$$

and $$\underset{\sim}{u} = \begin{Bmatrix} u_x \\ u_y \\ u_z \end{Bmatrix}$$

The stress and the strain are related by the constitutive matrix $\underset{\sim}{D}_T$ in incremental form as

$$d\underset{\sim}{\sigma}' = \underset{\sim}{D}_T \, (d\underset{\sim}{\varepsilon} - d\underset{\sim}{\varepsilon}^o) \qquad (7.3)$$

The equilibrium equation will now differ from the one in which no relative motion of fluid on solid occurs. We now have for the total energy

$$\underset{\sim}{L}^T \underset{\sim}{\sigma} + \rho \underset{\sim}{b} = \rho \ddot{\underset{\sim}{u}} + \rho_f \ddot{w} \qquad (7.4)$$

in which $\underset{\sim}{b}$ = the body force intensity, $\{b_x, b_y, b_z\}^T$

ρ, ρ_f = mass densities of bulk of fluid-solid and fluid respectively.

$\underset{\sim}{w}$ = fluid displacement relative to solid multiplied by porosity, n, i.e., averaged over total area, $\{w_x, w_y, w_z\}^T$.

The fluid phase: The equilibrium equation of the fluid phase can be represented as

$$\underset{\sim}{\nabla} p + \rho_f \underset{\sim}{b} = \rho_f \ddot{\underset{\sim}{u}} + \rho_f \frac{1}{n} \ddot{\underset{\sim}{w}} + \underset{\sim}{k}^{-1} \dot{\underset{\sim}{w}} \tag{7.5}$$

in which $\underset{\sim}{k}$ is a matrix of coefficients of permeability given in pressure terms. In the three dimensional case, if the orientation of coordinates is in the direction of the principal axes of the material, $\underset{\sim}{k}$ can be expressed as

$$\frac{1}{\underset{\sim}{k}} = \begin{bmatrix} \frac{1}{k_x} & 0 & 0 \\ 0 & \frac{1}{k_y} & 0 \\ 0 & 0 & \frac{1}{k_z} \end{bmatrix}$$

In future work we shall take $\underset{\sim}{k}^{-1}$ to be a scalar quantity $= \frac{1}{k}$. The permeability of soil will, in general, be a quantity strongly dependent on the total volumetric strain reached. However, in the present investigation, it is assumed constant throughout the analysis. Finally, the gradient operator is defined as

$$\underset{\sim}{\nabla} = \{\frac{\partial}{\partial x}, \frac{\partial}{\partial y}, \frac{\partial}{\partial z}\}^T$$

and the continuity condition can be represented as

$$\dot{\underset{\sim}{\varepsilon}}_v + \underset{\sim}{\nabla}^T \dot{\underset{\sim}{w}} = \dot{p} \frac{n}{K_f} \tag{7.6}$$

where $\dot{\varepsilon}_v = \underset{\sim}{m}^T \dot{\underset{\sim}{\varepsilon}}$

K_f = bulk modulus of fluid.

Equations (7.1) to (7.6) associated with the proper boundary conditions and initial conditions completely define the dynamics of nonlinear porous media.

If $\underset{\sim}{u}$ and $\underset{\sim}{w}$ in equations (7.1) to (7.6) are chosen as unknowns, then p can be eliminated by integrating equation (7.6) with respect

to time, using equation (7.2), we have

$$p = \frac{K_f}{\eta} (\underset{\sim}{m}^T \underset{\sim}{L} \underset{\sim}{u} + \underset{\sim}{\nabla}^T \underset{\sim}{w}) \qquad (a)$$

Upon substituting equation (a) into equation (7.1) we can write

$$\underset{\sim}{\sigma} = \underset{\sim}{\sigma}' + \underset{\sim}{m} \frac{K_f}{\eta} (\underset{\sim}{m}^T \underset{\sim}{L} \underset{\sim}{u} + \underset{\sim}{\nabla}^T \underset{\sim}{w}) \qquad (b)$$

Upon substituting equation (7.2) into equation (7.3) the resulting equation can be written as

$$d\underset{\sim}{\sigma}' = \underset{\sim}{D}_T (\underset{\sim}{L} d\underset{\sim}{u} - d\underset{\sim}{\varepsilon}^o) \qquad (c)$$

Upon eliminating p from equation (a) and equation (7.5) and then by simplifying we can write

$$\frac{K_f}{\eta} \underset{\sim}{\nabla} (\underset{\sim}{m}^T \underset{\sim}{L} \underset{\sim}{u} + \underset{\sim}{\nabla}^T \underset{\sim}{w}) + \rho_f \underset{\sim}{b} = \rho_f \ddot{\underset{\sim}{u}} + \frac{\rho_f}{\eta} \ddot{\underset{\sim}{w}} + \frac{1}{\underset{\sim}{k}} \underset{\sim}{w} \qquad (d)$$

The weak form of equation (7.4) using $\underset{\sim}{u} = \underset{\sim}{N}_u \bar{\underset{\sim}{u}}$, $\underset{\sim}{w} = \underset{\sim}{N}_w \bar{\underset{\sim}{w}}$ gives

$$- \int_\Omega \underset{\sim}{B}^T \underset{\sim}{\sigma} \, d\Omega + \int_\Gamma \underset{\sim}{N}_u^T \bar{\underset{\sim}{t}} \, d\Gamma + \int_\Omega \underset{\sim}{N}_u^T \rho \underset{\sim}{b} \, d\Omega = \underset{\sim}{M}_u \ddot{\bar{\underset{\sim}{u}}} + \underset{\sim}{M}_u \ddot{\bar{\underset{\sim}{w}}} \qquad (7.7)$$

in which $\underset{\sim}{M}_u = \int_\Omega \underset{\sim}{N}_u^T \rho \underset{\sim}{N}_u \, d\Omega$

$\underset{\sim}{M}_{uw} = \int_\Omega \underset{\sim}{N}_u^T \rho_f \underset{\sim}{N}_w \, d\Omega$ ($\underset{\sim}{M}_{uw}$ is proportional to $\underset{\sim}{M}_u$ if $\underset{\sim}{N}_w = \underset{\sim}{N}_u$)

Upon substituting equation (b) into (c) we can write

$$d\underset{\sim}{\sigma} = \underset{\sim}{D}_T (\underset{\sim}{L} d\underset{\sim}{u} - d\underset{\sim}{\varepsilon}^o) + \frac{K_f}{\eta} \underset{\sim}{m} \underset{\sim}{m}^T \underset{\sim}{B} d\bar{\underset{\sim}{u}} + \frac{K_f}{\eta} \underset{\sim}{m} \underset{\sim}{\nabla}^T \underset{\sim}{N}_w d\bar{\underset{\sim}{w}} \qquad (7.8)$$

Similarly, the weak form of equation (d) gives

$$- \int_\Omega \underset{\sim}{\nabla} \underset{\sim}{N}_w \frac{K_f}{\eta} \underset{\sim}{m}^T \underset{\sim}{B} \, d\Omega \, \bar{\underset{\sim}{u}} - \int_\Omega \underset{\sim}{\nabla} \underset{\sim}{N}_w \frac{K_f}{\eta} \underset{\sim}{\nabla} \underset{\sim}{N}_w \, d\bar{\underset{\sim}{w}} +$$

$$\int_\Omega \underset{\sim}{N}_w^T \rho_f \underset{\sim}{b} \, d\Omega = \underset{\sim}{M}_{wu} \ddot{\bar{\underset{\sim}{u}}} + \underset{\sim}{M}_w \ddot{\bar{\underset{\sim}{w}}} + \underset{\sim}{C} \dot{\bar{\underset{\sim}{w}}} \qquad (7.9)$$

in which $$\underset{\sim}{M}_{wu} = \int_{\Omega} \underset{\sim}{N}_w^T \rho_f \underset{\sim}{N}_u \, d\Omega \equiv \underset{\sim}{M}_{uw}^T$$

$$\underset{\sim}{M}_w = \int_{\Omega} \underset{\sim}{N}_w^T \frac{\rho_f}{n} \underset{\sim}{N}_w \, d\Omega$$

$$\underset{\sim}{C} = \int_{\Omega} \underset{\sim}{N}_w^T \frac{1}{k} \underset{\sim}{N}_w \, d\Omega$$

In the linear case, equation (7.8) can be integrated and finally, the following equation can be obtained

$$\begin{bmatrix} \underset{\sim}{M}_u & \underset{\sim}{M}_{uw} \\ \underset{\sim}{M}_{uw}^T & \underset{\sim}{M}_w \end{bmatrix} \begin{Bmatrix} \ddot{\underset{\sim}{u}} \\ \ddot{\underset{\sim}{w}} \end{Bmatrix} + \begin{bmatrix} \underset{\sim}{0} & \underset{\sim}{0} \\ \underset{\sim}{0} & \underset{\sim}{C} \end{bmatrix} \begin{Bmatrix} \dot{\underset{\sim}{u}} \\ \dot{\underset{\sim}{w}} \end{Bmatrix} + \begin{bmatrix} \underset{\sim}{K} & \underset{\sim}{E} \\ \underset{\sim}{E}^T & \bar{\underset{\sim}{K}} \end{bmatrix} \begin{Bmatrix} \underset{\sim}{u} \\ \underset{\sim}{w} \end{Bmatrix} = \begin{Bmatrix} \underset{\sim}{f} \\ \bar{\underset{\sim}{f}} \end{Bmatrix} \tag{7.10}$$

where $$\underset{\sim}{E} = \int_{\Omega} \underset{\sim}{B}^T \frac{K_f}{n} \underset{\sim}{m} \underset{\sim}{\nabla}^T \underset{\sim}{N}_w \, d\Omega$$

$$\bar{\underset{\sim}{K}} = \int_{\Omega} \underset{\sim}{N}_w \frac{K_f}{n} \underset{\sim}{\nabla}^T \underset{\sim}{N}_w \, d\Omega$$

$$\underset{\sim}{K} = \int_{\Omega} \underset{\sim}{B}^T \left(\underset{\sim}{D} + \frac{K_f}{n} \underset{\sim}{m} \underset{\sim}{m}^T \right) \underset{\sim}{B} \, d\Omega$$

$$\underset{\sim}{f} = \int_{\Gamma} \underset{\sim}{N}_u^T \bar{\underset{\sim}{t}} \, d\Gamma + \int_{\Omega} \underset{\sim}{N}_u^T \rho \underset{\sim}{b} \, d\Omega + \int_{\Omega} \underset{\sim}{B}^T \underset{\sim}{D} \, d\underset{\sim}{\varepsilon}^o \, d\Omega$$

$$\bar{\underset{\sim}{f}} = \int_{\Omega} \underset{\sim}{N}_w^T \rho_f \underset{\sim}{b} \, d\Omega$$

Equation (7.10) is identical to that presented by Ghaboussi and Wilson[6].

When the seepage velocity relative to the soil skeleton is small compared with its motion or if the permeability is low, the relative acceleration of the fluid with respect to solid can be assumed to be negligible. With this approximation, the unknown $\underset{\sim}{w}$ can be replaced by

p, thus the degrees of freedom reduce from 6 (u_x, u_y, u_z, w_x, w_y, w_z) to 4 (u_x, u_y, u_z, p). Therefore a cheaper and simpler formulation can be achieved. This simplification was first suggested by Zienkiewicz[9]. The detail of the derivation is given in the following.

By neglecting the $\ddot{\underset{\sim}{w}}$ term, equation (7.5) can be rewritten as

$$\underset{\sim}{w} = \underset{\sim}{k}\,\underset{\sim}{\nabla} p + \underset{\sim}{k}\,\rho_f\,\underset{\sim}{b} - \underset{\sim}{k}\,\rho_f\,\ddot{\underset{\sim}{u}} \qquad (e)$$

Substituting equations (e), (7.2) into (7.6) and simplifying leads to

$$\underset{\sim}{m}^T\,\underset{\sim}{L}\,\dot{\underset{\sim}{u}} + \underset{\sim}{\nabla}^T\,\underset{\sim}{k}\,\underset{\sim}{\nabla} p + \underset{\sim}{\nabla}^T\,\underset{\sim}{k}\,\rho_f\,\underset{\sim}{b} - \underset{\sim}{\nabla}^T\,\underset{\sim}{k}\,\rho_f\,\ddot{\underset{\sim}{u}} - \dot{p}\,\frac{K_f}{n} = 0 \qquad (f)$$

By neglecting the $\ddot{\underset{\sim}{w}}$ term equations (7.1), (7.3) and (7.4) can be written as follows

$$\underset{\sim}{\sigma} = \underset{\sim}{\sigma}' + \underset{\sim}{m}\,p \qquad (g)$$

$$d\underset{\sim}{\sigma}' = \underset{\sim}{D}_T\,(d\underset{\sim}{\varepsilon} - d\underset{\sim}{\varepsilon}^0) \qquad (h)$$

$$\underset{\sim}{L}^T\,\underset{\sim}{\sigma} + p\,\underset{\sim}{b} = \rho\,\ddot{\underset{\sim}{u}} \qquad (i)$$

Using $\underset{\sim}{u} = \underset{\sim}{N}_u\,\bar{\underset{\sim}{u}}$, $p = \underset{\sim}{N}_p\,\bar{p}$ and in view of equation (g), the weak form of equation (i) can be presented as

$$\int_\Omega \underset{\sim}{B}^T\,\underset{\sim}{\sigma}'\,d\Omega + \int_\Omega \underset{\sim}{B}^T\,\underset{\sim}{m}\,\underset{\sim}{N}_p\,d\Omega\,\bar{\underset{\sim}{p}} + \underset{\sim}{M}\,\ddot{\bar{\underset{\sim}{u}}} + \underset{\sim}{f} = 0 \qquad (j)$$

$$d\underset{\sim}{\sigma}' = \underset{\sim}{D}_T\,(\underset{\sim}{L}\,d\underset{\sim}{u} - d\underset{\sim}{\varepsilon}^0) \qquad (k)$$

The weak form of (f) gives

$$\int_\Omega \underset{\sim}{N}_p^T\,\underset{\sim}{m}^T\,\underset{\sim}{B}\,d\Omega\,\dot{\bar{\underset{\sim}{u}}} - \int_\Omega \underset{\sim}{\nabla}\,\underset{\sim}{N}_p^T\,\underset{\sim}{k}\,\underset{\sim}{\nabla}\,\underset{\sim}{N}_p\,d\Omega\,\bar{\underset{\sim}{p}} - \int_\Omega \underset{\sim}{N}_p^T\,\frac{n}{K_f}\,\underset{\sim}{N}_p\,d\Omega\,\dot{\bar{\underset{\sim}{p}}}$$

$$- \int_\Omega \underset{\sim}{N}_p^T\,\underset{\sim}{\nabla}^T\,\underset{\sim}{k}\,\rho_f\,\underset{\sim}{N}_u\,d\Omega\,\ddot{\bar{\underset{\sim}{u}}} + \bar{\underset{\sim}{f}} = 0 \qquad (\ell)$$

in which $$\underset{\sim}{f} = -\int_{\Omega} \underset{\sim}{N}_u^T \rho \underset{\sim}{b}\, d\Omega - \int_{\Gamma} \underset{\sim}{N}_u^T \bar{t}\, d\Gamma$$

$$\bar{\underset{\sim}{f}} = \int_{\Omega} \underset{\sim}{N}_p^T \underset{\sim}{\nabla}^T \underset{\sim}{k}\, \rho_f \underset{\sim}{b}\, d\Omega + \int_{\Omega} \underset{\sim}{N}_p^T \bar{q}\, d\Gamma$$

where q is the outflow across the boundary Γ. Therefore, the general equations can be rewritten as

$$\int_{\Omega} \underset{\sim}{B}^T \sigma'\, d\Omega + \underset{\sim}{Q}\, \bar{\underset{\sim}{p}} + \underset{\sim}{M}\, \ddot{\bar{\underset{\sim}{u}}} + \underset{\sim}{f} = 0 \qquad (7.11a)$$

$$d\underset{\sim}{\sigma}' = \underset{\sim}{D}_T \left(\underset{\sim}{B}\, d\bar{\underset{\sim}{u}} - d\underset{\sim}{\varepsilon}^0\right) \qquad (7.11b)$$

$$\underset{\sim}{H}\, \bar{\underset{\sim}{p}} + \underset{\sim}{T}\, \dot{\bar{\underset{\sim}{p}}} - \underset{\sim}{Q}^T \dot{\bar{\underset{\sim}{u}}} + \hat{\underset{\sim}{M}}\, \ddot{\bar{\underset{\sim}{u}}} - \bar{\underset{\sim}{f}} = 0 \qquad (7.11c)$$

in which

$$\underset{\sim}{Q} = \int_{\Omega} \underset{\sim}{B}^T \underset{\sim}{m}\, \underset{\sim}{N}_p\, d\Omega$$

$$\hat{\underset{\sim}{M}} = \int_{\Omega} \underset{\sim}{N}_u^T \rho\, \underset{\sim}{N}_u\, d\Omega$$

$$\underset{\sim}{H} = \int_{\Omega} (\underset{\sim}{\nabla}\, \underset{\sim}{N}_p)^T \underset{\sim}{k}\, \underset{\sim}{\nabla}\, \underset{\sim}{N}_p\, d\Omega$$

$$\underset{\sim}{T} = \int_{\Omega} \underset{\sim}{N}_p^T \frac{n}{K_f}\, \underset{\sim}{N}_p\, d\Omega$$

Equations (7.11.a,b,c) can be regarded as a set of ordinary differential equations and solved using time stepping procedure. The sequence at any time step can be summarized as follows, (the details of the computer program implementation are presented in Appendix D).

(1) Start with $^{t}\underset{\sim}{u}$, $^{t-\Delta t}\underset{\sim}{u}$, $^{t}\underset{\sim}{\sigma}'$ and ^{t}p.

(2) Using equation (7.11.a) evaluate $^{t+\Delta t}\underset{\sim}{u}$ as described in Chapter 4 and hence $^{t+\Delta t}\underset{\sim}{\varepsilon}$ and $^{t+\Delta t}\underset{\sim}{\sigma}$.

(3) Using equation (7.11.c) obtain $^{t+\Delta t}p$ with known values of $^{t+\Delta t}\dot{\underset{\sim}{u}}$ and $^{t+\Delta t}\ddot{\underset{\sim}{u}}$.

(4) Update t to t+Δt and if $t \leq t_{max}$ go to step (1), otherwise stop.

It is of interest to examine step (3) in some more detail. Equation (7.11c) may be numerically integrated over the time interval t, t+Δt as follows,

$$\underset{\sim}{H}\left[\theta\{^{t+\Delta t}\underset{\sim}{p}\} + (1-\theta)\{^{t}\underset{\sim}{p}\}\right]\Delta t + \underset{\sim}{I}\left[^{t+\Delta t}\underset{\sim}{p} - ^{t}\underset{\sim}{p}\right] - \hat{\underset{\sim}{f}}\,\Delta t = 0$$

or

$$\underset{\sim}{A}\,^{t+\Delta t}\underset{\sim}{p} = \underset{\sim}{R} \qquad (7.12)$$

in which

$$\underset{\sim}{A} = \theta\,\Delta t\,\underset{\sim}{H} + \underset{\sim}{I}$$

$$\underset{\sim}{R} = \left[\underset{\sim}{I} - (1-\theta)\,\Delta t\,\underset{\sim}{H}\right]\,^{t}\underset{\sim}{p} + \hat{\underset{\sim}{f}}\,\Delta t$$

$$\hat{\underset{\sim}{f}} = \underset{\sim}{Q}^{T}\,^{t}\dot{\underset{\sim}{u}} - \hat{\underset{\sim}{M}}\,^{t}\ddot{\underset{\sim}{u}} + \bar{\underset{\sim}{f}}$$

and the superscripts t, t+Δt indicate the values of a variable at time t, t+Δt respectively. Different values of θ correspond to different approximations; if $\theta \geq 0.5$ the integration procedure is always stable[10]. When θ = 1, the backward difference scheme is adopted in the present study. With the above algorithm, the dynamic program along with a FRONTAL solution technique[11] can be used to estimate the excess pore pressure at each time step.

It is of interest to note that for the conventional (Terzaghi) consolidation problem[12-16], (i.e., $\ddot{\underset{\sim}{w}} = \ddot{\underset{\sim}{u}} = 0$ with a known total stress, $\underset{\sim}{\sigma}$) the seepage equation can be shown to be

$$-\underset{\sim}{\nabla}^{T}\,k\,\underset{\sim}{\nabla}\,p + \left(\frac{n}{K_f} + \underset{\sim}{m}^{T}\,\underset{\sim}{D}_{T}^{-1}\,\underset{\sim}{m}\right)\dot{p} = \underset{\sim}{m}^{T}\,\dot{\underset{\sim}{\varepsilon}}^{o} + \underset{\sim}{m}^{T}\,\underset{\sim}{D}_{T}^{-1}\,\dot{\underset{\sim}{\sigma}} \qquad (7.13)$$

Again a finite element discretization of the above equation can be performed by using the standard procedure and incorporating any prescribed flow boundary conditions as described in the text by Zienkiewicz[10]. The discretization leads to

$$\underset{\sim}{H}\,\bar{\underset{\sim}{p}} + \underset{\sim}{T}\,\dot{\bar{\underset{\sim}{p}}} - \underset{\sim}{f} = 0 \qquad (7.14)$$

in which

$$\underset{\sim}{H} = \int_{\Omega} (\nabla \underset{\sim}{N}_p)^T \, k \, (\nabla \underset{\sim}{N}_p) \, d\Omega$$

$$\underset{\sim}{T} = \int_{\Omega} \underset{\sim}{N}_p^T \left(\frac{n}{K_f} + \underset{\sim}{m}^T \underset{\sim}{D}_T^{-1} \underset{\sim}{m}\right) \underset{\sim}{N}_p \, d\Omega$$

$$\underset{\sim}{f} = \int_{\Omega} \underset{\sim}{N}_p^T \left(\underset{\sim}{m}^T \dot{\underset{\sim}{\varepsilon}}^o + \underset{\sim}{m}^T \underset{\sim}{D}_T^{-1} \dot{\underset{\sim}{\sigma}}\right) d\Omega$$

Equation (7.14) is of exactly the same form as equation (7.11.c) and hence the computational algorithm presented earlier can be applied here. If $\dot{\underset{\sim}{\sigma}} = 0$, i.e., no change of total stress, equation (7.14) gives the change of excess pore pressure due to $\underset{\sim}{m}^T \dot{\underset{\sim}{\varepsilon}}^o$ alone in which $\underset{\sim}{m}^T \dot{\underset{\sim}{\varepsilon}}^o$ is equivalent to the autogenous volumetric strain as given in Chapter 5.

7.3 EXAMPLES

In this section two examples are presented which illustrate the application of the method of analysis described in previous sections.

Example 1 A saturated half space subjected to a harmonic loading on the surface.

This example is to investigate the effect of dynamic terms on seepage formulation. Therefore, only the study of analytic linear elastic steady state solution is carried out. Owing to the nature of the problem, the saturated half space subjected to a harmonic loading

on the surface can be treated as a one dimensional saturated soil column with the appropriate material properties.

For the one dimensional problem, equation (7.10) can be rewritten as

$$\left(D + \frac{K_f}{\eta} \right) \frac{\partial^2 u}{\partial z^2} + \frac{K_f}{\eta} \frac{\partial^2 w}{\partial z^2} = \rho \frac{\partial^2 u}{\partial t^2} + \rho_f \frac{\partial^2 w}{\partial t^2}$$

$$\frac{K_f}{\eta} \frac{\partial^2 u}{\partial z^2} + \frac{K_f}{\eta} \frac{\partial^2 w}{\partial z^2} = \rho_f \frac{\partial^2 u}{\partial t^2} + \frac{\rho_f}{\eta} \frac{\partial^2 w}{\partial t^2} + \frac{1}{k} \frac{\partial w}{\partial t} \qquad (7.15)$$

in which D denotes the elastic property of the solid skeleton and can be expressed as

$$D = \frac{E(1-\nu)}{(1+\nu)\ (1-2\nu)} \qquad (7.16)$$

in which E, ν are Young's modulus and Poisson's ratio of the material respectively.

The surface harmonic loading, f, can be represented as

$$f = f_o e^{i\Omega t} \qquad (7.17)$$

where f_o and Ω are respectively the amplitude and the frequency of the applied load. Since only the steady state solution is interested, the steady state responses can be represented by the following expressions

$$u = (u_R + i\ u_I)\ e^{i\Omega t} = \bar{u}\ e^{i\Omega t}$$

$$w = (w_R + i\ w_I)\ e^{i\Omega t} = \bar{w}\ e^{i\Omega t} \qquad (7.18)$$

in which u_R, u_I and w_R, w_I are respectively the real parts and the imaginary parts of the displacements u and w.

Substituting equation (7.18) into equation (7.15), in view of the following parameters,

$$\kappa = \frac{K_f/\eta}{D + K_f/\eta}$$

$$\beta = \rho_f/\rho$$

$$V_c = \sqrt{\frac{D+K_f/\eta}{\rho}}$$

$$\bar{z} = z/L \qquad (7.19)$$

where L is the height of the soil column, then nondimensionizing the results give

$$\frac{V_c^2}{L^2}\frac{d^2\bar{u}}{d\bar{z}^2} + \frac{V_c^2\,\kappa}{L^2}\frac{d^2\bar{w}}{d\bar{z}} = -\Omega^2\,\bar{u} - \beta\,\Omega^2\,\bar{w}$$

$$\frac{V_c^2\,\kappa}{L^2}\frac{d\,\bar{u}}{d\bar{z}^2} + \frac{V_c^2\,\kappa}{L^2}\frac{d^2\bar{w}}{d\bar{z}^2} = -\beta\,\Omega^2\bar{u} - \frac{\beta}{\eta}\Omega^2\,\bar{w} + \frac{i\Omega}{k\rho}\bar{w}$$

or

$$\frac{d^2\bar{u}}{d\bar{z}^2} + \kappa\frac{d^2\bar{w}}{d\bar{z}^2} = -\frac{\Omega^2\,L^2}{V_c^2}\bar{u} - \beta\frac{\Omega^2\,L^2}{V_c^2}\bar{w}$$

$$\kappa\frac{d^2\bar{u}}{d\bar{z}^2} + \frac{d^2\bar{w}}{d\bar{z}^2} = -\beta\frac{\Omega^2\,L^2}{V_c^2}\bar{u} - \frac{\beta}{\eta}\frac{\Omega^2 L^2}{V_c^2}\bar{w} + \frac{i\Omega\,L^2}{k\rho\,V_c^2}\bar{w} \qquad (7.20)$$

By defining the following nondimensional parameters

$$\pi_1 = \frac{k\rho\,V_c^2}{\Omega\,L^2}$$

$$\pi_2 = \frac{\Omega^2\,L^2}{V_c^2} \qquad (7.21)$$

equation (7.20) can be further represented as

$$\frac{d^2\bar{u}}{d\bar{z}^2} + \kappa \frac{d^2\bar{w}}{d\bar{z}^2} = \cdot\cdot \pi_2 \bar{u} - \beta \pi_2 \bar{w}$$

$$\kappa \frac{d^2\bar{u}}{d\bar{z}^2} + \kappa \frac{d^2\bar{w}}{d\bar{z}^2} = - \beta \pi_2 \bar{u} - \frac{\beta}{\eta} \pi_2 \bar{w} + \frac{i}{\pi_1} \bar{w} \qquad (7.22)$$

Now, the system becomes a set of simultaneous second order ordinary linear differential equations which can readily be solved by using a computer for the following boundary conditions

$$\sigma_{\bar{z}=0} = f_o$$

$$p_{\bar{z}=0} = 0$$

$$\bar{u}_{\bar{z}=1} = 0 \qquad (7.23)$$

$$\left.\frac{dp}{d\bar{z}}\right|_{\bar{z}=1} = 0$$

Equation (7.22) gives respectively the following two sets of equations when $\ddot{w}$ and when both $\ddot{u}$ and $\ddot{w}$ are neglected, i.e.,

$$\frac{d^2\bar{u}}{d\bar{z}^2} + \kappa \frac{d^2\bar{w}}{d\bar{z}^2} = - \pi_2 \bar{u}$$

$$\kappa \frac{d^2\bar{u}}{d\bar{z}^2} + \kappa \frac{d^2\bar{w}}{d\bar{z}^2} = - \beta\pi_2 \bar{u} + \frac{i}{\pi_1} \bar{w} \qquad (7.24)$$

and

$$\frac{d^2\bar{u}}{d\bar{z}} + \kappa \frac{d^2\bar{w}}{d\bar{z}} = 0$$

$$\kappa \frac{d^2\bar{u}}{d\bar{z}^2} + \kappa \frac{d^2\bar{w}}{d\bar{z}^2} = \frac{i}{\pi_1} \bar{w} \qquad (7.25)$$

Similarly, equations (7.24) and (7.25) associated with the boundary conditions as defined by equation (7.23) can easily be solved with the aid of computer.

It is worthwhile mentioning that equations (7.24) and (7.25) can also be expressed and solved in terms of unknowns u and p and identical results can be obtained.

It is of interest to investigate the responses for various values of the parameters represented in equations (7.19) and (7.21). However it can be noted that the parameters in equation (7.19) are nearly constant. Therefore, in the following parametric studies, these parameters are fixed as follows

$$\kappa = 0.973; \quad \beta = 0.333; \quad \eta = 0.333 \qquad (7.26)$$

The applied load f_o is nondimensionalised as $f_o/(K_f/\eta)$ and its value is chosen as 8.333×10^{-6}.

The results of computation with different values of π_1 and π_2 contain the absolute values of and the arguments of u, w, p and σ. But only the absolute values of u, w and p are shown in Figures 7.1, 7.2 and 7.3 respectively. The summary of the parametric studies is presented in Table 7.1 from which the ranges, wherein the $\ddot{w}$ or $\ddot{u}$ and $\ddot{w}$ terms in the formulation can be neglected, are readily seen.

From the results of this study, it can be concluded that unless the frequency of exciting force is very high, 50 cycles/sec. or above, and the coefficient of permeability is equivalent to that of sand, the Zienkiewicz's simplified formulation gives a reasonable approximation. Therefore this simplified formulation is adopted in the present study.

Example 2 A saturated sand layer subjected to N-S component of El Centro earthquake of May 1940 scaled to 0.1g.

A 50 foot layer of sand with water table at 5 feet below the ground surface is shown in Figure 7.4. This layer is subjected to the NS component of the El Centro earthquake scaled to a maximum acceleration of 0.1g. The results are presented in Figures 7.5 to 7.9. Figures 7.5, 7.6 and 7.7 show respectively the acceleration time history and displacement time history of the surface of the layer and the shear stress time history at point x. The rise of excess pore water pressure at various times are represented in Figure 7.8. The build up of excess pore water pressure with respect to time at point x_1 is shown in Figure 7.9. The effect of seepage on responses can easily be seen from the present study.

REFERENCES

1. BIOT, M.A.
'General Theory of Three-Dimensional Consolidation'
Jnl. of Applied Physics, Vol. 12, 155-164 (1941)

2. BIOT, M.A.
'Theory of Elasticity and Consolidation for a Porous Anisotropic Solid'
Jnl. of Applied Physics, Vol. 26, 182-185 (1955)

3. BIOT, M.A.
'General Solutions of the Equations of Elasticity and Consolidation for a Porous Material'
Jnl. of Applied Mechanics, Proc. ASME, Vol.23, 91-96 (1956)

4. BIOT, M.A.
'Mechanics of Deformation and Acoustic Propagation in Porous Media'
Jnl. of Applied Physics, Vol. 33, 1482-1498 (1961)

5. SANDHU, R.S. and WILSON, E.L.
'Finite Element Analysis of Flow in Saturated Porous Media'
Proc. ASCE, Vol. 95, 641-652 (1969)

6. GHABOUSSI, J. and WILSON, E.L.
'Variational Formulation of Dynamics of Fluid Saturated Porous Elastic Solids'
Jnl. of the Engineering Mechanics Division, ASCE, Vol.98, No. EM44, 947-963 (1972)

7. GHABOUSSI, J. and WILSON, E.L.
'Flow of Compressible Fluid in Porous Elastic Solids'
Int. Jnl. Num. Meth. Engng. Vol. 5, 419-442 (1973)

8. GHABOUSSI, J. and WILSON, E.L.
'Seismic Analysis of Earth Dam-Reservoir Systems'
Jnl. of the Soil Mechanics and Foundations Division, ASCE, Vol. 99, No. SM10 (1973)

9. ZIENKIEWICZ, O.C.
Lecture Note
'Basic Formulation of Soil Mechanics in Finite Element Analysis'
Course on Finite Elements in Geotechnical Engineering Held at Swansea, 1978

10. ZIENKIEWICZ, O.C.
'The Finite Element Method'
McGraw-Hill, London (1977)

11. HINTON, E. and OWEN, D.R.J.
'Finite Element Programming'
Academic Press (1977)

12. ZIENKIEWICZ, O.C., HUMPHESON, C. and LEWIS, R.W.
'A Unified Approach to Soil Mechanics Including Plasticity and Viscoplasticity'
Int. Symp. on Num. Methods in Soil Mechanics, Karlsruhe (1975)

13. ZIENKIEWICZ, O.C., NORRIS, V.A., WINNICKI, L.A., NAYLOR, D.J. and LEWIS, R.W.
'A Unified Approach to the Soil Mechanics Problems of Offshore Foundations, Numerical Methods in Offshore Engineering'
Ed. by Zienkiewicz, O.C., Lewis, R.W., and Stagg, K.G.,
John Wiley & Sons (1978)

14. SEED, H.B., MARTIN, P.P. and LYSMER, L.
'The Generation and Dissipation of Pore Water Pressure During Soil Liquefaction'
Report No. EERC-75-26, Earthquake Engineering Research Center, University of California, Berkeley, California (1975)

15. FINN, W.D.L., LEE, K.W. and MARTIN, G.R.
'Seismic Pore Water Pressure Generation and Dissipation'
Symp. on Soil Liquefaction ASCE National Convention, Philadelphia (1976)

16. FINN, W.D.L., LEE, K.W., BYRNE, P.M. and MARTIN, G.R.
'Response of Saturated Sands to Earthquake and Wave Induced Forces'
Numerical Methods in Offshore Engineering, Ed. by Zienkiewicz, O.C., Lewis, R.W. and Stagg, K.G.,
John Wiley & Sons (1978)

TABLE 7.1 SUMMARY OF PARAMETRIC STUDY

π_2 \ π_1	10^5	10^4	10^3	10^2	10^1	10^0	10^{-1}	10^{-2}
10^3	B	B	B	B	B	B*	B	B
10^1	B	B	B	B	B*	B	B,Z	B,Z**
10^{-1}	B	B	B	B*	B,Z	B,Z	B,Z	B,Z**
10^{-3}	B,Z,C	B,Z,C*	B,Z,C	B,Z,C	B,Z,C	B,Z,C	B,Z,C	B,Z,C**

Notes: 1. B denotes Biot's complete formulation; Z denotes Zienkiewicz's simplified formulation; C denotes conventional consolidation.
2. For values of π_2 below the double lines, all formulations give the identical responses
3. * denotes upper bounds, for values of π_1, left to * the results for all cases are identical and equivalent to the fully drained conditions.
4. ** denotes lower bounds, for values of π_1, right to ** the results for all cases are identical and equivalent to the fully undrained conditions.

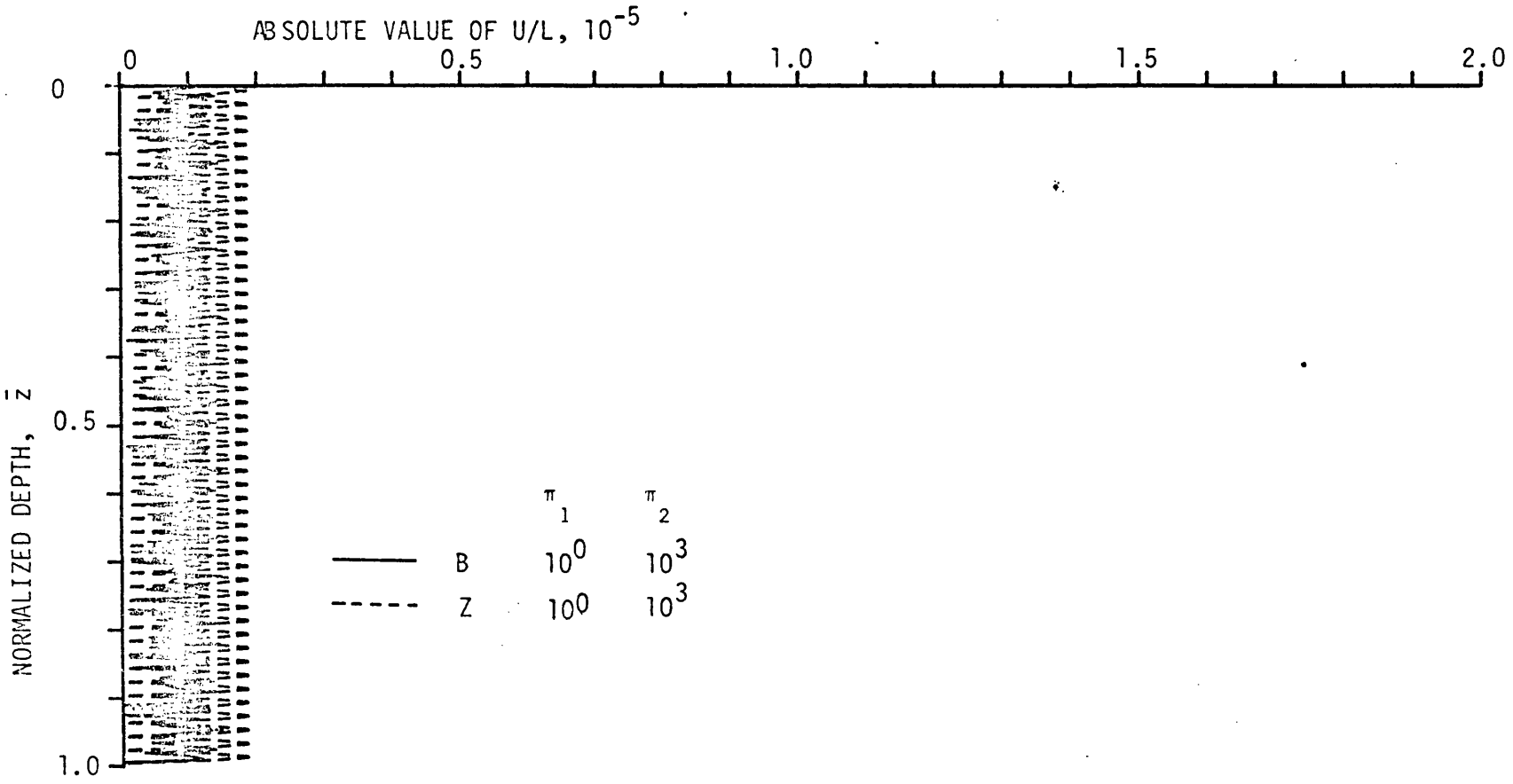

FIGURE 7.1 ABSOLUTE VALUE OF U/L

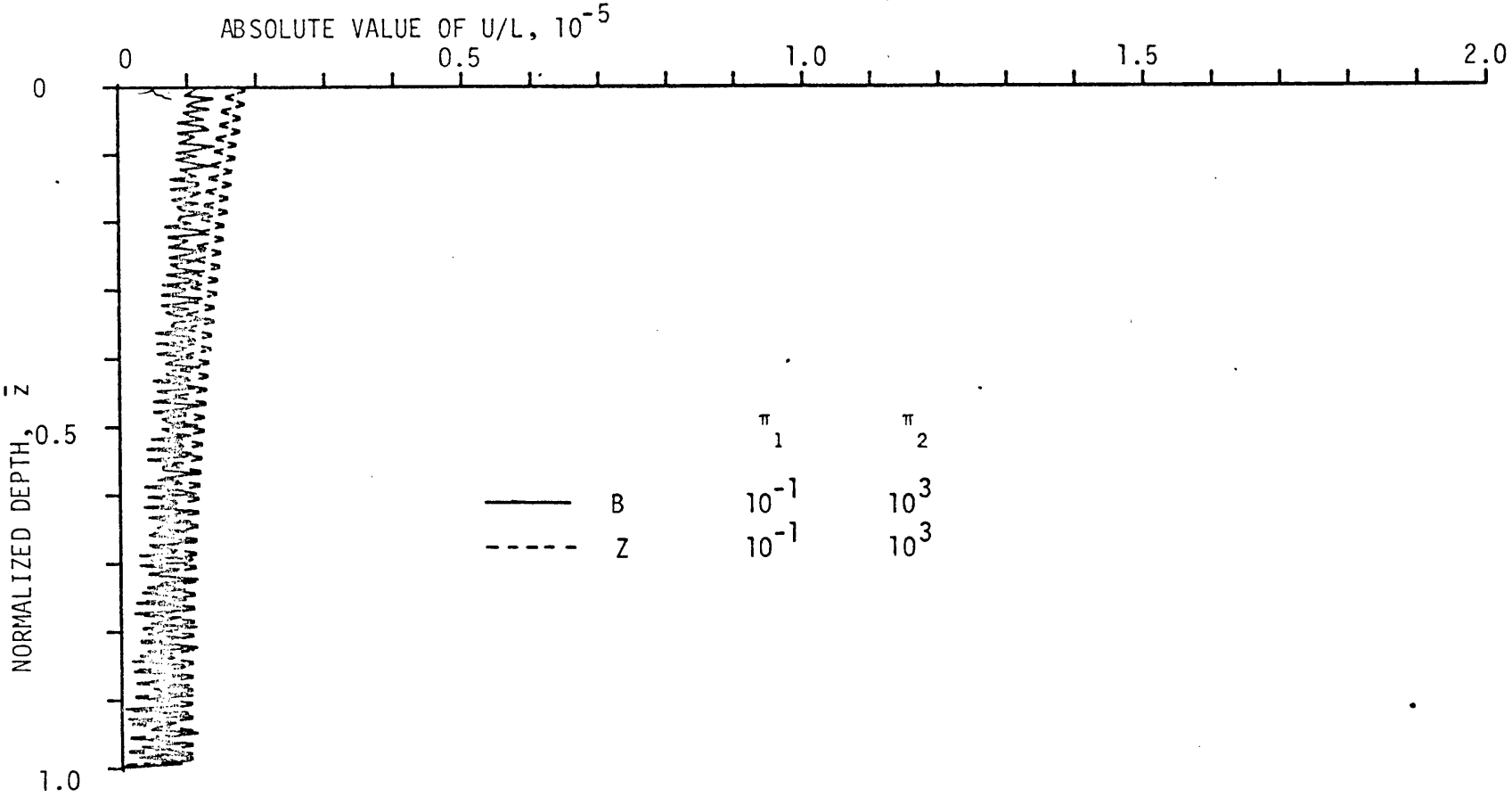

FIGURE 7.1 (cont'd)

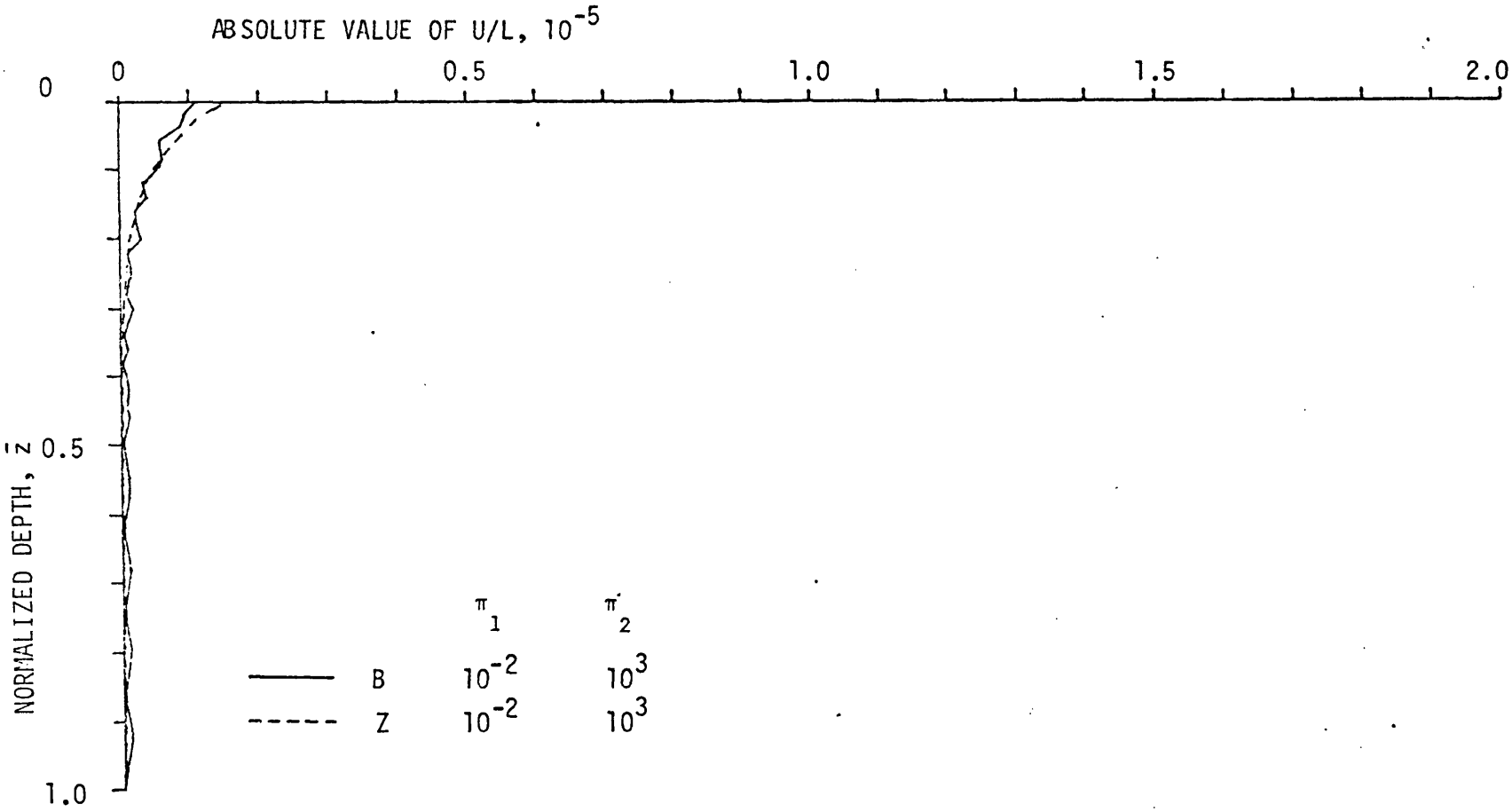

FIGURE 7.1 (cont'd)

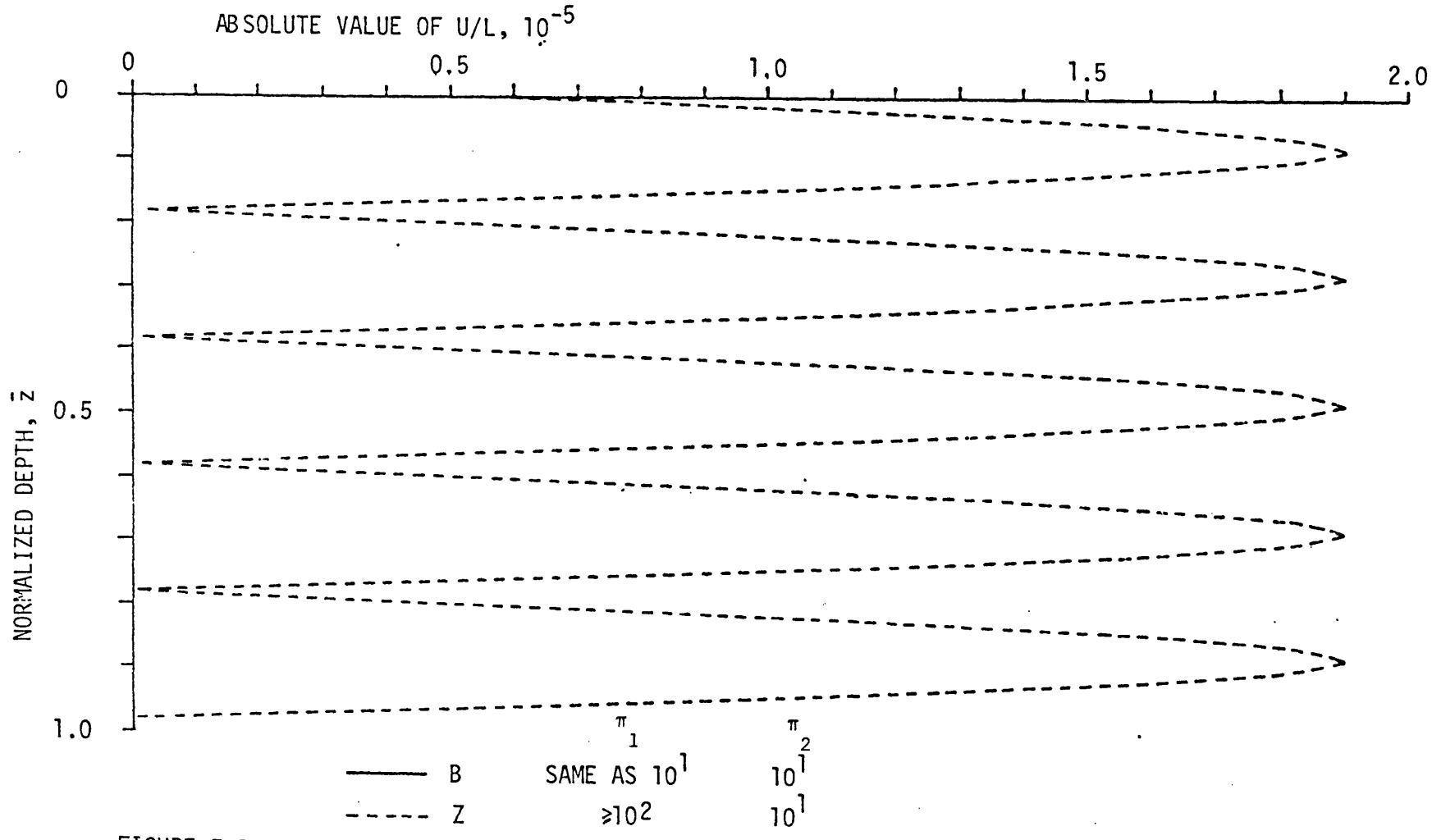

FIGURE 7.1 (cont'd)

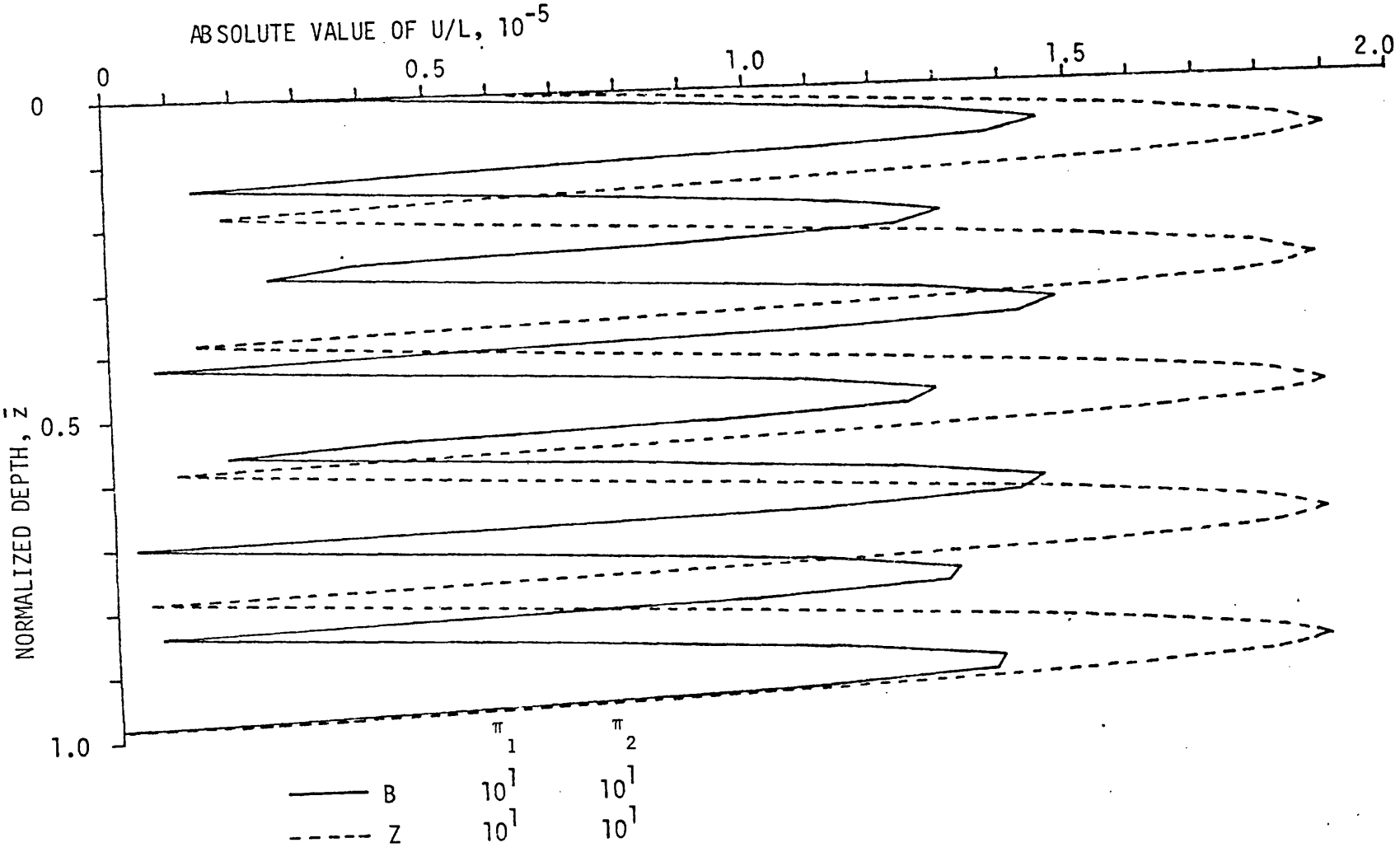

FIGURE 7.1 (cont'd)

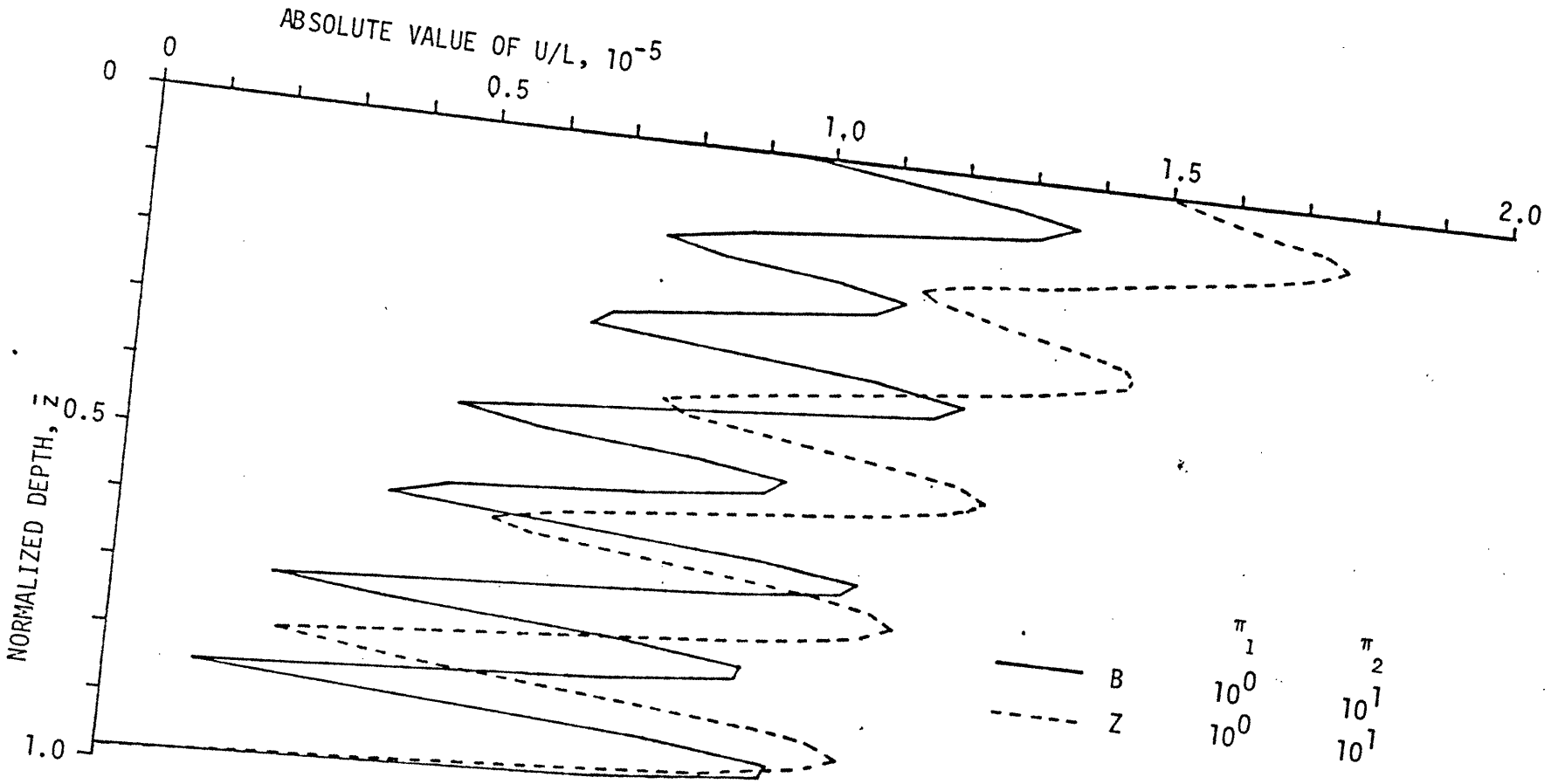

FIGURE 7.1 (cont'd)

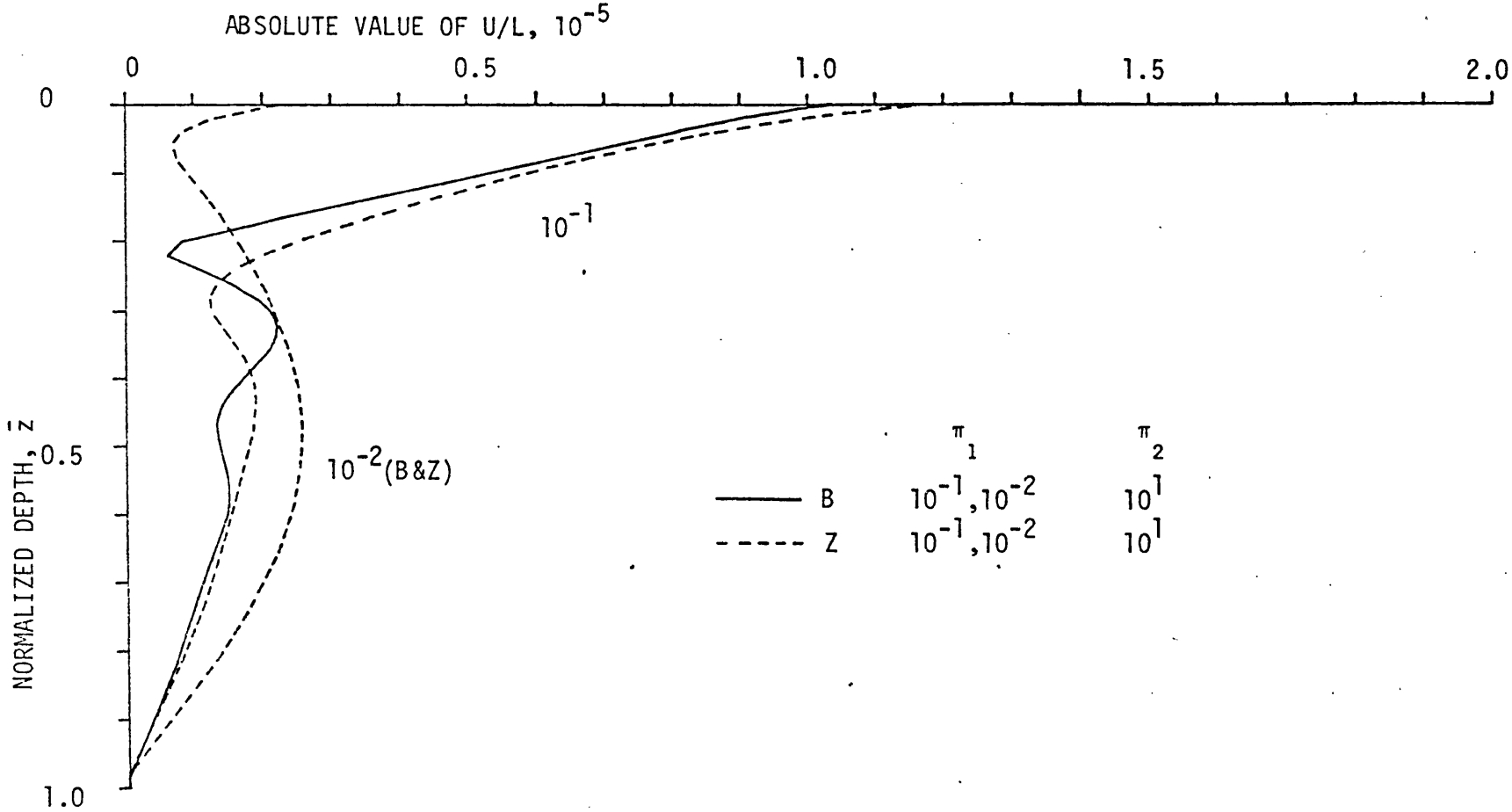

FIGURE 7.1 (cont'd)

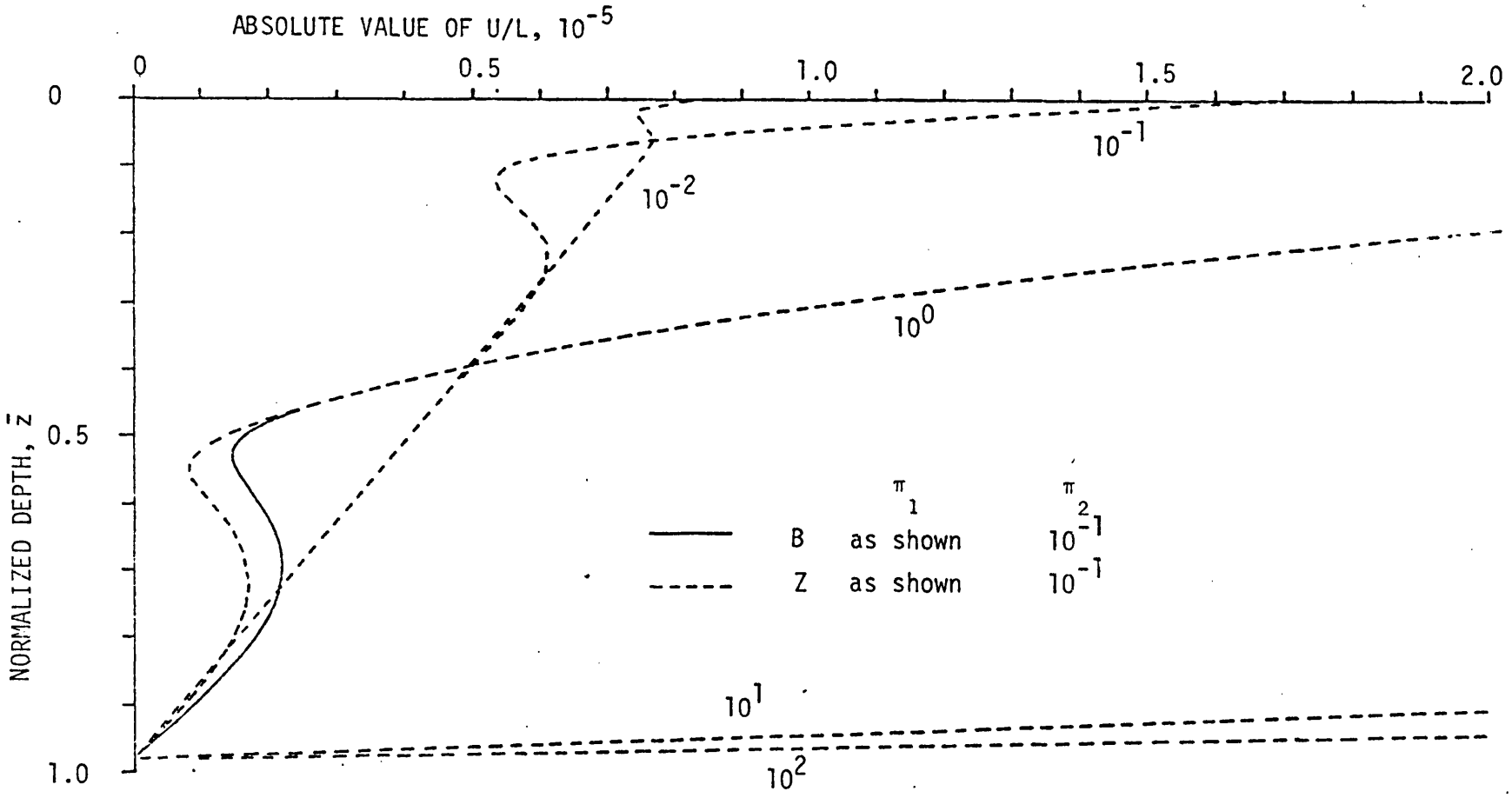

FIGURE 7.1 (cont'd)

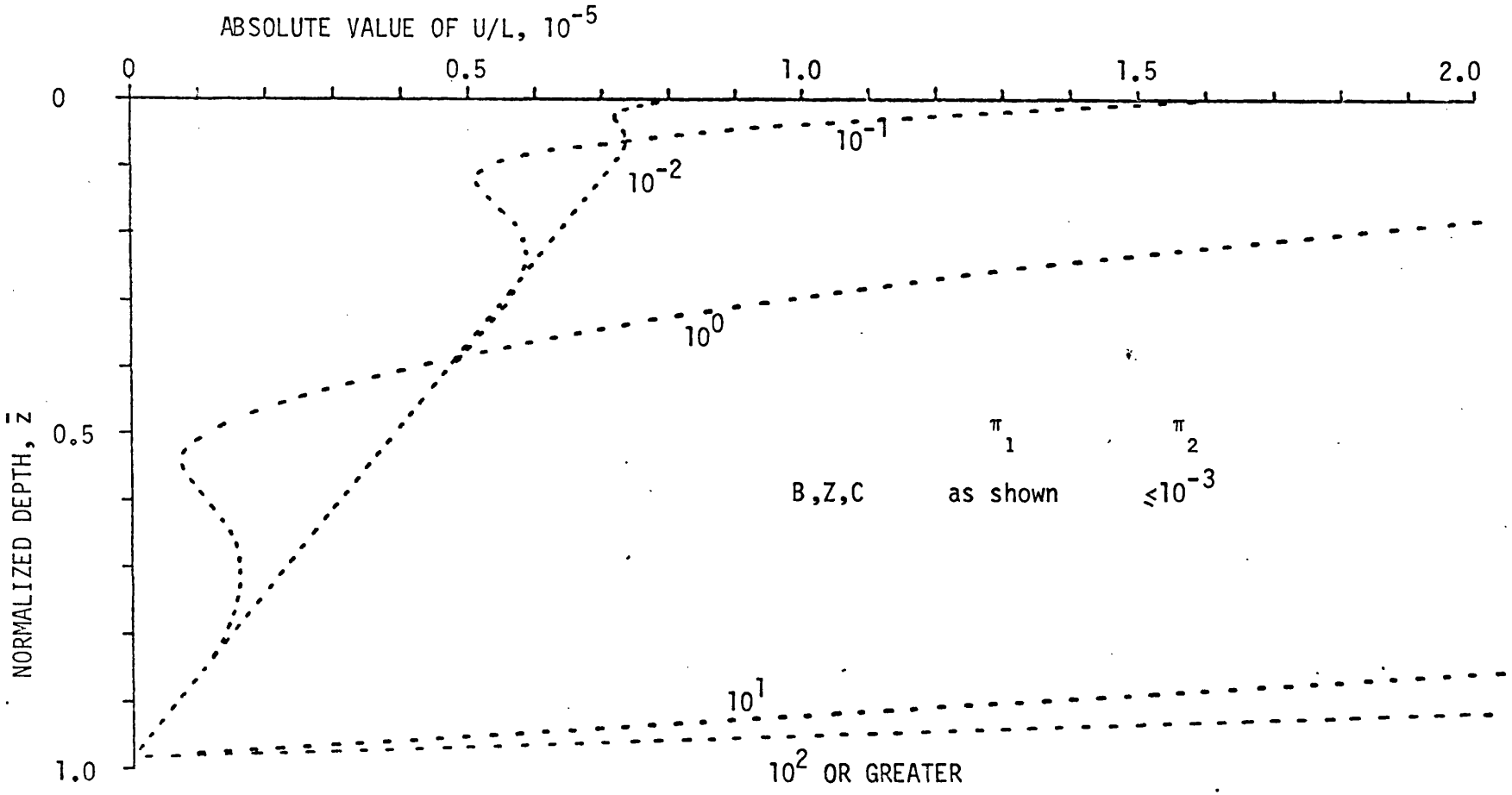

FIGURE 7.1 (cont'd)

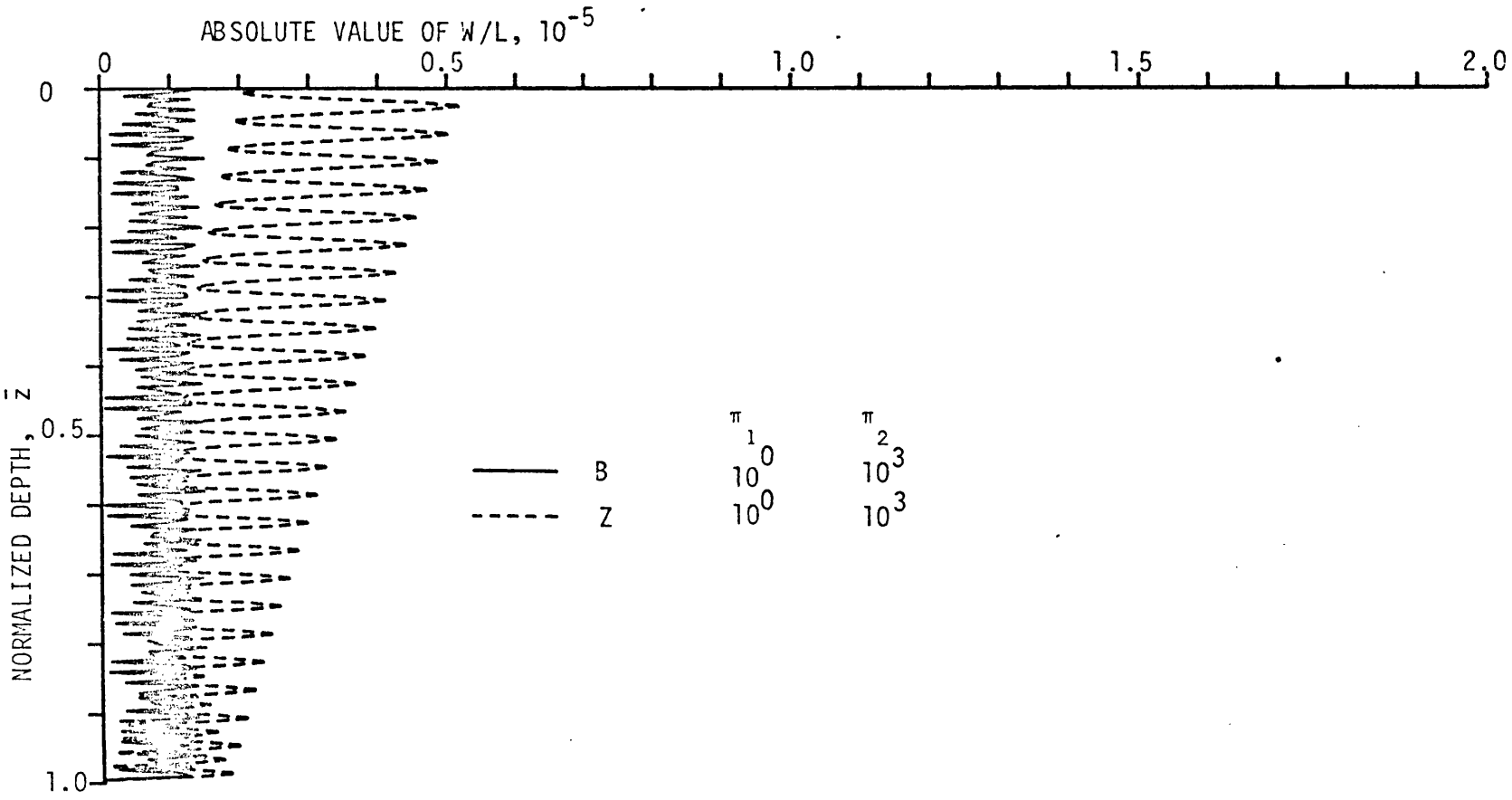

FIGURE 7.2 ABSOLUTE VALUE OF W/L

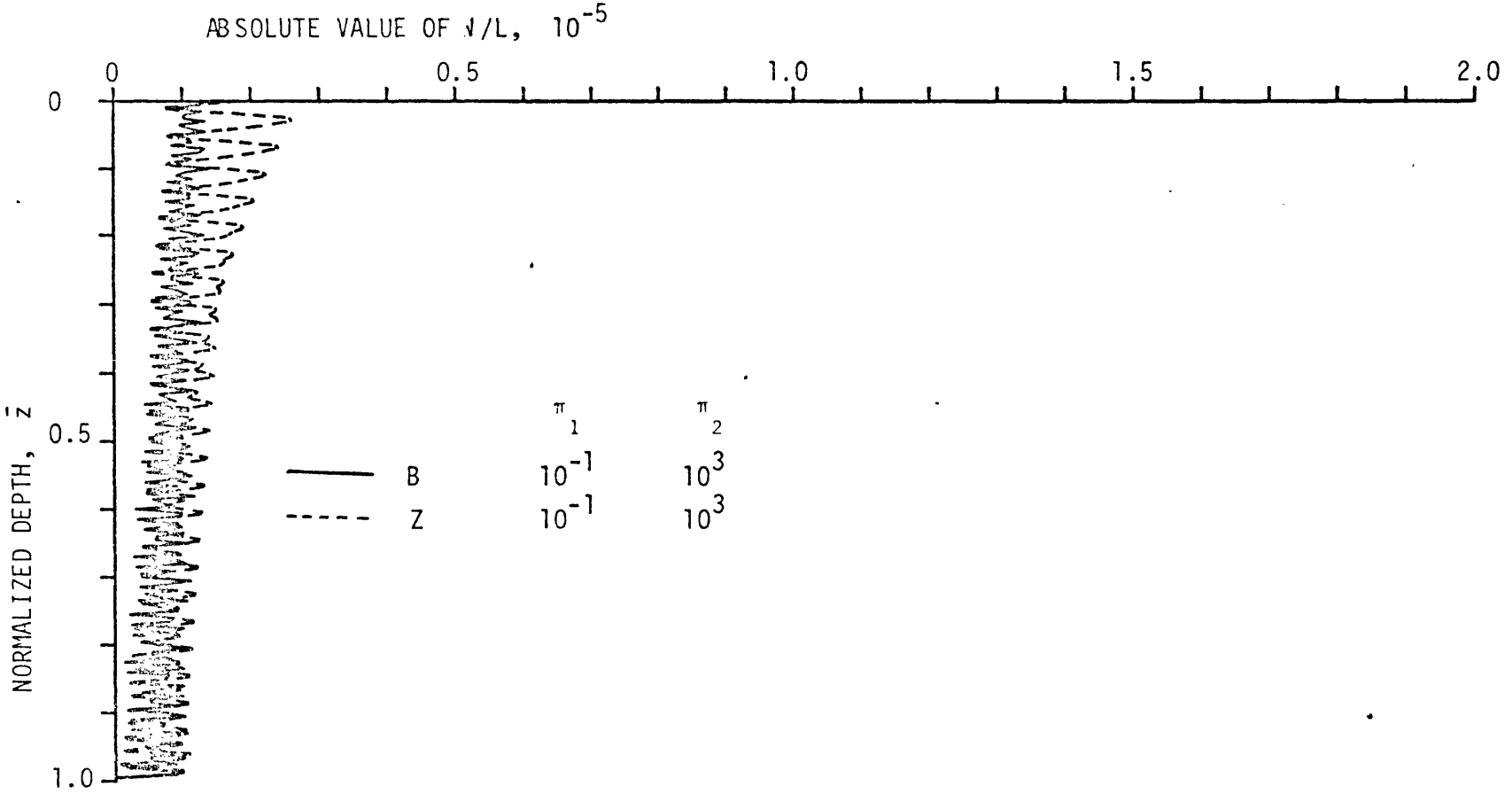

FIGURE 7.2 (cont'd)

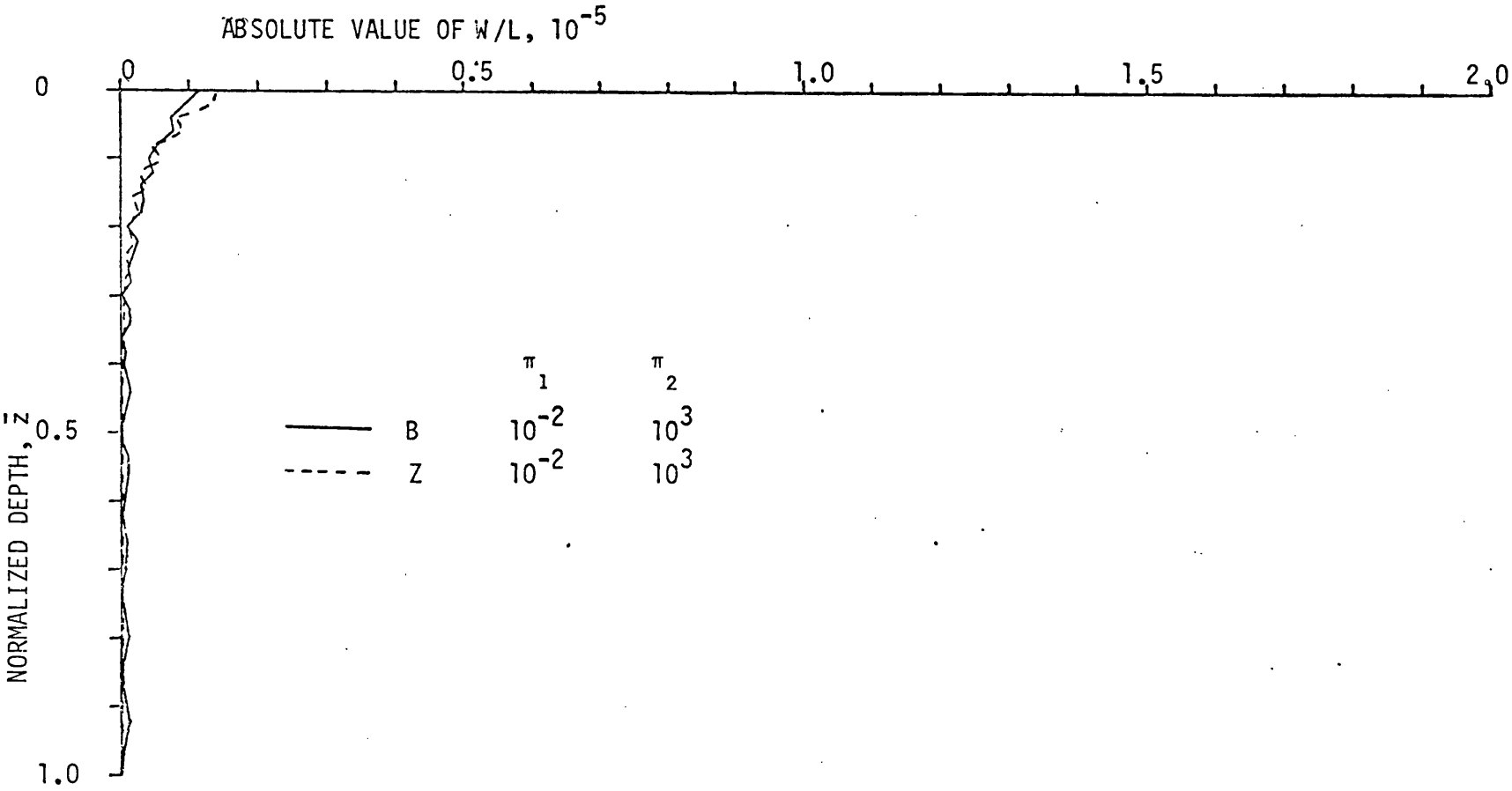

FIGURE 7.2 (cont'd)

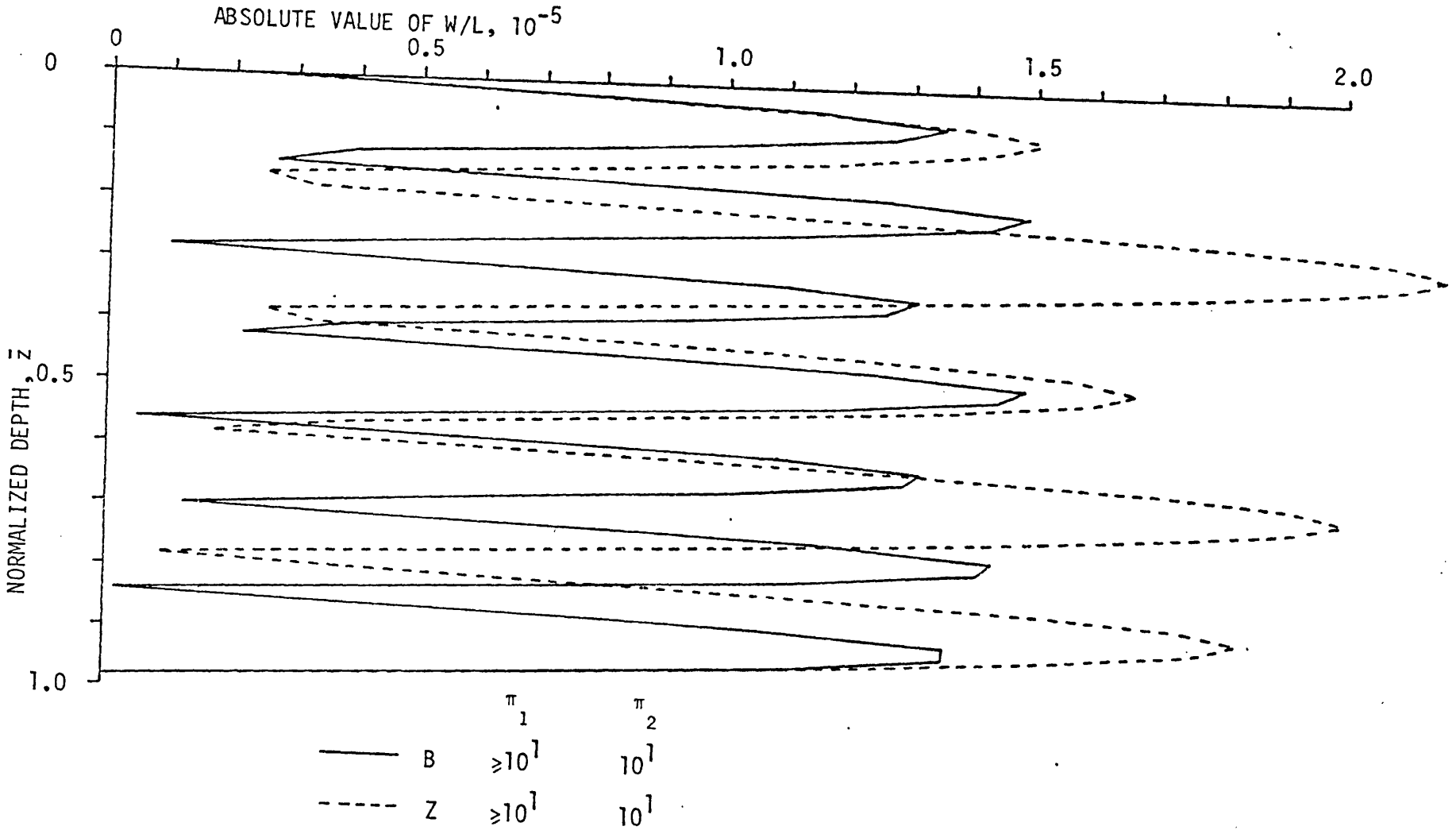

FIGURE 7.2 (cont'd)

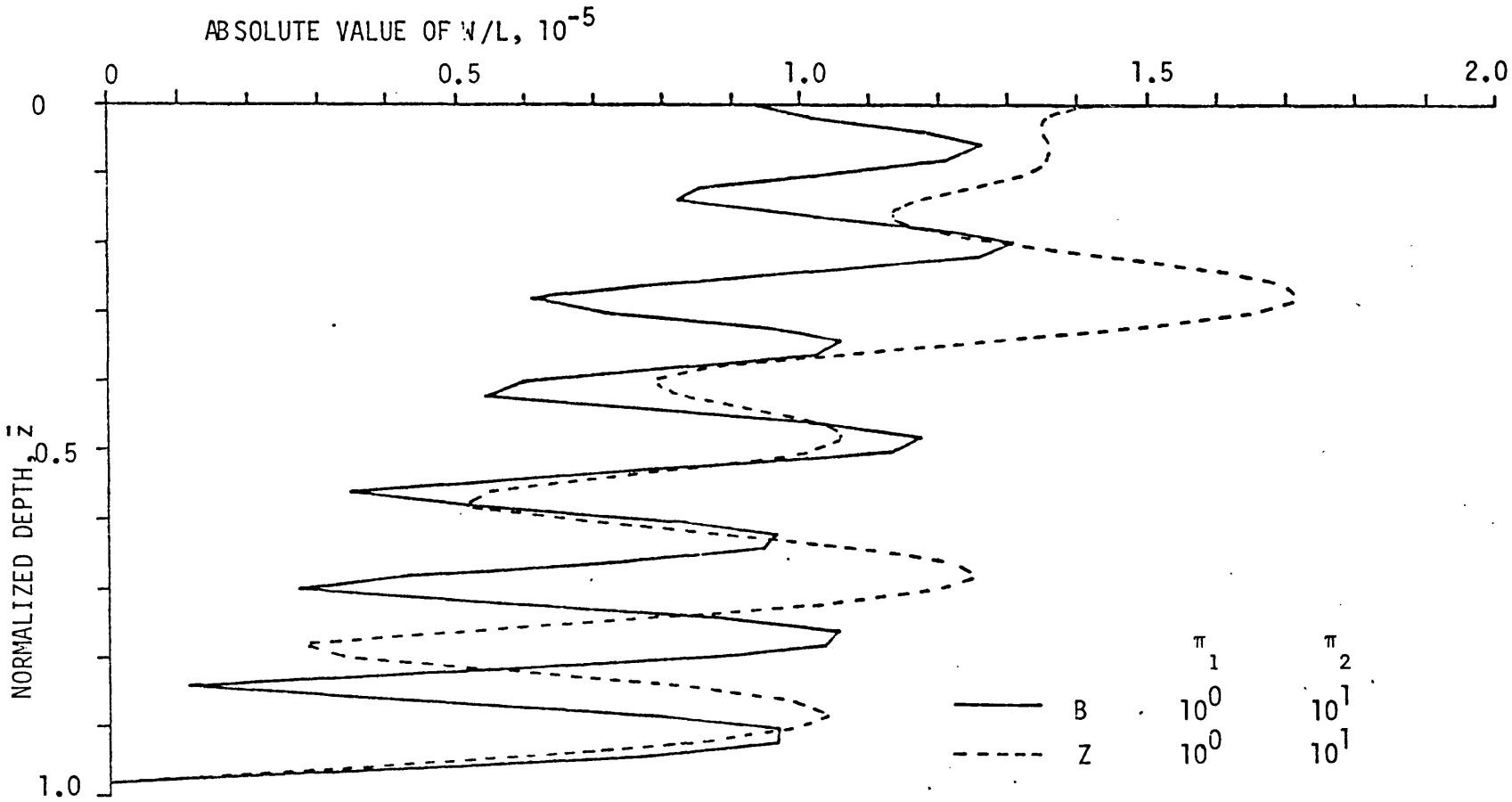

FIGURE 7.2 (cont'd)

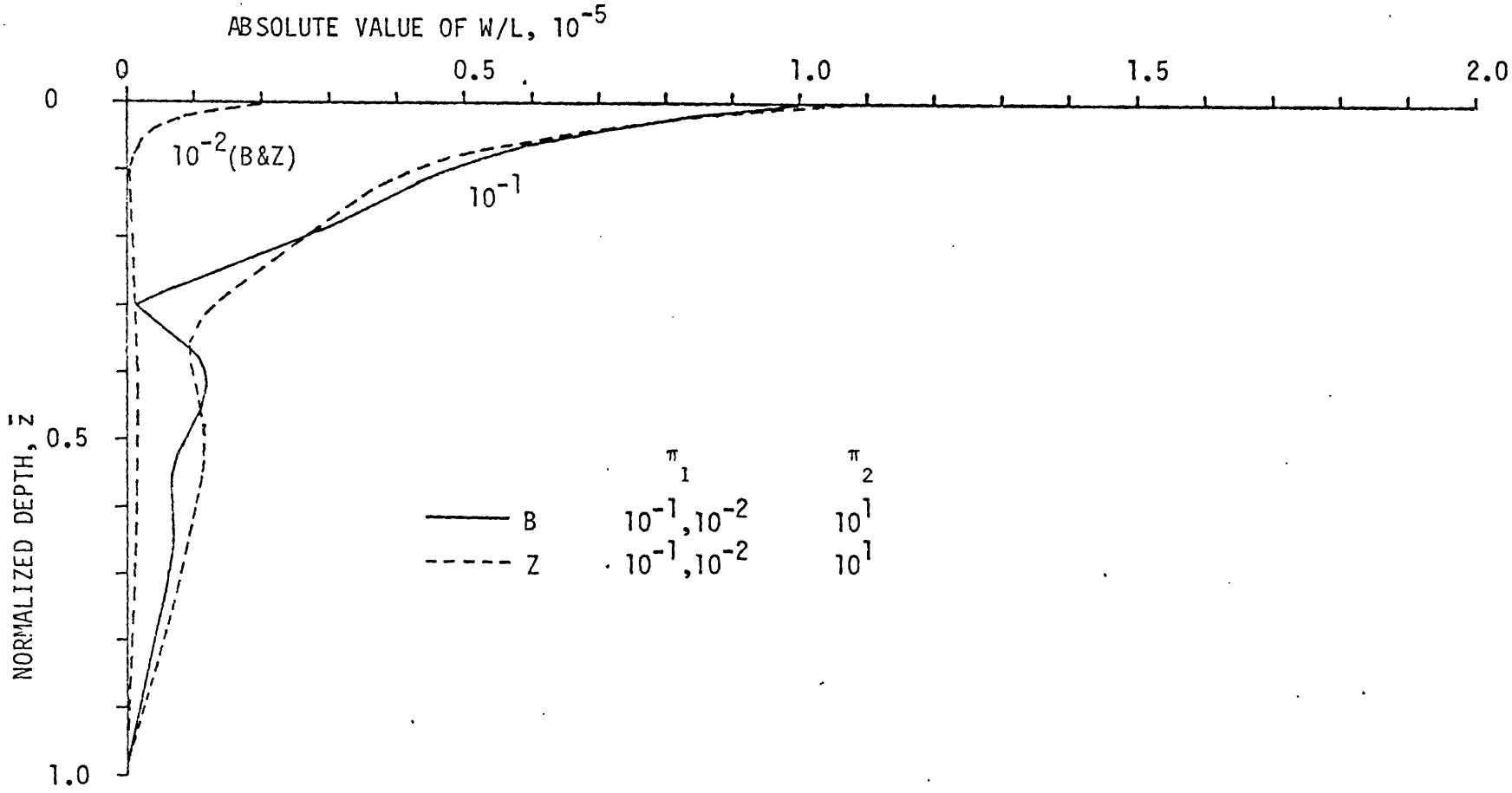

FIGURE 7.2 (cont'd)

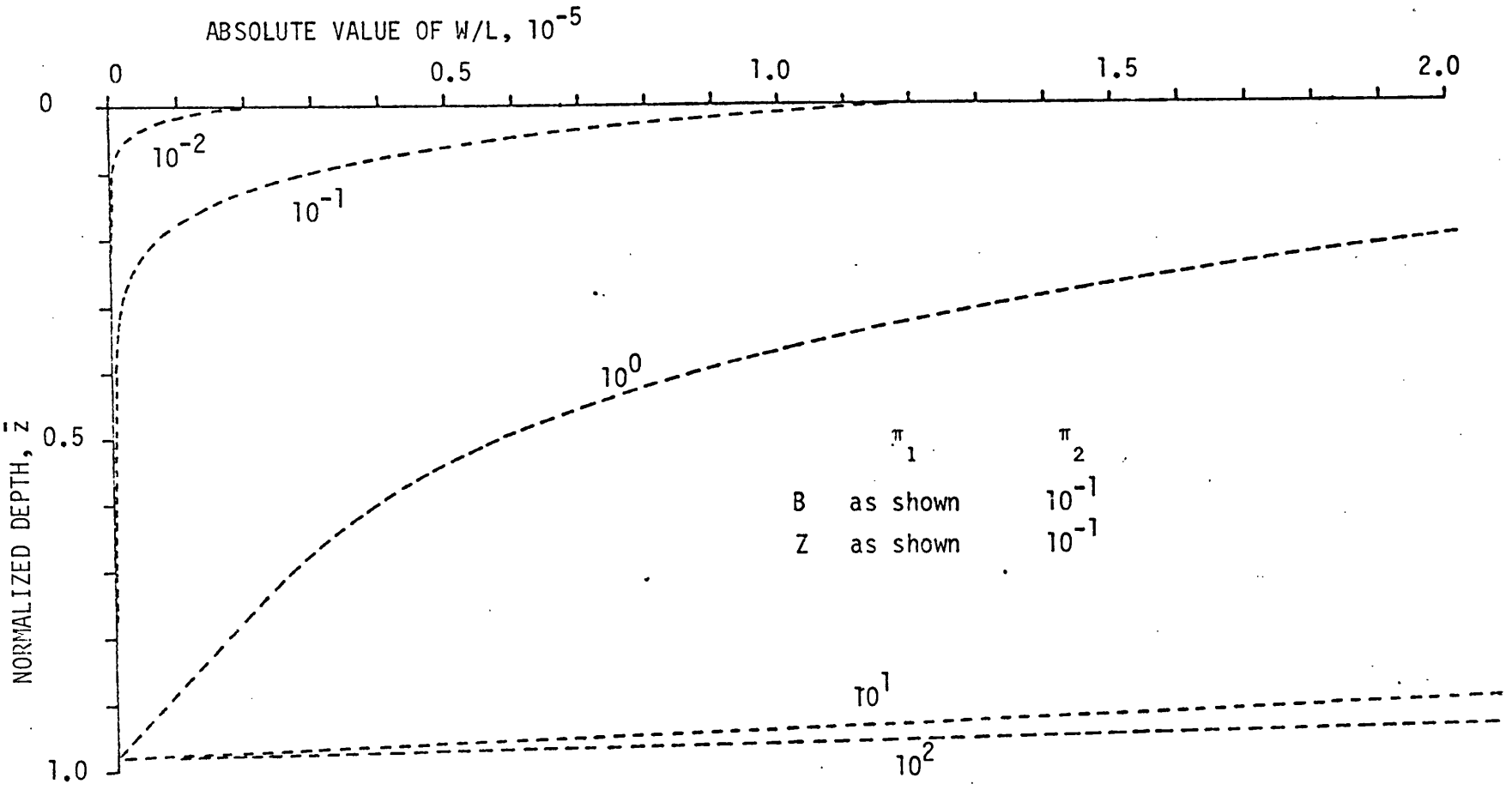

FIGURE 7.2 (cont'd)

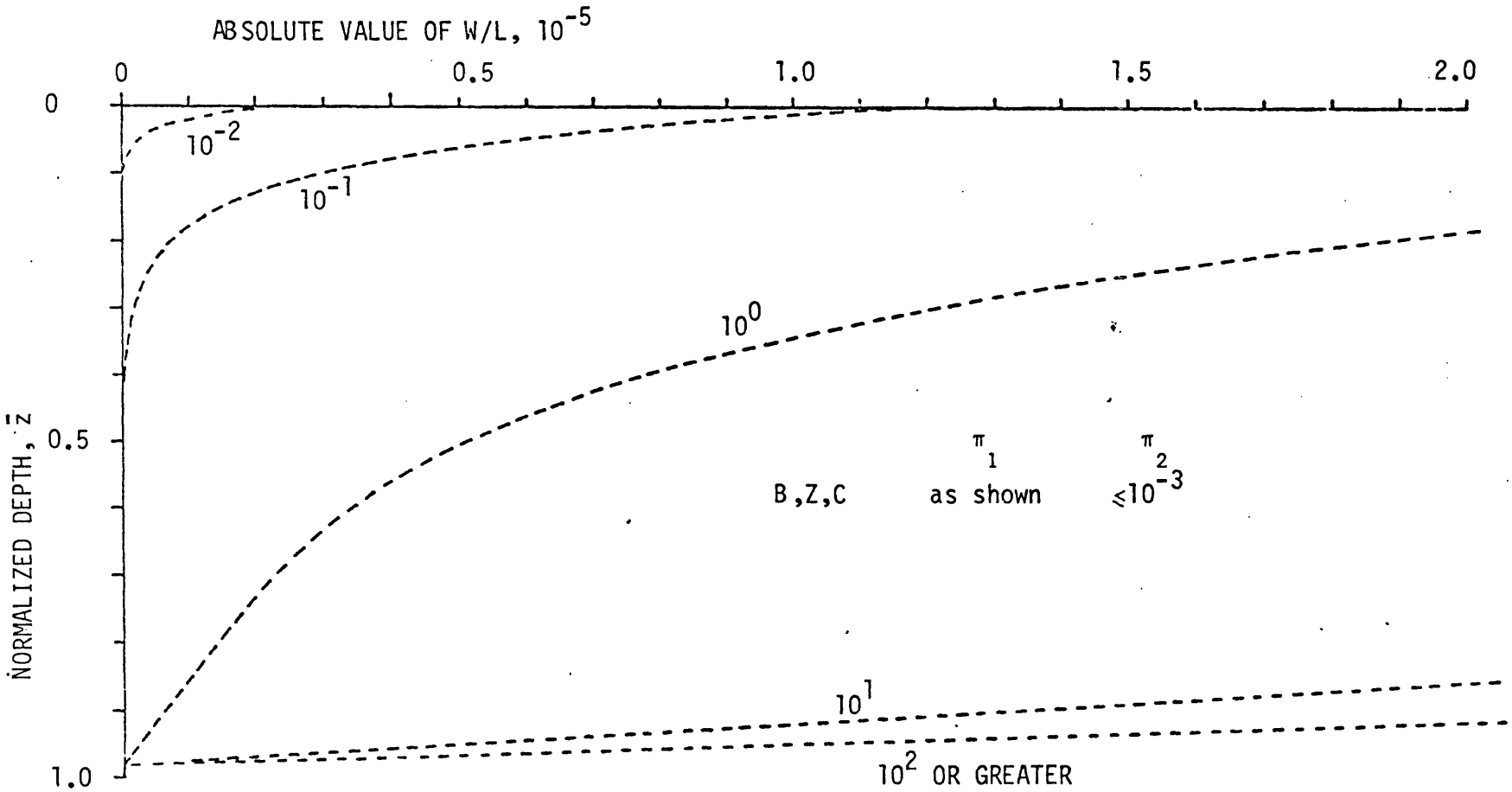

FIGURE 7.2 (cont'd)

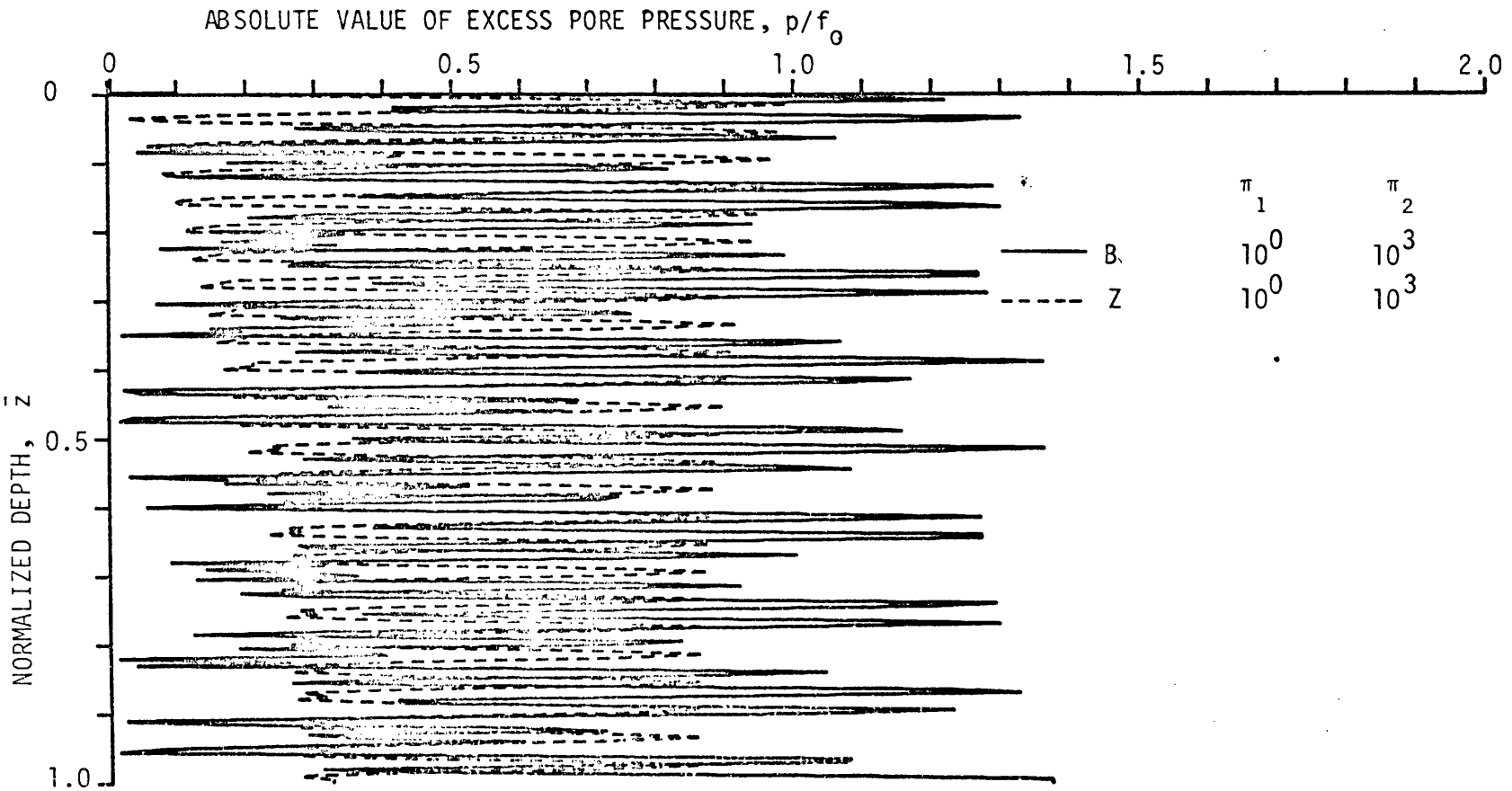

FIGURE 7.3 ABSOLUTE VALUE OF EXCESS PORE PRESSURE p/f_o

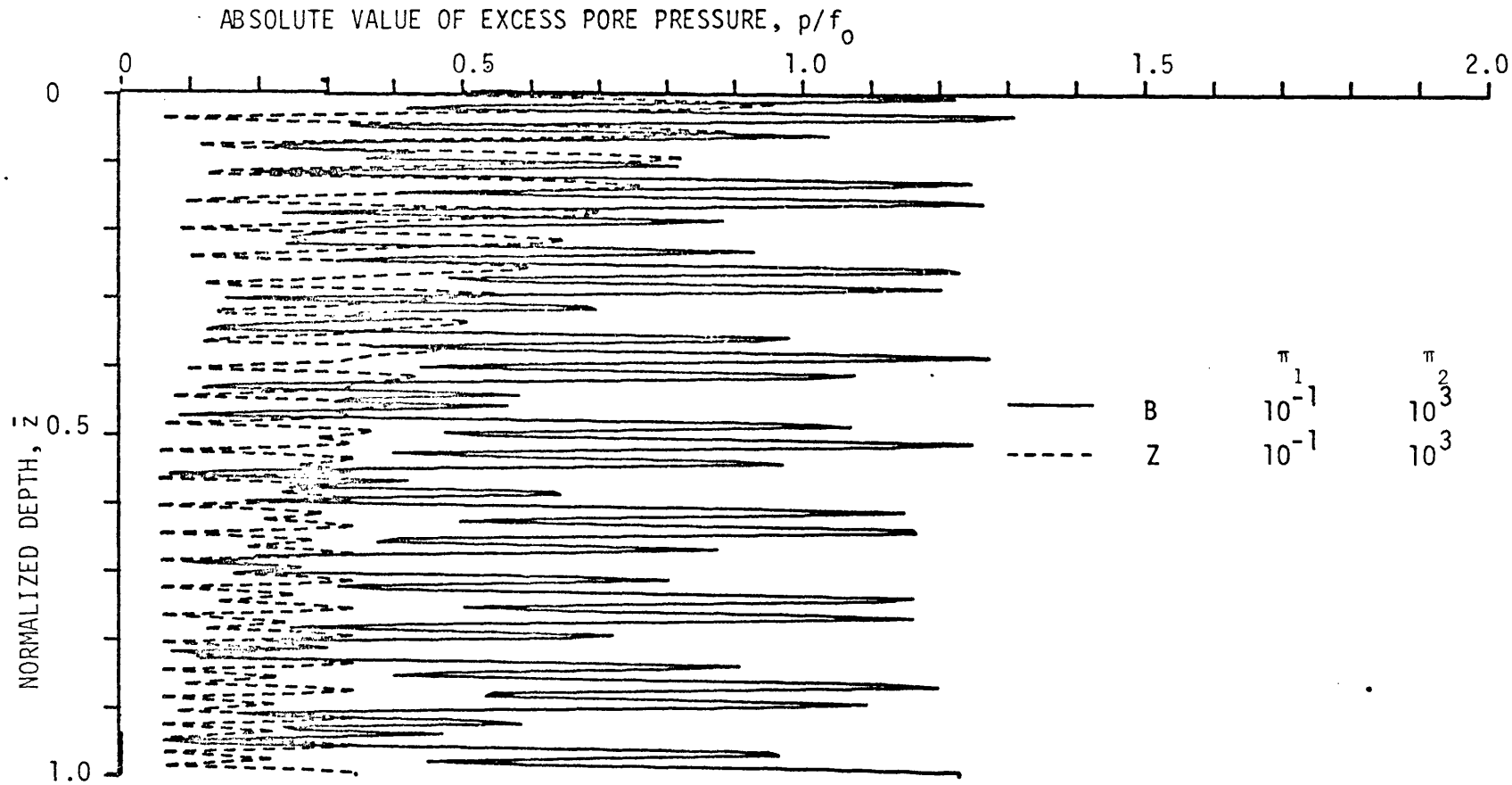

FIGURE 7.3 (cont'd)

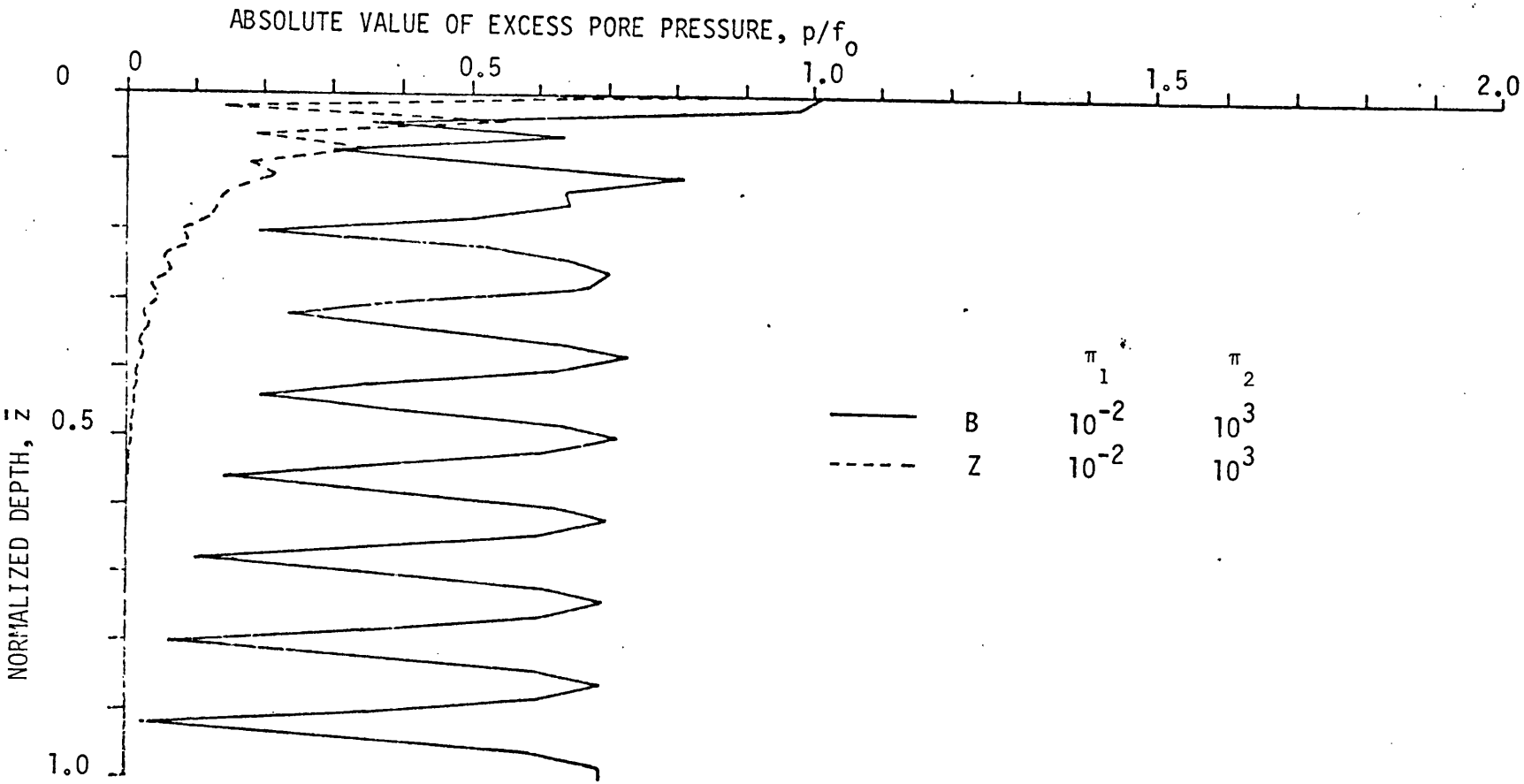

FIGURE 7.3 (cont'd)

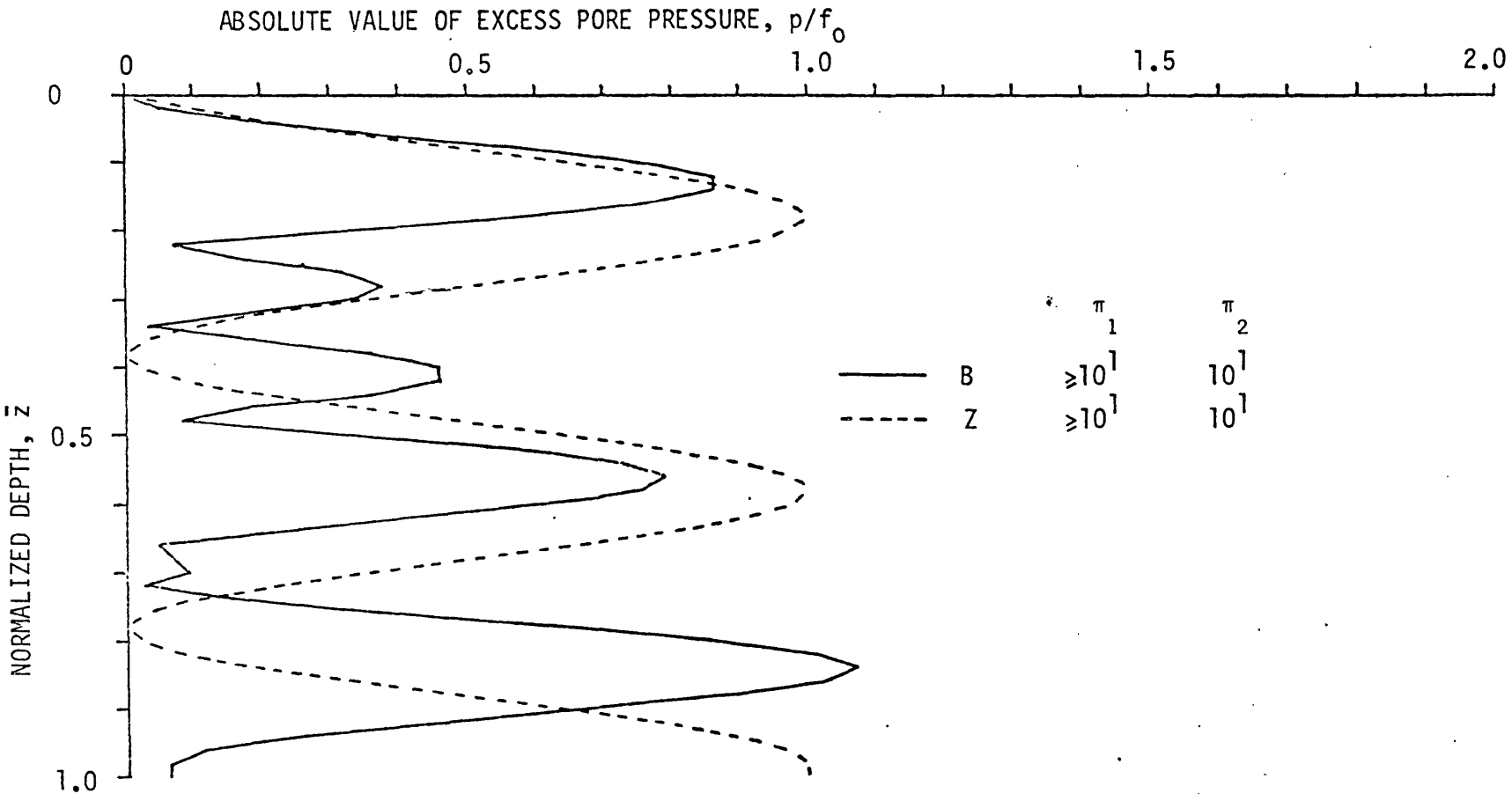

FIGURE 7.3 (cont'd)

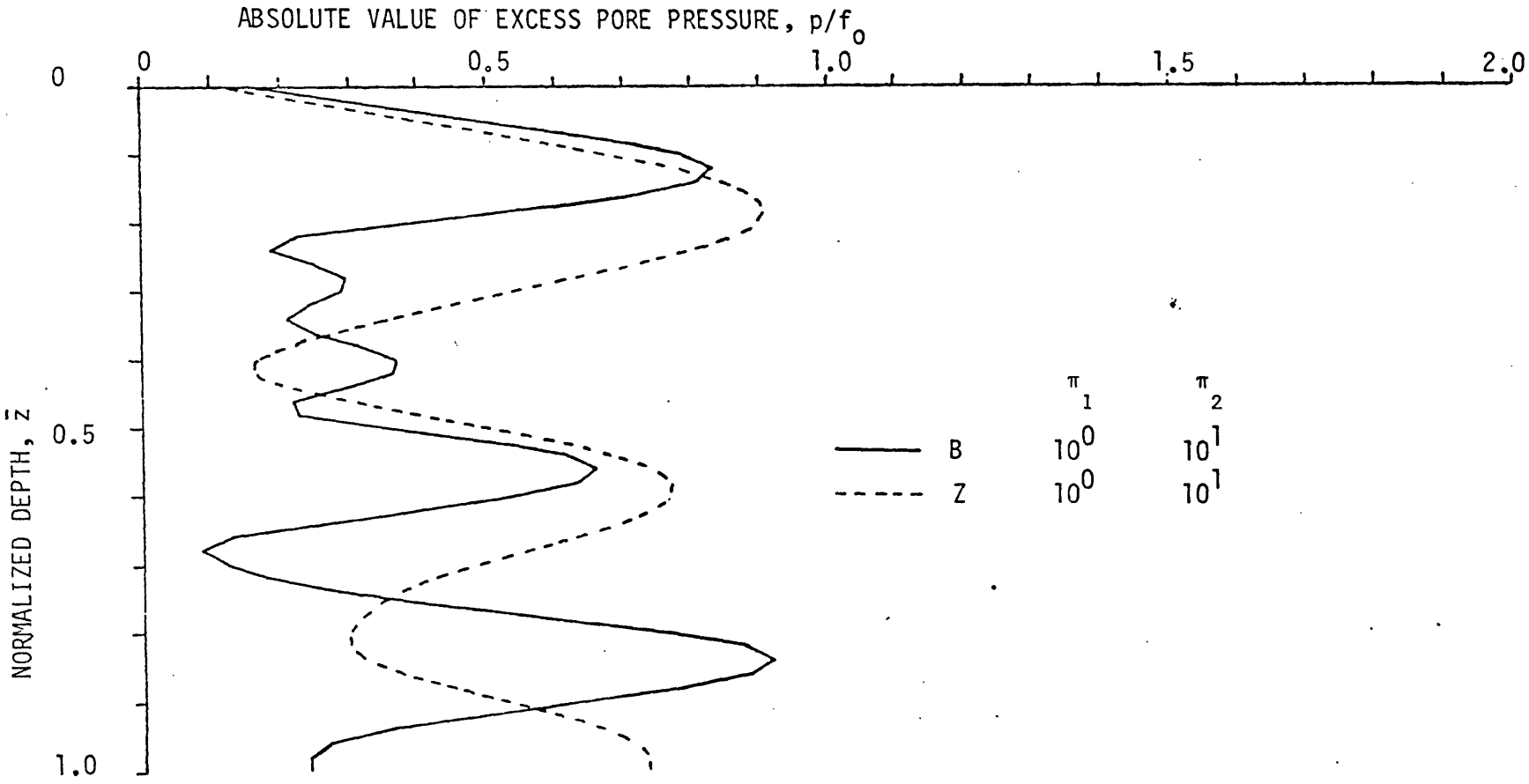

FIGURE 7.3 (cont'd)

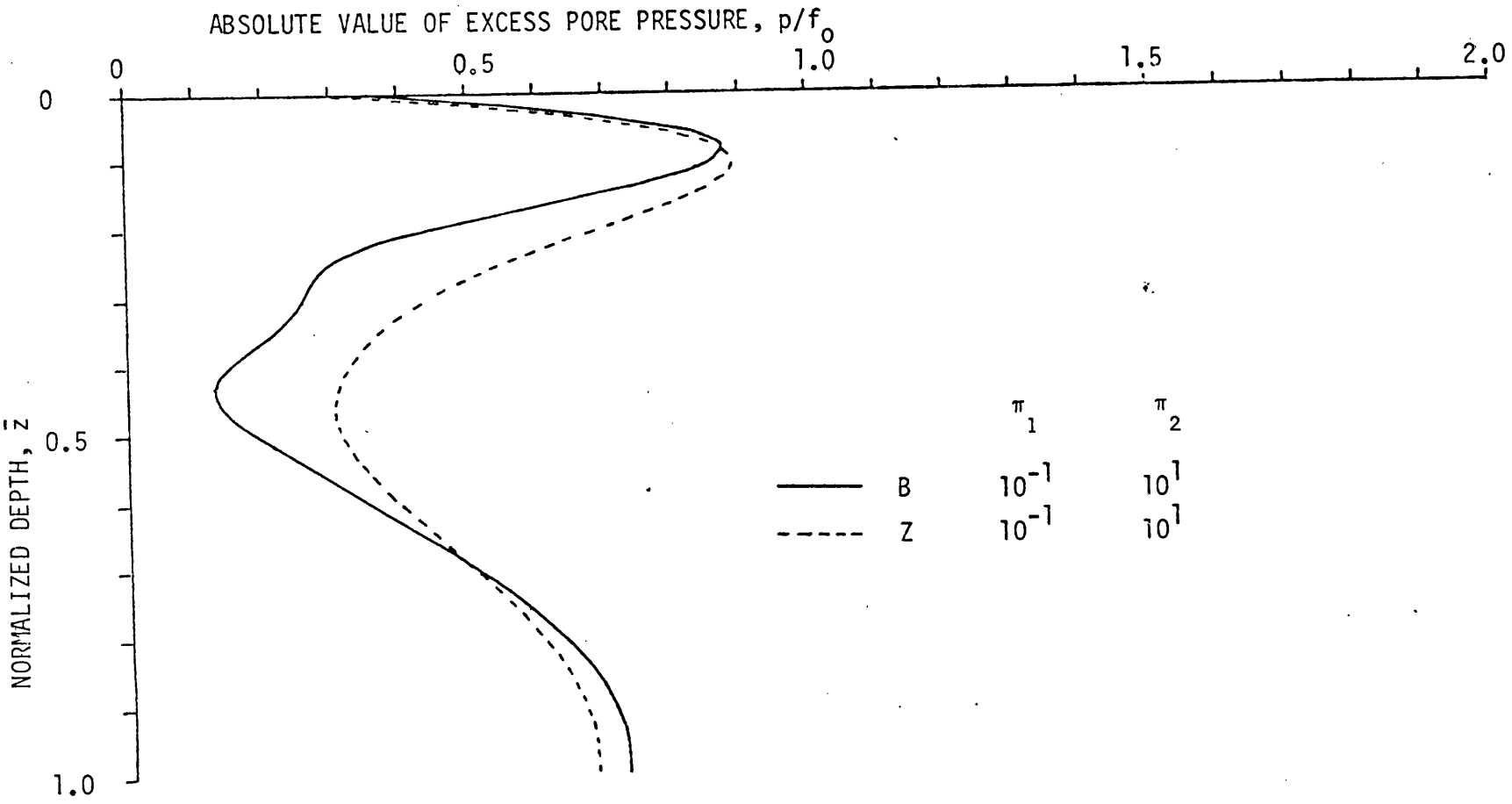

FIGURE 7.3 (cont'd)

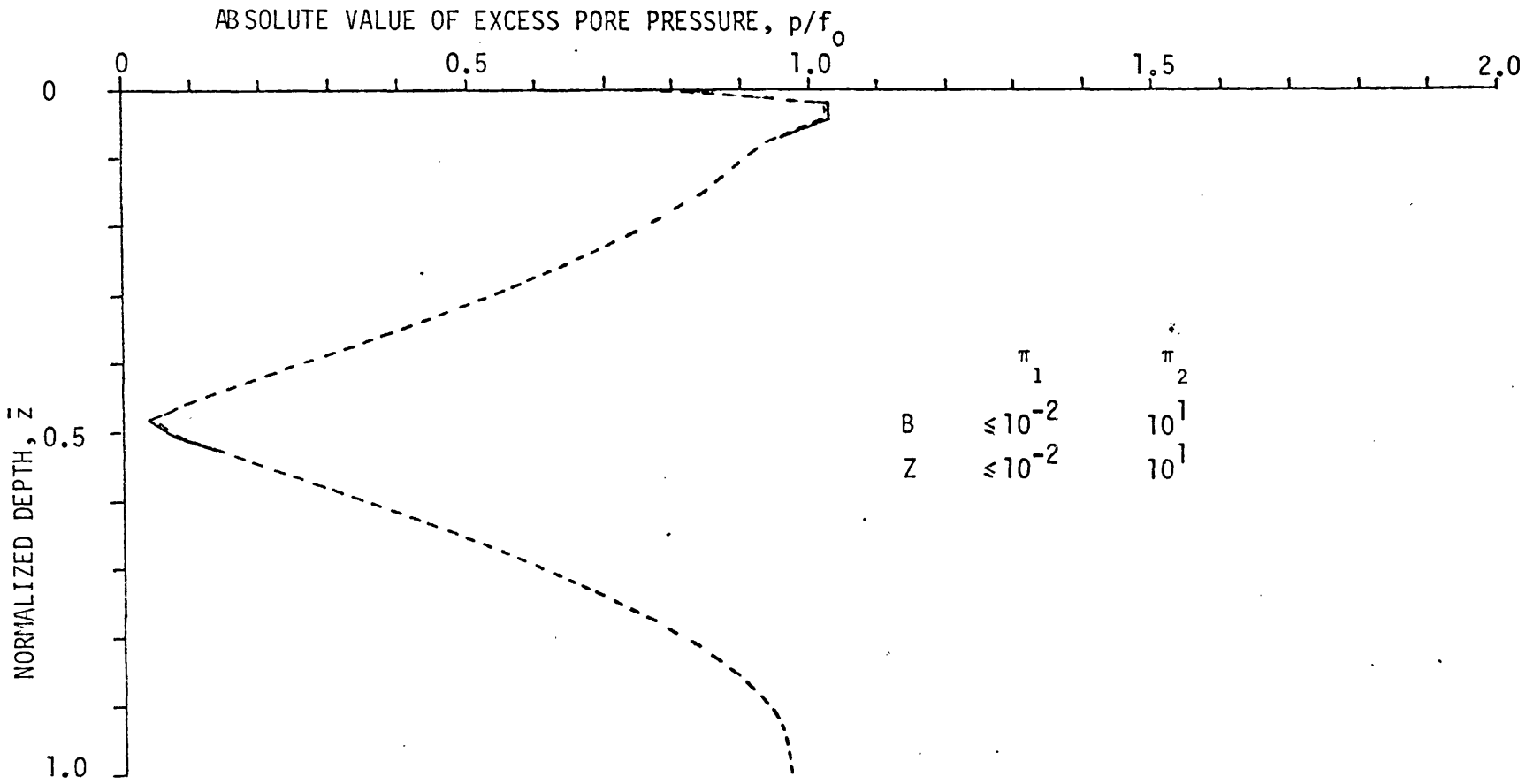

FIGURE 7.3 (cont'd)

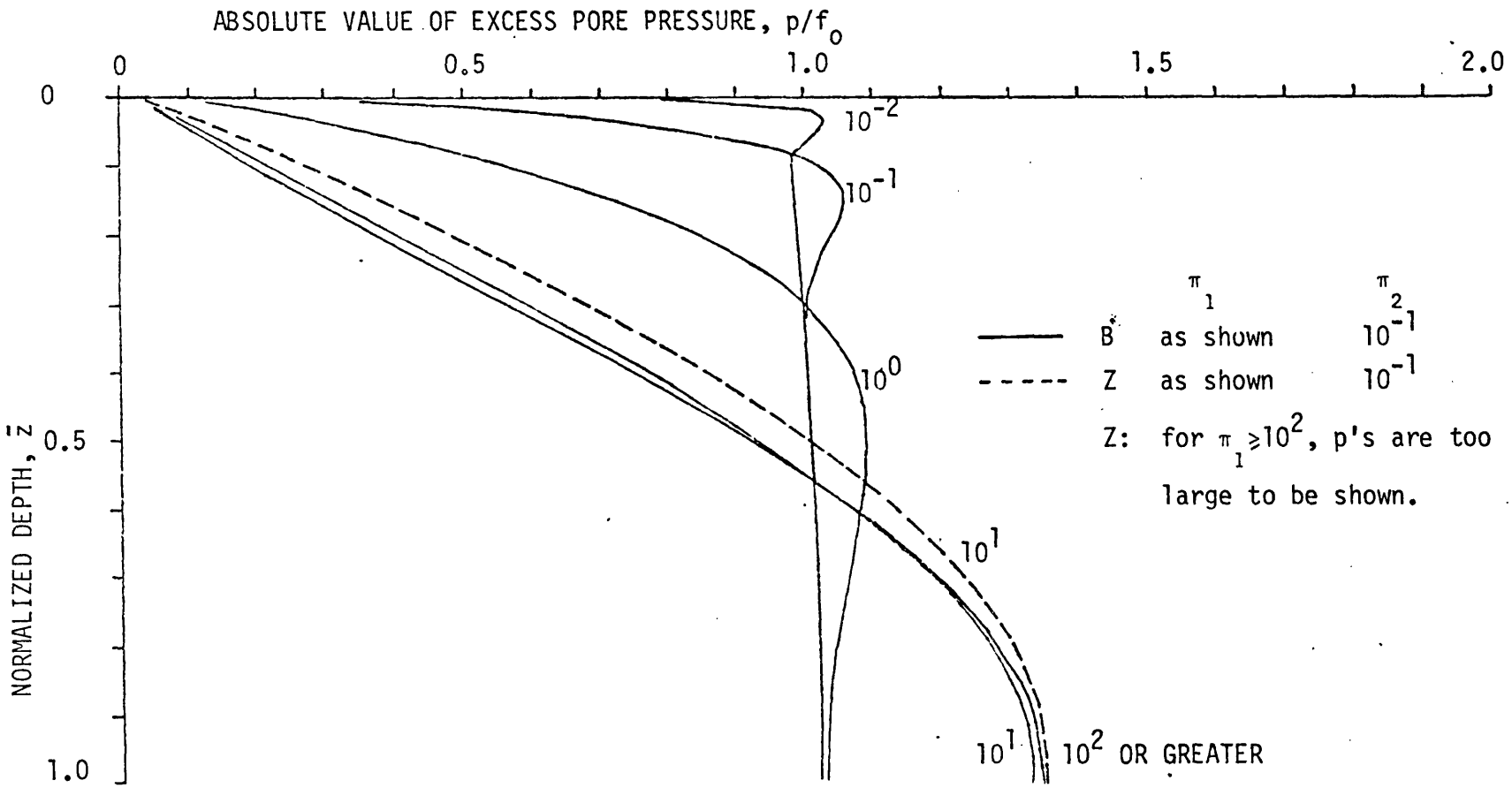

FIGURE 7.3 (cont'd)

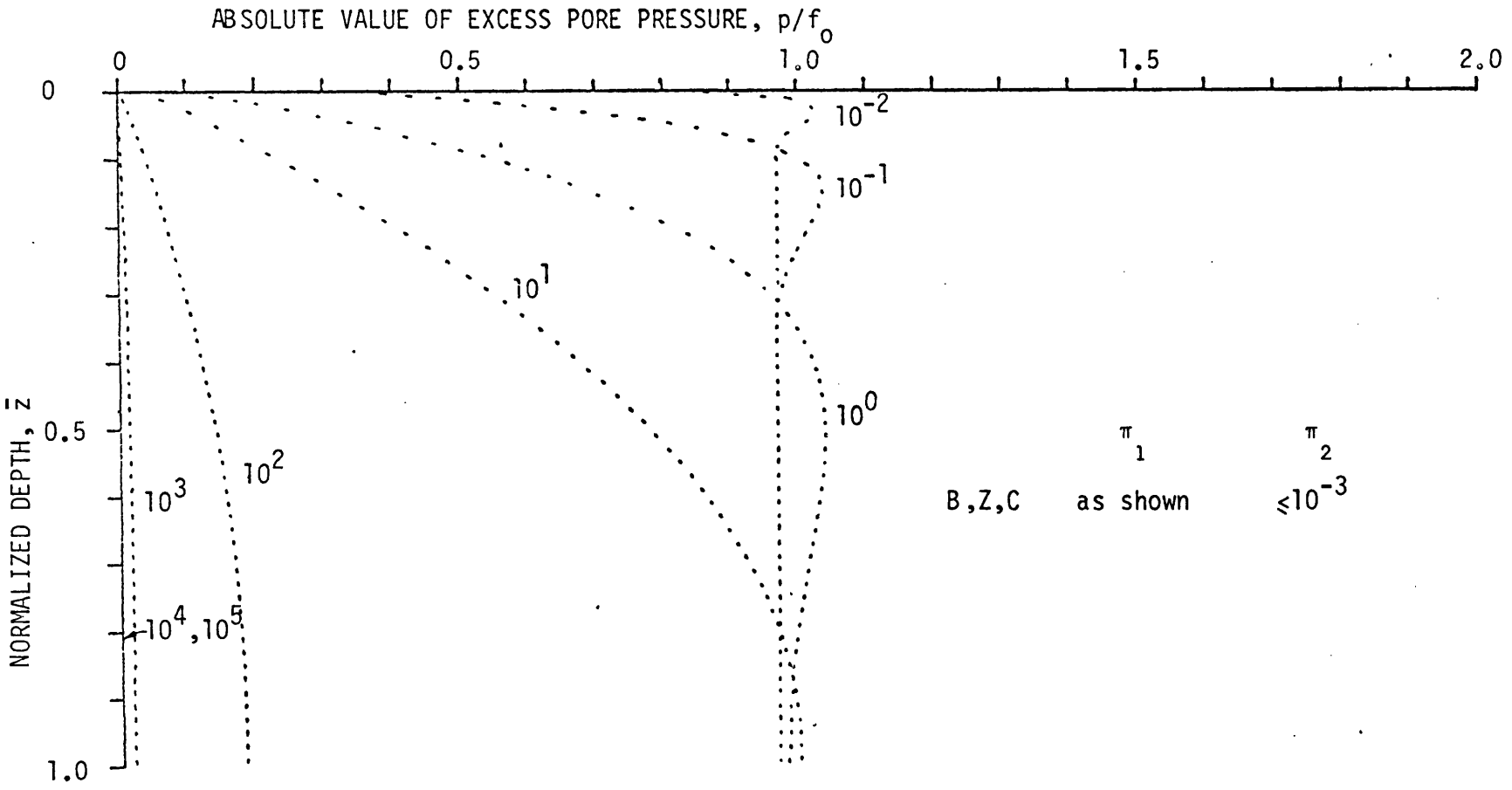

FIGURE 7.3 (cont'd)

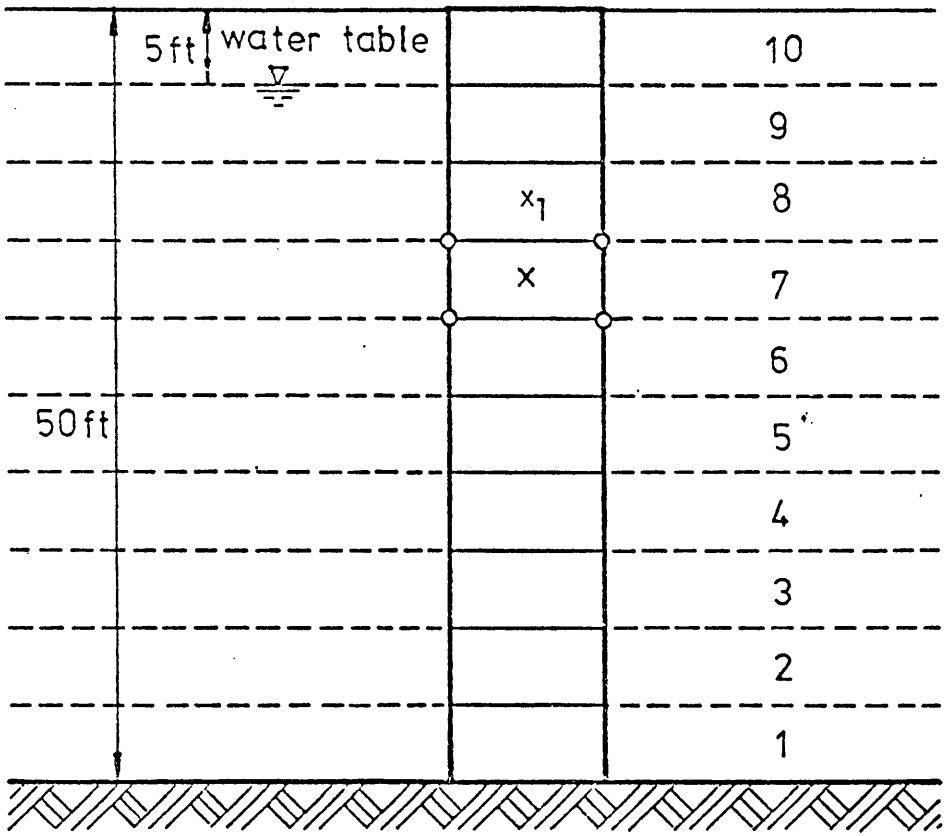

Material properties: Young's mod E = 2,000 kip/ft^2
Poisson ratio ν = 0.15
Friction angle ϕ = 40°
Cohesion C = 20 psf
Unit weight = 110 pcf

FIGURE 7.4 SATURATED SOIL STRATUM

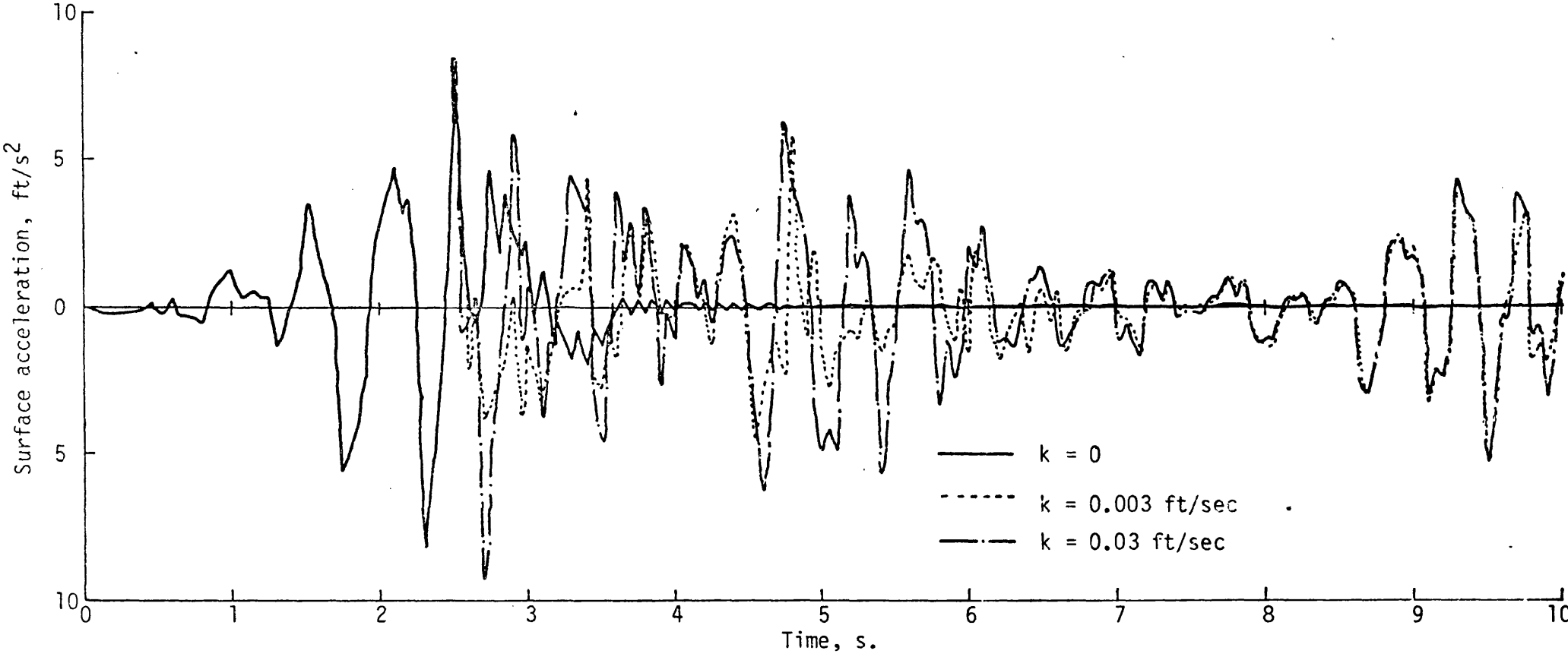

FIGURE 7.5 SURFACE HORIZONTAL ACCELERATION TIME HISTORY OF HORIZONTALLY LAYERED SATURATED SOIL SUBJECTED TO EL CENTRO EARTHQUAKE OF MAY 1941 SCALED TO 0.1g AT THE BASE

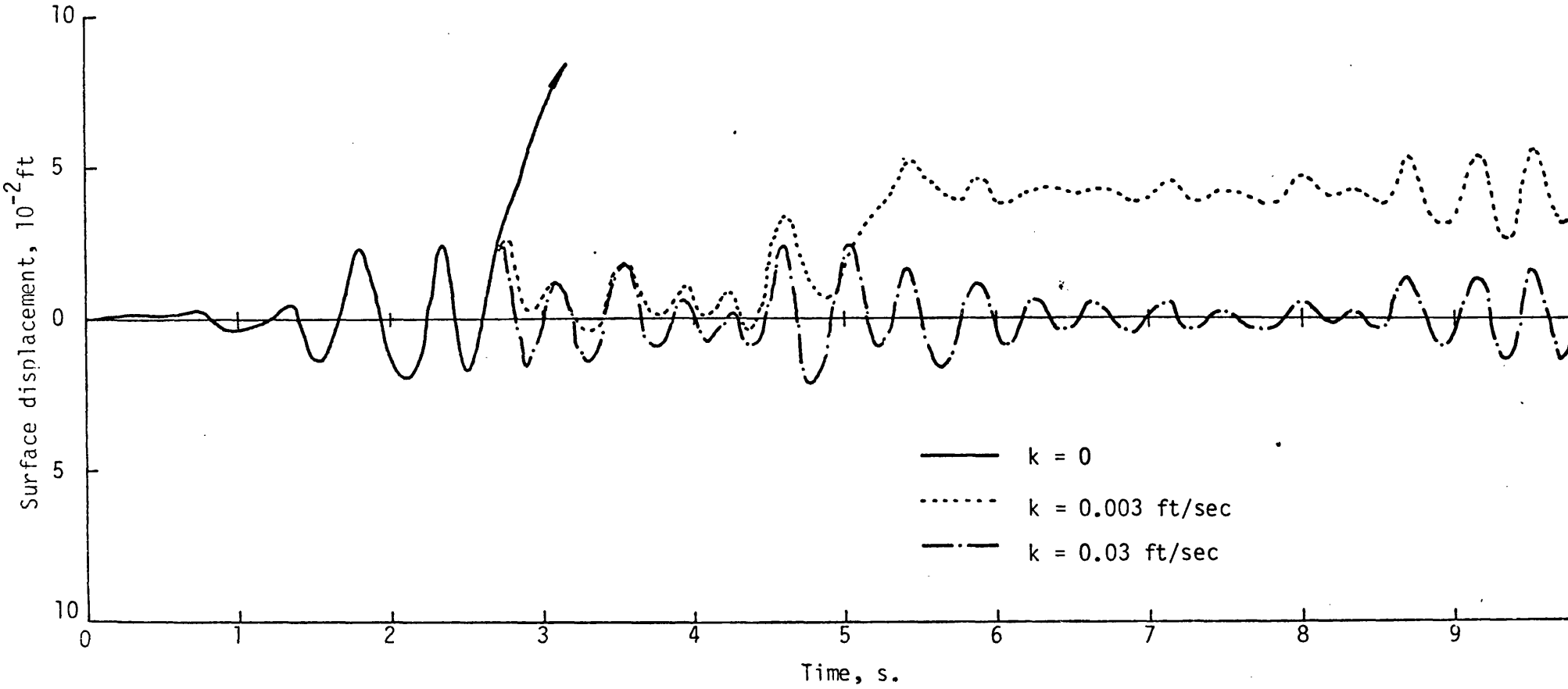

FIGURE 7.6 SURFACE HORIZONTAL DISPLACEMENT TIME HISTORY OF HORIZONTALLY LAYERED SATURATED SOIL SUBJECTED TO EL CENTR
EARTHQUAKE OF MAY 1940 SCALED TO 0.1g AT THE BASE

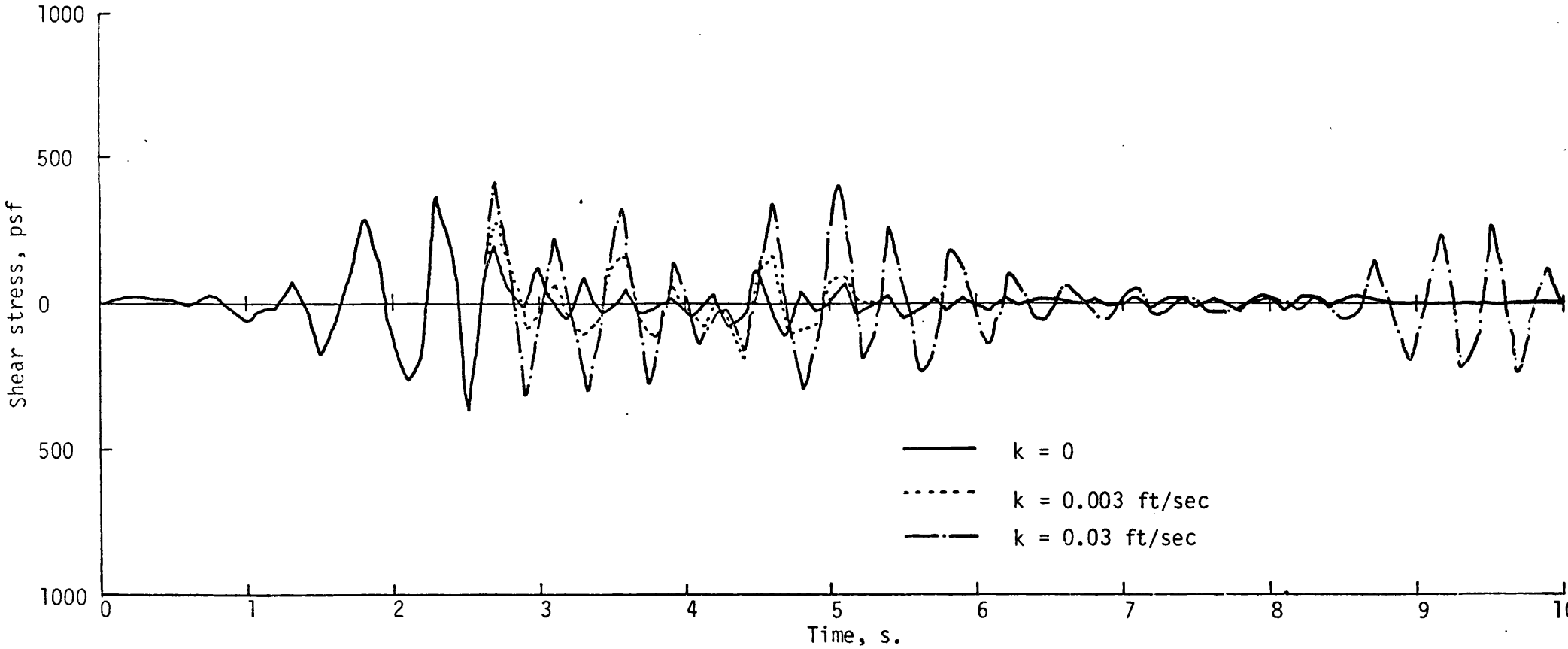

FIGURE 7.7 SHEAR STRESS TIME HISTORY IN LAYER 7 OF HORIZONTALLY LAYERED SATURATED SOIL SUBJECTED TO EL CENTRO EARTHQUAKE OF MAY 1940 SCALED TO 0.1g AT THE BASE

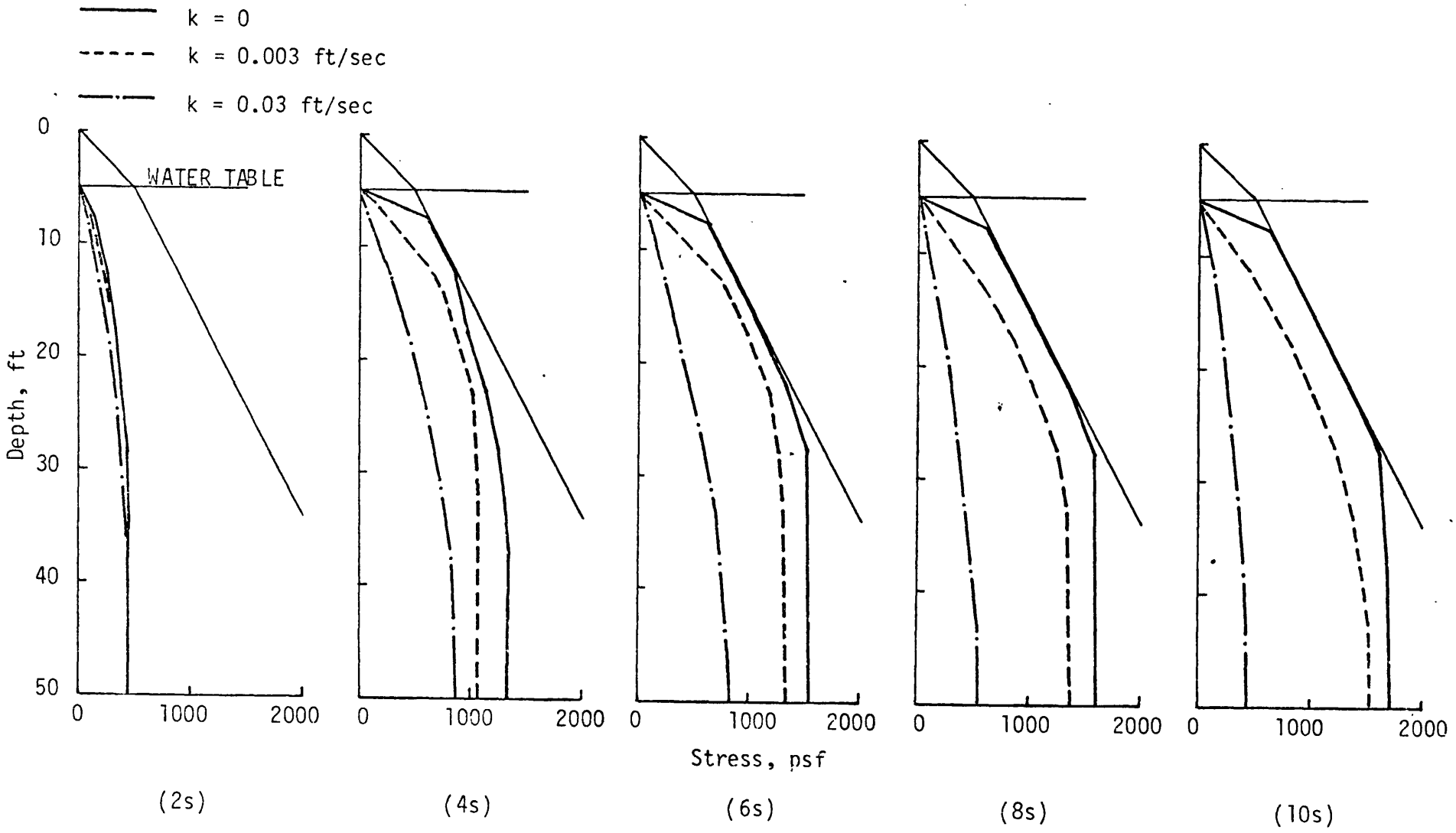

FIGURE 7.8 BUILD UP OF EXCESS PORE WATER PRESSURE AT 1sINTERVALS FROM THE START OF MOTION

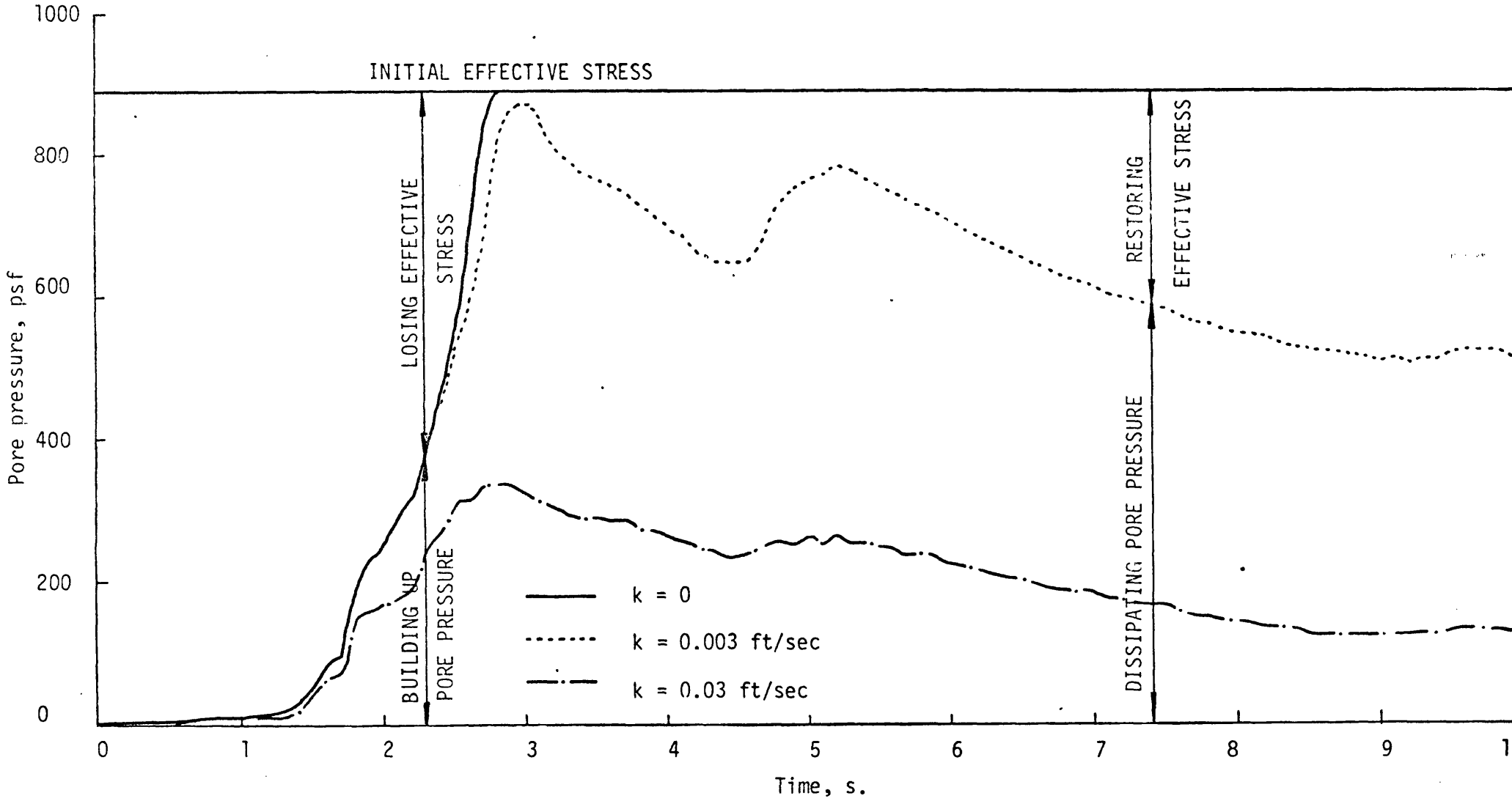

FIGURE 7.9 BUILD UP OF EXCESS PORE WATER PRESSURE WITH RESPECT TO TIME IN LAYER 8 DUE TO EL CENTRO EARTHQUAKE OF MAY 1940 SCALED TO 0.1g AT THE BASE

CHAPTER 8

NONLINEAR RESPONSE OF EARTH DAMS IN EARTHQUAKES

8.1 INTRODUCTION

In order to illustrate the process of dynamic analysis of embankment dams, the study of a typical embankment dam constructed on a rock foundation shown in Figure 8.1 subjected to the recorded earthquake of El Centro, May 1940, has been carried out. The results are presented graphically and the safety of the dam undergoing the passage of the earthquake can therefore readily be assessed. However, before the presentation of the results, a brief description of the procedures needed to carry out the dynamic analysis of an embankment is reviewed.

8.2 THE DYNAMIC ANALYSIS OF EMBANKMENT DAMS

The major steps in the nonlinear dynamic analysis of embankment dams subjected to an earthquake can be summarised as follows:

1. Determine the proper analytical model and data such as reservoir levels, dam sections and finite element meshes for analysis.
2. Determine the characteristics of the ground motions developed in the rock under the dam, if any, or its soil foundation during the earthquake.
3. Determine the initial stresses in the dam before the earthquake.
4. Determine the dynamic properties of the constituent material of the dam.

5. Evaluate the response of the dam to the base rock excitation. The results of a finite element analysis give the displacement at each nodal point and stresses at each Gauss integration point.

6. Presentation and interpretation of the results.

Items (1) to (5) have already been discussed in the previous chapters. Therefore, this chapter concentrates on the presentation and interpretation of the results.

8.3 EFFECTS OF THE VERTICAL COMPONENT OF AN EARTHQUAKE ON THE DAM RESPONSE

It has been pointed out by Seed[1] and widely accepted in practice[2,3] that the effects of vertical motions induced by the earthquake may be neglected for the following reasons:-

1. the shear stresses in a dam caused by vertical motions are much less than those due to horizontal motions.

2. extensive laboratory tests have shown that the tendency for volume changes and associated pore pressure development caused by vertical vibrations is small in comparison with those resulting from shear deformation.

3. such pore pressures as may be introduced by vertical motions in the absence of shear stresses will be neutral pressures and thereby will have no influence on the shear resistance of the soil.

Accordingly, it seems reasonable to conclude that both the shear stresses and the shear strength are primarily determined by the horizontal shaking induced by an earthquake. However, in order to study this

conclusion, the dam, shown in Figure 8.1, subjected to horizontal component alone and subjected to both horizontal component and vertical component of El Centro earthquake has been analysed. The results are presented in Figures 8.2 (a,b,c,d). It can be noted from Figures 8.2 (a,b,c,d) that the conclusion made by Seed is quite reasonable.

8.4. UNDRAINED SEISMIC ANALYSIS OF AN EARTH DAM

It is of interest to investigate, at first, the undrained behaviour of an earth dam during the passage of an earthquake. Figure 8.3 presents the horizontal displacement time histories at the dam crest. Figure 8.4 shows the shear stress time histories at Gauss point x. Figure 8.5 shows contours of the build up of excess pore pressure at 2-second intervals from the start of motion. The normalized vertical effective stress and excess pore water pressure at various heights along the axis of dam are plotted against time in Figure 8.6. In order to offer a comparison, indeed,to evaluate the accuracy of the present approach, a separate 70 metres earth dam which is subjected to the same accelerogram as the previous example has been studied and the contours of the build up of excess pore water pressure are presented at 2-second intervals from the start of motion in Figure 8.7. From the results of the present study, it can be seen that, as with the soil layer problem, the risk of liquefaction of the upper portion of a high dam is higher than that of the lower portion. This is due to the amplification of the excitation and also to the fact that the effective stress at the top is smaller than that of the bottom. Consequently, in order to preclude the possibility of soil liquefaction in practical design, special

attention should be paid to the upper portion of the dam.

It is worthwhile noting that the responses shown in Figure 8.3 and 8.4 for the analysis which neglect the autogenous volumetric strain are equivalent to fully drained conditions, i.e., no build up of excess pore pressure.

8.5 UNDRAINED VS PARTIALLY DRAINED SEISMIC ANALYSIS OF EARTH DAM

It is of interest to study the effect of seepage flow during earthquake on the dynamic responses of the dam. Figures 8.8 (a,b) present the horizontal displacements of the dam crest and the build up of excess pore pressure at Gauss point of element 70. It can be seen from Figures 8.8 that the drained conditions and the undrained conditions provide no significant difference in displacements. But, the average change in excess pore pressure is about 10 percent.

8.6 EVALUATION OF DAM SAFETY

The dynamic response analysis of a dam provides the time histories of displacement and stress induced throughout the dam for the duration of the applied base rock motion. The following presentations cover each 2-second interval from the start of motion. The typical displacement time histories and shear stress time histories have been presented previously. The deformed configurations of the dam are presented in Figure 8.9. The x displacement contours are shown in Figure 8.10. The contours of σ_x, σ_y, σ_z, τ_{xy}, principal stresses σ_1 and σ_2 are represented in Figures 8.11 (a,b,c,d,e,f) respectively. The principal stress vectors are presented in Figure 8.12.

Figure 8.13 shows the contours of dissipated energy, Q, which is defined as

$$Q = \int_0^t \underset{\sim}{\sigma}^T \dot{\underset{\sim}{\varepsilon}}_{VP} \, dt$$

The figures presented are rather typical and the responses seem reasonable. However, for comparison, a separate study of the 70 meters high dam mentioned previously was again made and the contours of the dissipated energy are shown in Figure 8.14. It can be seen from both Figures 8.13 and 8.14 that the contours of dissipated energy are quite similar.

The factors governing the safety of a dam under an earthquake are displacement and stress. Based on the results of the present study, the evaluation of the safety of the dam under the earthquake can readily be made, provided that the criteria of the maximum allowable displacement and stress have been specified. These values will differ from dam to dam. Thus the safety of the dam can be ascertained.

A comprehensive investigation of the collapse of the Lower San Fernando Dam during the earthquake of 9th February 1971 is being undertaken. It is hoped that some additional results will be obtained in the near future.

REFERENCES

1. SEED, H.B., LEE,K.L., IDRISS,I.M. and MAKDISI,F.
'Slides in the San Fernando Dams during the earthquake of Feb. 9, 1971'
Journal of the Geotechnical Division, ASCE, pp. 651-688 (1975).

2. KRAMER,R.W., MACDONALD,R.B., TIEDEMANN,D.A. and VIKSNE,A.
'Dynamic analysis of Tsengwen Dam'
Bureau of Reclamation, Denver, Colorado, (1975).

3. ARTHUR,H.G., et. al.
'Dynamic analysis of embankment dams'
United States Department of the Interior, Bureau of Reclamation, Engineering and Research Center, Denver, Colorado, (1976).

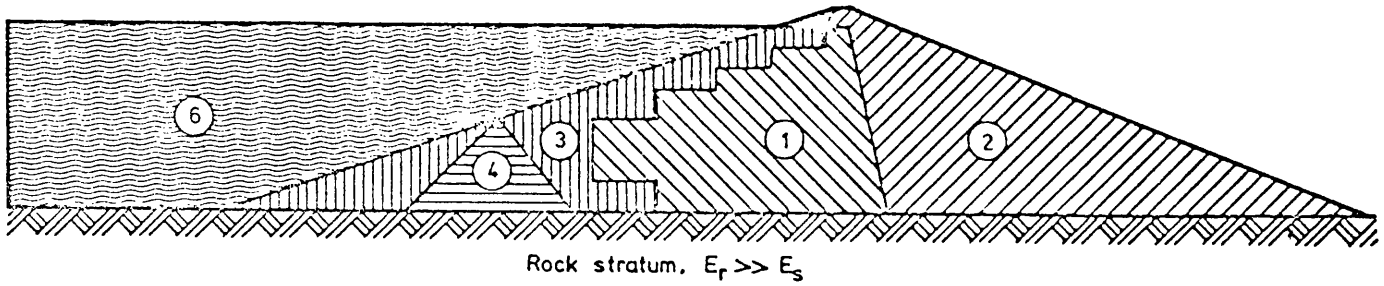

(1)

Material zone	E MN/m^2	ν	ϕ degree	C kN/m^2	Unit weight kg/m^3
1	100	0.45	33	10	2250
2	100	0.40	33	10	2260
3	230	0.45	38	80	2400
4	100	0.45	33	10	2160
5	230	0.45	38	80	2400
6	2250 *	0.50	-	-	1000

* BULK MODULUS

	Pre-I.L.	Post-I.L.
βA	120	5
B	55.5	0.51

(3)

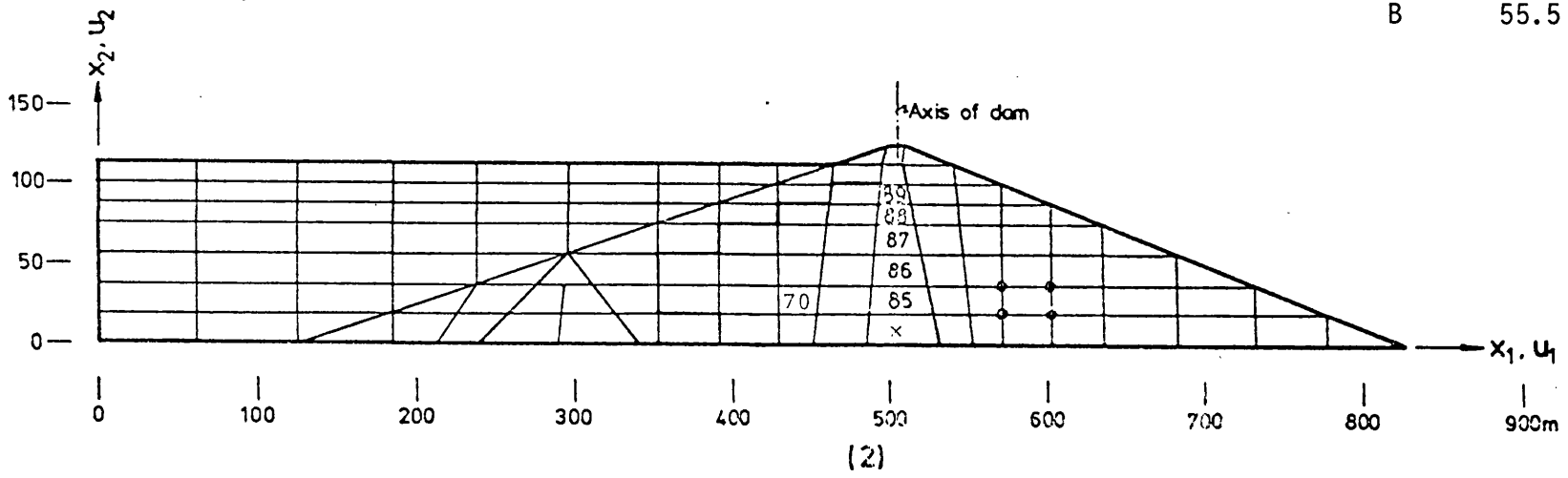

(2)

FIGURE 8.1 EARTHDAM: (1) MATERIAL ZONES; (2) FINITE ELEMENT MESH; (3) MATERIAL PROPERTIES

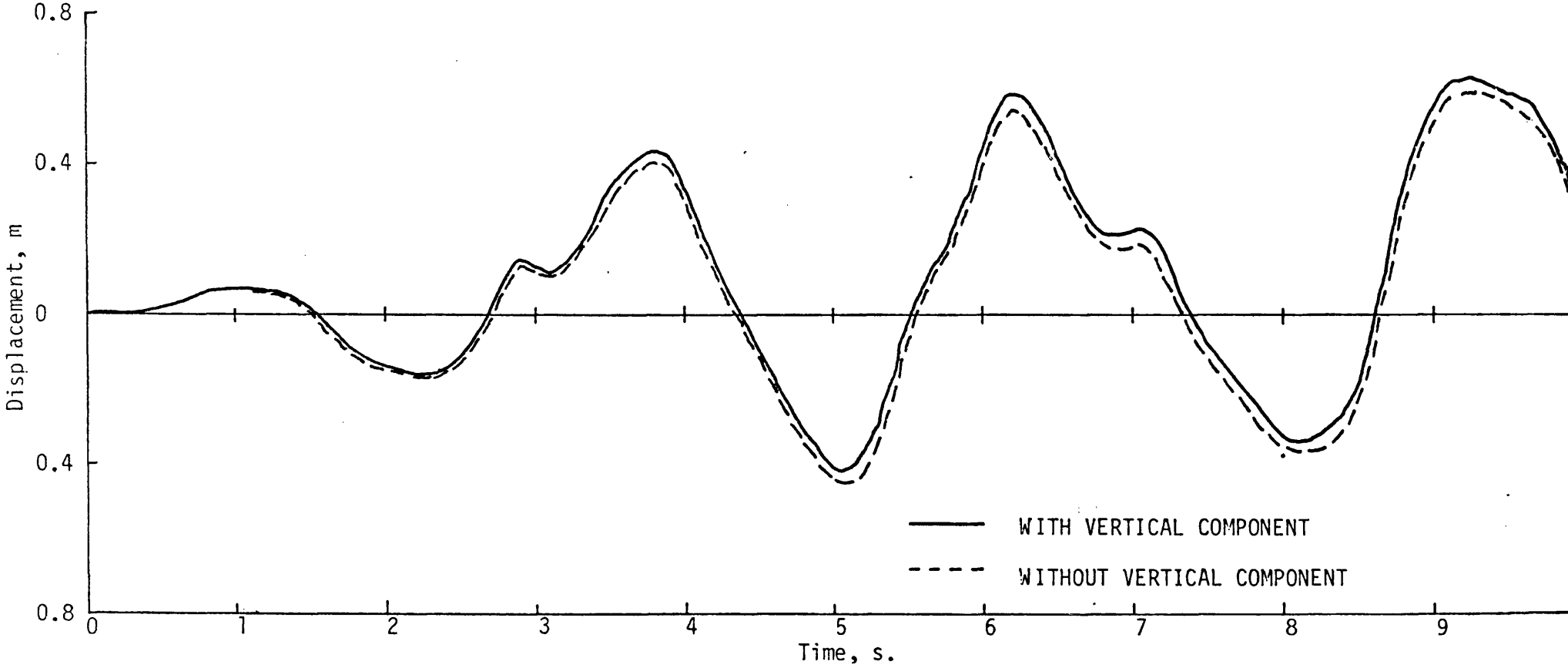

FIGURE 8.2(a) HORIZONTAL DISPLACEMENT TIME HISTORY AT DAM CREST

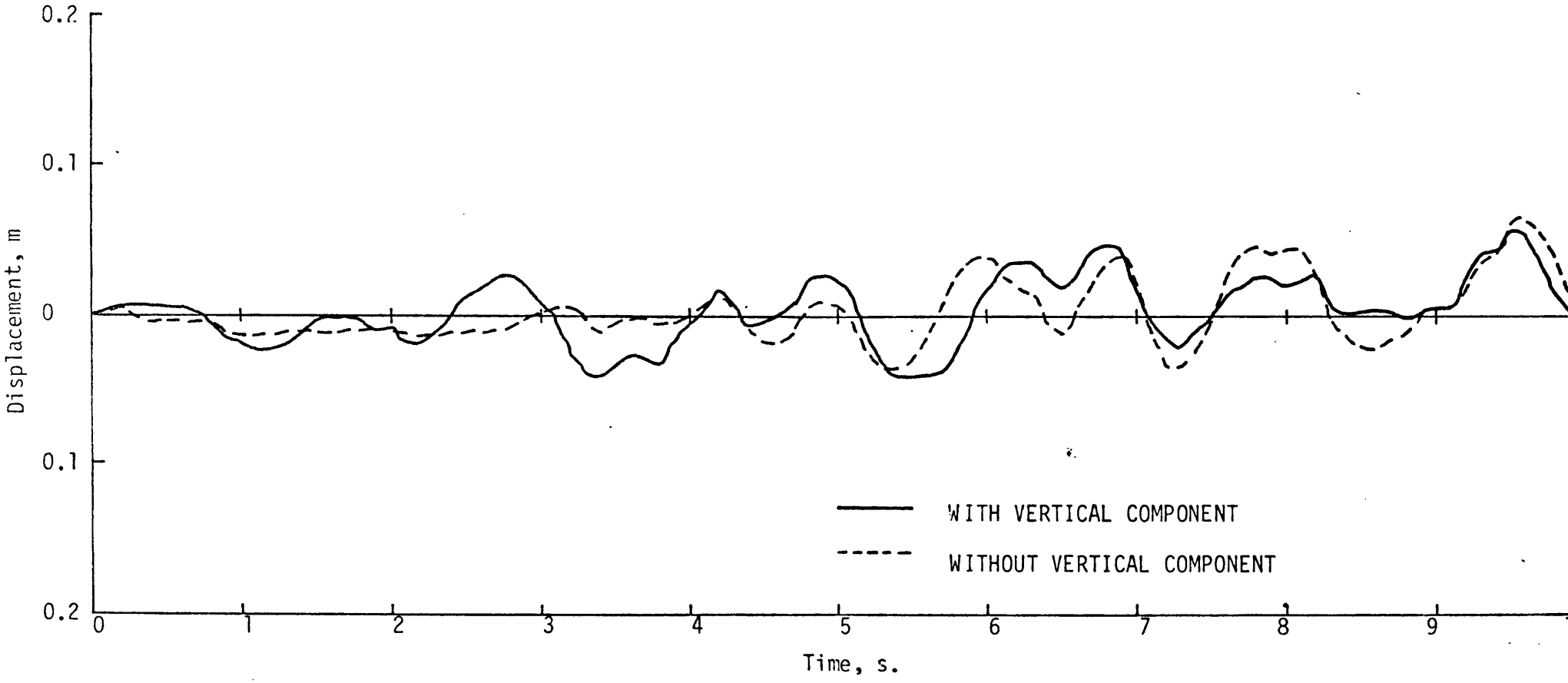

FIGURE 8.2(b) VERTICAL DISPLACEMENT TIME HISTORY AT DAM CREST

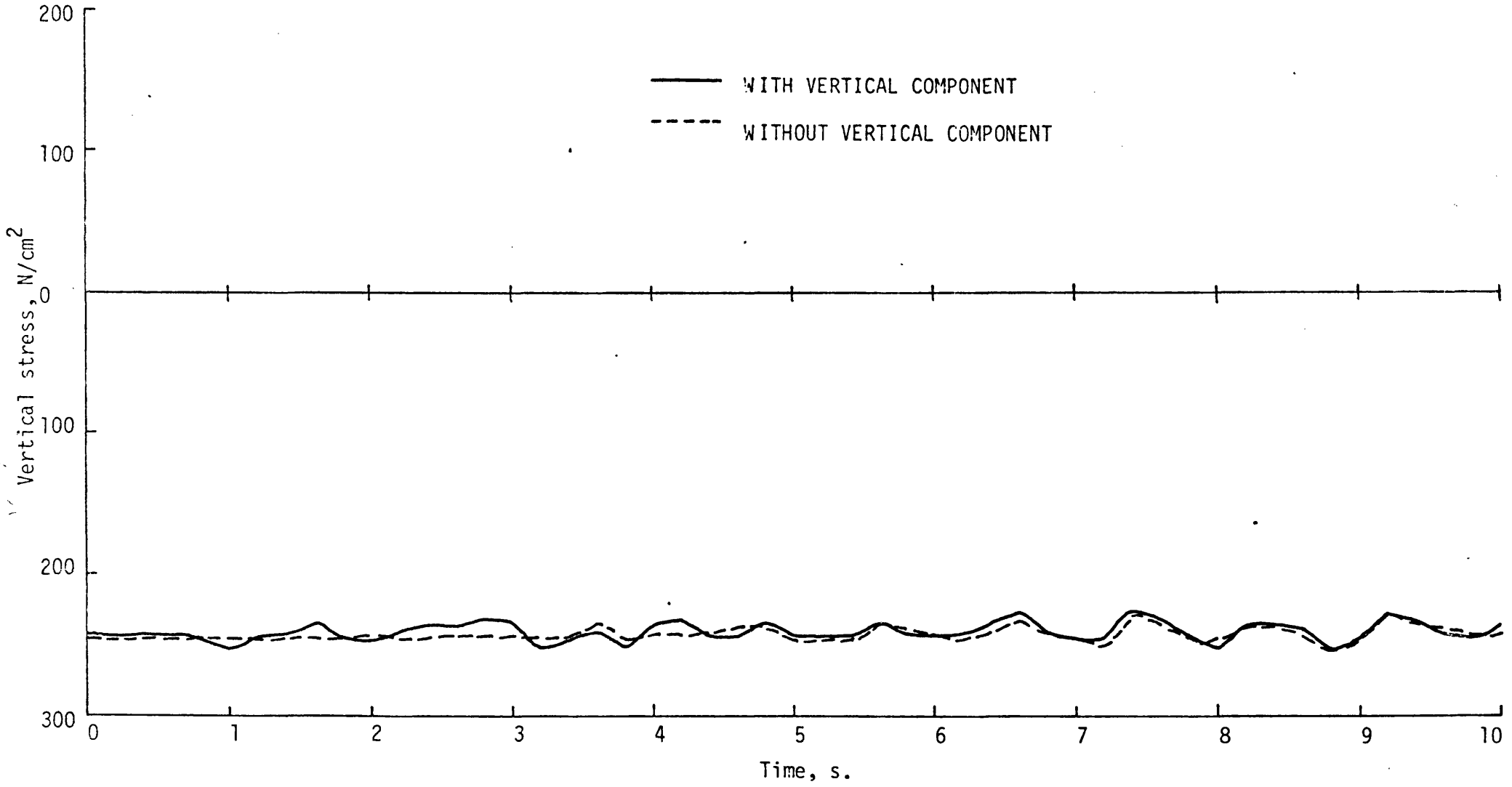

FIGURE 8.2(c) VERTICAL STRESS TIME HISTORY AT POINT X

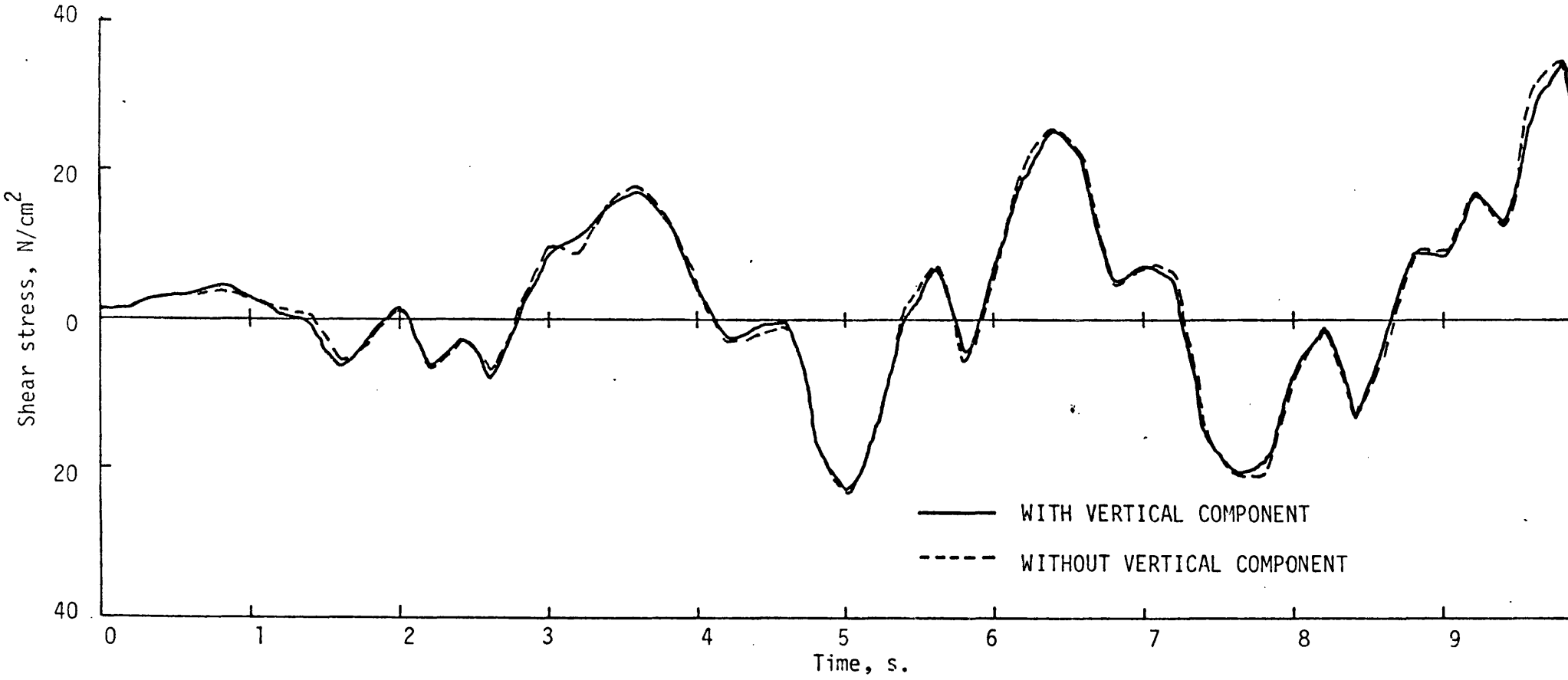

FIGURE 8.2(d) SHEAR STRESS TIME HISTORY AT POINT X

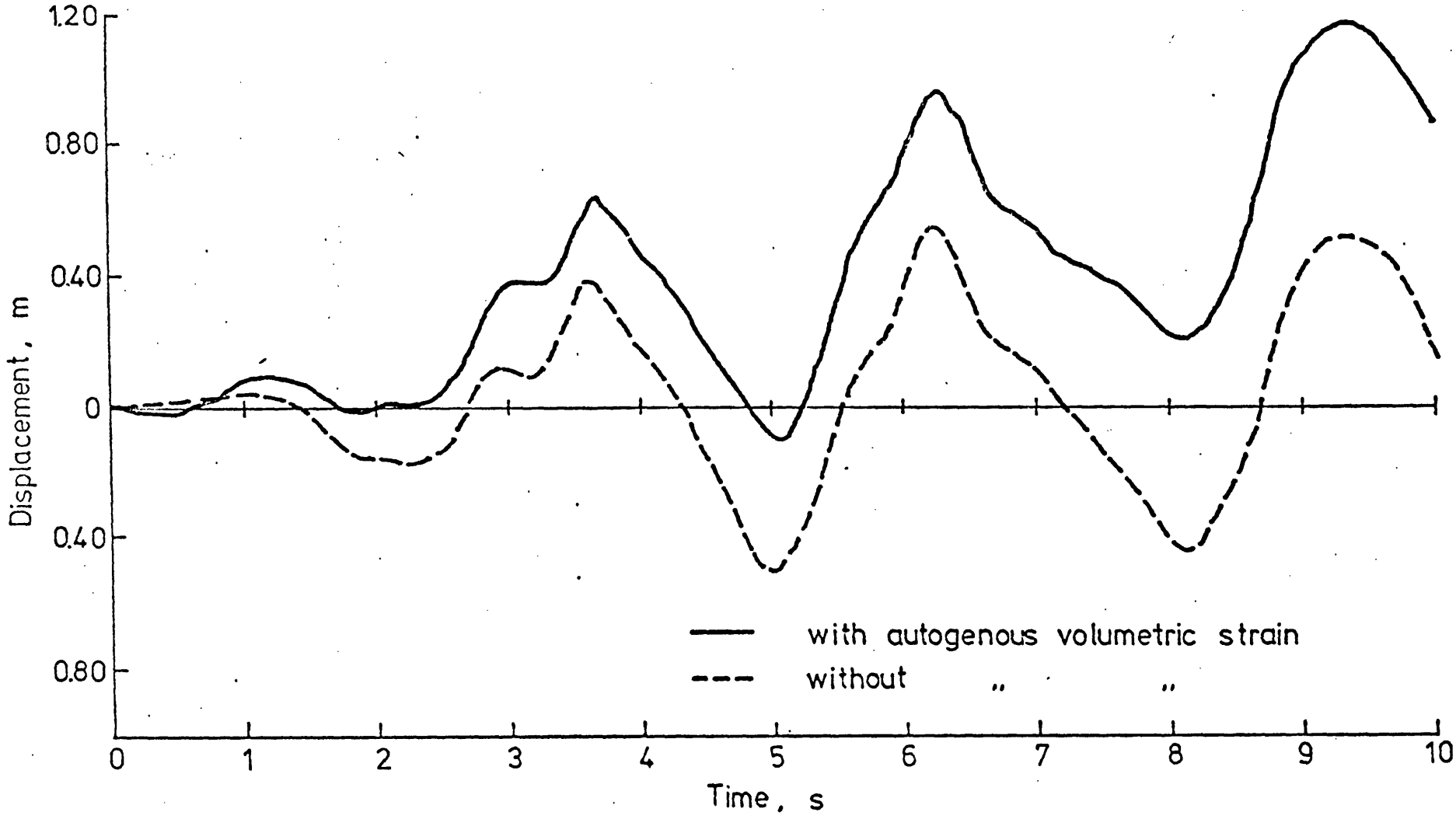

FIGURE 8.3 HORIZONTAL DISPLACEMENT TIME HISTORY AT DAM CREST WITH FULLY UNDRAINED CONDITIONS

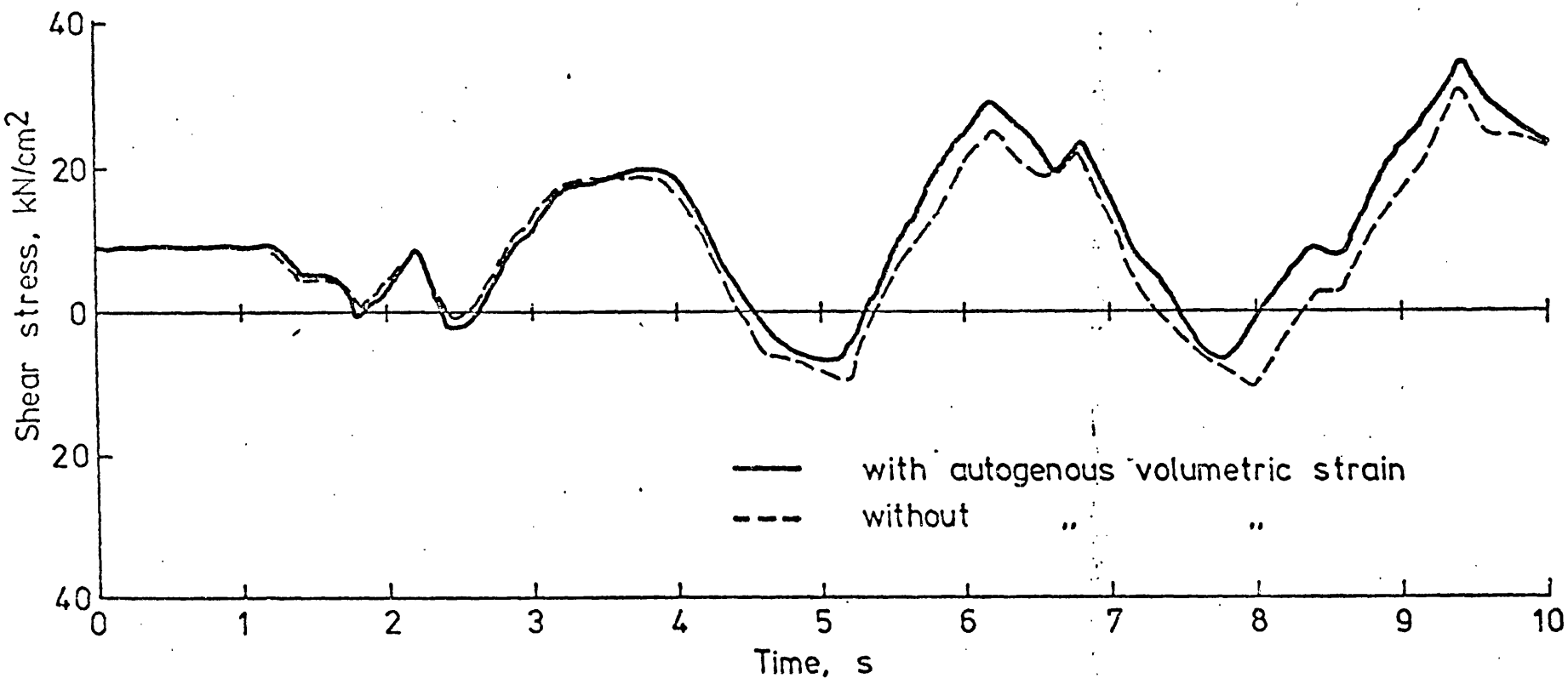

FIGURE 8.4 SHEAR STRESS TIME HISTORY AT THE GAUSS POINT OF ELEMENT 85

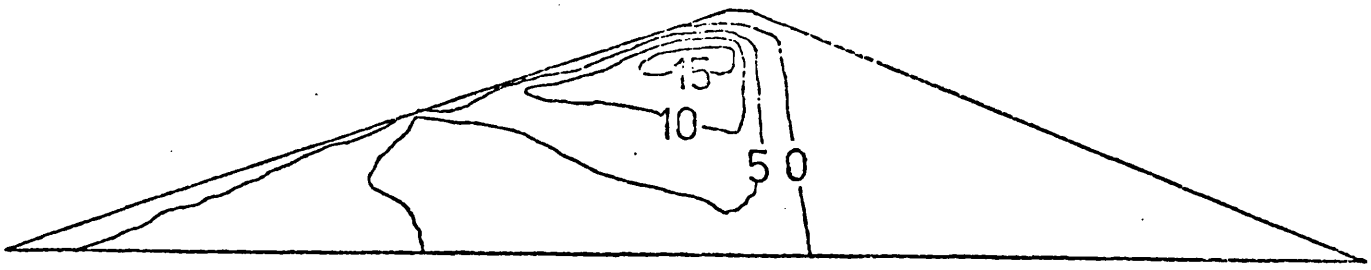

(2s)

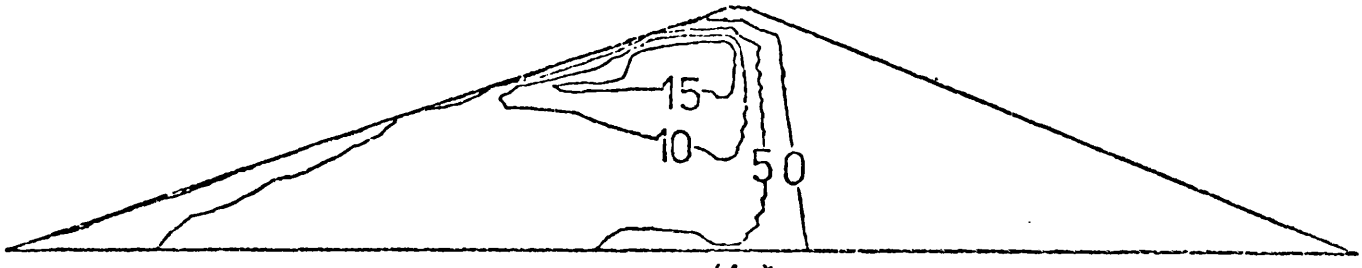

(4s)

CONTOUR UNIT: N/cm^2

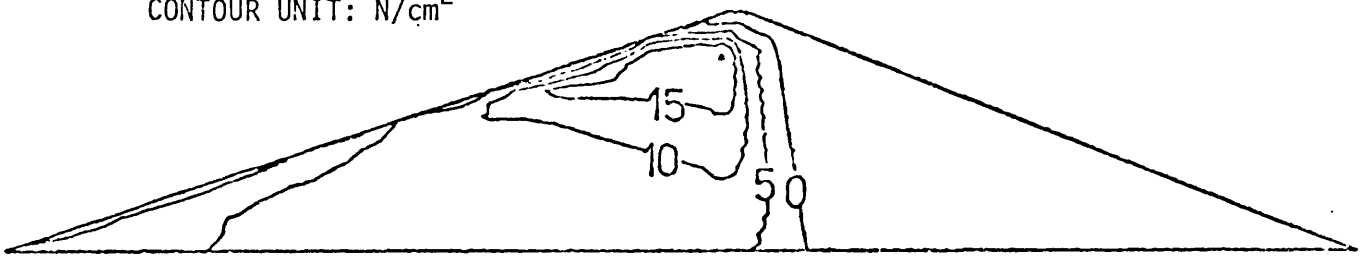

(6s)

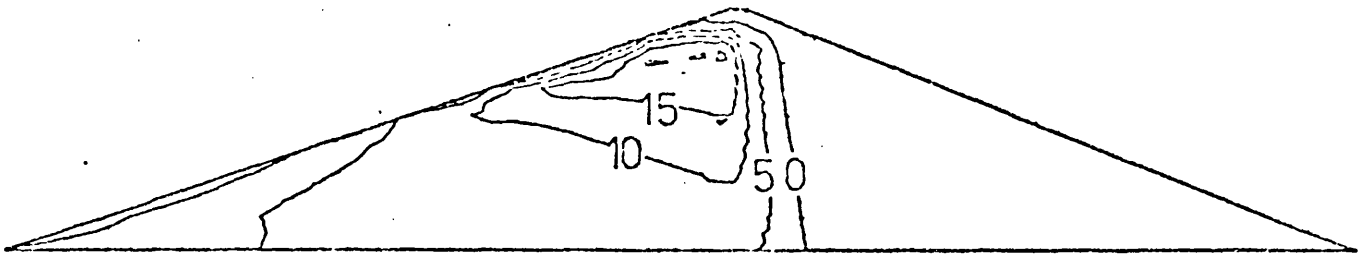

(8s)

FIGURE 8.5 EXCESS PORE PRESSURE CONTOUR

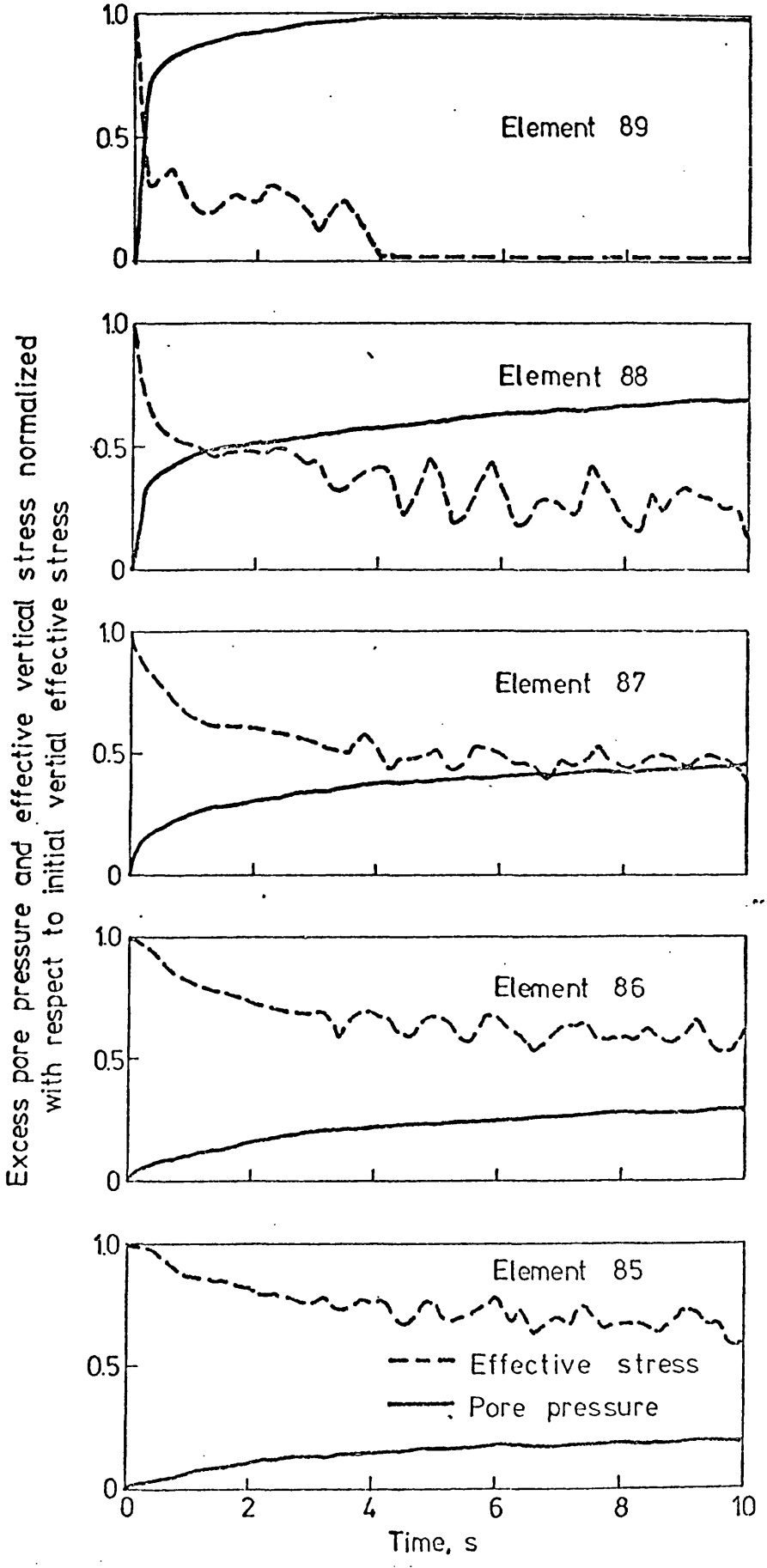

FIGURE 8.6 NORMALIZED VERTICAL EFFECTIVE STRESS AND EXCESS PORE PRESSURE AT VARIOUS HEIGHTS ALONG THE AXIS OF DAM

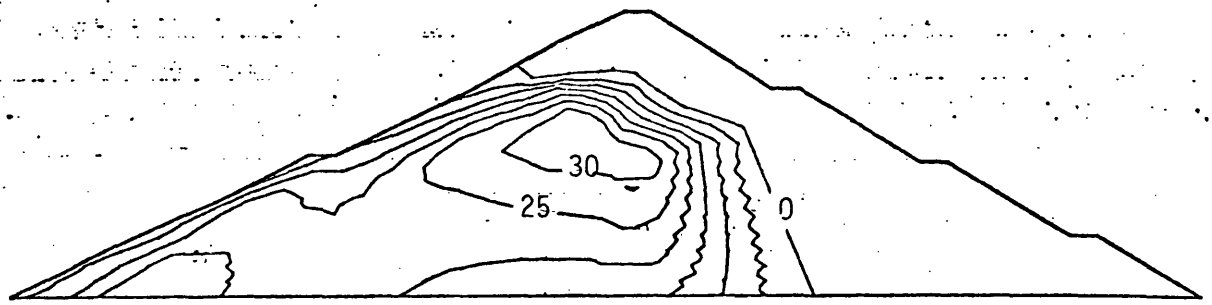

(2s)

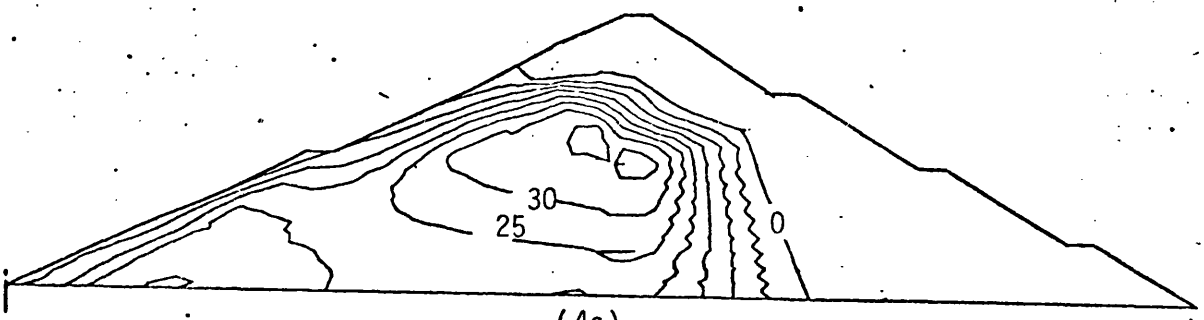

(4s)

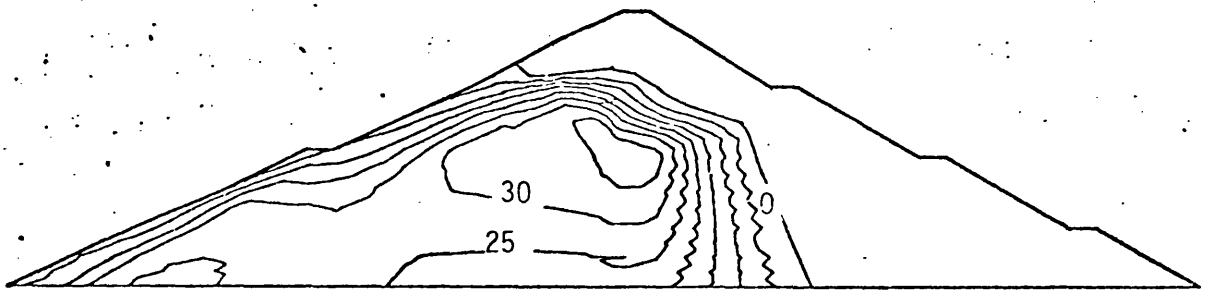

(6s)

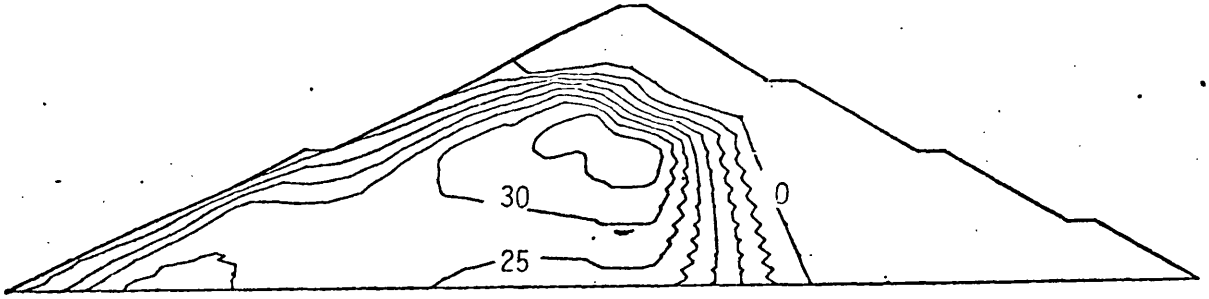

(8s)

CONTOUR UNIT: N/cm^2

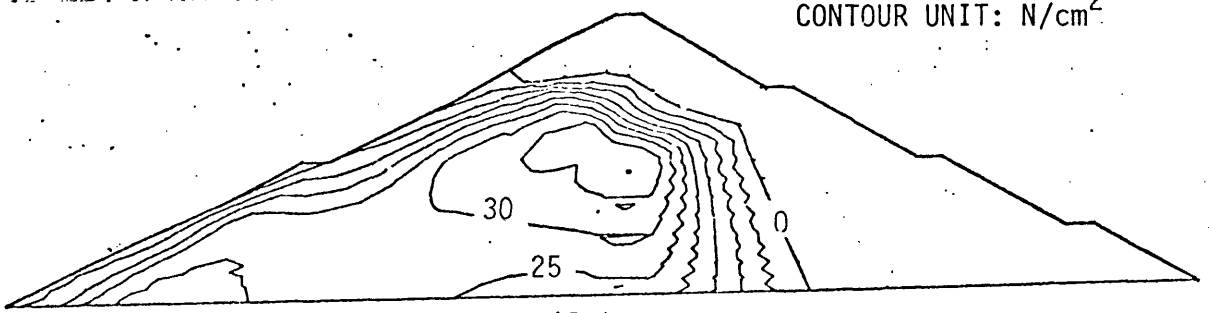

(10)

FIGURE 8.7 EXCESS PORE PRESSURE CONTOUR

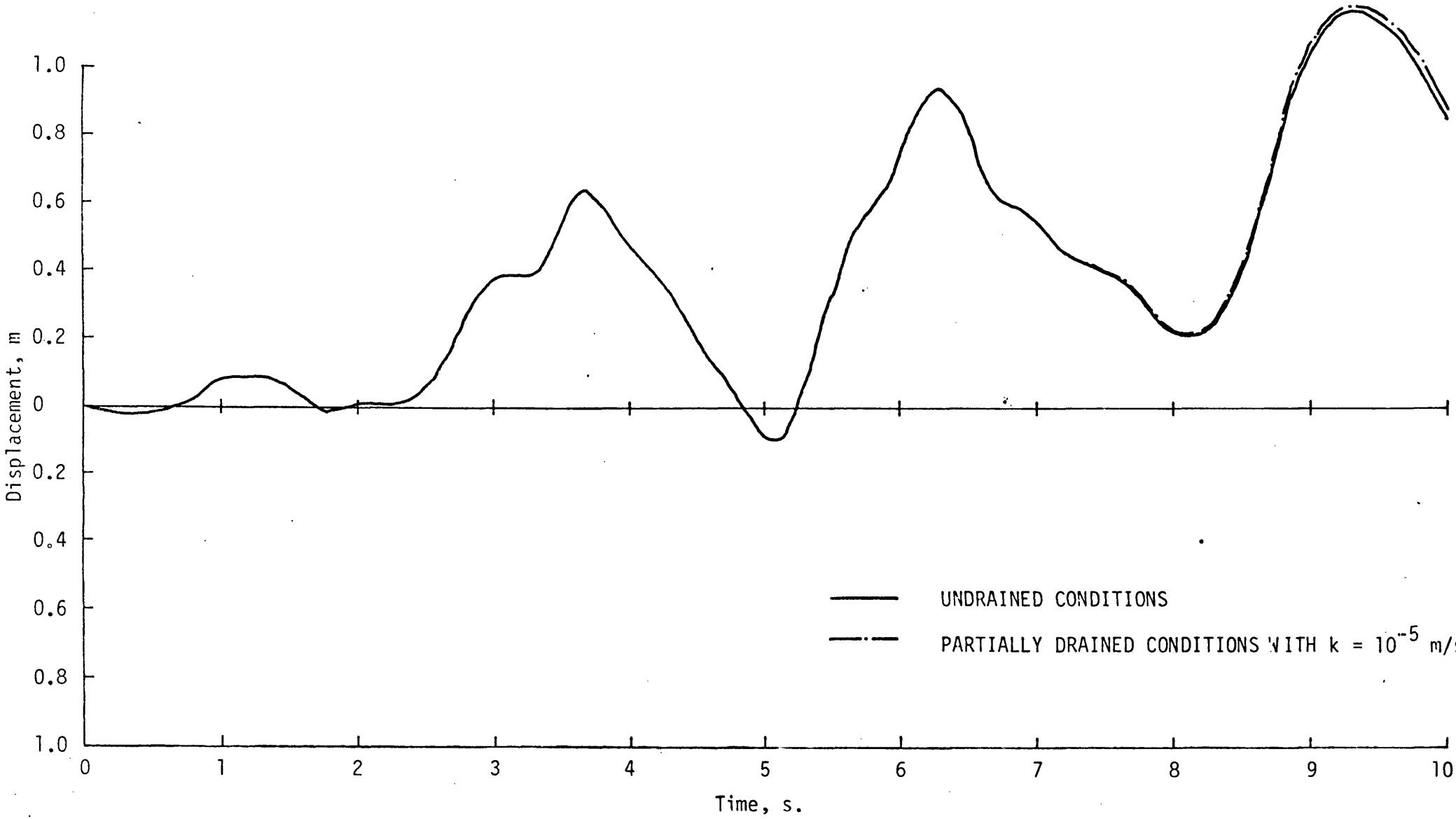

FIGURE 8.8(a) HORIZONTAL DISPLACEMENT TIME HISTORY AT DAM CREST WITH PARTIALLY DRAINED CONDITIONS

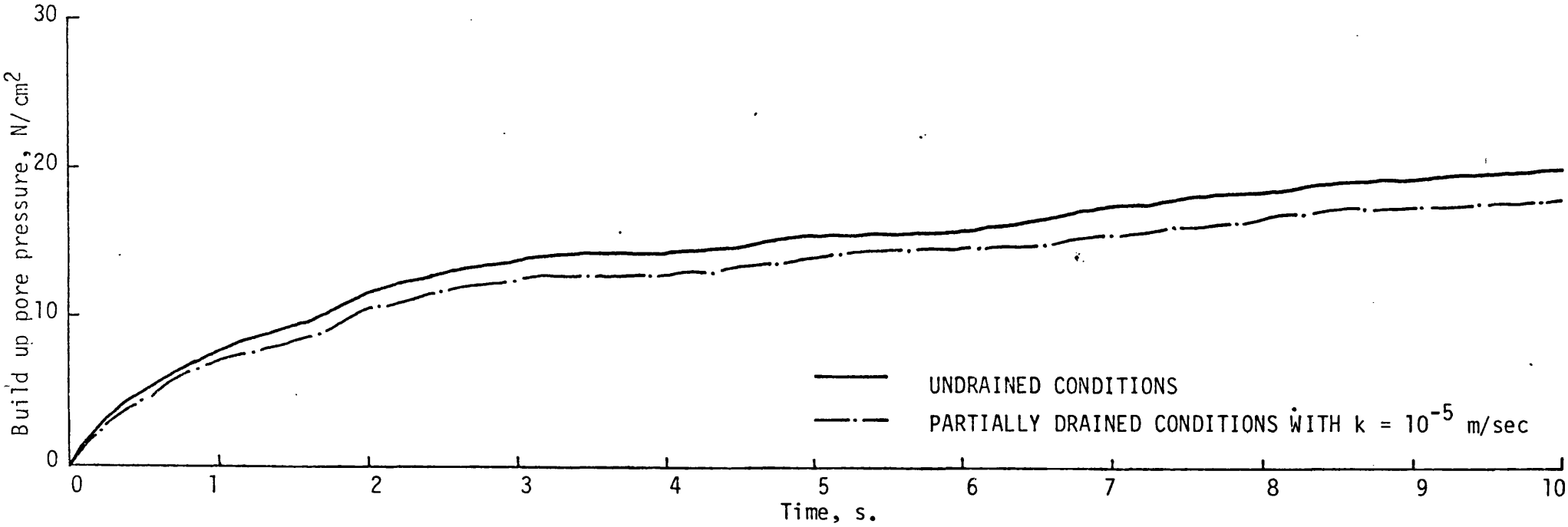

FIGURE 8.8(b) EXCESS PORE PRESSURE CHANGE AT THE GAUSS POINT OF ELEMENT 70

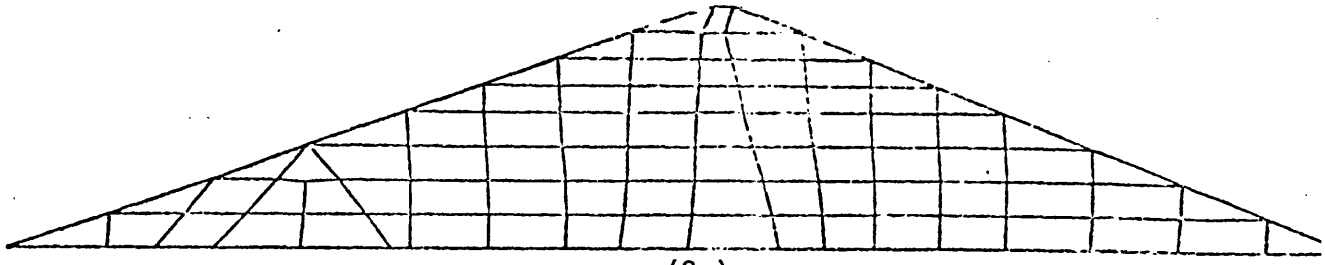

(2s)

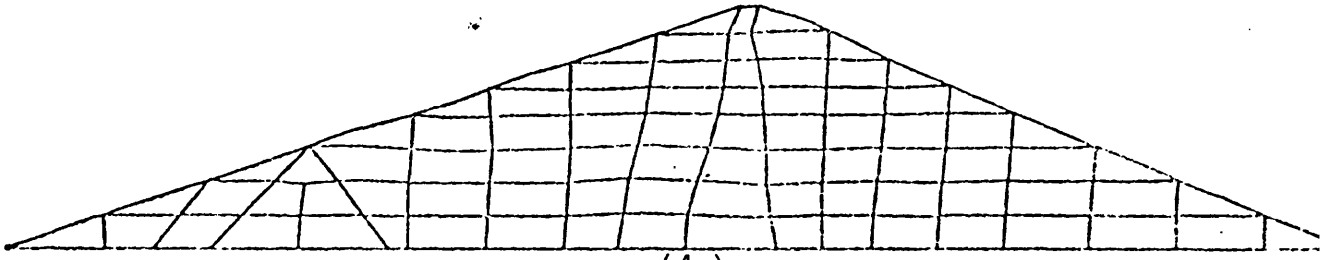

(4s)

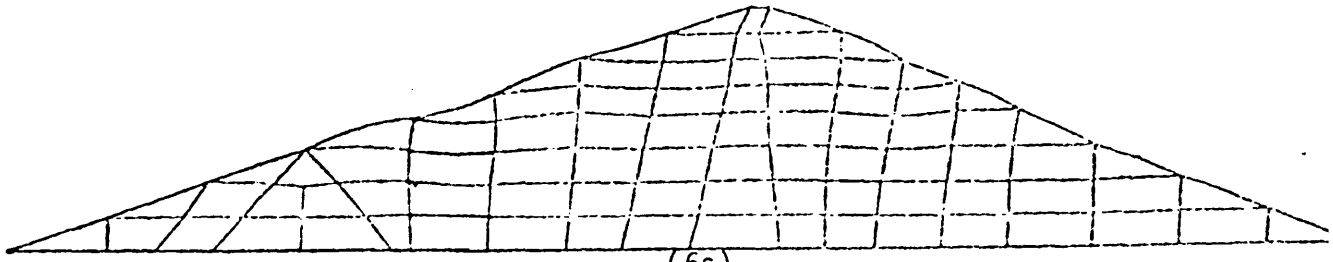

(6s)

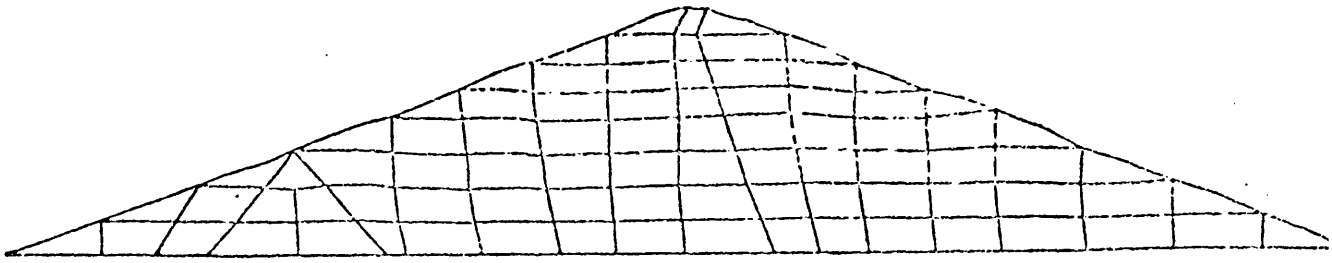

(8s)

FIGURE 8.9 DEFORMED MESH (DISPLACEMENT x 40)

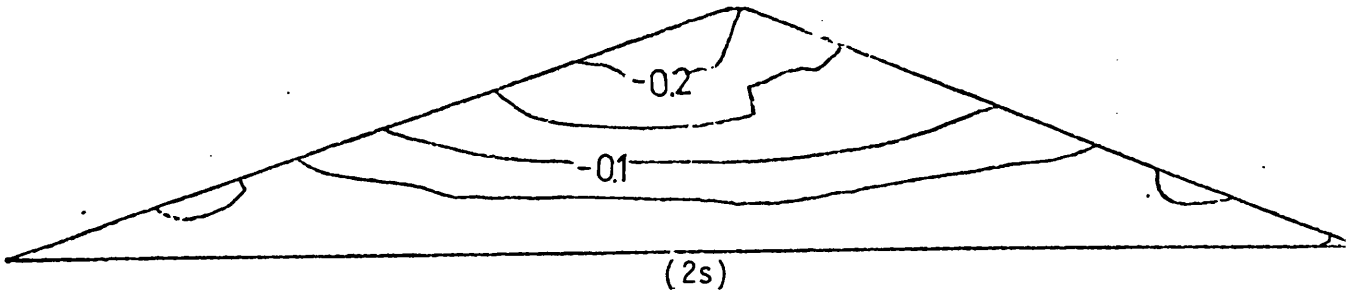

(2s)

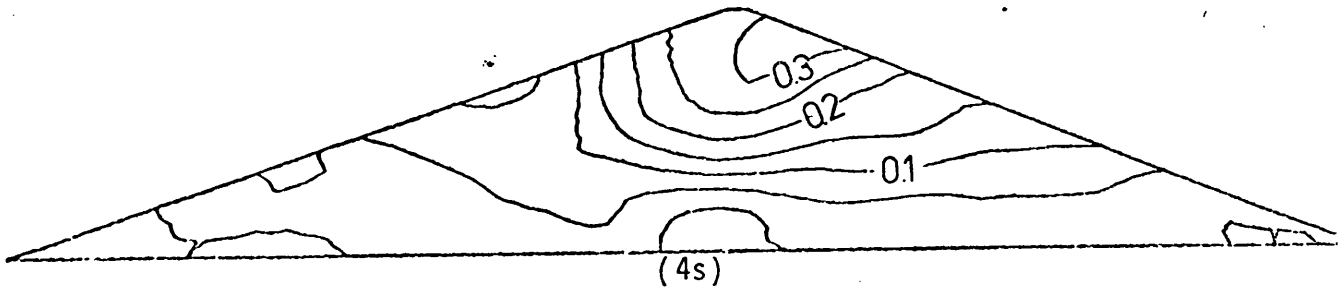

(4s)

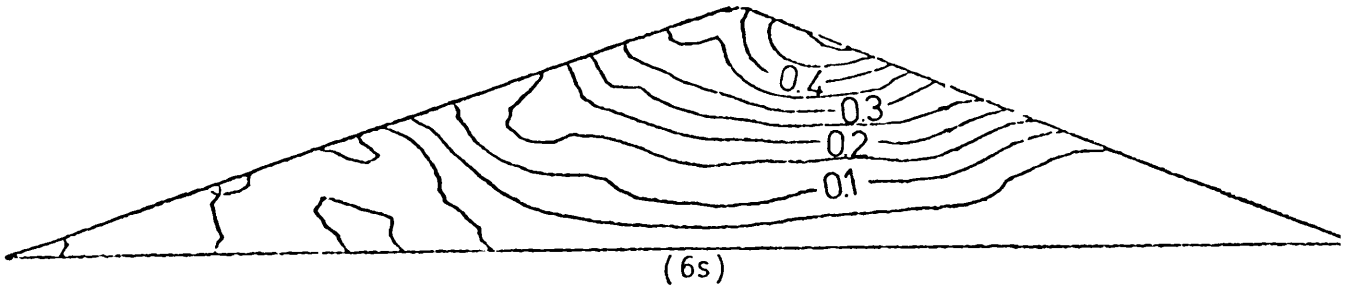

(6s)

CONTOUR UNIT: m

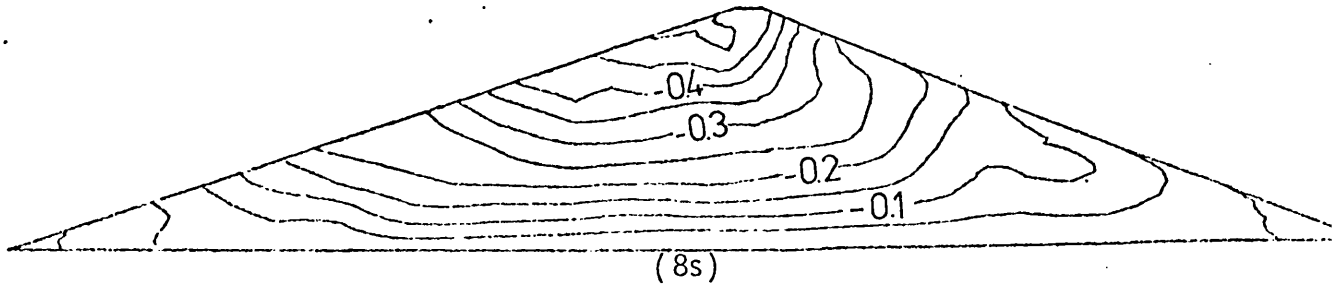

(8s)

FIGURE 8.10 DISPLACEMENT CONTOUR

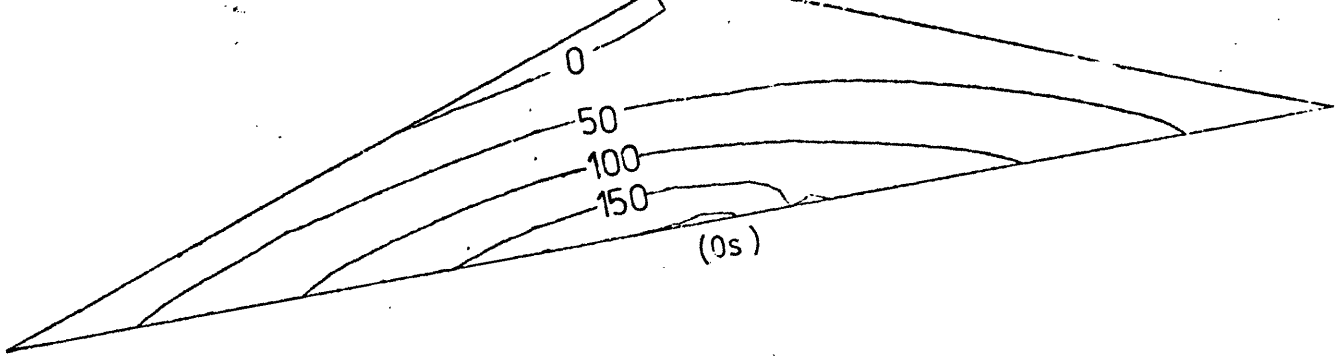

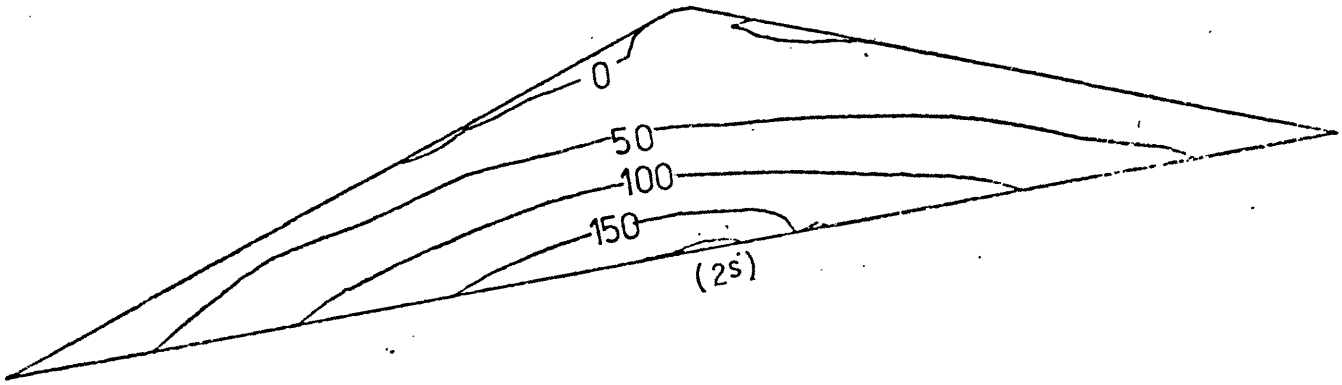

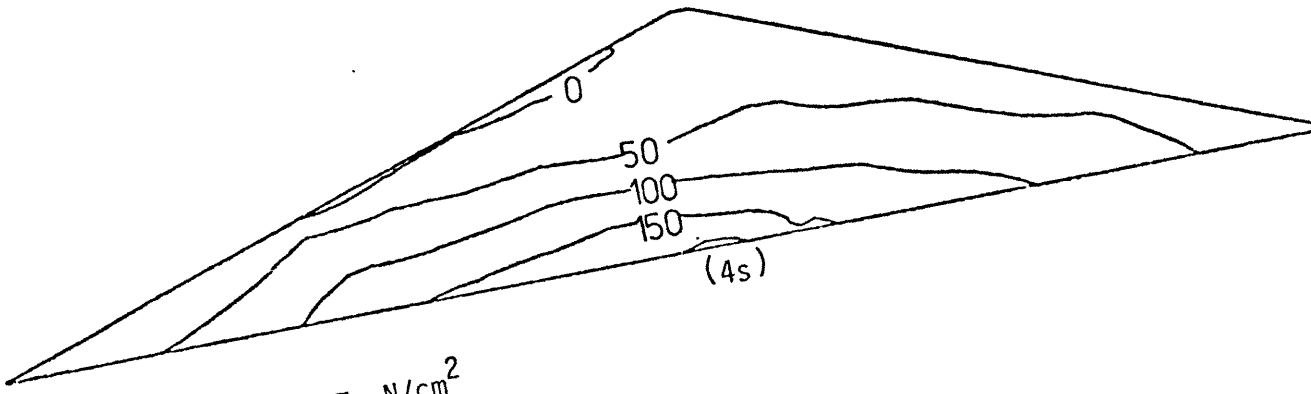

CONTOUR UNIT: N/cm^2

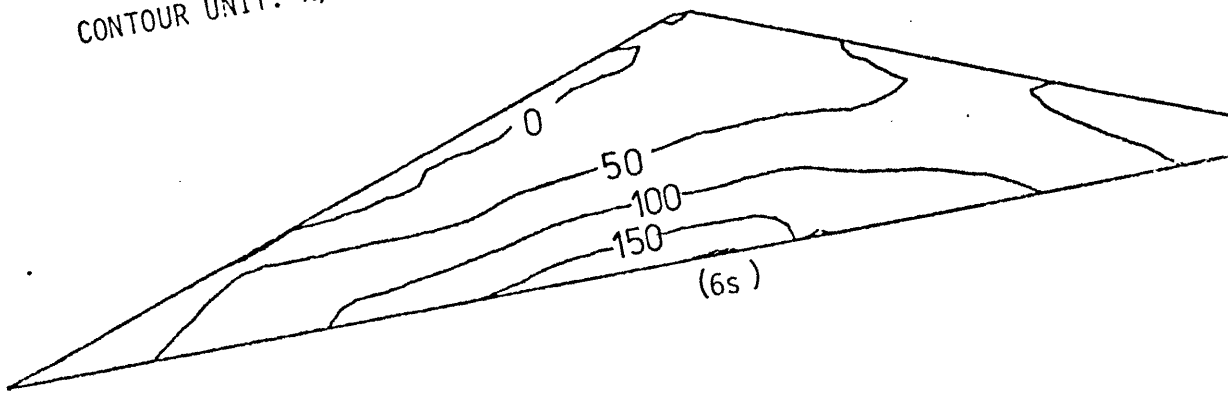

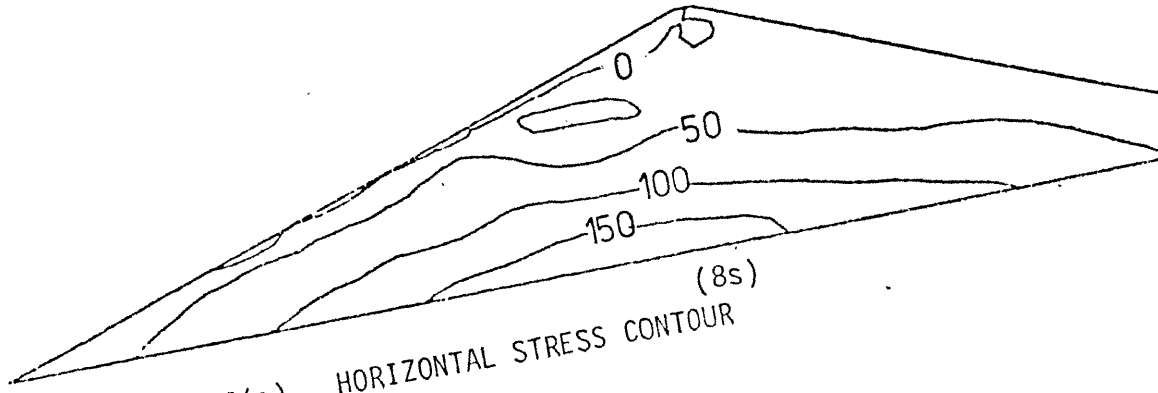

FIGURE 8.11(a) HORIZONTAL STRESS CONTOUR

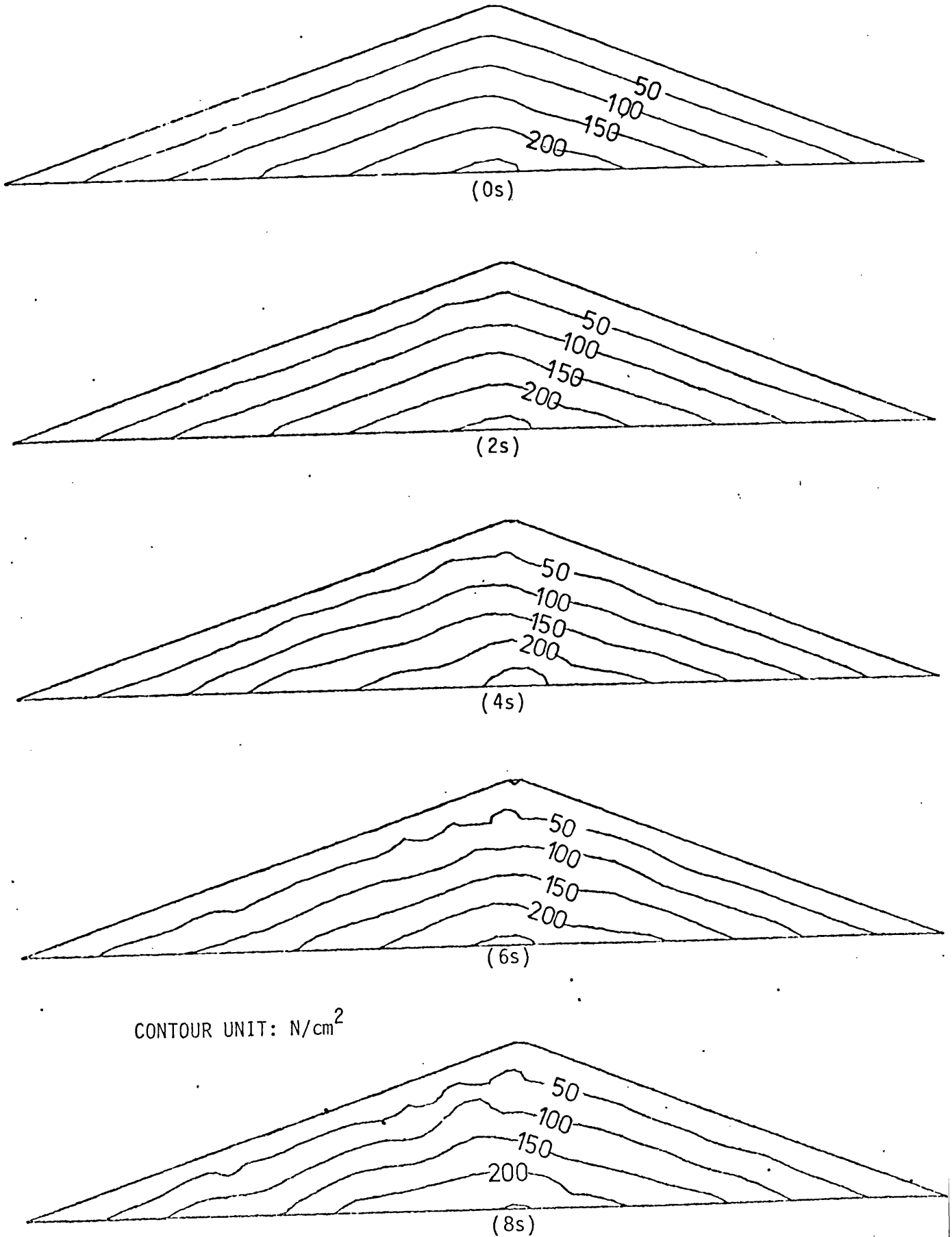

FIGURE 8.11(b) VERTICAL STRESS CONTOUR

50
100
150
(0s)
50
100
150
(2s)
50
100
150
(4s)
50
100
150
(6s)
CONTOUR UNIT: N/cm²
50
100
150
(8s)
z-COMPONENT STRESS CONTOUR

FIGURE 8.11(c)

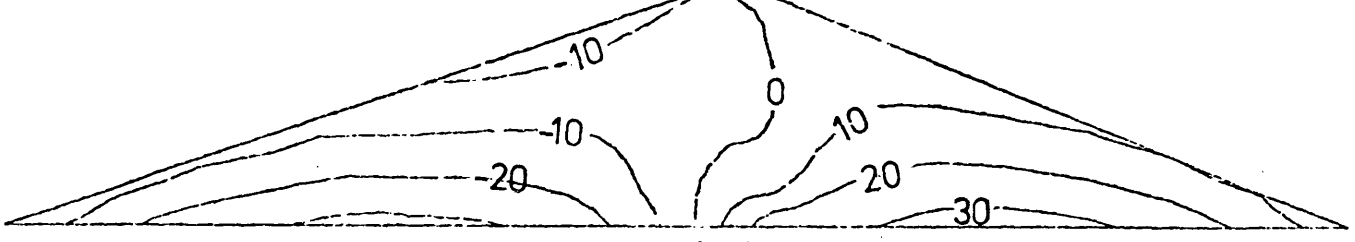

(0s)

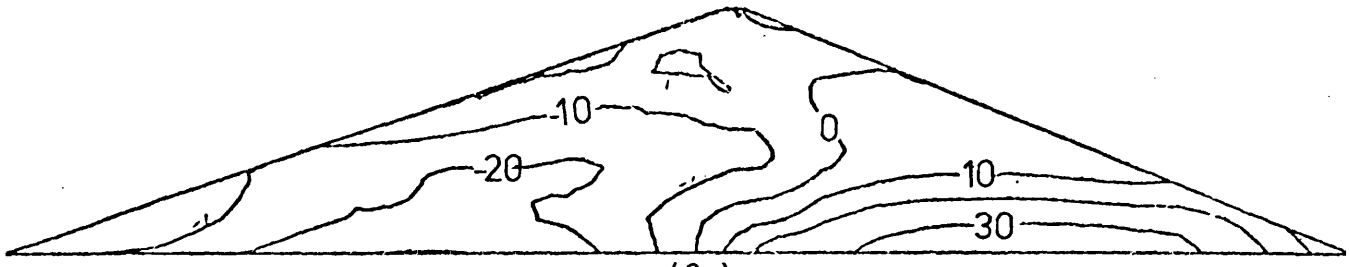

(2s)

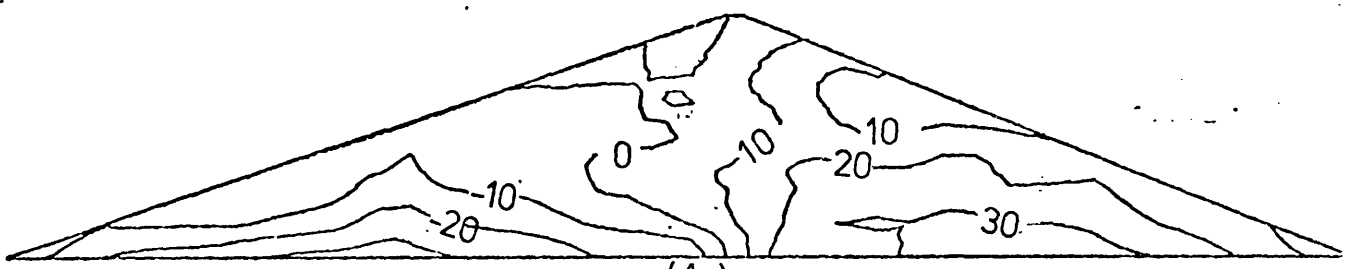

(4s)

(6s)

CONTOUR UNIT: N/cm^2

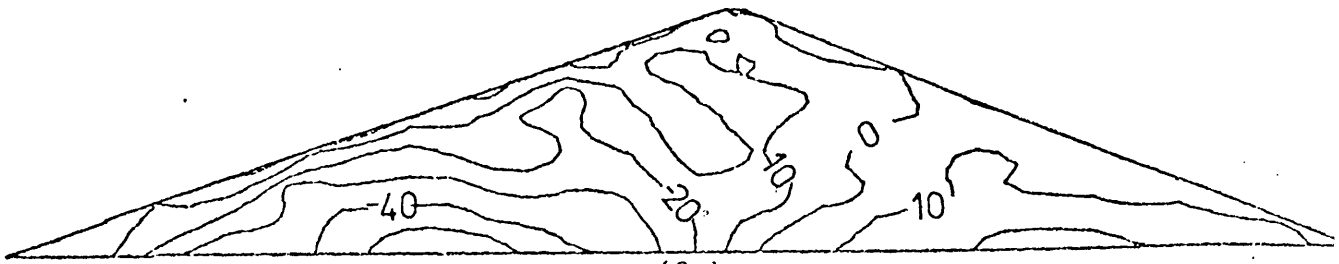

(8s)

FIGURE 8.11(d) SHEAR STRESS CONTOUR

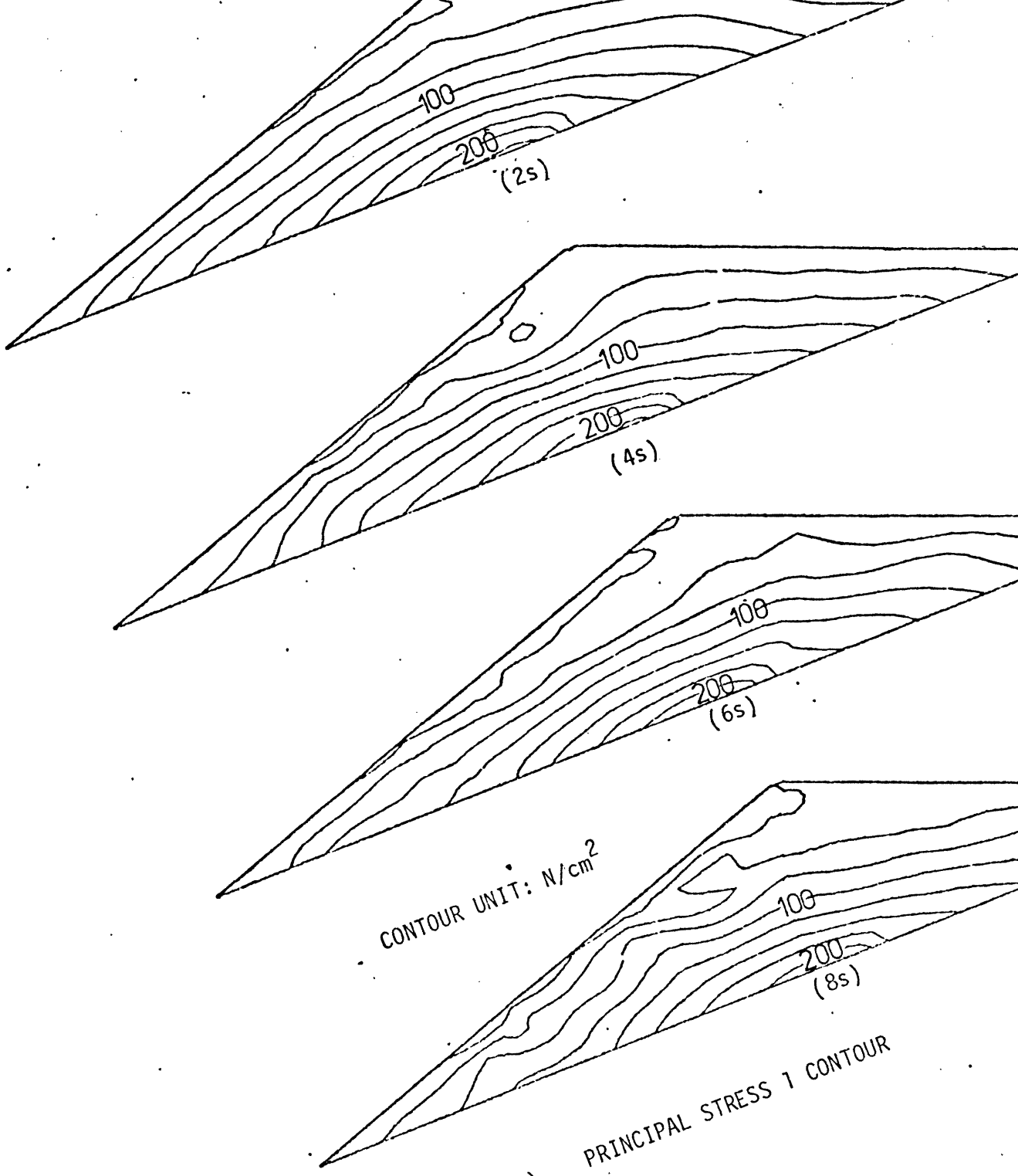

FIGURE 8.11(e) PRINCIPAL STRESS 1 CONTOUR

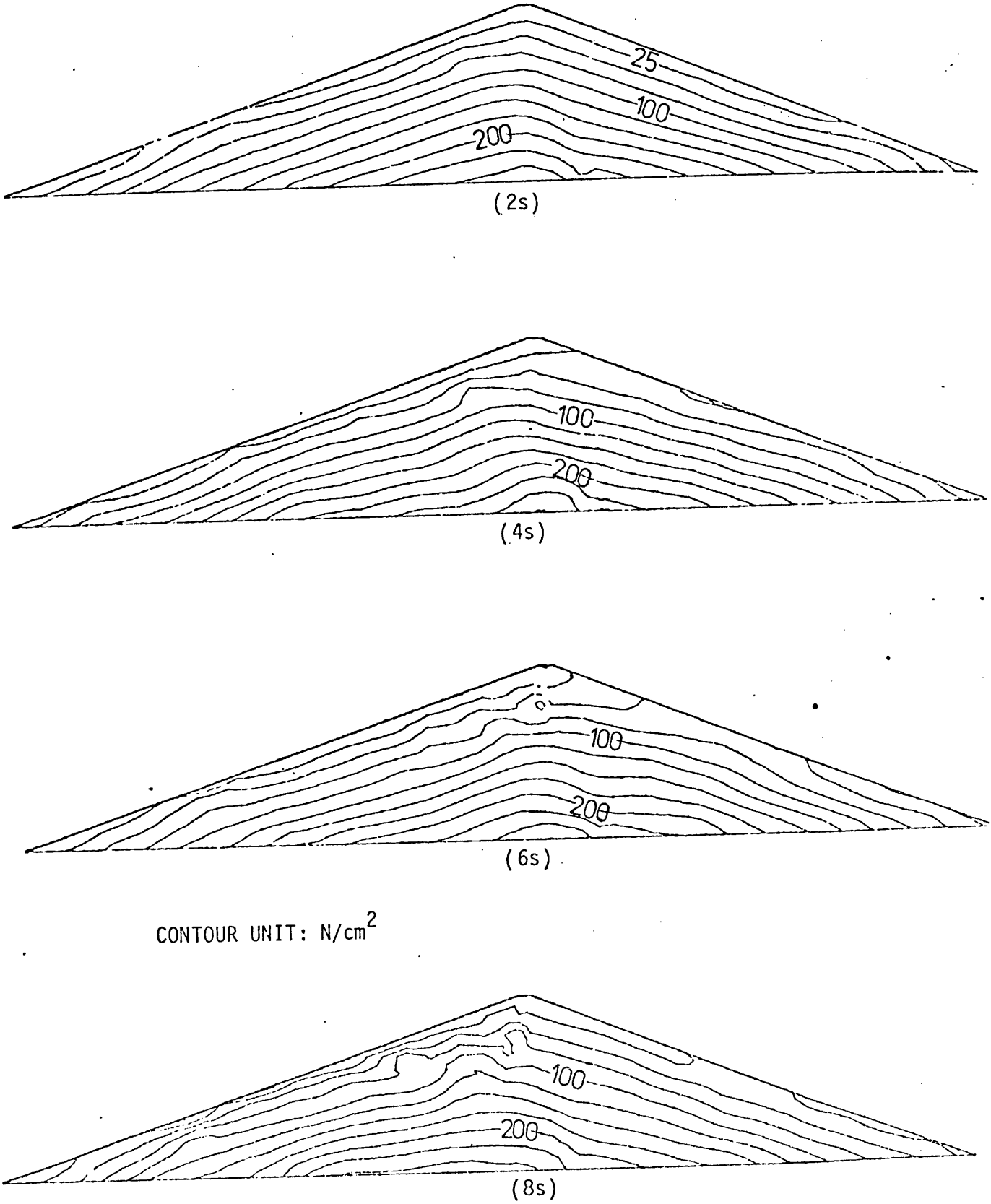

FIGURE 8.11(f) PRINCIPAL STRESS 2 CONTOUR

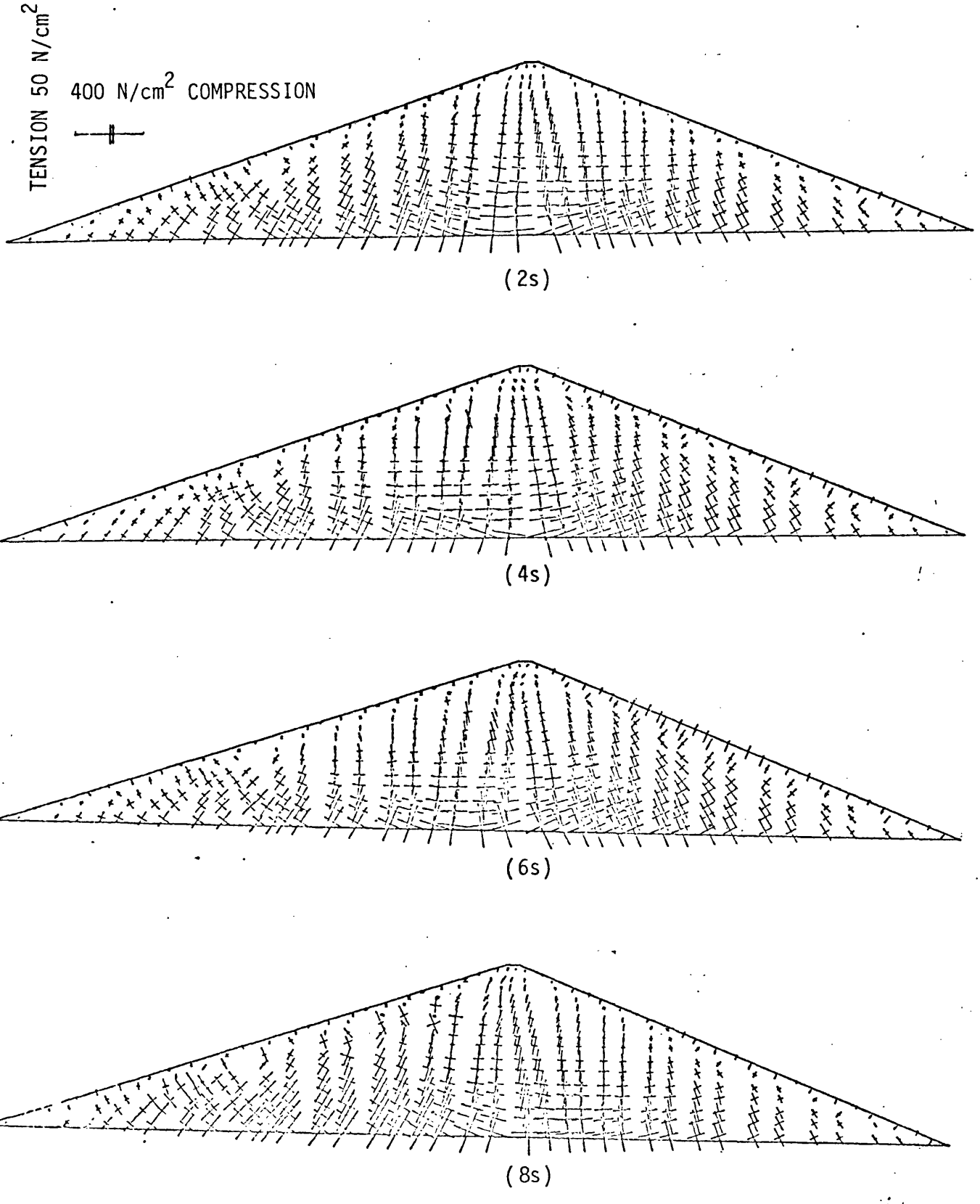

FIGURE 8.12 PRINCIPAL STRESS VECTOR DISTRIBUTION

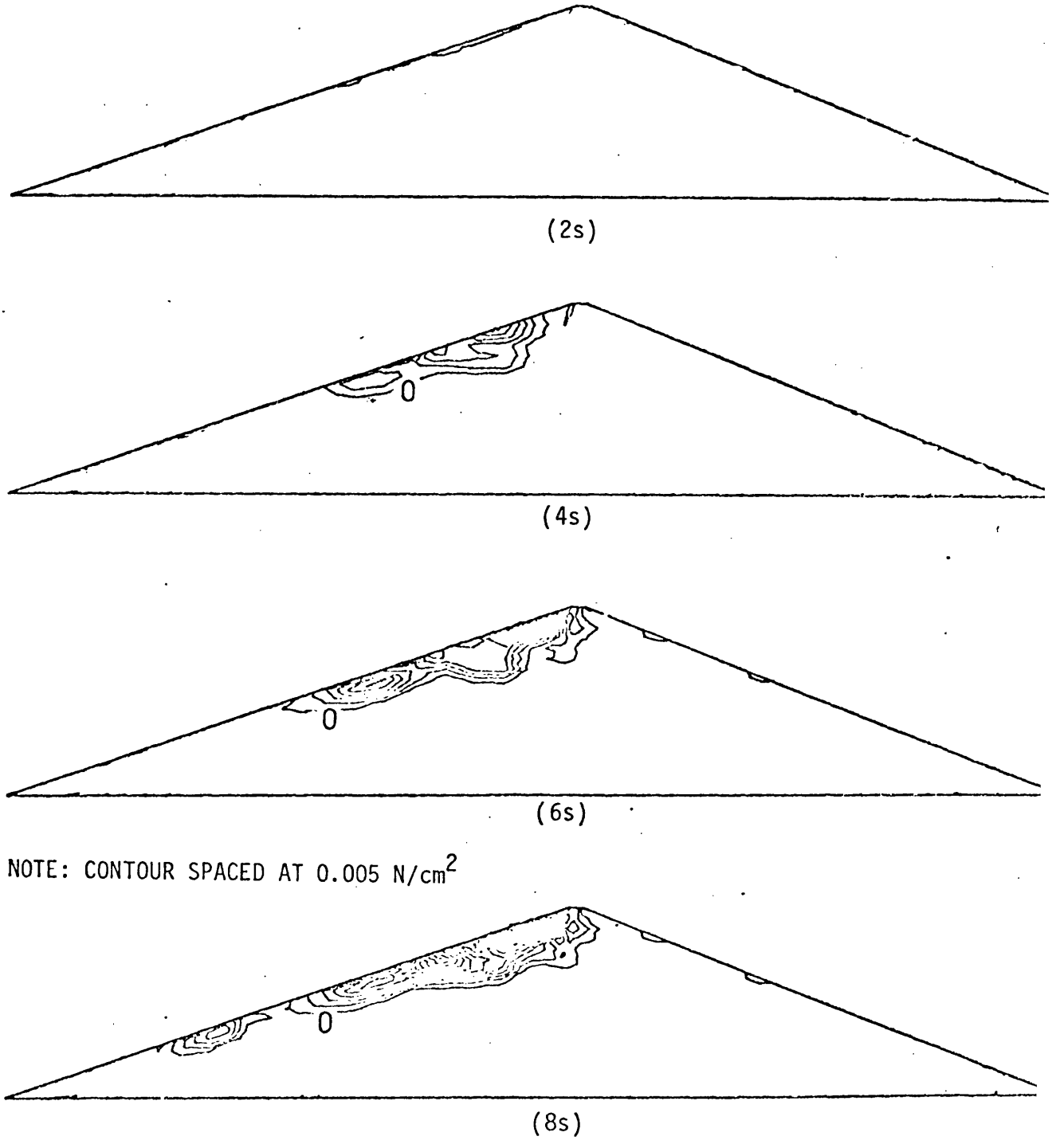

FIGURE 8.13 DISSIPATED ENERGY CONTOUR

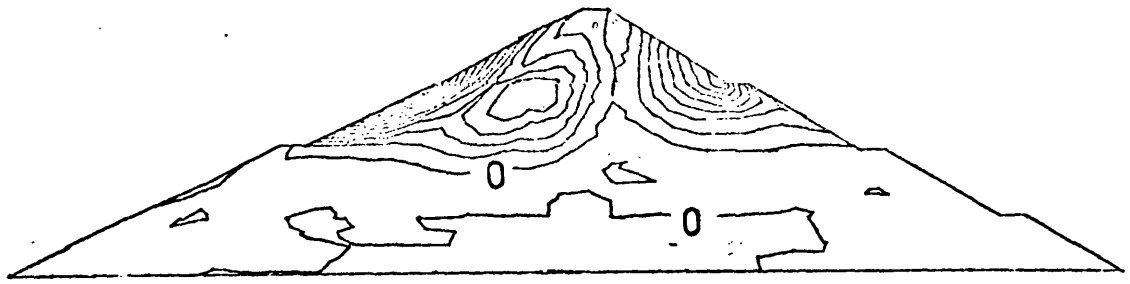

(2s)

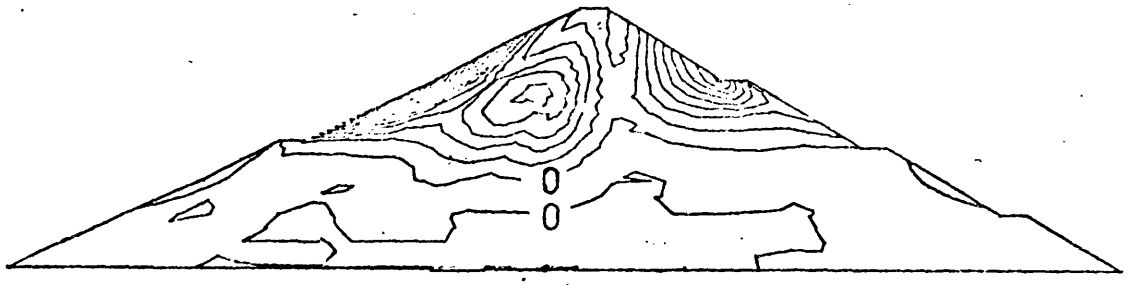

(4s)

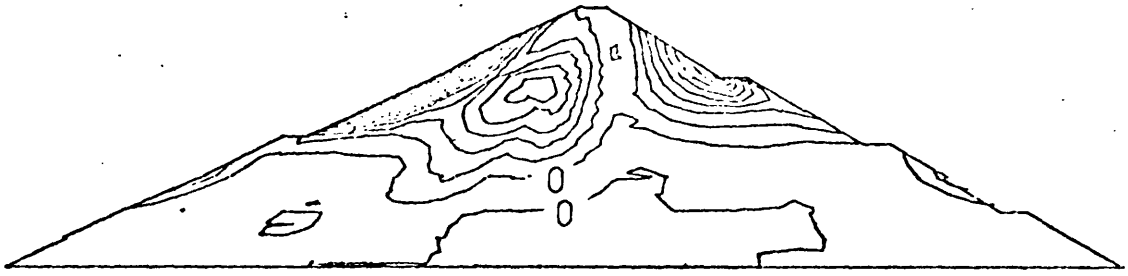

(6s)

NOTE: CONTOUR SPACED AT 0.005 N/cm^2

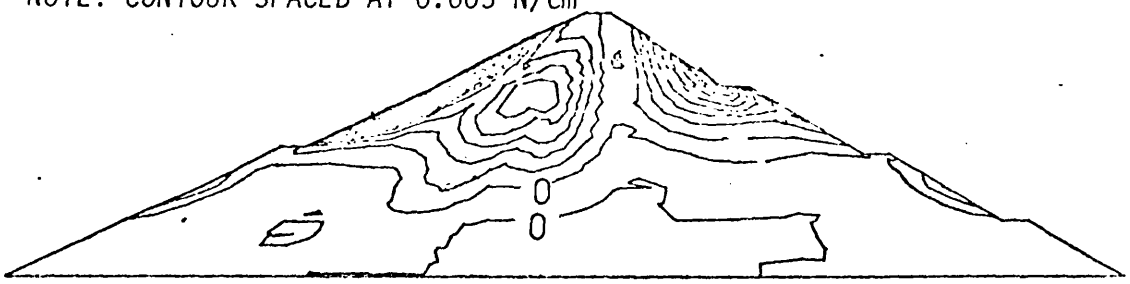

(8s)

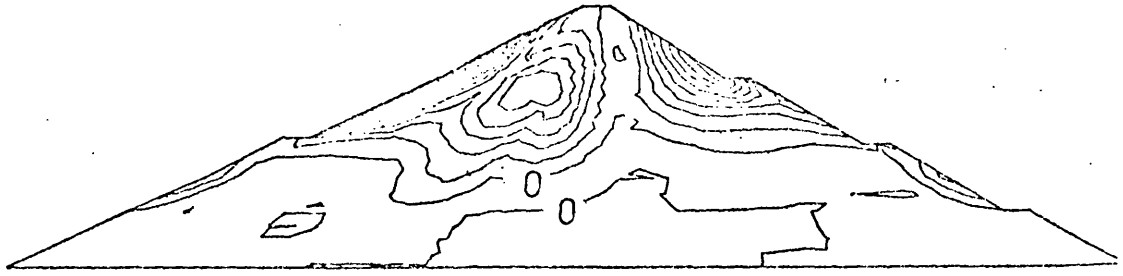

(10s)

FIGURE 8.14 DISSIPATED ENERGY CONTOUR

CHAPTER 9

CONCLUSIONS AND RECOMMENDATIONS

9.1 CONCLUSIONS

As pointed out at the beginning of the thesis, the main objectives of the study are: (1) to look for a suitable method in nonlinear dynamic analysis, (2) to consider a proper nonlinear material model for the soil, (3) to investigate the phenomena of liquefaction. Now a general conclusion based on the results of the study can be summarized as follows:

(1) First of all, it can be seen that the nonlinear dynamic analysis of earth dams by a finite element spatial discretization and a central difference time stepping scheme has proved efficient in describing the response and behaviour of the dam undergoing the passage of seismic excitation.

(2) It appears that the implicit time stepping scheme is cheaper in comparison with the explicit time stepping scheme. This is because the implicit time stepping scheme is unconditionally stable, therefore a relatively large size of time step length can be adopted. On the other hand, the explicit central difference scheme is conditionally stable in which the time step length is limited by a critical time step length.

(3) A general model for the analysis of seismic response and liquefaction of saturated soil has been presented.

The model allows the progressive build up of excess pore water pressure and consequently the successively decreasing of the effective stress until the point of structural failure.

(4) In most earth dams, the permeability of the constituent material is usually very low, and the seismic excitation occurs for a short period. Therefore, the seismic response analysis can be treated using a fully undrained condition.

(5) A combination of local liquefaction and multiple shear failure is a likely mechanism of failure of the earth dams during earthquakes.

9.2 RECOMMENDATIONS

In any research of this nature there is always a scope for further study. A few suggestions are given as follows:

(1) It is worthwhile carrying out extensive soil tests to generalize the expression for autogenous volumetric strain.

(2) An anisotropic hardening model for soils developed by Mroz, et. al.,[1,2] should be applied in the cyclic load and liquefaction studies.

(3) It is worthwhile fully developing the implicit time stepping scheme since the nature of seepage formulation does not allow seepage equation to be solved without matrix factorization.

REFERENCES

1. MROZ,Z., NORRIS,V.A. and ZIENKIEWICZ,O.C.
'An anisotropic hardening model for soils and its application to cyclic loading'
Int. J. Num. Anal. Methods in Geomechanics, Vol.2, 203-221 (1978).

2. MROZ,Z., NORRIS,V.A. and ZIENKIEWICZ,O.C.
'Application of an anisotropic hardening model in the analysis of elasto-plastic deformation of soils'
(to be published).

APPENDIX A

LIST OF SYMBOLS

Although all notations have been defined as they first appear in the text, a list of principal symbols used in this thesis is presented for easy reference. On many occasions additional ones have to be used in a minor context and a non-uniqueness arises. Dots are used to denote differentiation with respect to time.

$\underset{\sim}{a}$ nodel displacement

$\underset{\sim}{B}$ Matrix of shape function derivatives

$\underset{\sim}{C}$ Damping matrix

C Cohesion of soil

$\left[C_T\right] = \left[D_T\right]^{-1}$

c Wave speed

$\underset{\sim}{D}$ Elasticity matrix

D_r Relative density

$\underset{\sim}{D}_T$ Tangential elasticity matrix

E Young's modulus

$\underset{\sim}{e}$ Deviatoric strain

F Yield function

G Shear modulus

K Bulk modulus

$\underset{\sim}{K}$ Stiffness matrix

K_f Bulk modulus of fluid

K_T The bulk tangential modulus

$\underset{\sim}{L}$ Strain operator

$\underset{\sim}{M}$ Mass matrix

M_{cs} Critical state line

$\underset{\sim}{m}$ Vector equivalent to Kronecker delta, i.e. $\{1,1,1,0,0,0\}^T$

$\underset{\sim}{N}_i$ Shape function

P Pore pressure

P_o Half the preconsolidation pressure

Q Plastic potential function

$\underset{\sim}{s}$ Deviatoric stress

T Natural period

$t, t+\Delta t$ Represent times at t and $t + \Delta t$

$\underset{\sim}{u}$ Displacement vector

$\underset{\sim}{w}$ Fluid displacement relative to solid skeleton in porous media

x,y,z Cartesian co-ordinates

α = Lode angle

$\alpha = \frac{K_f}{n}$

$\beta = \frac{1}{n/K_f + 1/K_T}$

γ Shear strain

γ Fluidity parameter

$\underset{\sim}{\varepsilon}$ strain vector

ζ Damping ratio

η, ξ Element curvilinear co-ordinates

θ $\frac{\bar{\sigma}'}{\sigma'_{mo}}$

κ Strain path length

λ Characteristic number

μ Viscosity

ν Poisson's ratio

$\xi = \sqrt{\frac{1}{2} d\underset{\sim}{e}^T d\underset{\sim}{e}}$

ρ, ρ_f Mass density of material and fluid respectively

$\underset{\sim}{\sigma}$	Stress vector
$\bar{\sigma}'$	The second effective stress invariant
σ'_{mo}	The average effective mean stress at t = 0
ϕ	Angle of internal friction
ω	Circular frequency

APPENDIX B

AN INTRODUCTION TO DYNAMIC RELAXATION

B.1 INTRODUCTION

The problems of interest include linear and nonlinear stress analysis, electrostatics, magnetostatics, steady state heat conduction and fluid flow in porous media. After the appropriate finite element discretization such problems, known as equilibrium problems, can be represented by a set of simultaneous equations of the form

$$\underset{\sim}{K}\,\underset{\sim}{a} = \underset{\sim}{f} \tag{B.1}$$

where for example in a structural analysis problem in which the displacement method is used, $\underset{\sim}{f}$ represents the vector of applied nodal force, $\underset{\sim}{K}$ is the stiffness matrix of the structure, and $\underset{\sim}{a}$ is the vector of nodal displacement. In the other applications $\underset{\sim}{f}$, $\underset{\sim}{K}$, and $\underset{\sim}{a}$ have their own physical significance.

A problem represented by (B.1) may be transformed into an equivalent second order transient problem and then a standard method for solving such a problem can be used. For example, if dynamic terms involving inertia and viscous damping are added to the governing equation (B.1) then the static solution can be obtained from the dynamic analysis of the problem. This method has been named the dynamic relaxation (DR) technique and following its introduction by Day[1] it has been used as an alternative procedure for solving a wide range of linear and nonlinear problems[2-15].

The DR technique basically involves the step by step integration of critically damped vibrations using viscous damping to ensure the

attainment of steady static solution. By a suitable choice of damping factor the oscillations associated with the dynamic problem rapidly converge to the static solution.

The main advantage of the DR technique, which in its standard form is an explicit method which uses a central difference time stepping scheme, is that it avoids the solution of simultaneous equations and instead simply reduces to a step by step procedure in which the equations for the unknown variables uncouple at each step. Consequently it is very simple and easy to program. The core storage requirements for such a program are small and for less than those required for a direct finite element solution for the majority of cases. The technique is therefore ideally suited for nonlinear finite element problems involving large bandwidths and it is also of use with minicomputers.

B.2 STANDARD DYNAMIC RELAXATION METHOD

It is well known that the displacements of a damped dynamically loaded structural system eventually converges to the corresponding static solution. The rate of convergence to the static solution depends on the damping factors assigned. If critical damping is adopted, the oscillations dampen down most rapidly to the corresponding static solution as can be seen in the examples given later. If a damping factor is used which is greater than the critical factor, then the convergence to the static solution is asymptotic and although the difference between displacement values of successive time steps may be small, the solution may be just converging slowly and may still be far from the static value. On the other hand, if a smaller damping factor

is selected, the oscillations die down with successively smaller amplitudes. This idea has been developed into a method of structural analysis which depends on following the dynamic behaviour of the structure until it has dampened down to its static configuration. There is a considerable amount of literature on the application of DR to the analysis of plates, shells and three dimensional solids, e.g.[23-25].

The idea can be extended to solve any system with governing equations of the same form as equation (B.1) which can be rewritten in pseudo dynamic equations in the following form

$$\underset{\sim}{M}\,\ddot{\underset{\sim}{a}} + \underset{\sim}{C}\,\dot{\underset{\sim}{a}} + \underset{\sim}{K}\,\underset{\sim}{a} = \underset{\sim}{f} \qquad \text{(B.2)}$$

where $\underset{\sim}{M}$ is the fictitious mass matrix

$\underset{\sim}{C}$ is the damping matrix

$\underset{\sim}{K}$ is the stiffness matrix (For nonlinear problems $\underset{\sim}{K}\,\underset{\sim}{a}$ can be represented by $\int_{\Omega} B^T \sigma \, d\Omega$ in which $\underset{\sim}{B}$ denotes the strain matrix $\underset{\sim}{\sigma}$ is the stress vector)

a dot refers to differentiation with respect to time, and $\underset{\sim}{a}$ and $\underset{\sim}{f}$ are as defined previously.

Various methods of solving DR problems have been discussed in the literature (7-11). The most efficient and the one which is presented here is the explicit difference scheme.

There is a wide choice of $\underset{\sim}{M}$ and $\underset{\sim}{C}$, the fictitious mass and damping matrices. The selection of these matrices is now discussed.

Fictitious mass matrix Various forms of the fictitious mass matrix can be applied[15]. The three most convenient forms are:

(1) a diagonal lumped mass matrix; (i.e., the real mass matrix)

(2) a mass matrix in which the diagonal elements of $\underset{\sim}{M}$ are equal to the corresponding elements of $\underset{\sim}{K}$, i.e., $m_{ii} = k_{ii}$;

(3) a mass matrix in which the diagonal elements of $\underset{\sim}{M}$ are equal to the sum of the absolute vector of all the elements in the corresponding row of the stiffness matrix $\underset{\sim}{K}$, i.e.,

$m_{ii} = \sum_{j=1}^{m} |k_{ij}|$ where m is the order of stiffness matrix.

All forms of fictitious mass matrices are purely diagonal. The relative merits of each fictitious mass matrix can be seen in the examples.

Damping matrix The damping matrix can be expressed by Rayleigh damping as follows:

$$\underset{\sim}{C} = \alpha\underset{\sim}{M} + \beta\underset{\sim}{K} \tag{B.3}$$

where α and β are arbitrary proportionality factors.

It can be shown that the damping matrix adopted is $\zeta_r \underset{\sim}{C}_r$ where $\underset{\sim}{C}_r$ is the damping matrix associated with critical damping of the r^{th} mode.

The damping ratio ζ_r associated with the r^{th} mode of the system can be expressed in terms of α and β by the relation

$$\zeta_r = \frac{\alpha}{2\omega_1} + \frac{\beta\,\omega_r}{2} \tag{B.4}$$

in which ω_r is the circular frequency in the r^{th} mode. In a low frequency dominant system, usually the contribution of the second term in equation (B.4) is negligible. Therefore, the damping ratio ζ_r can

be simplified as

$$\zeta_r = \frac{\alpha}{2\omega_r} \tag{B.5}$$

For the critical damping, $\zeta_r = 1$, leads to

$$\alpha = 2\omega_r \tag{B.6}$$

Finally, the critical damping matrix is given as

$$\underset{\sim}{C} = 2\omega_r \underset{\sim}{M} \tag{B.7}$$

B.3 THE CENTRAL DIFFERENCE SCHEME AND STABILITY CONSIDERATIONS

With the mass and damping matrices specified, equation (B.2) can be solved by the centred finite difference approximation which can be written, for the i^{th} node, as

$$M_i \frac{{}^{t+\Delta t}a_i - 2\,{}^{t}a_i + {}^{t-\Delta t}a_i}{\Delta t^2} + C_i \frac{{}^{t+\Delta t}a_i - {}^{t-\Delta t}a_i}{2\Delta t} + \sum_{j=1}^{m} K_{ij}\,{}^{t}a_i = {}^{t}f_i$$

or ${}^{t+\Delta t}a_i$ can be presented explicitly as

$${}^{t+\Delta t}a_i = \frac{1}{M_i + C_i \frac{\Delta t}{2}} \left\{ (\Delta t)^2 \left(-{}^{t}f_i - \sum_{j=1}^{m} K_{ij}\,{}^{t}a_i\right) + 2M_i\,{}^{t}a_i - \right.$$

$$\left. - \left(M_i - C_i \frac{\Delta t}{2}\right) {}^{t-\Delta t}a_i \right\} \tag{B.8}$$

in which $t+\Delta t$, t, $t-\Delta t$ denote three successive time intervals. Therefore, the computation of ${}^{t+\Delta t}a_i$ is straightforward since all terms in the right hand side of equation (B.8) are known at time t.

It is noted that the central difference scheme is conditionally stable. That is, it would be unstable if the length of time step is

greater than some critical time step length. The critical time step length for linear problems is limited by the highest frequency λ_{max} of the finite element mesh. Thus

$$\Delta t \leq \frac{2}{\lambda_{max}} \tag{B.9}$$

when Δt does not satisfy the above inequality, a spurious increase in the computed displacements will take place and this leads to numerical instability.

The estimate of the critical time step length for conditionally stable schemes apparently necessitates the solution of the eigenvalue problem for the whole system. However, a bound on the highest eigenvalue can be simply obtained by the consideration of an individual element. It has been proved that the highest system eigenvalue must always be less than the highest eigenvalue of the individual elements. This allows an easily obtained and conservative estimate of the critical time step length.

The fact that equation (B.9) is necessary and sufficient for stability of the central difference scheme has been proved only for linear systems. There is, however, considerable empirical evidence that equation (B.9) is also sufficient for stability in nonlinear problems.

It can be shown that for a given finite element mesh

$$\lambda_{max} = \frac{2C}{\ell} \tag{B.10}$$

where C is the current wave speed and ℓ the minimum length of an element. Combining equation (B.9) and (B.10), and introducing a reduction factor β_1 which is normally less than unity and is element type dependent factor, leads to

$$\Delta t \leq \frac{\beta_1 \ell}{C} \tag{B.11}$$

which shows that the time step length must be bounded by the smallest traversal time of the wave across an element.

The critical time step length is governed by the highest frequency of the discrete mesh λ_{max}, and as mentioned earlier λ_{max} is directly related to the speed of wave propagation and for various fictitious mass matrices yield different λ_{max}. It can be shown that for a real mass matrix

$$\lambda_{max} = \frac{2}{\ell} \sqrt{\frac{E(1-\nu)}{\rho(1+\nu)\ (1-2\nu)}} \tag{B.12}$$

in which E, ν and ρ are respectively Young's modulus, Poisson's ratio and mass density of the material.

For mass matrix equal to the leading diagonal elements of stiffness matrix, i.e., $m_i = k_{ii}$, the highest eigenvalue of the discrete mesh from practical experience is $2 \leq \lambda_{max}$. For mass matrix equal to the sum of the corresponding row of stiffness matrix, i.e., $m_i = \sum_{j=1}^{m} |k_{ij}|$, the highest eigenvalue of the discrete mesh according to Gerschgorin's theorem is $\lambda_{max} = 1$. These factors can be used as a rough guide for selecting the lengths of critical time step.

As pointed out previously, the efficiency of convergence to the static solution depends on the choice of damping factor. The most efficient approach is to choose a critical damping factor given by equation (B.7). It is noted that the critical damping factor is governed by the lowest frequency of the system. This lowest frequency can be obtained directly by eigenvalue analysis or by step by step integration of equation (B.8) without damping.

B.4 EXAMPLES

In order to show the versatility of the DR technique and indeed the procedures as described above, two examples are given as follows:

Example 1: A cantilever beam under uniformly distributed load is considered. Figure B.1 illustrates this problem in which a cantilever beam is modelled by five plane stress elements and is subjected to a uniformly distributed load. It can be seen that the results with various fictitious mass matrices converge well to the static solution. As shown in Table B.1, the results obtained using fictitious mass schemes 2 and 3 are cheaper than those obtained using a real mass i.e. scheme 1. Strictly speaking, methods based on fictitious mass schemes 2 and 3 should be of equal cost. However, as indicated in Table B.1, methods based on mass scheme 3 are slightly cheaper than those based on mass scheme 2. This can be attributed to numerical approximation of damping factor, i.e., mass scheme 2 was overdamped.

Example 2: This problem is concerned with the linear and nonlinear stress analysis of an earth dam. An earth dam with dimensions and material properties is presented in Figure B.2. The static displacement at the crest ofdam and stress at Gauss point marked x in Figure B.2 are respectively shown in Figures B.3 and B.4. The static displacement and stress obtained by dynamic relaxation are reasonably consistent with the values obtained by a separate static program. In the present case the static analysis is cheaper than the analysis based on dynamic relaxation. However, dynamic relaxation could be more competitive in 3-dimensional and/or highly nonlinear problems with large bandwidth

since dynamic relaxation is only influenced slightly by these effects in terms of cost of analysis and computer storages. The cost of static nonlinear computation is directly related to these factors.

B.5 CONCLUSIONS

The main attractions of the dynamic relaxation methods in nonlinear finite element problems can be summarized as follows:

(1) They use less computer storages and the programming is generally simpler. They are especially suitable for a large bandwidth (or frontwidth) systems such as 3-D problems or as a means of solving fairly large practical problems on minicomputers.

(2) They are also suitable for the solution of nonlinear problems.

REFERENCES

1. DAY,A.S.
'An introduction to dynamic relaxation'
Engineer, 219, 218-221 (1965).

2. OTTER,J.R.H.
'Computations for prestressed concrete reaction pressure vessels using dynamic relaxation'
Nucl. Struct. Engng, 1, 65-75 (1965).

3. OTTER,J.R.H.
'Dynamic relaxation compared with other iterative treatments of partial differential equations'
Mech. Engng Des. 3, 183-185 (1966).

4. DAY,A.S.
'Analysis of plates by dynamic relaxation with special reference to boundary conditions'
Proc. Int. Symp. Digital Computers Struct. Analysis, University of Newcastle Upon Tyne, 1966.

5. CHAUDHURY,J.K., BROTTON,D.M. and MERCHANT,W.
'A numerical method for dynamic analysis of structural frameworks'
Int. J. Mech. Sci. 8, 149-162 (1966).

6. OTTER,J.R.H., CASSEL,E. and HOBBS,R.E.
'Dynamic relaxation'
Proc. Inst. Civ. Engrs 35, 633-656 (1966).

7. WOOD,W.L., CUBITT,N.J. and HUSSEY,M.J.L.
'Discussion of dynamic relaxation, Proc. Inst. Civ. Engrs 37, 723-750 (1967).

8. WOOD,W.L.
'Comparison of dynamic relaxation with three other iterative methods'
Engineer, 224, 683-687 (1967).

9. CASSEL,A.L., KINSEY,P.J. and SEFTON,D.J.
'Cylindrical shell analysis by dynamic relaxation'
Proc. Inst. Civ. Engrs 39, 75-84 (1968).

10. WOOD,W.L.
'Discussion on dynamic relaxation'
Proc. Inst. Civ. Engrs 40, 249-250 (1968).

11. WOOD,W.L.
'On an explicit numerical method for solving the biharmonic equation'
Num. Math., 11, 413-426 (1968).

12. RUSHTON,K.R.
'Dynamic relaxation solutions of elastic plate problems'
J. Strain Analysis, 3, 23-32 (1968).

13. RUSHTON,K.R. and LAING,L.M.
'A digital computer solution of the Laplace equation using the dynamic relaxation method'
Aeronaut.Q. 19, 375-387 (1968).

14. RUSHTON,K.R.
'Large deflexions of variable thickness plates'
Int. J. Mech. Sci. 10, 723-735 (1968).

15. BREW,J.S. and BROTTON,D.M.
'Nonlinear structural analysis by dynamic relaxation'
Int. Jnl Num. Meth. Engng 3, 463-483 (1971).

16. CRANDALL,S.H.
'Engineering Analysis'
McGraw-Hill, 1956.

17. HINTON,E. and OWEN,D.R.J.
'Finite Element Programming'
Academic Press, 1977.

18. ZIENKIEWICZ,O.C.
'The Finite Element Method'
McGraw-Hill, London, 1977.

19. JENNINGS,A. and MAJID,K.
'Elastic-plastic analysis of computer of framed structures loaded up to collapse'
Struct. Engr, 43, 407-412 (1965).

20. BATHE,K.J. and WILSON,E.L.
'Stability and accuracy analysis of direct integration methods'
Int. J. Earthquake Eng. and Struct. Dyn. 1, 283-291.

21. FELIPPA,C.A.
'Procedures for computer analysis of large nonlinear structural systems'
Paper presented at the International Symposium on Large Engineering Systems, the University of Manitoba, Winnipeg, Canada, 1976.

22. IRONS,B.M.
'A frontal solution program for finite element analysis'
Int. Jnl Num. Meth. Engng 2, 5-32 (1970).

23. ALWAR,R.S. and RAO,N.R.
'Large elastic deformations of clamped skewed plates by dynamic relaxation'
Comput. Struct. 4, 381-398 (1974).

24. ALWAR,R.S. and RAO,N.R.
'Nonlinear analysis of orthotropic skew plates'
AIAA J. 11 (4), 495-498 (1973).

25. ALWAR,R.S., RAO,N.R. and RAO,M.S.
'An alternative procedure in dynamic relaxation'
Computers and Structures, 5, 271-274 (1975).

26. CHAPLIN,T.K.
'Metadynamic relaxation applied to automatic analysis of slabs, plates and beams on elastic foundations'
The Interaction of Structure and Foundation, 76-83.

27. SHANTARAM,D., OWEN,D.R.J. and ZIENKIEWICZ,O.C.
'Dynamic transient behaviour of two- and three-dimensional structures including plasticity, large deformation effects and fluid interaction'
Int. J. Earthquake Eng. and Struct. Dyn. 4, 561-578.

28. PAREKH,C.J.
'Dynamic relaxation solution of seepage problems'
Numerical Methods in Geomechanics, Second International Conference at Virginia Polytechnic Institute and State University, Blacksburg, Virginia, USA, 1976.

29. ZIENKIEWICZ,O.C. and CORMEAU,I.C.
'Visco-plasticity-plasticity and creep in elastic solids, A unified numerical solution approach'
Int. Jnl Num. Meth. Engng 8, 821-845.

TABLE 1. Number of time steps required to reach static solution using various fictitious mass matrices

Mass scheme	scheme 1	scheme 2	scheme 3
Period (S)	0.0058	1737.9	4600.0
Critical time step length (S)	2.0×10^{-6}	1.0	2.75
No. of steps needed to reach static solution	4950	2960	2730
$\frac{\text{No. of steps of various schemes}}{\text{No. of steps of scheme 3}}$	1.81	1.08	1

(a) Geometry and material properties of the beam

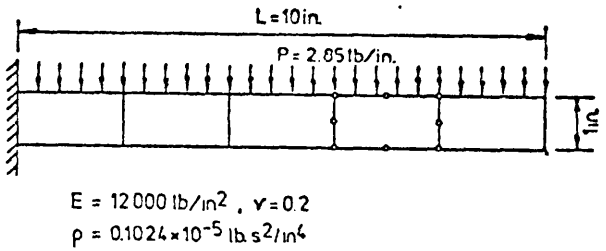

(b) Key for figures (1,3 and 4)

------	static solution
.....	α = o
———	α = critical damping , α_{cr}
—·—·—	α = 0.6α_{cr}

(c) Pseudo-transient solution based on mass scheme 1

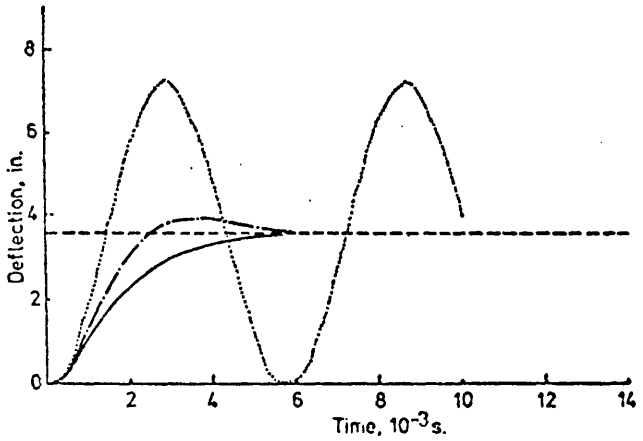

(d) Pseudo-transient solution based on mass scheme 2

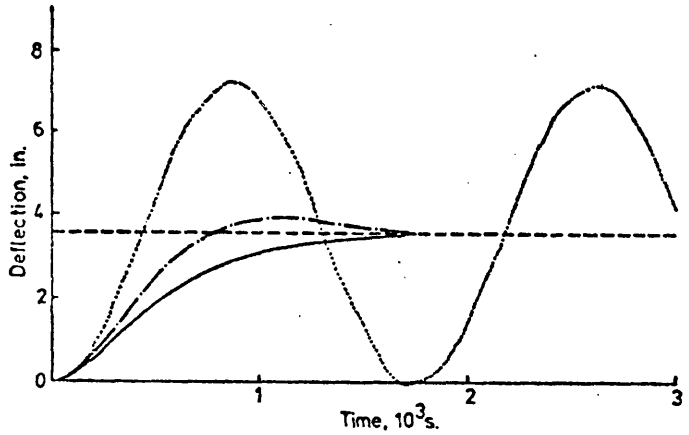

(e) Pseudo-transient solution based on mass scheme 3

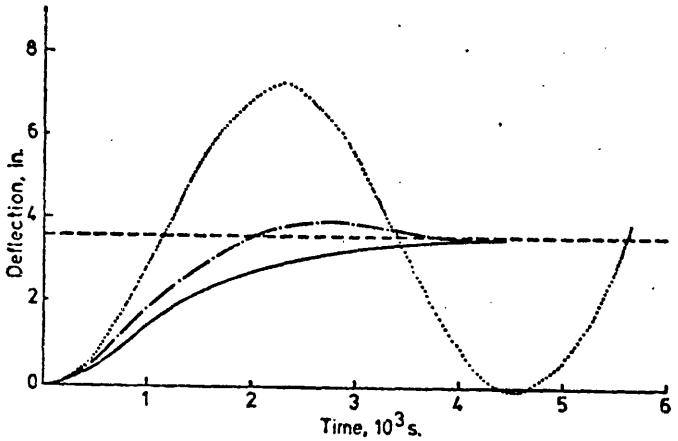

Figure 3.1 Free end deflection of a cantilever beam subjected to uniformly distributed load

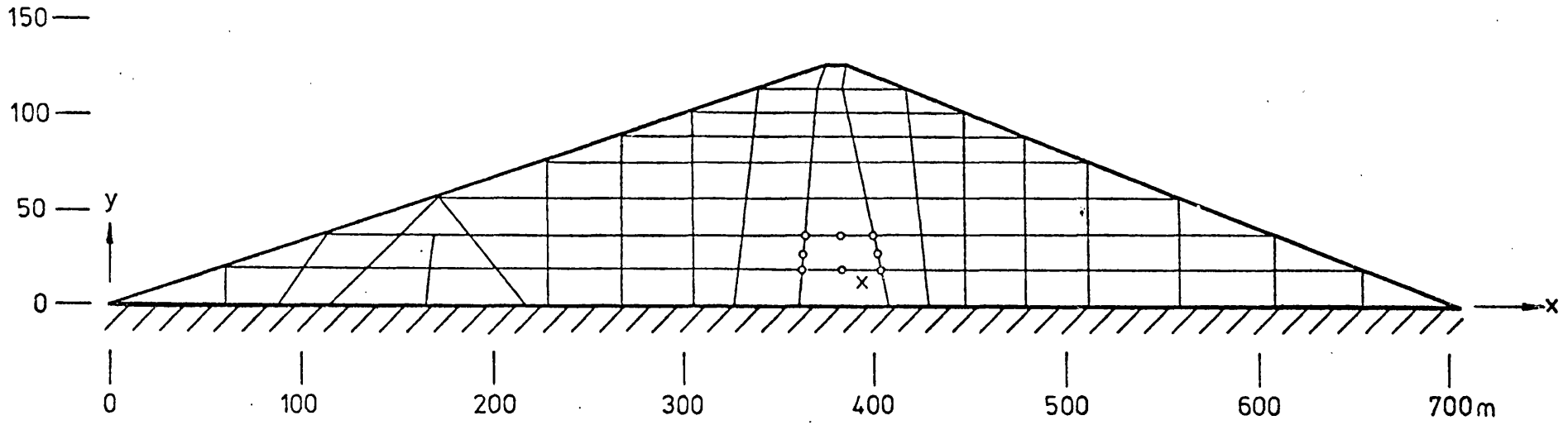

$E = 100000\ KN/m^2$, $\nu = 0.4$, $\rho = 2310\ kg/m^3$

Figure B.2 Geometry and material properties of earthdam problem

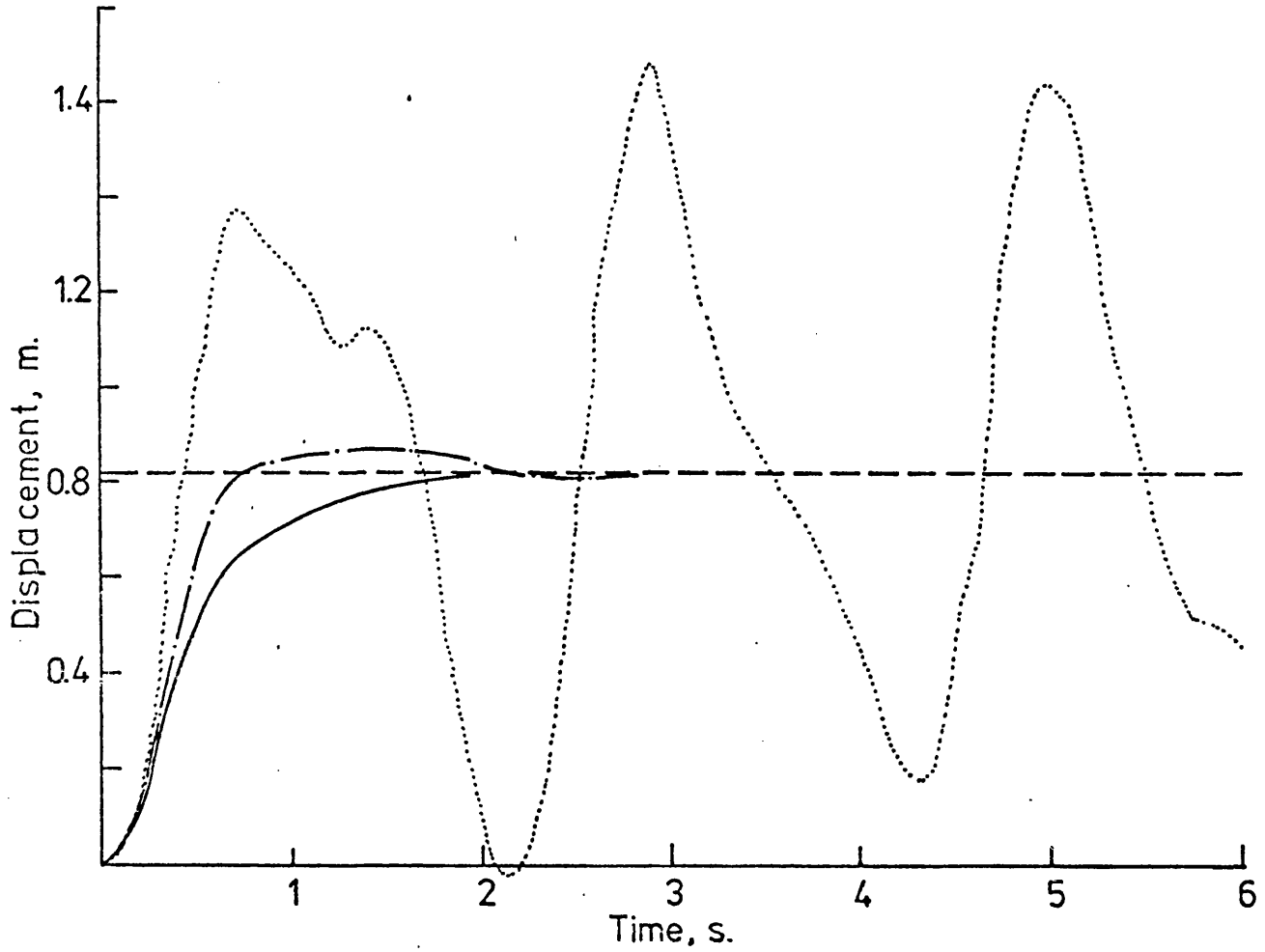

Figure B.3 Static displacement at dam crest

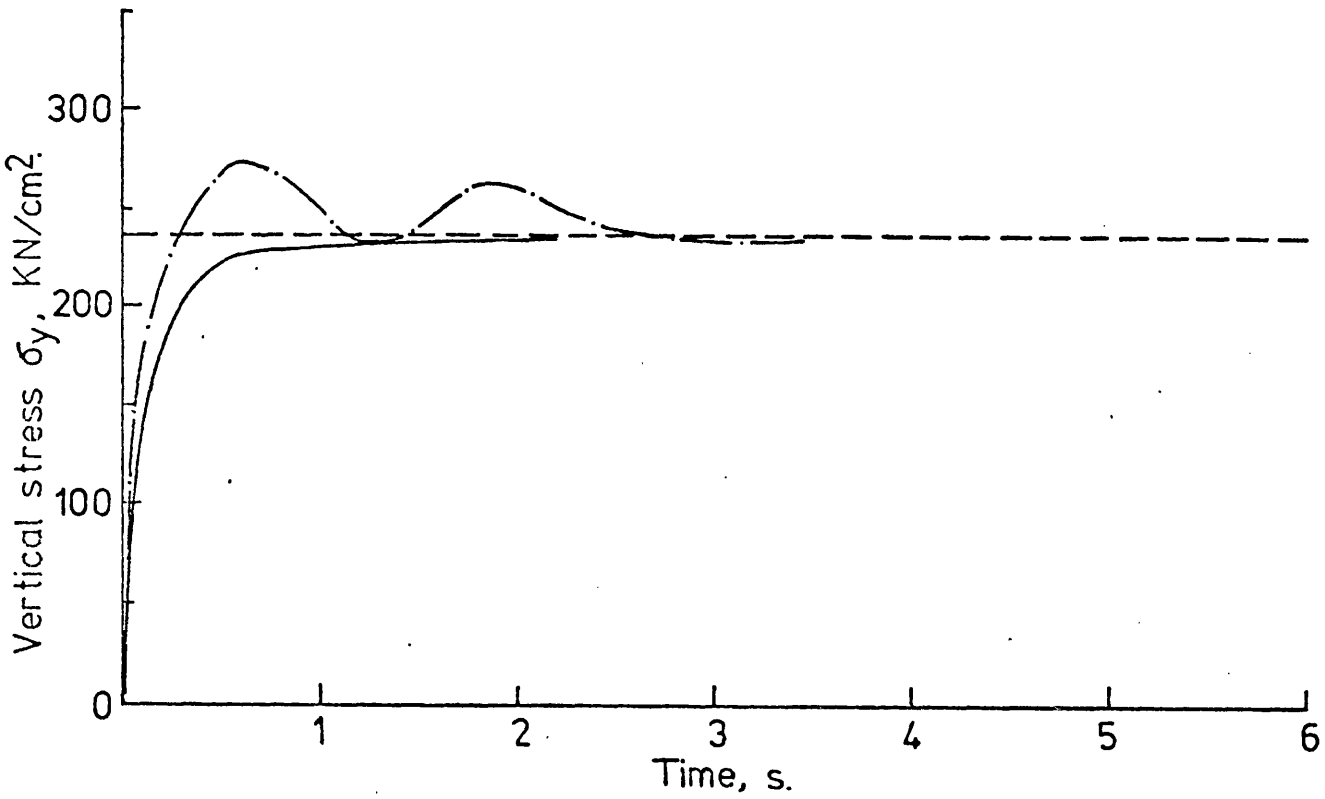

Figure B.4 Static stress at Gauss point x

APPENDIX C

NONLINEAR RESPONSE OF A QUAYWALL IN AN EARTHQUAKE

C.1 INTRODUCTION:

It has been shown that the explicit central difference time stepping scheme appears to be a feasible way of obtaining full nonlinear solution. It has also been pointed out that this scheme is conditionally stable. It will be unstable if the time stepping length is more than the critical one which is materially dependent as can be seen from the expression which was given in Chapter 4, equation (4.15). Therefore if a system is composed of different materials and one material is much stiffer than the rest, then it would be uneconomical to use the explicit central difference time stepping scheme directly without any special treatment. However, if a special technique such as one equivalent to static condensation is employed so that the stiffer region can be eliminated, then the critical time step length will no longer be governed by the stiffer material. Therefore a considerable reduction of computer time can be achieved. This appendix is to introduce the static condensation technique and an example will be given.

C.2 Static Condensation Technique[1,2]

The equations of motion under earthquake excitation are retrieved in the following

$$\underset{\sim}{M}\,\ddot{\underset{\sim}{a}} + \underset{\sim}{C}\,\dot{\underset{\sim}{a}} + \underset{\sim}{P}(a) = -\underset{\sim}{M}\,\ddot{\underset{\sim}{u}}_g \qquad (C.1)$$

A quaywall with backfill and foundation is shown in Figure C.1. If this system is subjected to an earthquake, since the quaywall is much stiffer than the backfill and the foundation, therefore, it can be assumed that the quaywall will undergo a rigid body movement during the earthquake. This movement can be represented by the following expression

$$\underset{\sim}{a}^R = \begin{bmatrix} u \\ v \\ \alpha \end{bmatrix} \tag{C.2}$$

where u and v represent the rigid body translations in x and y directions respectively and α denotes the rigid body rotation. It is also assumed that there is no slippage taking place along the contact face between the rigid block and the surrounding elements.

Let the total displacement vector $\underset{\sim}{a}$ in equation (C.1) be divided into two parts

$$\underset{\sim}{a} = \begin{pmatrix} \underset{\sim}{a}^D \\ \underset{\sim}{a}^I \end{pmatrix} \tag{C.3}$$

where $\underset{\sim}{a}^D$ denotes those displacement components directly related to the movement of the rigid block, $\underset{\sim}{a}^R$, while $\underset{\sim}{a}^I$ represents those displacement components free from the movement of the rigid block. Thus a transformation matrix $\underset{\sim}{T}$ can be uniquely defined as follows

$$\underset{\sim}{a}^D = \underset{\sim}{T}\,\underset{\sim}{a}^R$$

$$\underset{\sim}{a}^I = \underset{\sim}{I}\,\underset{\sim}{a}^I$$

or

$$\underset{\sim}{a} = \begin{bmatrix} \underset{\sim}{a}^D \\ \underset{\sim}{a}^I \end{bmatrix} = \begin{pmatrix} \underset{\sim}{T} & \underset{\sim}{0} \\ \underset{\sim}{0} & \underset{\sim}{I} \end{pmatrix} \begin{pmatrix} \underset{\sim}{a}^R \\ \underset{\sim}{a}^I \end{pmatrix} \tag{C.4}$$

in which $\underset{\sim}{T}$ is the matrix specifying the dependence, and $\underset{\sim}{I}$ is a unit vector and $\underset{\sim}{0}$ are null matrices.

Let

$$\underset{\sim}{a}^m = \begin{pmatrix} \underset{\sim}{a}^R \\ \underset{\sim}{a}^I \end{pmatrix} \tag{C.5}$$

and

$$T^* = \begin{pmatrix} \underset{\sim}{T} & \underset{\sim}{0} \\ \underset{\sim}{0} & \underset{\sim}{I} \end{pmatrix}$$

then a unique expression relating $\underset{\sim}{a}$ to $\underset{\sim}{a}^m$ can be obtained as follows

$$\underset{\sim}{a} = \underset{\sim}{T}^* \underset{\sim}{a}^m \tag{C.7}$$

Substituting equation (C.7) into equation (C.1) and using the principles of transformation as follows[3]

$$\underset{\sim}{M}\ \underset{\sim}{T}^*\ddot{\underset{\sim}{a}}^m + \underset{\sim}{C}\ \underset{\sim}{T}^*\ \dot{\underset{\sim}{a}}^m + \int_\Omega \underset{\sim}{B}^T\ \underset{\sim}{D}\ \underset{\sim}{B}\ \underset{\sim}{T}^*\ \underset{\sim}{a}\ \underset{\sim}{d}\ \Omega = -\ \underset{\sim}{M}\ \ddot{\underset{\sim}{u}}_g \tag{C.8}$$

Premultiplying equation (C.8) by $\underset{\sim}{T}^{*T}$ gives

$$\underset{\sim}{T}^{*T}\ \underset{\sim}{M}\ \underset{\sim}{T}^*\ \ddot{\underset{\sim}{a}}^m + \underset{\sim}{T}^{*T}\ \underset{\sim}{C}\ \underset{\sim}{T}^*\ \dot{\underset{\sim}{a}}^m + \int_\Omega \underset{\sim}{T}^{*T}\ \underset{\sim}{B}^T\ \underset{\sim}{D}\ \underset{\sim}{B}\ \underset{\sim}{T}^*\ a^m\ d\,\Omega = \underset{\sim}{T}^{*T}\ \underset{\sim}{M}\ \ddot{\underset{\sim}{u}}_g \tag{C.9}$$

or

$$\underset{\sim}{M}^*\ \ddot{\underset{\sim}{a}}^m + \underset{\sim}{C}^*\ \dot{\underset{\sim}{a}}^m + \int_\Omega B^{*T}\ \underset{\sim}{\sigma}^*\ d\ \Omega = -\ \underset{\sim}{T}^{*T}\ \underset{\sim}{M}\ \ddot{\underset{\sim}{u}}_g \tag{C.10}$$

in which

$$\underset{\sim}{M}^* = \underset{\sim}{T}^{*T}\ \underset{\sim}{M}\ \underset{\sim}{T}^*$$

$$\underset{\sim}{C}^* = \underset{\sim}{T}^{*T}\ \underset{\sim}{C}\ \underset{\sim}{T}^*$$

$$\underset{\sim}{B}^* = \underset{\sim}{B}\ \underset{\sim}{T}^*$$

$$\underset{\sim}{\sigma}^* = \underset{\sim}{D}\ \underset{\sim}{B}^*\ \underset{\sim}{a}^m$$

It can be seen in equation (C.10) that after transformation the vector $\underset{\sim}{a}^D$ has been eliminated from equations of motion. Therefore any displacement component belonging to the stiffer block disappears and the critical time stepping length is independent of the stiffer block.

C.3 Example:

A quaywall with backfill and foundation is shown in Figure C.1. The quaywall is considered as a rigid block. The material properties of the backfill and the foundation are also given in Figure C.1. The system is subjected to the base excitation of the May 1940 El Centro earthquake. The displacement time history at the top of the quaywall is presented in Figure C.2. The deformed shapes at 2 second intervals from the start of motion are presented in Figure C.3. From Figure C.3, it can clearly be seen that the quaywall is maintaining a rigid body movement. It is worthwhile to note that the critical time step length is no longer governed by the quaywall.

C.4 Conclusions:

As demonstrated in the example, the static condensation technique can be applied in a nonlinear response study for a system consisting of materials of different stiffness. The computation time can be tremendously reduced by using such techniques to get rid of the displacement components only relevant to the stiffer material.

REFERENCES

1. CLOUGH, R.W. and PENZIEN, J.
'Dynamics of Structures'
McGraw-Hill Book Co., New York (1975)

2. BATHE, K.J. and WILSON, E.L.
'Numerical Methods in Finite Element Analyses'
Prentice-Hall (1976)

3. ZIENKIEWICZ, O.C.
'The Finite Element Method'
McGraw-Hill Book Co., London (1977)

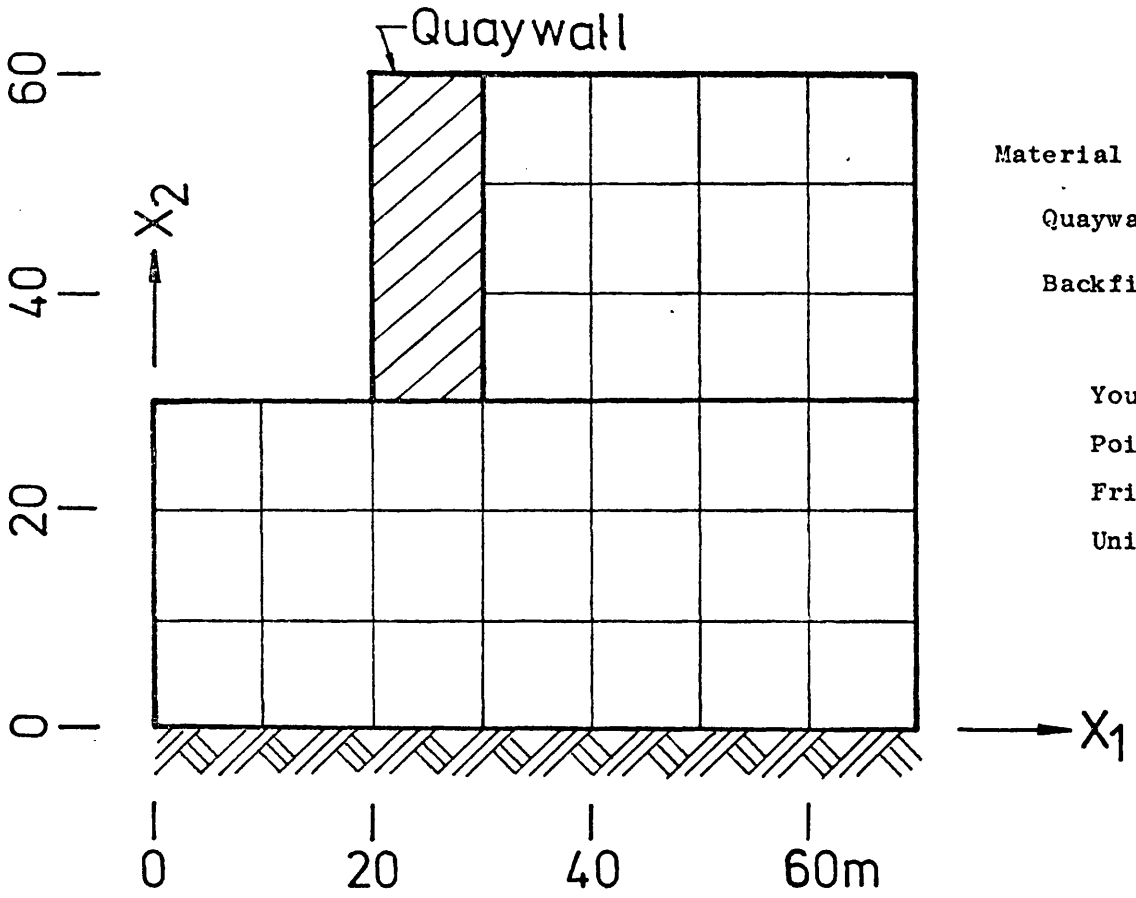

Material properties:

Quaywall: considered as a rigid block

Backfill and Foundation:

Young mod.E = 100 $^{MN}/_{m^2}$

Poisson's ratio ν = 0.4

Friction angle ϕ = 40°

Unit weight = 2200 $^{Kg}/_{m^3}$

Fig. C.1: GEOMETRY AND MATERIAL PROPERTIES OF QUAY WALL

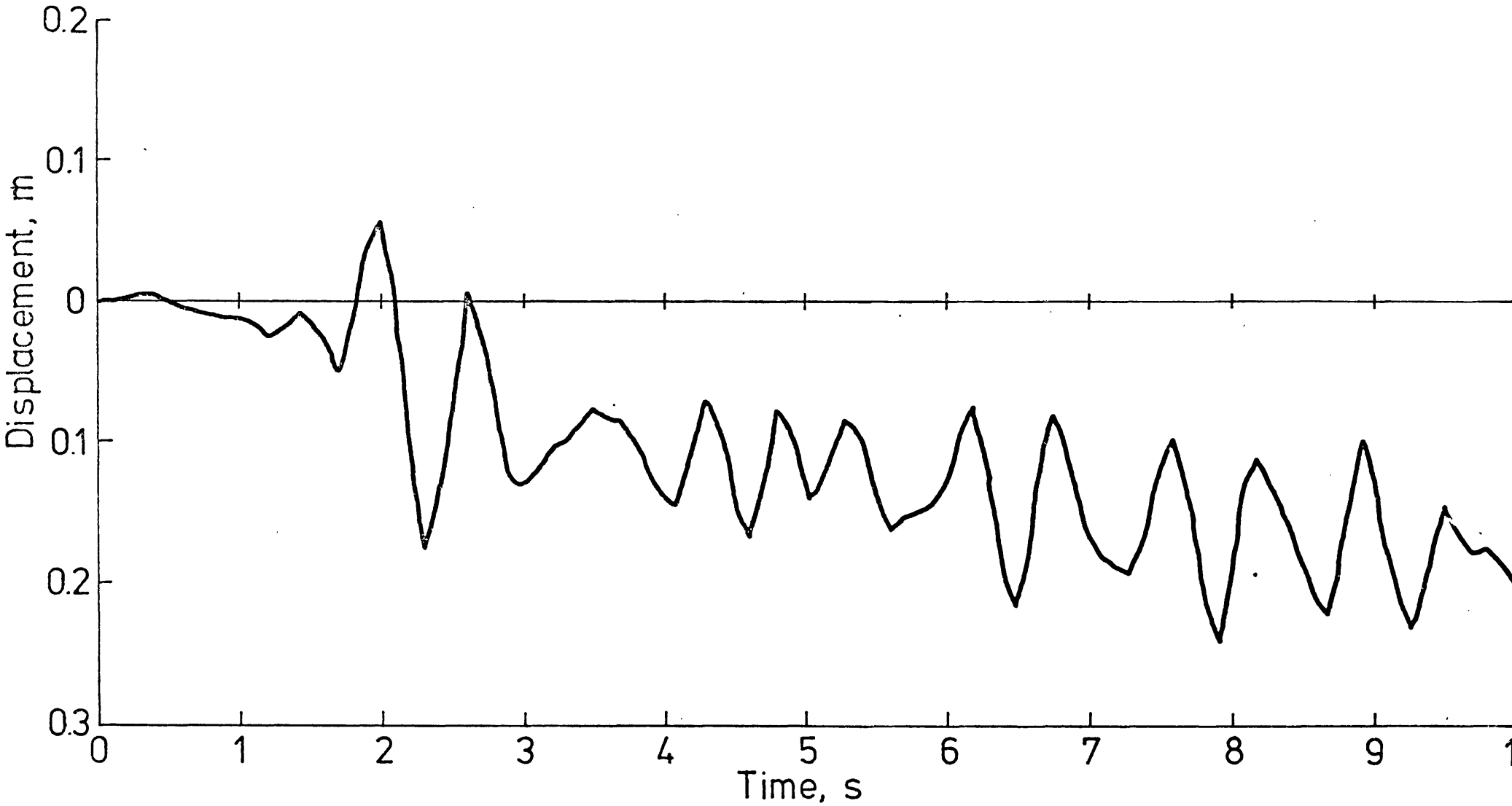

Fig. C.2 HORIZONTAL DISPLACEMENT TIME HISTORY AT THE TOP OF QUAY WALL

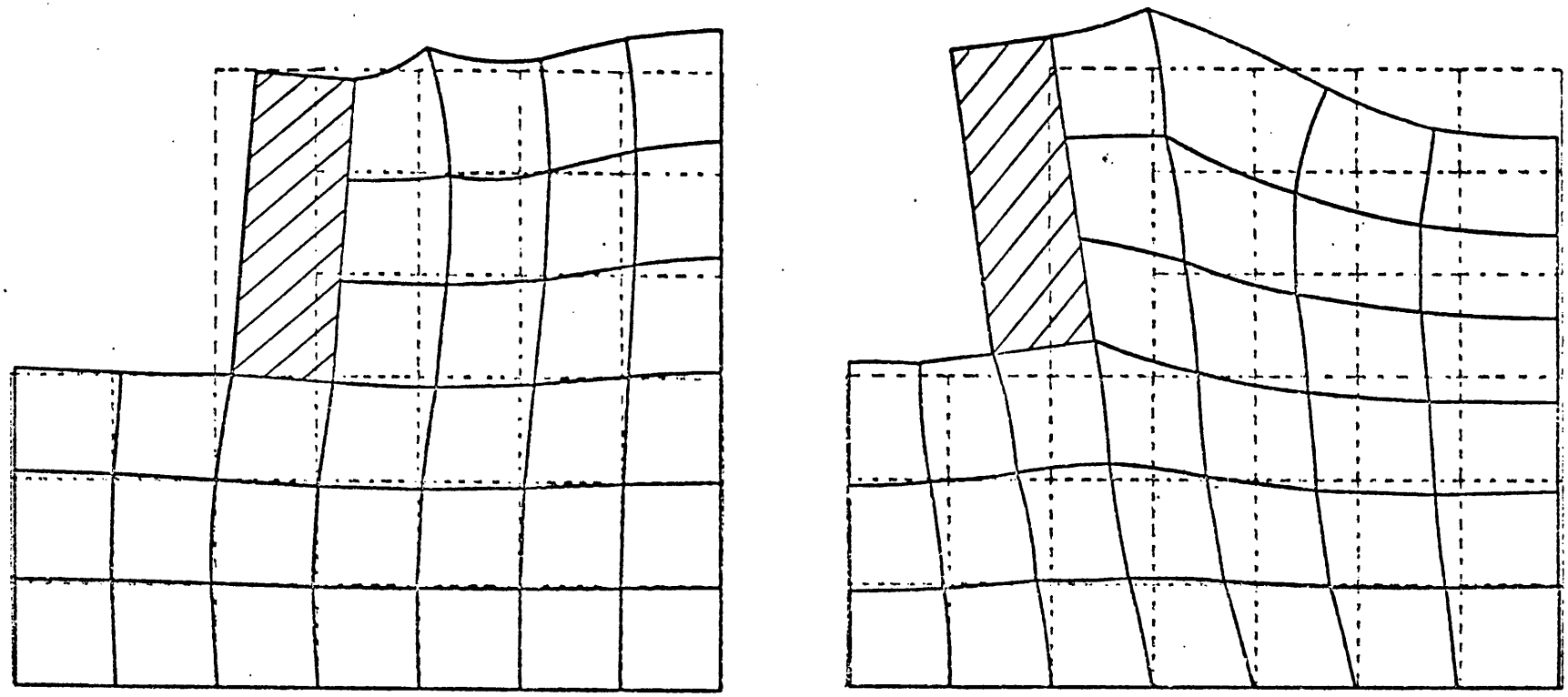

(1) 2 sec

(2) 4 sec

Fig.C.3(a) Deformed shape of a quaywall subjected to earthquake excitation

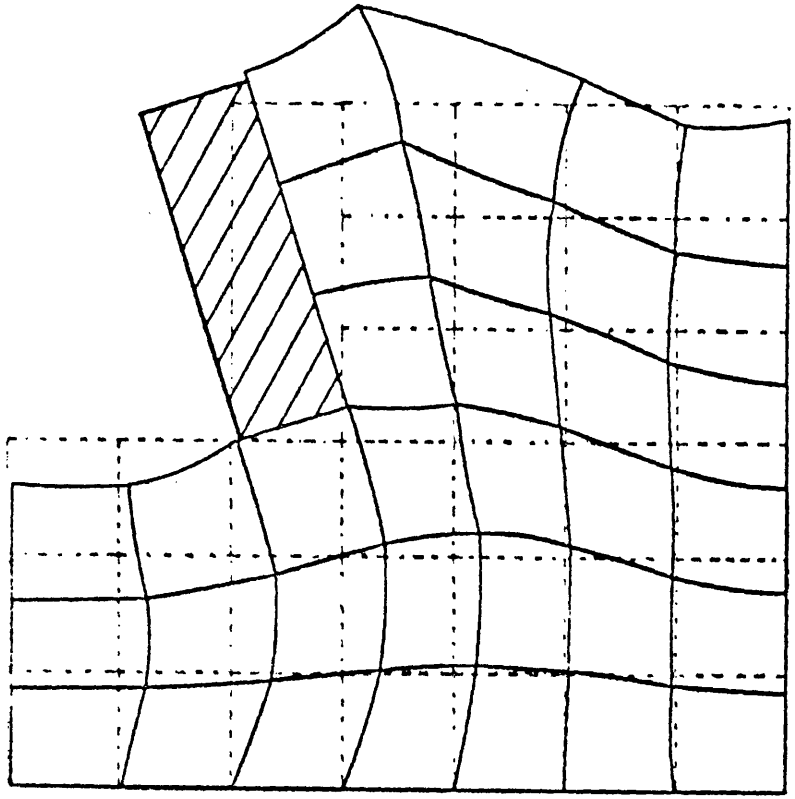

(3) 6 sec

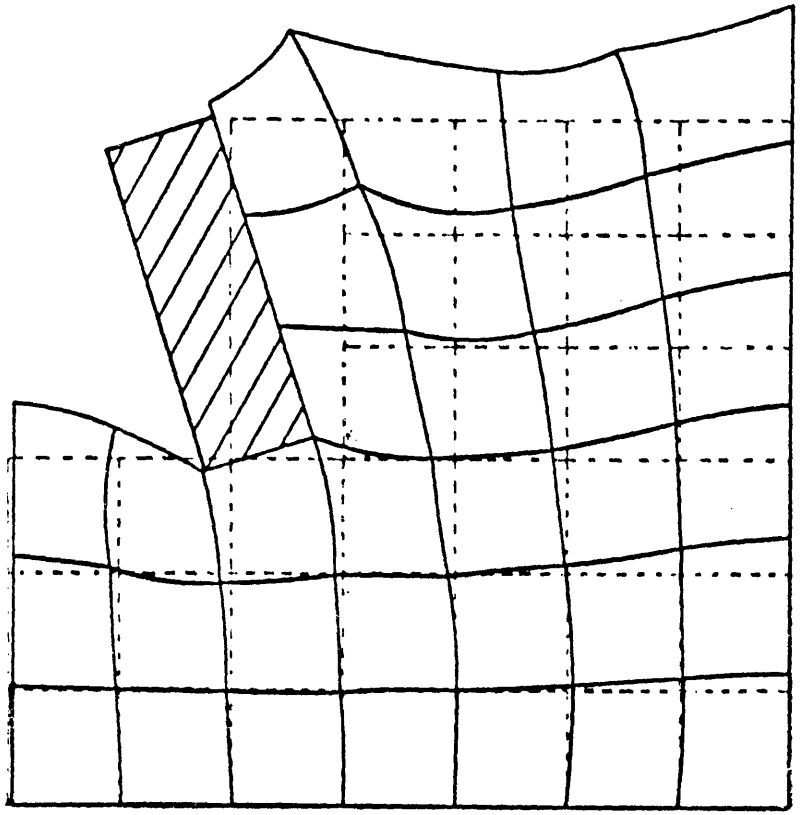

(4) 8 sec

Fig. C.3(b)

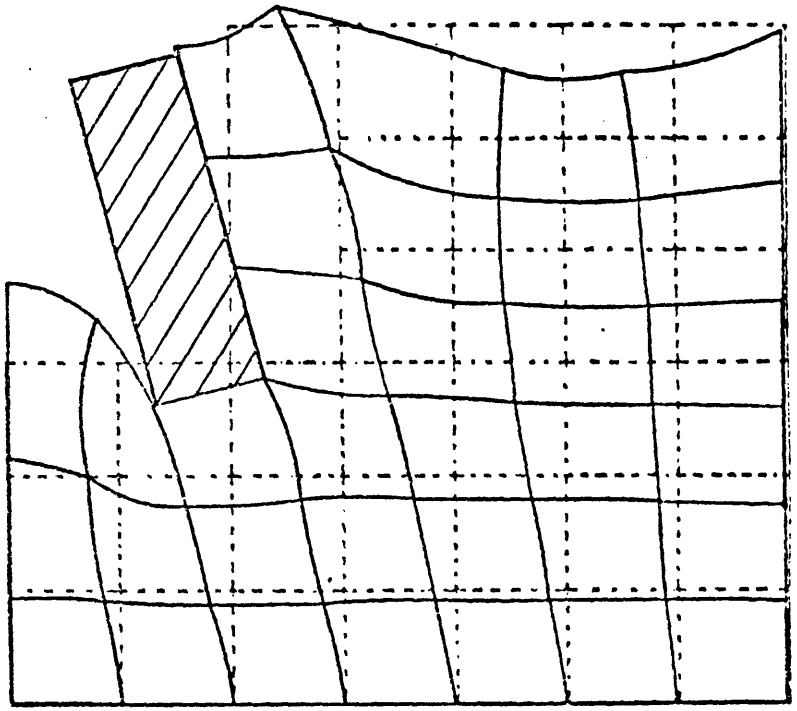

(5) 10 sec

Fig. C-3(c)

APPENDIX D

COMPUTER IMPLEMENTATION

D.1 INTRODUCTION

This appendix is devoted to a description of the computer programs QUAKE and EXACT. Therefore, it can be divided into two parts: Part I presents the detail description of QUAKE; Part II describes EXACT.

QUAKE was originally coded by Hinton and Owen to solve plane stress/strain-transient dynamic problems using the elasto/viscoplastic model with small strain and 4 and 8 noded elements. Now, it has been extended to include the elastoplastic model and large deformations using 9 noded elements to deal with a wide range of transient dynamic problems of saturated porous media under the drained, undrained or partially drained conditions. The total Langrangian strains with Piola Kirchoff stress are adopted. The equation of motion is solved by the central difference time stepping scheme. The seepage equation is solved within each dynamic time step by the FRONTAL solution technique. The style of QUAKE follows closely to the text by Hinton and Owen[1] and therefore all conventions and terms not mentioned in this appendix are to be found in their text. Since the output of the dynamic response by the finite element method covers the displacements at each nodal point and stresses at each Gauss integration point, it is useful to represent the output through various graphic forms. Therefore, a brief description of the procedures from the input to graphic production is also given in Part I.

EXACT was written to solve the one dimensional dynamic problems of porous media subjected to a sinusoidal loading on the surface by an analytical approach. For the sake of clarity, the theoretical derivation of the solution used in EXACT is also given. The program uses complex variables and the results are plotted by EDPLOT[2] which was implemented in EXACT.

PART I: QUAKE

D.2 GENERAL ORGANIZATION OF QUAKE

The general organization of QUAKE is given in Figure D.1 which consists of one master segment and 24 primary and auxilliary subroutines. The primary subroutines rely on auxialliary subroutines to carry out the secondary operations. The auxilliary subroutines may be required by more than one primary subroutine as shown in Figure D.1. The order of calling the primary subroutines is controlled by the master segment.

In order to efficiently use the nature of CDC 7600 computer, the variables from master to subroutines or from primary subroutines to auxilliary subroutines and viceversa are transimitted through COMMON blocks. The COMMON blocks are stored in a COMMON deck. Therefore any change in the COMMON blocks, it is only needed to correct the common deck once, then all COMMON blocks are corrected automatically by the computer.

The function of each subroutine is given as follows:

SUBROUTINE BMATPS	sets up B matrix
SUBROUTINE FIXITY	imposes the boundary conditions

SUBROUTINE FLOW	calculates the viscoplastic strain rate or plastic strain
SUBROUTINE FRONT	solves seepage equations
FUNCTION FUNCT	interpolates the accelerogram
SUBROUTINE GAUSSQ	sets up the Gauss sampling point positions and weighting factors for numerical integration
SUBROUTINE INPUT	reads in data required to define control parameters, nodal co-ordinates and element topology, boundary conditions and material properties.
SUBROUTINE INVAR	calculates the stress invariants and the yield stress with various yield criteria
SUBROUTINE JACOB2	computes the Jacobian matrix and its inverse
SUBROUTINE JACOBD	sets up large displacement Jacobian matrix and its inverse
SUBROUTINE LINEAR	calculates total strains, elastic strain and the corresponding stress.
SUBROUTINE LOADS	deals with various loadings input and computes the equivalent nodel forces
SUBROUTINE LUMASS	diagonalizes the mass matrix by a special lumping scheme[3].
SUBROUTINE MODPS	sets up the elasticity matrix D
SUBROUTINE NODEXY	calculates co-ordinates of midside nodes which lie on a straight line connecting two adjacent nodes and of the center nodes of the 9 noded elements
SUBROUTINE OUTPUT	prints out the displacements at nodel points and stresses at Gauss points and writes the results on tapes for the input data files of plotting programs

SUBROUTINE RESIDU	calculates the values of $\int_{\Omega} \underset{\sim}{B}^{T} \underset{\sim}{\sigma} d\Omega$
SUBROUTINE SEEPAGE	computes the seepage
SUBROUTINE SEEPS1	computes value of each element of seepage matrix
SUBROUTINE SEEPSTF	forms seepage matrix
SUBROUTINE SFR2	sets up the shape functions and their derivatives
SUBROUTINE STEP1	calculates the displacements at first time step
SUBROUTINE STEPN	calculates the displacements at time steps greater than 1
SUBROUTINE TIEUP	is used when selected nodes are constrained to have same displacement in a prescribed direction

D.3 USER INSTRUCTIONS

**** Card 1 (16I5)

1-5 NPOIN	total number of nodal points
6-10 NELEM	total number of elements
11-15 NVFIX	number of nodel points with restrained degrees of freedom
16-20 NCASE	number of time step for intermediate stop
21-25 NTYPE	type of problem (1 plane stress, 2 plane strain)
26-30 NNODE	number of nodes per element
31-35 NDOFN	number of degrees of freedom per node
36-40 NMATS	number of different materials
41-45 NPROP	number of material properties

46-50 NGAUS	Gauss integration rule
51-55 NDIME	number of dimensions (=2)
56-60 NSTRE	number of stress component (=3)
61-65 NALGO	number of time step for intermediate start
66-70 NCRIT	yield criteria (=1, Von Mises; =2, Tresca; =3, Drucker Prager; =4, Mohr/Coulomb, =5, Cambridge Critical State)
71-75 NTAPE	code for input through tape, (=1, COORD, LNODS, IFPRE are input through Tape 8; =0 All input data are through cards)
76-80 NREAD	the last nodal point to be read in

**** Card 2 (I10, 6FI0.5)

1-10 IPOIN	current nodal point
11-20 COORD (IPOIN,1)	x co-ordinate
21-30 COORD (IPOIN,2)	y co-ordinate

* the last IPOIN must be NREAD

** only corner points need to be specified, midside nodes and central nodes are interpolated by SUBROUTINE NODEXY if not specified

**** Card 3 (16I5)

1-5 NUMEL	element number
6-10 MATNO (NUMEL)	material indicator
11-15 LNODS (NUMEL,1)	
16-20 LNODS (NUMEL,2)	
21-25 LNODS (NUMEL,3)	
26-30 LNODS (NUMEL,4)	
. . . . .	end for 4 noded element

31-35 LNODS (NUMEL,5)

36-40 LNODS (NUMEL,6)

41-45 LNODS (NUMEL,7)

46-50 LNODS (NUMEL,8)

. . . . . end for 8 noded element

51-55 LNODS (NUMEL,9)

. . . . . end for 9 noded element

* total of NELEM cards

**** Card 4 (1X, I4, I5)

2-5 NOFIX (IVFIX) number of the node with restrained degrees of freedom

6-10 IFPRE (IVFIX) Fixity code

(=10 Y free
=01 X free
=11 both X and Y fixed)

* total of NVFIX cards

**** Card 5/A (I5)

1-5 NUMAT material identification number

**** Card 5/B (8E10.4)

1-10 PROPS (NUMAT,1) Young's modulus

11-20 PROPS (NUMAT,2) Poisson's ratio

21-30 PROPS (NUMAT,3) thickness for plane stress problem

31-40 PROPS (NUMAT,4) mass density per unit volume

41-50 PROPS (NUMAT,5) temperature coefficient alpha

51-60 PROPS (NUMAT,6) reference yield value Fo or cohesion C

61-70 PROPS (NUMAT,7) hardening parameter

71-80 PROPS (NUMAT,8) friction angle

**** Card 5/C (8E10.4)

1-10 PROPS (NUMAT,9) fluidity parameter gamma

11-20 PROPS (NUMAT,10) exponent delta

21-30 PROPS (NUMAT,11) NFLOW Code (=1, power law; ≠1, exponent law; =10, elastoplastic model)

31-40 PROPS (NUMAT,12) - NONAS (=0, associated flow rule, ≠0, non-associated flow rule)

41-50 PROPS (NUMAT,13) - DILAN (dilatancy angle, or M_{cs})

51-60 PROPS (NUMAT,14) half preconsolidation pressure in the critical state model or k_x

61-70 PROPS (NUMAT,15) - χ in the critical state model or k_y

71-80 PROPS (NUMAT,16) bulk modulus of fluid

* NMATS times cards 5/A/B/C

**** Card 6 (3I5, 2F10.3, 5I5)

1-5 NSTEP total number of time steps

6-10 NOUTP(1) output for displacements required at every NOUTP(1) steps

11-15 NOUTP(2) output for stresses required at every NOUTP(2) steps

16-25 DTIME time step length

26-35 DTEND time when the external excitation ends

36-40 NTIED number of sets of variables to be tied up

41-45 NTIES maximum number of tied variables in each set

46-50 NREQD nodal number for selective output of displacements at every NOUTP(2) steps

51-55 NREQS nodal number for selective output of shear stress at every NOUTP(2) steps

56-60 NSEEP — code for partially drained analysis (=0, fully undrained ≠0, partially drained)

**** Card 7/A (I5, 2F10.5)

1-5 — nodal point

6-15 — initial X displacement

16-25 — initial Y displacement

* last nodal point must be specified

**** Card 7/B (I5, 2F10.5)

1-5 — nodal point

6-15 — initial X velocity

16-25 — initial Y velocity

* last nodal point must be specified

**** Card 8 (12A6)

1-72 Title — load case title

**** Card 9 (5I5)

1-5 IPCOD — point load control

6-10 IGRAV — gravity load control

11-15 IEDGE — edge load control

16-20 ITEMP — temperature load control

21-25 IITER — base acceleration control

**** Card 10 (I5, 2F10.3)

1-5 LODPT — node number

6-15 POINT(1) — load in X direction

16-25 POINT(2) — load in Y direction

* last node must be specified

**** Card 11 (2F10.3)

1-10	THETA	Angle of gravity axis to + Y axis
11-20	GRAVY	gravity constant

* If IGRAV = 0, omit this set

**** Card 12/A (I5)

1-5	NEDGE	number of loaded edges

**** Card 12/B (4I5)

1-5	NEASS	element number with edge load
6-10	NOPRS(1)	edge nodes 1,2,3
11-15	NOPRS (2)	
16-20	NOPRS (3)	

**** Card 12/C (6F10.3)

1-10	PRESS (1,1)	normal components for loaded edge nodes
11-20	PRESS (2,1)	
21-30	PRESS (3,1)	
31-40	PRESS(1,2)	tangential components for loaded edge nodes
41-50	PRESS (2,2)	
51-60	PRESS (3,2)	

* repeat card 12/B/C NEDGE times

** If IEDGE = 0, omit this set

**** Card 13 (I5, F10.3)

1-5	NODPT	node number
6-15	TEMPE (NODPT)	nodal temperature change

* last node must be specified

** If ITEMP = 0, omit this set

**** Card 14 (4I5)

1-5	IACEE	number of accelerogram entries
6-10	IFIXD	fixed degree of freedom
11-15	NTIME	time steps required for DYNAMIC RELAXATION

**** Card 15 (2F10.3)

1-10	AFACT	ratio of time step length of accelerogram to DTIME
11-20	BFACT	damping factor, C = BFACT*M BFACT = 2 * ZETA * OWEGA

**** Card 16 (2I5, F10.0, 12I5)

1-5	NTSEQ	sequence of tied up variable
6-10	NPTIE (ITIEP)	number of tied up variables in NTSEQ set
11-20	TANGL (ITIED)	inclination of tied up variables with + x direction
21-25	NCURB (LABGN)	nodal points and tied up variables
26-30	NCURB (NPTIE (ITIED))	

** If NTIED = 0, omit this set

**** Card 17/A (4I5)

1-5	NPOEL	number of elements with pore pressure dissipation
6-10	NPOND	associated nodal numbers for NPOEL elements
11-15	NPOBC	number of boundary nodes with specified pore pressure
16-20	NPMAX	maximum nodal number in NPOND nodal points

**** Card 17/B (16I5)

(NPNOD (IPOIN) IPOIN = 1, NPOND) input all nodal points relevant to pore pressure dissipation

**** Card 17/C (16I5)

(NPELE (IELEM), IELEM = 1, NPOEL) input all elements with pore pressure dissipation

**** Card 17/D (16I5)

(NPBCN (IVFIX), IVFIX = 1, NPOBC) input all boundary nodes with prescribed pore pressure

* If NSEEP = 0, omit 17/A/B/C/D set

**** Accelerogram is input through Tape 7

**** If NTAPE = 1; Card2, Card 3 and Card 4 are input through Tape 8 which can be created by any static program in the same way as it is read.

D.4 GRAPHICAL REPRESENTATION

In any finite element analysis, especially in one that involves a time stepping routine, the information generated is considerable. Most of this information can be lost unless some form of graphical representation is employed. The process of plotting the time history of displacements or stresses or plotting the changing sequence of principal stress vectors or contours can be very tedious if one has to resort to hand-plotting. It is therefore imperative that results are stored on files so that they can then be used to generate an automatic plotting sequence. There are various processes by which one can display the results graphically, such as making use of the graphics system available on the 1904S or the PDP11 computer. The best method at present appears to be the use of the "graphomat" machine.

For design purposes, it is useful to plot the time histories of displacement and shear stress, to plot the contours of stresses and the principal stresses, to plot the principal stress vector distributions and the deformed shapes. In the present plotting program, the time histories are plotted by the program RESPONSEPLOT, the deformed shapes are plotted by DEFORMPLOT, the principal stress vectors and contours can be simultaneously plotted by CONTVECTPLOT. The procedures of plotting results are outlined as follows:

(1) Catalogue the output of QUAKE to the following filestores

Tape 3 displacement contour and deformed shape

Tape 4 stress contour

Tape 9 principal stress vector

Tape 10 displacement response at specified node NREQD

Tape 11 shear stress response at specified Gauss point NREQS

(2) After these files have been created, except stress contour plot requires to extrapolate the stress from Gauss point values to nodal point values using the program EXTRAPOLATE, the rest can readily be used as the input data of programs RESPONSEPLOT, DEFORMPLOT, and CONVECTPLOT. The flow chart of graphic production is given in Figure D.2

PART II: EXACT

D.5 Theoretical derivation

For one dimensional soil column under a harmonic exciting force on the surface, the non-dimensional equations of motion can be written as

$$\frac{d^2\bar{u}}{d\bar{z}^2} + \kappa \frac{d^2\bar{w}}{d\bar{z}^2} = -\pi_2\bar{u} - \beta\pi_2\bar{w} \tag{1.a}$$

$$\kappa \frac{d^2\bar{u}}{d\bar{z}^2} + \kappa \frac{d^2\bar{w}}{d\bar{z}^2} = -\beta\pi_2\bar{u} - \frac{\beta}{\eta}\pi_2\bar{w} + \frac{i}{\pi_1}\bar{w} \tag{1.b}$$

(1.a) x κ - (1.b) and simplifying, give

$$(\kappa^2-\kappa)\frac{d^2\bar{w}}{d\bar{z}^2} = \pi_2(\beta-\kappa)\bar{u}_2 + \pi_2\left\{\frac{\beta}{\eta} - \beta\kappa - \frac{i}{\pi_1\pi_2}\right\} \tag{2}$$

(1.a) x β - (1.b) gives

$$(\beta-\kappa)\frac{d^2\bar{u}}{d\bar{z}^2} + (\beta\kappa-\kappa)\frac{d^2\bar{w}}{d\bar{z}^2} = \bar{w}\left\{\frac{\beta}{\eta}\pi_2 - \beta^2\pi_2 - \frac{i}{\pi_1}\right\} \tag{3}$$

$\frac{d^2(2)}{d\bar{z}^2}$ gives

$$\left[\kappa^2-\kappa\right]\frac{d^4\bar{w}}{d\bar{z}^4} = \frac{d^2\bar{u}}{d\bar{z}^2}\pi_2(\beta-\kappa) + \pi_2\frac{d^2\bar{w}}{d\bar{z}^2}\left[\frac{\beta}{\eta} - \beta\kappa - \frac{i}{\pi_1\pi_2}\right] \tag{4}$$

Equation (3) gives

$$\frac{d^2\bar{u}}{d\bar{z}^2} = \frac{\frac{\beta}{\eta}\pi_2 - \beta^2\pi_2 - \frac{i}{\pi_1}}{\beta-\kappa}\bar{w} + \frac{(\kappa-\beta\kappa)}{\beta-\kappa}\frac{d^2\bar{w}}{d\bar{z}^2} \tag{5}$$

Substituting (5) into (4) and simplifying give

$$\{\kappa^2-\kappa\}\frac{d^4\bar{w}}{d\bar{z}^4} + \{\pi_2\kappa(2\beta-1) - \pi_2\frac{\beta}{\eta} + \frac{i}{\pi_1}\}\frac{d^2\bar{w}}{d\bar{z}^2} +$$

$$\pi_2\left[\pi_2\beta^2 - \frac{\pi_2\beta}{\eta} + \frac{i}{\pi_1}\right]\bar{w} = 0 \qquad (6)$$

Let $\frac{d^2\bar{w}}{d\bar{z}^2} = m^2$, $\frac{d^4\bar{w}}{d\bar{z}^4} = m^4$, equation (6) gives

$$\left[\kappa^2-\kappa\right]m^4 + \left[\pi_2\kappa(2\beta-1) - \pi_2\frac{\beta}{\eta} + \frac{i}{\pi_1}\right]m^2 +$$

$$\pi_2\left[\pi_2\beta^2 - \frac{\pi_2\beta}{\eta} + \frac{i}{\pi_1}\right] = 0 \qquad (7)$$

Further putting $m^2 = n$,

$$a = \kappa^2 - \kappa \quad \{a = \alpha^2\kappa^2 - \kappa\}^*$$

* represents expression used in EXACT

$$b = \pi_2\kappa(2\beta-1) - \pi_2\frac{\beta}{\eta} + \frac{i}{\pi_1}$$

$$\{b = \pi_2\kappa\left[(\lambda_1+\lambda_2)\alpha\beta - 1\right] - \lambda_1\pi_2\frac{\beta}{\eta} + \frac{i}{\pi_1}\}^*$$

$$c = \pi_2\left[\pi_2\beta^2 - \frac{\pi_2\beta}{\eta} + \frac{i}{\pi_1}\right]$$

$$\{c = \lambda_2\pi_2\{\lambda_1\beta^2\pi_2 - \lambda_1\frac{\pi_2\beta}{\eta} + \frac{i}{\pi_1}\}$$

Then equation (7) becomes

$$an^2 + bn + c = 0$$

and the roots are

$$n_1 = \frac{-b + \sqrt{b^2 - 4ac}}{2a}$$

$$n_2 = \frac{-b - \sqrt{b^2 - 4ac}}{2a}$$

or $$m_{1,2} = \pm\sqrt{n_1}$$

$$m_{3,4} = \pm\sqrt{n_2}$$

and

$$\bar{w} = c_1 e^{m_1 \bar{z}} + c_2 e^{m_2 \bar{z}} + c_3 e^{m_3 \bar{z}} + c_4 e^{m_4 \bar{z}} \qquad (8.a)$$

$$\frac{d\bar{w}}{d\bar{z}} = c_1 m_1 e^{m_1 \bar{z}} + c_2 m_2 e^{m_2 \bar{z}} + c_3 m_3 e^{m_3 \bar{z}} + c_4 m_4 e^{m_4 \bar{z}} \qquad (8.b)$$

$$\frac{d^2\bar{w}}{d\bar{z}^2} = c_1 m_1^2 e^{m_1 \bar{z}} + c_2 m_2 e^{m_2 \bar{z}} + c_3 m_3^2 e^{m_3 \bar{z}} + c_4 m_4^2 e^{m_4 \bar{z}} \qquad (8.c)$$

Substituting equation (8) into (2) gives

$$a \frac{d^2\bar{w}}{d\bar{z}^2} = c_1 a m_1^2 e^{m_1 \bar{z}} + c_2 a m_2^2 e^{m_2 \bar{z}} + c_3 a m_3^2 e^{m_3 \bar{z}} + c_4 a m_4^2 e^{m_4 \bar{z}}$$

$$= \pi_2 [\beta - \kappa] \bar{u} + \left[\frac{\beta \pi_2}{\eta} - \beta \kappa \pi_2 - \frac{i}{\pi_1} \right] (c_1 e^{m_1 \bar{z}} + c_2 e^{m_2 \bar{z}} + c_3 e^{m_3 \bar{z}} + c_4 e^{m_4 \bar{z}})$$

Let $d = \frac{\beta \pi_2}{\eta} - \beta \kappa \pi_2 - \frac{i}{\pi_1}$ $\{ d = \frac{\lambda_1 \beta \pi_2}{\eta} - \lambda_1 \beta \pi_2 \alpha \kappa - \frac{i}{\pi_1} \}^*$

$E = \pi_2 (\beta - \kappa)$ $\{ E = \lambda_2 \pi_2 (\beta - \alpha \kappa) \}^*$

then we have

$$\bar{u} = \frac{1}{E} \{c_1 e^{m_1 \bar{z}} (am_1^2 - d) + c_2 e^{m_2 \bar{z}} (am_2^2 - d) + c_3 e^{m_3 \bar{z}} (am_3^2 - d) + c_4 e^{m_4 \bar{z}} (am_4^2 - d) \} \quad (9.a)$$

$$\frac{d\bar{u}}{d\bar{z}} = \frac{1}{E} \{c_1 m_1 e^{m_1 \bar{z}} (am_1^2 - d) + c_2 m_2 e^{m_2 \bar{z}} (am_2^2 - d) + c_3 m_3 e^{m_3 \bar{z}} (am_3^2 - d) + c_4 m_4 e^{m_4 \bar{z}} (am_4^2 - d) \} \quad (9.b)$$

The boundary conditions are

$$P_{|\bar{z} = 0} = 0 = - \frac{M}{L} \{ \frac{d\bar{u}}{d\bar{z}} + \frac{d\bar{w}}{d\bar{z}} \} = 0 \quad (10.a)$$

$$\therefore \frac{d\bar{u}}{d\bar{z}} = - \frac{d\bar{w}}{d\bar{z}} \qquad \text{note } M = \frac{K_f}{r_i}$$

$$\bar{u}_{\bar{z} = 1} = 0 \quad (10.b)$$

$$\frac{dp}{d\bar{z}}_{|\bar{z} = 1} = \frac{M}{L^2} \{ \frac{d^2\bar{u}}{d\bar{z}^2} + \frac{d^2\bar{w}}{d\bar{z}^2} \} = 0 \quad (10.c)$$

$$\sigma_{z\ |\bar{z} = 0} = \{(D + M) \frac{d\bar{u}}{dz} + M \frac{d\bar{w}}{dz} \}$$

$$= \frac{M}{\kappa L} \{ \frac{d\bar{u}}{d\bar{z}} + \kappa \frac{d\bar{w}}{d\bar{z}} \} = f_o$$

or

$$\frac{d\bar{w}}{d\bar{z}} = \frac{f_o \kappa L}{M(\kappa - 1)} \qquad \{ \frac{d\bar{w}}{d\bar{z}} = \frac{f_o \kappa L \alpha}{M(\alpha^2 \kappa - 1)} \}^* \quad (10.d)$$

Applying (10.a) by substituting (8.b) and (9) into (10.a)

i.e. $\frac{d\bar{u}}{d\bar{z}} + \frac{d\bar{w}}{d\bar{z}} = 0$, and simplifying, give

$$c_1\{m_1 + \frac{m_1(am_1^2 - d)}{E}\} + c_2\{m_2 + \frac{m_2(am_2^2-d)}{E}\} +$$

$$c_3\{m_3 + \frac{m_3(am_3^2-d)}{E}\} + c_4\{m_4 + \frac{m_4(am_4^2-d)}{E}\} = 0 \qquad (11$$

Applying (10.b), equation (9.a) gives

$$c_1e^{m_1}(am_1^2-d) + c_2e^{m_2}(am_2^2-d) + c_3e^{m_3}(am_3^2-d) + c_4e^{m_4}(am_4^2-d) = 0 \qquad (11$$

Applying (10.c) by substituting equation (5) into (10.c), we have

$$\frac{\frac{\beta}{\eta}\pi_2 - \beta^2\pi_2 - \frac{i}{\pi_1}}{\beta - \kappa}\bar{w} + \frac{(1-k)}{\beta-\kappa}\frac{d\bar{w}^2}{d\bar{z}^2} = 0 \qquad (11$$

Let $g = \frac{\frac{\beta\pi_2}{\eta} - \beta^2\pi_2 - \frac{i}{\pi_1}}{\beta - \kappa}$ $\quad \{g = \frac{\alpha(\lambda_1\frac{\beta\pi_2}{\eta} - \beta^2\pi_2\lambda_1 - \frac{i}{\pi_1}}{\beta - \alpha\kappa}\}^*$

$f = \frac{\beta(1-k)}{\beta-\kappa}$ $\quad \{f = \frac{\beta(1-\alpha^2k)}{\beta-\kappa\alpha}\}^*$

Substituting equation (8.a) and (8.c) into equation (11.c) and simplifying lead to

$$(g+fm_1^2)\,e^{m_1}c_1 + (g+fm_2^2)\,e^{m_2}c_2 + (g+fm_3^2)\,e^{m_3}c_3 + (g+fm_4^2)\,e^{m_4}c_4 = 0 \qquad (11$$

pplying (10.d) by substituting equation (8.b) into $\frac{d\bar{w}}{d\bar{z}} = \frac{f_0 K L}{M(\kappa-1)}$ we have

$$c_1 m_1 + c_2 m_2 + c_3 m_3 + c_4 m_4 = \frac{f_0 K L}{M(\kappa-1)} \qquad (11.e)$$

ewrite equation (11) into the following form

$$\begin{bmatrix} 1 + \frac{m_1(am_1^2 - d)}{E} & m_2 + \frac{m_2(am_2^2-d)}{E} & m_3 + \frac{m_3(am_3^2-d)}{E} & m_4 + \frac{m_4(am_4^2-d)}{E} \\ m_1(am_1^2 - d) & e^{m_2}(am_2^2 - d) & e^{m_3}(am_3^2 - d) & e^{m_4}(am_4^2 - d) \\ g + fm_1^2)e^{m_1} & (g + fm_2^2)e^{m_2} & (g + fm_3^2)e^{m_3} & (g + fm_4^2)e^{m_4} \\ m_1 & m_2 & m_3 & m_4 \end{bmatrix} \begin{bmatrix} c_1 \\ c_2 \\ c_3 \\ c_4 \end{bmatrix} = \begin{bmatrix} 0 \\ 0 \\ 0 \\ \frac{f_0 K L}{M(\kappa-1)} \end{bmatrix} \qquad (12)$$

quation (12) may be solved for c_1, c_2, c_3, and c_4, then substituting he results into the expressions for $\bar{u}$, $\bar{w}$, p and σ, we can obtain the alues of $\bar{u}$, $\bar{w}$, p and σ.

Based on the above formulation, a computer program EXACT has been oded. The lists of source program QUAKE and EXACT are not given in this hesis. However, the complete document of these programs can be found in he report "EXPLICIT COMPUTATIONAL METHODS IN NONLINEAR DYNAMICS".

REFERENCES

1. HINTON,E. and Owen,D.R.J.
'Finite Element Programming'
Academic Press, (1977).

2. EDPLOT
User Instructions, C/R/709/74.

3. HINTON, E., ROCK,T.A. and ZIENKIEWICZ, O.C.
'A note on mass lumping and related processes in the finite element method'
Int. Jnl. Earthquake Eng. and Struct. Dyn., 4, 245-249, (1976).

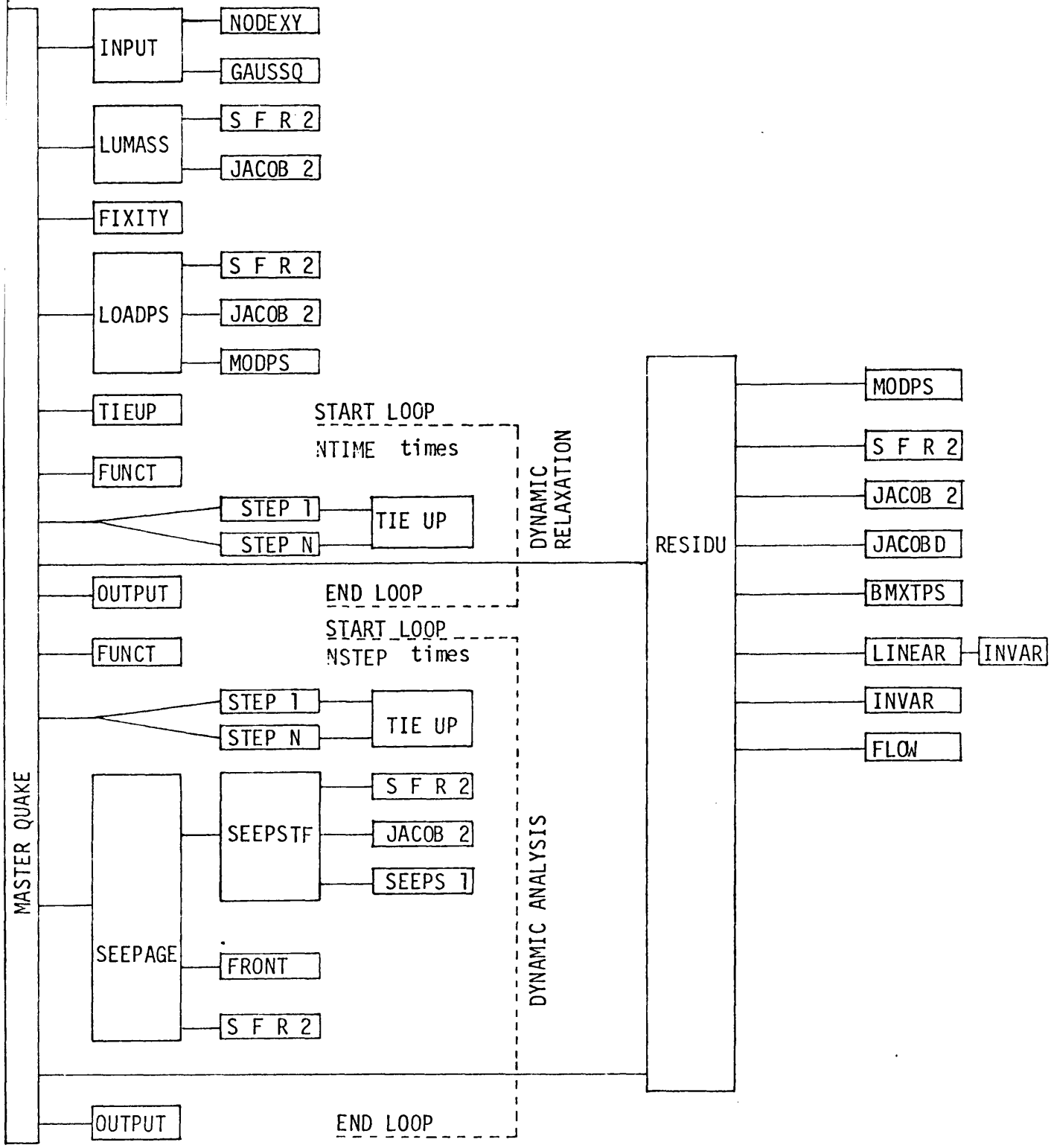

FIGURE D.1 Organization of QUAKE

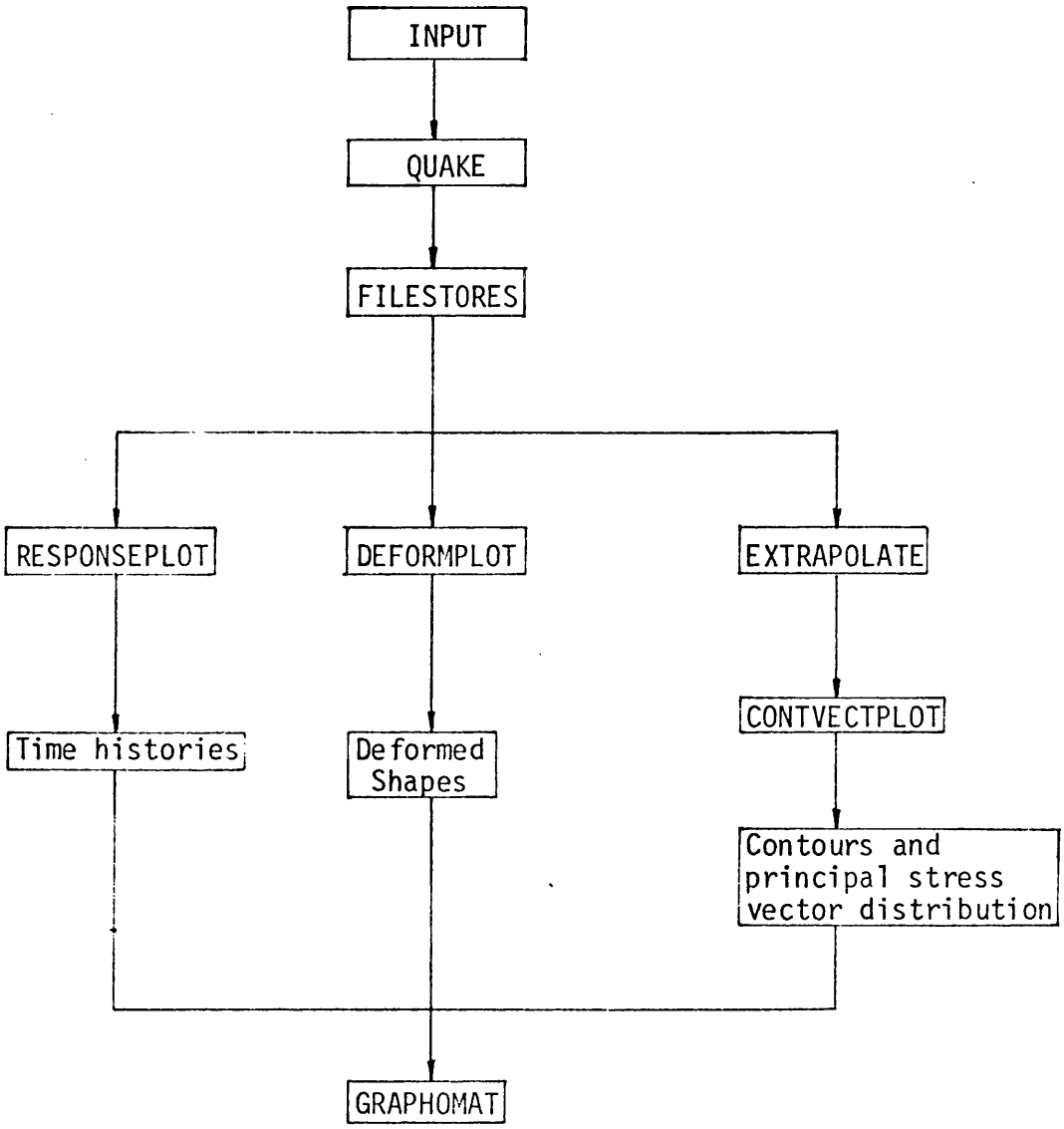

Figure D.2 Graphic Representation